# Reactive oxygen species and mitochondrial metabolism in acute myocardial ischaemia reperfusion injury: measurement and modulation

**John Francis Mulvey**
Department of Medicine
University of Cambridge

This thesis is submitted for the degree of
***Doctor of Philosophy***

St Edmund's College
September 2019

**Declaration**

This thesis is the result of work that I performed under the supervision of Dr Thomas Krieg from October 2015 to March 2019, with the exception of work done in collaboration which has been specifically declared throughout the text. Information collected from other sources has also been referenced accordingly. No part of this text has been or is being submitted for any other qualification at either the University of Cambridge or any other institution. And neither does it exceed the word limit of 60,000 words prescribed by the Clinical Medicine and Clinical Veterinary Medicine Degree Committee.

John Mulvey

September 2019

**Abstract**

Reactive oxygen species (ROS) are known to play a central role in the pathology of acute myocardial infarction (AMI), where their production is driven by the metabolism of the citric acid cyclic intermediate succinate that accumulates during ischaemia. This is a major driver of damage upon reperfusion of ischaemic tissue.

ROS are however increasingly understood to not only have negative effects, but also to act as biological signalling molecules that are able to activate protective pathways. In order to investigate how such antagonistic processes might interplay in the setting of ischaemia/reperfusion injury (IRI), it is necessary to have a tool that allows the titration of a precise amount of ROS, ideally occurring in a manner that closely mimics endogenous ROS production in both location and the exact reactive species. To this end we validate that the mitochondria-targeted compound MitoPQ produces ROS in this manner and also develop a bespoke control compound that matches the molecular properties of MitoPQ closely with the exception that it does not redox cycle at complex I in the mitochondrial respiratory chain.

These compounds are then used in model systems *in vitro* and in the mouse *in vivo* to show that whilst high doses of exogenous ROS are damaging to the heart undergoing ischaemia/reperfusion, low doses protect the heart against this insult as shown by smaller infarct sizes. Such a biphasic relationship is also seen between mitochondrial ROS and a range of cellular functions, and further allow us to demonstrate clearly for the first time that a primary increase in mitochondrial ROS may result in these changes rather than the other way around.

We also validate two further tools for use *in vivo* that enable the investigation of the effects of changes in mitochondrial redox status. MitoNeoD is an improved probe for the detection of mitochondrial superoxide using the exomarker approach, while MitoCDNB allows the selective disruption of mitochondrial thiol redox state.

The metabolic changes occurring in IRI are also investigated, applying mass spectrometry and magnetic resonance spectroscopy to measure the accumulation of succinate during ischaemia and show that the existing cardioprotective strategies of ischaemic preconditioning and moderate cooling do not alter the extent to which succinate is accumulated during ischaemia.

The use of disodium malonate to inhibit the metabolism of succinate at reperfusion is conversely found to protect the heart against IRI.

A pilot experiment is also conducted to validate a protocol of volitional exercise post AMI that has been reported to have beneficial effects on heart function during the development of heart failure with a view to investigating a potential role of succinate, but no difference is observed between exercised and sedentary mice in our hands.

**Acknowledgements**

I would first and foremost like to thank Dr Thomas Krieg for his support and guidance throughout my PhD, whilst also providing the space for my own ideas to develop. I am especially grateful for the opportunities he facilitated to present the work contained here to the scientific community.

I'd also like to recognise and thank all the collaborators mentioned in this work, most notably Professor Mike Murphy, Professor Richard Hartley and Professor Fabio Di Lisa. Salvo, Lee, Hiran and others – it has been a pleasure to work with you.

I am also indebted to all members of the Krieg lab during my time there - for your expert scientific tutelage, endless patience and as a sounding board for when progress was hard to come by. And for the company during long hours in the animal house, that too.

## Contents

**List of figures and tables**

**Abbreviations**

ACN - acetonitrile
AM – acetoxymethyl
AMI – acute myocardial infarction
BCA – bicinchoninic acid
B-Mode - brightness-mode
BSA – bovine serum albumin
CoQ – coenzyme Q
cpYFP – circularly permuted yellow fluorescent protein
CsA – cyclosporin A
CuZnSOD – copper/zinc superoxide dismutase
Cys39 – cysteine 39, ND3 subunit, mammalian complex I
db/db - BKS.Cg- Dock7$^{m}$ *Lepr*$^{db}$/J
DMM – dimethyl malonate
DSM – disodium malonate
DTND – 2-nitrobenzoic acid
ECG – electrocardiogram
ETC – electron transport chain
FBS – fetal bovine serum
FCCP - carbonyl cyanide-p-trifluoromethoxyphenylhydrazone
FMN – flavin mononucleotide
GABA – γ-aminobutryic acid
GGT - γ-glutamyl transpeptidase
GPX – glutathione peroxidase
GR – glutathione reductase
Grx - glutaredoxin
GS – glutathione synthetase
GSH - glutathione
GSSG – glutathione disulfide
GST – glutathione s-transferase
HBSS – Hank's balanced salt solution
HE – hydroethidine
HFrEF – heart failure with reduced ejection fraction
HIIT – high intensity interval training
HPLC – high performance liquid chromatography
HRP – horseradish peroxidase
i.p. - intraperitoneal
i.v. - intravenous
IMM – inner mitochondrial membrane
IPost – ischaemic postconditioning
IRI – ischaemia/reperfusion injury
LAD – left anterior descending coronary artery
LC – liquid chromatography
LDH – lactate dehydrogenase
LV – left ventricle
LVDP - left ventricular developed pressure
MAS – malate/aspartate shuttle
MCU – mitochondrial calcium uniporter
MEM – minimum essential media

MI – myocardial infarction
MICT – moderate intensity continuous training
MitoPQ – mitoparaquat
M-Mode – motion-mode
MnSOD – manganese superoxide dismutase
MPG - 2-mercapto- propionyl-glycine
MPTP – mitochondrial permeability transition pore
MR – magnetic resonance
MRM – multiple reaction monitoring
MRS – magnetic resonance spectroscopy
MS – mass spectrometry
MSMS – tandem mass spectrometry
MSR – methionine sulfoxide reductase
NAC- n-acetyl cysteine
NMR – nuclear magnetic resonance
NNT - nicotinamide nucleotide transhydrogenase
NRVM – neonatal rat ventricular myocytes
NSTEMI – non-ST elevated myocardial infarction
OMM – outer mitochondrial membrane
PNC – purine nucleotide cycle
PPCI – primary percutaneous coronary intervention
PQ – paraquat
PRESS – point resolved spectroscopy sequence
PSLX – parasternal long axis
PSAX – parasternal short axis
RET – reverse electron transport
ROS – reactive oxygen species
SDH – succinate dehydrogenase (alternatively complex II)
SOD – superoxide dismutase
SDH – succinate dehydrogenase
SDS-PAGE – sodium dodecyl sulfate polyacrylamide gel electrophoresis
STEAM – stimulated echo acquisition mode
STEMI – ST elevated myocardial infarction
TCEP - tris(2-carboxyethyl)phosphine
TFA – trifluoracetic acid
TMRM – tetramethylrhodamine
TNB – 5'-thio-2-nitrobenzoic acid
TPP – triphenylphosphonium
TrxR – thioredoxin reductase
TTC - tripheyltetrazolium chloride
T2DM – type 2 diabetes mellitus
WET – water suppression enhanced through $T_1$ effects
γGCL - γ-glutamate cysteine ligase

# Chapter 1 – General Background

## Heart attack as a clinical problem

According to the World Health Organisation coronary heart disease is the leading cause of death and disability worldwide, with the majority of mortality and morbidity attributable to acute myocardial ischaemia/reperfusion injury (IRI) (Mathers et al. 2006). This occurs when a coronary artery is acutely occluded, subjecting the myocardium supplied by that vessel (the 'area at risk') to ischaemia. Where the artery is completely occluded, patients typically present with an elevation of the ST-segment in the electrocardiogram (ST-segment elevation myocardial infarction; STEMI) as shown in figure 1.1. If the occlusion is only partial, the ST segment does not typically elevate (non-ST-segment elevation myocardial infarction; NSTEMI) and normally a smaller area of the heart is damaged. The majority of research is focussed on STEMI as both the more damaging and more clear-cut situation. When a patient presents to hospital with typical symptoms of a heart attack (chest pain, often radiating into the shoulder and arm, often alongside shortness of breath and weakness) much of the current focus is on diagnosing and treating the problem as quickly as possible in order to restore blood flow to the tissue and salvage as much myocardium as possible. This is typically done through either thrombolysis (i.e. chemical removal of the offending blockage), thrombectomy (mechanical removal of the blockage) or angioplasty in order to remove the stenosis in the artery. Often stenting is also used in this case to ensure that the vessel remains open after the procedure.

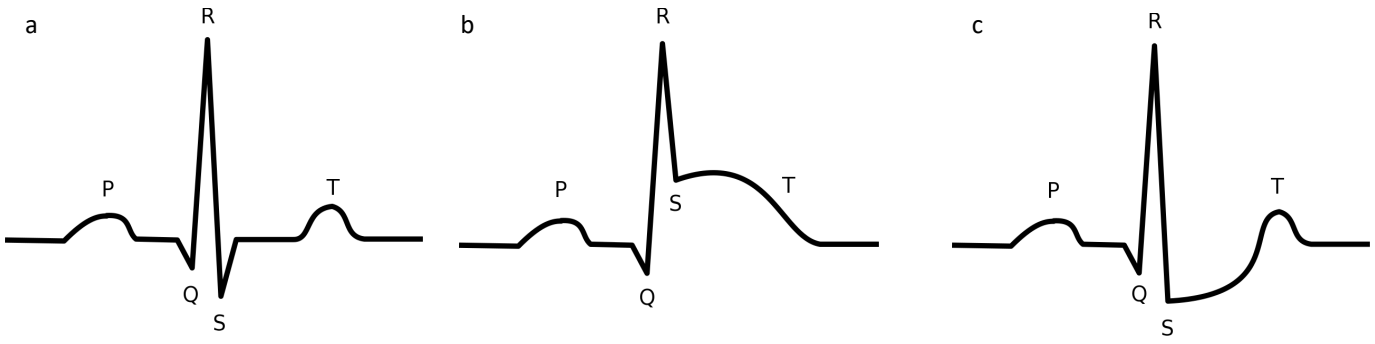


**Figure 1.1 Stereotypical human lead I electrocardiogram during acute myocardial infarction.**

**A.** ECG of a healthy patient **B.** ECG of patient undergoing a STEMI with the characteristic elevation of the ST segment **C.** An example of one possible ECG pattern in NSTEMI patients, showing ST segment depression.

**Ischaemia reperfusion injury – history of research, relative contributions of ischaemia and reperfusion, reperfusion injury as therapeutically amenable**

Whilst with current knowledge it may seem to be obvious, the suggestion that the occlusion of a coronary artery was responsible for the presence of myocardial infarcts in dead patients was initially controversial, and indeed it wasn't until 1980 that this was really demonstrated beyond all doubt. There had been suggestions as early as the 19th century from experimentalists in the dog that similar damage to that seen in patients at autopsy could be produced by the deliberate occlusion of a coronary artery (Weigert, 1880). DeWood et al. were the first to show conclusively that patients nearly always had an observable thrombus in a vessel supplying the ischaemic region, and moreover that lysis of this thrombus both restored blood flow to the tissue and reversed the clinical signs, including those such as ST-elevation in the ECG (DeWood et al., 1980). We now know that if patients die more than 24 hours after the infarction occurs, the offending thrombus will often not be found due to spontaneous lysis by fibrinolysins from surrounding epithelium, but at the time this was a major confounding factor in the analysis of post-mortem patients.

Further than the link between coronary occlusion and myocardial infarction, in 1974 Braunwald noted that the prognosis for patients with acute myocardial infarction was inversely related to the amount of tissue that was lost, and proposed that treatments should target reducing the amount of tissue death following the ischaemic insult: providing a clearly defined goal in treating acute myocardial infarction patients (Braunwald et al., 1974).

The most effective clinical intervention to achieve this currently involves minimising the ischaemic time from the onset of symptoms until the instigation of reperfusion by any of the methods discussed previously. If a coronary artery is occluded and significant collateral blood flow is absent, the area at risk will become ischaemic and eventually necrotic as cells are unable to meet their energy requirements or remove waste products. Reperfusion of ischaemic tissue is therefore essential for its survival, but it is widely acknowledged to exacerbate myocardial cell death: increasing infarct size over and above that caused by the initial ischaemic insult as originally postulated by (Jennings et al. (1960). This phenomenon is known as reperfusion injury (Figure 1.2). Any therapeutics that may either decrease ischaemic cell death or reduce the extent of reperfusion injury are termed 'cardioprotective' and should significantly improve the outcome for patients with acute myocardial IRI. Reperfusion injury in particular is a highly

sort after target, as patients will be reperfused in the hospital which provides the opportunity to provide an intervention immediately before, during or after it. In contrast a therapy targeted at reducing ischaemic cell death could only be administered towards the end of the ischaemic period.

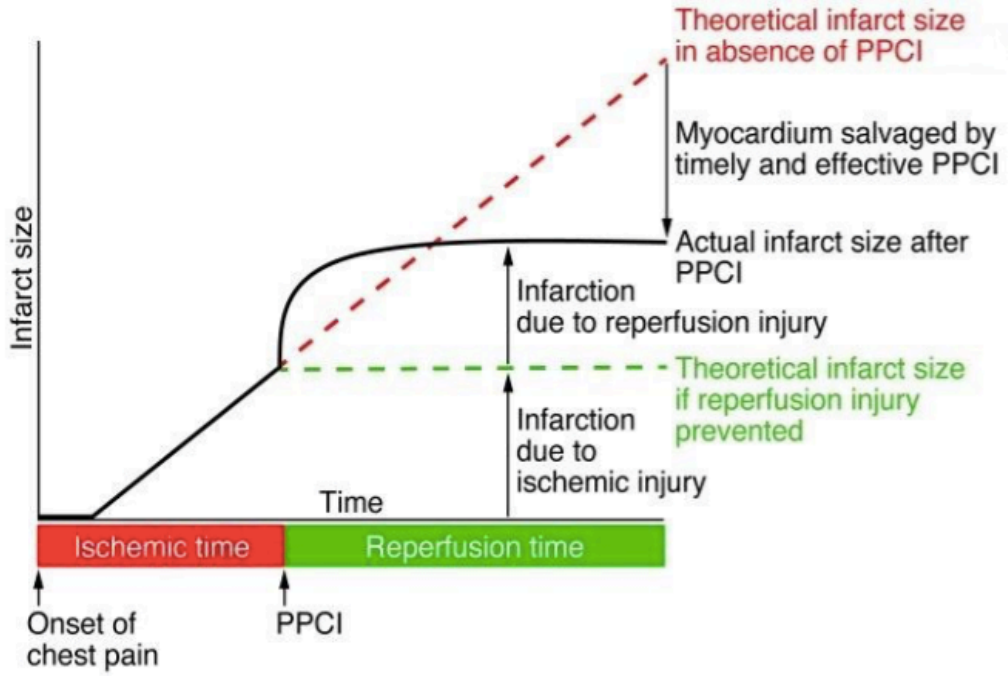


**Figure 1.2 The relative contribution of ischaemic and reperfusion injuries to myocardial infarct size.**

Myocardial infarct size is related not only to the ischaemic time, but is exacerbated by reperfusion itself: a phenomenon known as reperfusion injury. Current clinical interventions are focused on minimising ischaemic time (red dashed line) by decreasing the time between patients reporting symptoms and undergoing a primary percutaneous coronary intervention (PPCI) to restore blood flow. A therapy that is able to decrease reperfusion injury may also give a large reduction in infarct size (green dashed line). Reproduced from Hausenloy and Yellon (2013).

## Role of mitochondria

The primary deficiency that occurs during ischaemia is a lack of sufficient oxygen to meet the metabolic needs of the tissue. The heart has incredibly high energetic requirements due to its

function as a pump, consuming approximate 16 kg of ATP per day in a typical human (Neubauer, 2007). The vast majority of this energy is produced aerobically within mitochondria, whose importance in the (contractile) cardiomyocyte is shown by the fact they occupy up to 30% of cell volume (Tait and Green, 2012). Mitochondria function to provide the ATP required to power cellular processes through oxidative phosphorylation during aerobic respiration. In oxidative phosphorylation, electrons are passed from suitable electron donors (NADH, $FADH_2$) to electron acceptors (such as oxygen) along a series of linked protein carriers in the mitochondrial inner membrane. The energy released by this flow of electrons is used to transport protons across the inner mitochondrial membrane, generating an electrochemical gradient that is then used to drive ATP production by the $F_1F_0$ ATPase (Balaban et al., 2005) in a process known as chemiosmosis (Mitchell, 1961). Oxygen is required as the terminal electron acceptor in order that the process may continue, and hence when blood flow and oxygen supply ceases during myocardial infarction the heart tissue in the area at risk ceases to be able to meet its energetic demands. This leads to the time-dependent cell death during ischaemic injury.

Mitochondria are however increasingly being understood to play a central role in reperfusion injury as well due to their production of reactive oxygen species (ROS), and thus represent a viable target for the reduction of infarct size (Ertracht et al., 2014).

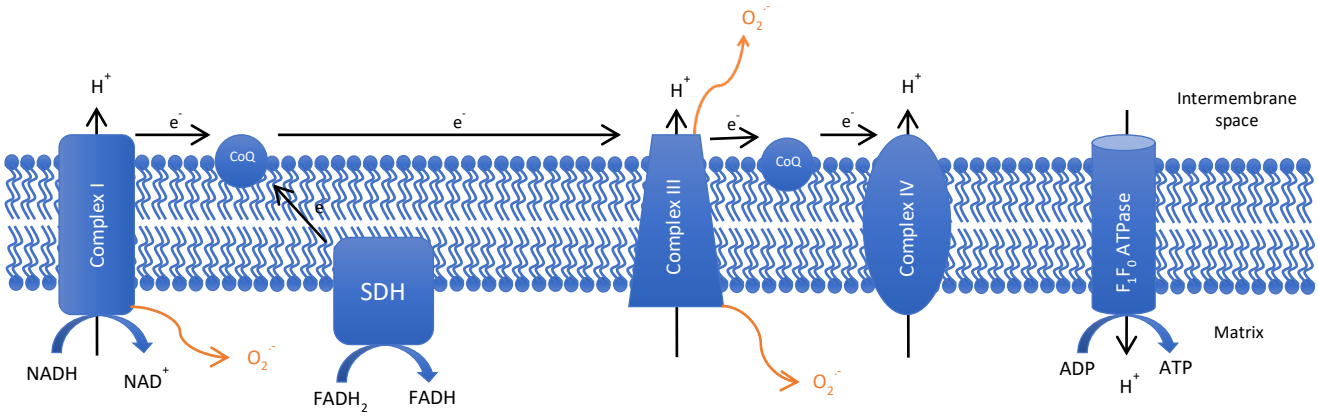


**Figure 1.3 The mitochondrial electron transport chain.**

Electrons enter the electron transport chain at either complex I or complex II (SDH) from NADH or succinate via FADH2 respectively, before passing through complexes III and IV. These redox reactions are coupled to the translocation of protons across the inner mitochondrial membrane, creating an electrochemical gradient that drives the production of ATP at the $F_1F_0$

ATPase. Complexes I and III represent the primary sites of superoxide production, the primary ROS species in the mitochondria.

**Mitochondrial reactive oxygen species production in general terms**

The concept of an 'oxygen paradox' was first described by Helmut (Davies, 2016), which states that although oxygen is essential for aerobic beings, it is also inherently toxic due to the production of reactive species. When the tissue is reperfused, injury is also driven directly from the reintroduction of oxygen by the production of reactive oxygen species (ROS). The mitochondrial electron transport chain is quantitatively the principal source of ROS production within the cardiomyocyte, and will thus be the focus of discussion here (Murphy, 2009). It is however worth noting that there are also other sources of ROS within both the mitochondria and the wider cell, and whilst they are thought to play a comparatively minor role particularly in IRI the ETC is not the sole source of ROS.

In the mitochondria at the ETC, superoxide is produced as the proximal ROS by the one electron reduction of oxygen, as its ground state of having two unpaired electrons in antibonding orbitals with parallel spins means that it will accept one electron at a time (Sawyer and Valentine, 1981). We can model this process using the Nernst equation, which shows that the rate of superoxide formation will depend on the relative concentrations of oxygen and superoxide.

$$E_h(mV) = -160 + 61.5 \log_{10} \frac{[O_2]}{[O_2{}^{\bullet -}]}$$

The rate at which this one electron reduction occurs is then the rate at which ROS production will occur in mitochondria. The dependency of ROS production upon oxygen tension may be used to explain the oxygen paradox, as the presence of oxygen must inevitably favour ROS production.

As with almost all biological processes, this is dependent upon catalysis by proteins containing either residues or prosthetic groups that may exist in a redox form that is able to interact with oxygen to form superoxide. Whilst thermodynamically favoured, the acceptance of an electron by molecular oxygen to form superoxide is spin-forbidden, and so most commonly occurs through spin-orbital coupling to a catalyst. When first considering a single protein, at any one

moment in time only a proportion of it will be in the applicable redox state, which will then catalyse the reaction by some second order rate constant. Thus:

$$\left(\frac{\mathrm{d}[O_2^{\bullet -}]}{\mathrm{d}t}\right)_E = k_E[O_2]P_{\mathrm{R}}[E]$$

Or in the more general case where multiple proteins are considered:

$$\left(\frac{\mathrm{d}[O_2^{\bullet -}]}{\mathrm{d}t}\right)_{Total} = [O_2]\sum_i (k_E P_{\mathrm{R}}[E])$$

When taken as a whole, the quantity of ROS produced in any given situation will depend on the:

a) $[O_2]$ - Oxygen tension
b) [E] – concentration of enzyme
c) $k_E$ – rate constant
d) $P_R$ – proportion of the enzyme that is in a catalytically active state

Of these, $P_R$ is of the most interest here as it is able to change rapidly in a range of biological situations. This will be discussed in greater detail in chapter 4.

**Reactive oxygen species: sources and sinks**

Whilst superoxide is the proximal ROS, it will react to form a variety of other products. ROS are often chemically defined as oxygen containing molecules with an unpaired electron, although here we use a wider definition that also encompasses species such as hydrogen peroxide that are still biologically highly reactive. The structures of some common ROS that are discussed here are shown for reference in Figure 1.4.

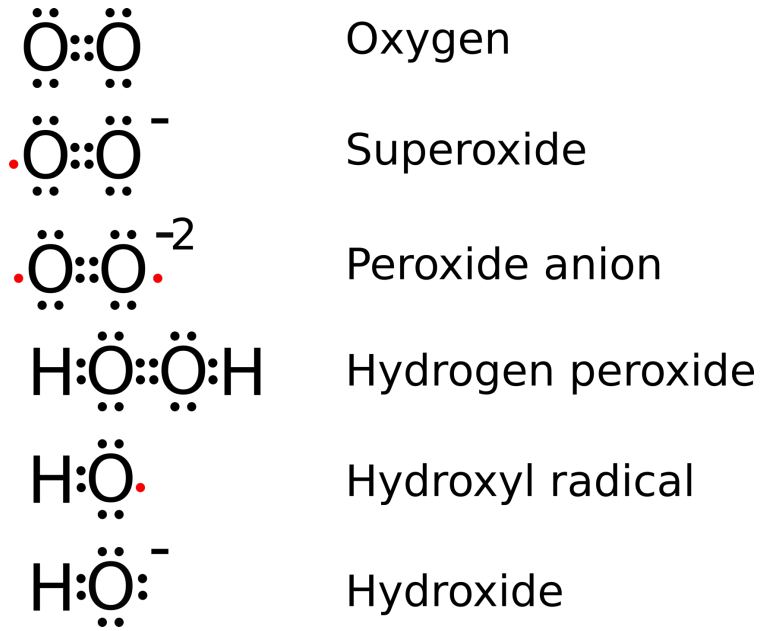


**Figure 1.4 Electron structures of some commonly referred to reactive oxygen species.** Unpaired electrons are shown in red.

Cellular levels of a given ROS species may be modelled as the sum of its sources and sinks, along with their relative rates. We have discussed how a ROS such a superoxide may be produced, but there are also multiple mechanisms by which it may be removed.

There are micromolar concentrations of manganese superoxide dismutase (MnSOD) in the mitochondrial matrix, causing its rapid ($k \sim 2.3 \times 10^9$ $M^{-1}s^{-1}$) dismutation to form hydrogen peroxide ($H_2O_2$) (Turrens, 2003). Copper/zinc superoxide dismutase (CuZnSOD) may also catalyse the same reaction within the intermembrane space. Alternatively, superoxide may react rapidly with nitric oxide (NO) to form peroxynitrite ($ONOO^-$; $k \sim 6.7 \times 10^9$ $M^{-1}s^{-1}$ (Huie and Padmaja, 1993)). As first proposed by Harber and Weiss, superoxide may also further react with $H_2O_2$ to form the hydroxyl radical (equations a and b), a process catalysed in biological systems by ferrous iron and known as the Fenton reaction (McCord and Day, 1978; Rigo et al., 1977).

$$O_2^{\bullet-} + Fe^{3+} \rightarrow O_2 + Fe^{2+} \qquad (a)$$

$$Fe^{3+} + H_2O_2 \rightarrow Fe^{3+} + OH^- + OH^{\bullet} \qquad (b)$$

$$O_2^{\bullet-} + H_2O_2 \rightarrow OH^- + OH^{\bullet} + O_2 \qquad (net)$$

Superoxide is not freely diffusible through membranes but may pass through channels. $H_2O_2$ is however membrane permeable although it appears that most transport across membranes occurs via aquaporins. This is thus a potentially regulatory step by which to modulate its levels between different cellular compartments (Bienert and Chaumont, 2014).

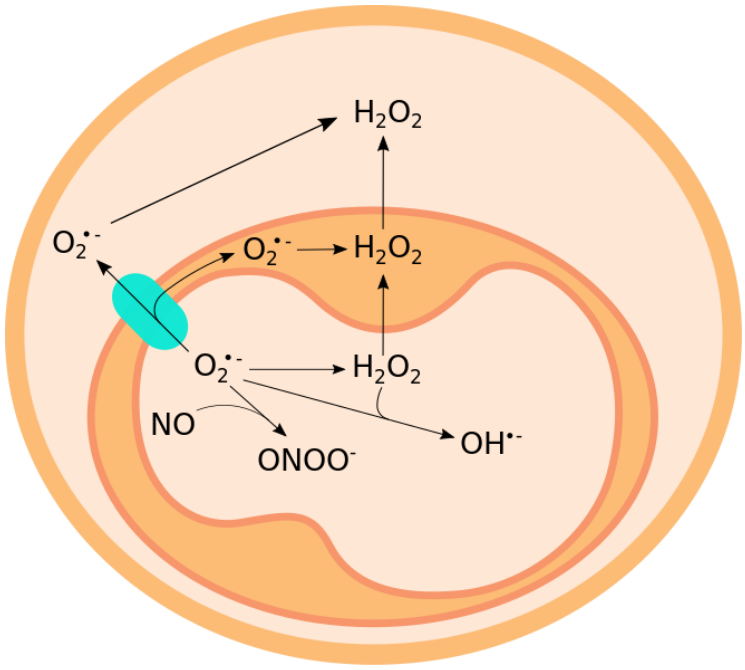


**Figure 1.5 Summary of mitochondrial superoxide fluxes.**

Superoxide produced in the mitochondrial matrix has a range of possible fates. Its passage across the inner and outer mitochondrial membranes is facilitated by channels such as aquaporins. The majority undergoes enzymatic dismutation to form hydrogen peroxide, catalyzed by MnSOD in the mitochondrial matrix or by CuZnSOD in the intermembrane space and cytosol. It may also react with nitric oxide to form peroxynitrite, or by Harber-Weiss chemistry to form hydroxyl radicals.

Steady state concentrations of a ROS such as superoxide are challenging to measure but it appears that in general the sinks outweigh the sources and thus concentrations are likely to be very low in normal physiology, estimated at 10-200 pM (Cadenas and Davies, 2000; Chance et al., 1979).

**Reactive oxygen species production as the key mediator of damage at reperfusion through decision step of mitochondrial permeability transition pore opening**

The mechanisms by which high quantities of ROS induce cell death in pathological situations such as reperfusion injury remain incompletely understood. The ROS may be directly damaging themselves, often by causing damage to essential macromolecules such as nucleic acids, proteins, polyunsaturated fatty acids in lipids (lipid peroxidation) or inactivation of enzymes due to the oxidation of co-factors. These mechanisms then lead to detriments in cell function. For example, both lipid peroxidation and the oxidation of thiol groups on membrane proteins are reported to lead to changes in membrane permeability and membrane lipid bilayer dysfunction (Prime et al., 2012).

However, the key decision step leading to gross cell death and thus infarction in IRI is not merely the accumulation of cellular damage from ROS, but the opening of the mitochondrial permeability transition pore (MPTP). This is a non-specific pore in the inner mitochondrial membrane permeable to molecules <1500 Da in weight (Bernardi and Di Lisa, 2015). The MPTP has been described as the 'arbiter of cell fate' following IRI, with the extent of its opening determining whether the cell recovers or undergoes apoptosis or necrosis (Honda and Ping, 2006).

The biochemical conditions that lead to MPTP opening at reperfusion have been well studied. Without oxygen during ischaemia, cellular metabolism must occur via anaerobic glycolysis due to the lack of a terminal electron acceptor for oxidative phosphorylation. This leads to the production of lactate which reduces intracellular pH. Intracellular acidification activates the $Na^+$-$H^+$ exchanger, pumping $H^+$ out in return for sodium entry, which is exacerbated by decreased function of the $Na^+$-$K^+$ ATPase due to ATP depletion. Sodium overload then activates the $Na^+$-$Ca^{2+}$ exchanger to function in reverse to extrude sodium, and leads to intracellular calcium overload (Avkiran and Marber, 2002). As glycolysis alone is insufficient

to meet the cells energy requirements, breakdown of ATP occurs in addition as it is used not only for normal energy requiring processes in the cell but also by the $F_1F_0$ ATPase as it functions in reverse to maintain the mitochondrial membrane potential. This hydrolysis of ATP and other adenine nucleotides leads to an accumulation of inorganic phosphate. Combined, these three conditions of high [calcium], high [phosphate] and low free [ATP] provide a strong stimulus for MPTP opening, but yet the pore is prevented from forming during ischaemia due to the acidic pH (Halestrap, 1991).

Upon reperfusion, pH is rapidly restored due to washout of lactate and increased action of the $Na^+$-$H^+$ exchanger as well as the $Na^+$-$HCO^-$ symporter once the sodium gradient is restored. A major inhibitor of MPTP formation is then removed, but ROS production also acts as a stimulus for the opening of the pore (Crompton et al., 1987; Zorov et al., 2000). The relative contributions of the different stimuli to MPTP opening however remain an open question, as changes in mitochondrial calcium and ROS are experimentally very challenging to tease apart with conventional methods.

As a high conductance pore permeable to solutes <1500 Daltons in weight, once the MPTP does open it leads to mitochondrial depolarisation and uncoupling of phosphorylation. This results in ATP depletion and energetic failure (Hausenloy and Yellon, 2003). A net influx of solutes then causes matrix swelling driven by the increased oncotic pressure. Since the surface area of the IMM greatly exceeds that of the OMM, matrix swelling may lead to rupture of the OMM, releasing pro-apoptotic molecules such a cytochrome c and apoptosis inducing factor from the intermembrane space (Zamzami et al., 2001). Cell death, and in the case of IRI infarct generation, thus occur.

**Metabolic changes during ischaemia: the selective accumulation of succinate**

Comparative metabolomic approaches have identified succinate as hallmark of ischaemic tissues, being one of only 3 metabolites that were accumulated universally across a range of tissues *in vivo*. The other two, xanthine and hypoxanthine, are breakdown products of purine nucleotides and so are well characterised and are of less interest here given our focus on mitochondrial metabolism as they are metabolised outside of the mitochondria by xanthine oxidoreductase in the cytosol. The accumulation of succinate is also substantial, with a 3-19

fold increase reported compared to baseline levels, corresponding to 61-729 ng $mg^{-1}$ wet weight of tissue (Chouchani et al., 2014).

Initial *ex vivo* experiments in the perfused mouse heart suggested that this accumulation of succinate during ischaemia occurred due to the reverse action of succinate dehydrogenase (SDH), which in turn is driven by the overflow of fumarate from the purine nucleotide cycle (PNC) and the malate/aspartate shuttle (MAS). This was done using stable isotope labelled substrates to examine pathways that produce succinate in normoxia, such as glycolysis, beta-oxidation and glutamine metabolism which indicated no significant contribution to ischaemic succinate. Likewise, inhibition of the gamma-aminobutyric acid (GABA) shunt with vigabatrin has no effect. *In silico* flux analysis of mitochondrial metabolism suggested that SDH would operate in reverse during ischaemia, oxidising fumarate to produce succinate, and indeed this was shown by inhibition with the membrane permeable competitive inhibitor dimethyl malonate in the mouse undergoing myocardial ischaemia *in vivo*. Administration of $^{13}C$ labelled aspartate also resulted in significantly accumulation of the isotopic label in the pool of ischaemic succinate (Chouchani et al., 2014), indicating that this fumarate originated from the PNC and the MAS which both utilise aspartate as a common carbon source.

Reversal of SDH has not previously been reported in ischaemic tissues, but there is good reason to suspect that it may occur due to the prevailing conditions during ischaemia. The lack of oxygen as a terminal electron acceptor means that there is an accumulation of electrons further up the respiratory chain. NADH passes electrons through complex I onto the coenzyme Q (CoQ) pool, giving it reduced state which drives SDH to function in reverse to reduce fumarate to succinate. This is thermodynamically feasible given the reaction exhibits a Gibbs free energy of -0.59 kJ/mol (Chinopoulos, 2013). Evidence of this phenomenon has also been demonstrated in isolated SDH preparations (Hirst et al., 1996), submitochondrial particles (Sanadi and Fluharty, 1963; Wilson and Cascarano, 1970) and in bacteria (Maklashina et al., 1998). It is also supported by experiments using the membrane permeable SDH inhibitor dimethyl malonate in the mouse *in vivo* which caused a decreased accumulation of succinate when it was administered prior to ischaemia (Chouchani et al., 2014).

Data reported since have however questioned the quantitative contribution of SDH reversal to the accumulation of succinate. Using the Langendorff perfused mouse heart and stable isotope labelled substrates, SDH reversal is suggested to contribute only ~6% of the succinate

accumulated (Zhang et al., 2018a). Small contributions are also found from glutamine anaplerosis (8%) and aspartate anaplerosis into canonical Krebs cycle activity (10%) (i.e. not via fumarate from the MAS). This leaves approximately three quarters unaccounted for, which is therefore believed to originate from pre-existing Krebs cycle metabolites. An open question therefore remains in the literature regrading which of these sources of ischaemic succinate is quantitatively dominant (Chinopoulos, 2019).

Succinate accumulation: a therapeutic opportunity

Decreasing the accumulation of succinate during ischaemia with the membrane permeant competitive inhibitor of SDH dimethyl malonate has been shown to protect the heart against IRI, and conversely the normal degree of injury could be recapitulated by the co-administration of the membrane permeable succinate derivative dimethyl succinate (Chouchani et al., 2014). This demonstrates that the accumulation of succinate is sufficient to drive cellular injury at reperfusion, but it is not known if this is necessary. There are a wide variety of strategies that have been shown in basic research to protect the heart against IRI, but little is known about their effects on cellular metabolism.

Ischaemic preconditioning was first demonstrated by Charles Murry in his seminal work over 3 decades ago (Murry et al., 1986). In this intervention, short cycles of ischaemia and reperfusion (typically 3 cycles of 5 min ischaemia and 5 min reperfusion followed by a washout period of 10 minutes in the mouse) are applied before the index ischaemia. Much work has been done since to unravel the signalling cascades responsible and to develop pharmacological mimics, but their application to patients will always be hampered due to the fact that in the clinic outside of a few elective scenarios it is not possible to apply any intervention before the index ischaemia as symptoms only develop following the onset of ischaemia. It however remains perhaps the most robust cardioprotective strategy.

## Succinate metabolism at reperfusion is a major driver of ROS production

The accumulation of succinate during ischaemia and strategies to ameliorate it, are principally of interest due to the direct link between its metabolism at reperfusion and tissue damage. The succinate pool may be viewed as a large store of electrons that accrue due to the fact that oxygen, which normally functions as the terminal electron acceptor in the mitochondrial

electron transport chain, is not available during ischaemia. Due to the stochiometric dependence of ROS production on oxygen tension, this means that ROS generation during ischaemia is generally considered to be low.

In contrast, a large quantity of ROS is generated in the first moments of reperfusion following an ischaemic insult (Zweier et al., 1987). In *in vitro* experiments complex I and complex III have been identified as quantitatively the main sites of ROS production under normal conditions, but the source of ROS production at reperfusion has been the focus of much recent work. Historically there has been a tacit assumption that this ROS production results from the interaction of oxygen into a dysfunctional respiratory chain in a non-specific manner, but it has now been shown to a specific and now well characterised process (Chouchani et al., 2014). This occurs due to the rapid metabolism of ischaemically accumulated succinate, with baseline levels re-established within 5 minutes (Ashrafian et al., 2012; Chouchani et al., 2014).

The set of prevailing conditions at the end of ischaemia include a high concentration of succinate, as well as a reduced CoQ pool and a high NAD/NADH ratio due to respiratory chain arrest without oxygen to accept electrons from complex IV. At reperfusion ATP generation returns and the proton motive force is restored, which then causes reverse electron transport (RET) to occur as the electrons contained within the succinate pool pass in the reverse direction through complex I and driving ROS production there. This is believed to occur at the FMN site, corresponding to complete backflow of electrons through the complex (Brand, 2016). RET has been well described *in vitro* but its importance and occurrence *in vivo* has only been recently understood (Chouchani et al., 2016). Since RET requires this highly specific set of conditions to occur (Robb et al., 2018) it is likely limited to the first seconds or minutes of reperfusion. Whilst historically complex III has been regarded as a key site of superoxide generation in mitochondria (Cadenas et al., 1977; Turrens et al., 1985) under the conditions found at reperfusion superoxide production by complex III is now thought to be negligible (Murphy, 2009).

Succinate metabolism at reperfusion: another therapeutic opportunity

In addition to there being an interest in therapies to reduce the accumulation of succinate during ischaemia, it is also possible to protect the heart against IRI by decreasing the rate of succinate metabolism upon reperfusion and so reduce the generation of ROS that occurs. This has been

shown experimentally by the inhibition of succinate dehydrogenase at reperfusion using disodium malonate which protected the heart against injury (Valls-Lacalle et al., 2015). This inhibition resulted in less ROS production and a decrease in MPTP opening and suggests that decreasing succinate metabolism at reperfusion is a potential therapeutic target in IRI.

## Mitochondria-targeted compounds

The general approach to generate mitochondrial-targeted compounds has been to create a positively charged molecule, whose selective accumulation is then driven across both the plasma membrane (due to the inside negative membrane potential of -30 to -60 mV) and into the mitochondria (due to the membrane potential of -150 to -180 mV) (Smith et al., 2003). Theoretical equilibrium values of uptake may be calculated from the Nernst equation.

$$\frac{[ion]_{outside}}{[ion]_{inside}} = e^{\frac{VZF}{RT}}$$

where V = membrane potential
Z = charge of cation
F = Faraday's constant
R = ideal gas constant
T = temperature in Kelvin

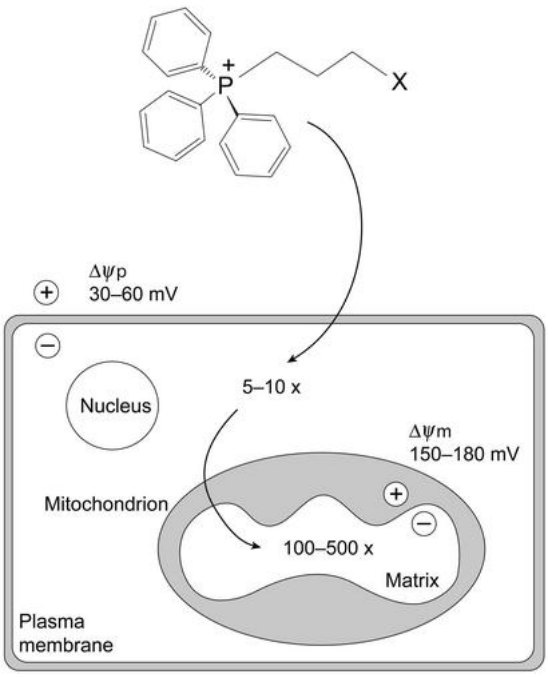

**Figure 1.6 Targeting compounds to the mitochondria via conjugation to the TPP cation.** The moiety of interest (X) is conjugated to the lipophilic cation TPP, driving its selective accumulation across both the cell and mitochondrial membrane due to the electrical potentials across these membranes. This results in a 100-500 fold accumulation of the compound within the mitochondrial matrix compared to the extracellular milieu. Reproduced from Smith et al. (2003).

Consideration must also be given to the membrane permeability of the resultant molecule and thus a commonly used strategy has emerged of conjugating the molecule of interest to a lipophilic cation, most commonly triphenylphosphonium (TPP). The positive charge on TPP is delocalised and thus unusually for a cation it is hydrophilic and can pass favourably through the phospholipid bilayers of the cell and organelle membranes (Ross et al., 2005). TPP itself was originally used to assess mitochondrial membrane potential (Liberman and Skulachev, 1970; Liberman et al., 1969) but TPP conjugation has now emerged as a successful approach to generate mitochondria-targeted molecules. The TPP targeting moiety is conjugated to a molecule of interest with a hydrocarbon linker, typically by displacing a leaving group with triphenylphosphine late in the chemical synthesis scheme (Smith et al., 2004). Care must be taken as the hydrocarbon linker itself will also affect the uptake properties of the molecule by altering its hydrophobicity: Reily et al. (Reily et al., 2013) for example demonstrate longer alkyl chain results in faster accumulation into mitochondria due to increased hydrophobicity. Successful examples of this approach include mitochondria-targeted antioxidants (Smith and Murphy, 2010), *S*-nitrosating agents (Chouchani et al., 2013), hydrogen peroxide probes (Cochemé et al., 2012) and membrane potential probes (Logan et al., 2016). It is therefore both a well-established and well-characterised approach.

A number of new compounds utilising this strategy are presented in this thesis, which are developed for use as tools of direct relevance to investigating the mechanisms of IRI that we have discussed. MitoParaquat (MitoPQ; (Robb et al., 2015)) has already been reported as a tool to selectively generate superoxide at the matrix face of complex I in the mitochondrial respiratory chain. However like all small molecule approaches, it is likely to have effects upon both the mitochondria and the cell aside from its primary actions upon complex I – due to either the paraquat or TPP moieties. The bespoke design and synthesis of compounds such as MitoPQ by Professor Richard Hartley (University of Glasgow) gives rise to the opportunity to also develop a control compound, with chemical and physical properties that replicate those of

MitoPQ apart from a small change that renders it unable it generate superoxide. The off-target properties can be hypothesised to remain unchanged from those of MitoPQ, and so enable its use as a highly specific positive experimental control.

MitoCDNB brings about the opposite change in mitochondrial redox state by causing the depletion of glutathione selectively within the mitochondria. There is also an unmet need to adequately measure the production of superoxide within the mitochondria given its position as the proximal ROS species. The development of MitoB to measure hydrogen peroxide within the mitochondria and its adoption by the research community demonstrates the successful use of the 'exomarker' approach in which an exogenous probe is transformed by a biological reaction to produce a diagnostic exomarker (Logan et al., 2014, 2015). However there is a need for a probe that is specific for superoxide rather than relying on downstream species as indirect measures.

**Development of heart failure after myocardial infarction**

Heart failure may be defined as "a clinical syndrome resulting from any structural or functional cardiac disorder that impairs the ability of the ventricle to fill or eject blood" (Yancy et al., 2013). The aetiology of heart failure is diverse, but a major cause is due to the pathological remodelling of the heart that occurs following AMI: particularly changes in the shape, size and composition of the left ventricle (Konstam et al., 2011). Incidence of heart failure in the clinic following AMI differs significantly between different studies, but ranges between 18 – 37%. One-year mortality following the diagnosis of heart failure is then reported to be between 16 – 39%. However unlike the successful decline in mortality of AMI itself due to efforts to decrease "door to balloon" times, the mortality of post AMI heart failure has showed no improvement over time (Hellermann et al., 2002). It is therefore an area in which further research is warranted.

As noted earlier in this chapter, the link between infarct size and prognosis following AMI in patients was first described by Braunwald (1974). Research in animal models has shown this to be due to pathological remodeling. For example Pfeffer and Braunwald used a surgical model of AMI in the rat to show that larger infarct sizes are also associated with a greater degree of ventricular remodeling over time (Pfeffer and Braunwald, 1990). This has since

been substantiated by a multitude of studies in patients (Chareonthaitawee et al., 1995; van Gilst et al., 1996; McKay R G et al., 1986).

Following AMI there is also an activation of a stereotyped inflammatory cascade, comprising three phases of ingress, proliferation and maturation. In the first neutrophils are recruited and begin to clear the infarct of necrotic cardiomyocytes and cellular debris. The proliferative phase then occurs when monocytes invade the infarct and differentiate into macrophages. In mice this typically occurs around 2–7 days post-AMI. Neovessels are formed to support the proliferation of fibroblasts in the infarcted area, and these then deposit extracellular matrix proteins including the collagen necessary for scar formation. Lastly during the maturation phase these fibroblasts undergo apoptosis and the neovessels regress from the infarct which allows the collagen-based matrix to condense to form the mature scar. It is crucial that this happen as early as possible due to the weak mechanical properties of the infarcted tissue which leave the heart particularly susceptible to rupture (Frangogiannis, 2006).

The scar area however does not just correspond to the area of necrotic tissue that results from the injury of ischaemia/reperfusion. Infarct expansion refers to the spread of the infarct due to tissue death not resulting directly from IRI (Jackson et al., 2002). Recruitment of adjacent tissue into the infarct scar decreases the proportion of viable contractile myocardium and thus is linked to decreases in pump function. This results in the development of systolic heart failure (or heart failure with reduced ejection fraction; HFrEF). HFrEF appears to be critical to future prognosis, with more serious left ventricular impairments subject to worse outcomes. Within the ‘remote’ myocardium that is not directly impacted by the scar there is therefore a hypertrophic response due to increased workload imposed on the heart by large infarcts. It is worth noting that this appears to be molecularly distinct from the hypertrophy induced by exercise (Strøm et al., 2005), and correspondingly is associated with worse rather than better outcomes (McMullen and Jennings, 2007).

The formation of a fibrous scar is typically accompanied by ventricular dilatation as the heart struggles to main systolic function and mean ventricular pressure increases. Scar formation has also been shown to account for the majority of the ventricular dilatation that occurs during the first hours to weeks after AMI, left ventricular end systolic volume not stabilising until after 1 month in mice (Ross et al., 2002). This also results in thinning of the ventricular

wall over time. As summarised in Laplace's law all three of these factors combine to increase the tensile stress upon the ventricle wall.

$$T \sim \frac{\Delta P * r}{h}$$

Where:

T = tensile stress

r = radius

h = wall thickness

**Δ**P = transmural pressure = $pressure_{inside}$ - $pressure_{outside}$

This combines with the reduced compliance of the scar and hypertrophy of remote myocardium to alter the stress-strain relationship of the ventricle and thus greatly increase the chance of ventricular aneurysm and subsequent rupture. It is of note that in the case of aneurysm there is a positive feedback loop as the greater curvature of the aneurysm leads to even greater wall stress being placed upon the already weakened wall.

**The beneficial effects of exercise**

Exercise, or physical activity, has almost universally been shown to be beneficial upon a wide range of physiological and pathological processes, in both epidemiological and interventional studies in humans, as well as in animal models (Pedersen and Saltin, 2006; Warburton and Bredin, 2017). It also has a number of theoretical advantages as a medical intervention: it is either cheaply or freely available, has a marked lack of negative side effects and an exceptional safety profile when compared with pharmacological interventions (Vina et al., 2012).

Of most relevance here is the positive effect that exercise has been shown to have upon heart function. In healthy people exercise is demonstrated to be an effective prophylactic strategy against the development of cardiovascular disease since the seminal works of Morris and colleagues in the 1950s, decreasing the occurrence of AMI and also improving prognosis should it occur (Morris et al., 1953). More recently is has been shown that some of this benefit is conferred via changes in the remodeling of the heart that occurs during the development of heart failure following AMI – even when the exercise occurs prior to the

ischaemic event (Maessen et al., 2017). Inevitably these findings lead to investigations as to whether exercise following AMI could improve the prognosis of patients with chronic heart failure. Historically the recommendation from clinicians has been to avoid any physical activity after an acute cardiovascular event, with exercise being slowly reintroduced as part of cardiac rehabilitation programs with the aim of preventing secondary AMIs. This is well supported by interventional evidence with improvements in longevity as well as quality of life (Taylor et al., 2004).

Exercise training has however also been reported to effect left ventricular remodeling after AMI. A small number of randomised controlled trials have been conducted, with a meta-analysis suggesting that greatest benefits occurring when training starts earlier following MI (as soon as one week) and lasts longer than 3 months (Haykowsky et al., 2011). Some mechanistic insight has been provided by animal studies, but as would be expected given the multifactorial benefits of exercise (Booth and Laye, 2009) a multitude of mechanisms are at play, with the basic science literature not even consistent regarding what benefits it may confer. For example one of the pioneering groups in the field is that of Duncker and colleagues who have variously reported exercise to have no effect upon LV remodelling (de Waard Monique C. et al., 2007), beneficial effects (de Waard et al., 2010) or detrimental effects (van Deel et al., 2018) depending on the disease model and exercise protocol that is used. Clearly further work is required in order to coalesce our understanding such that we can make appropriate recommendations to patients.

**Aims and objectives**

The aim of this work it to better characterise the role played by reactive oxygen species in AMI. This requires first the generation and validation of better tools with which to modulate and measure ROS. To this end we will provide further validation of MitoPQ, which generates superoxide at the matrix face of complex I within the mitochondria, and develop MitoPQ control compound 2 as a bespoke control compound. MitoCDNB conversely results in the opposite change in mitochondrial redox state by the depletion of glutathione selectively within the mitochondria and is tested for the first time *in vivo* to validate its actions *in vitro*. MitoNeoD, used to measure specifically the levels of superoxide within the mitochondria, will again be validated for the first time *in vivo* by its administration to mice both alone and in concert with MitoPQ.

Chapter 4 applies MitoPQ and its control compound to the situation of AMI, where ROS have been shown to both be major drivers of damage at reperfusion but also to be involved in signaling protection against IRI. We shall test the dose-response relationship of exogenous ROS generated by MitoPQ in both a primary cell model of anoxia/reoxygenation as well as in an *in vivo* surgical model of AMI in the mouse. We also assess its effects upon mitochondrial and cell function, with the aim to tease apart the primacy of changes in mitochondrial ROS and calcium: two closely interlinked parameters that cannot be conclusively unpicked using conventional methodologies.

Chapter 5 investigates the role of metabolism in IRI, focusing on the accumulation of succinate during ischaemia and its metabolism at reperfusion. We first aim to measure in the heart the succinate that is accumulated during ischaemia in a non-invasive manner by utilising magnetic resonance spectroscopy. We shall also assess whether existing cardioprotective strategies involve decreases in the accumulation of succinate during ischaemia, or if they are potentially additive to therapies targeting the accumulation and metabolism of succinate. The application of disodium malonate at reperfusion is examined as one particular strategy.

The last part of this thesis presents data from a pilot experiment on the effect of volitional exercise upon the development of heart failure post MI in mice. A future aim is to investigate a potential role for succinate in the beneficial effects of exercise upon the heart, but we first

attempt to validate a published protocol that is reported to have beneficial effects upon heart function as measured by echocardiography.

# Chapter 2 – Materials and methods

## Animals

Male C57BL/6J mice aged 8-12 weeks (22-32 g) were obtained from Charles River, UK. Male Sprague Dawley rats aged 10 weeks (250-275 g) were also obtained from Charles River, UK. These were all housed under standard laboratory conditions, with food and water available *ad libitum*. All procedures were carried out in accordance with the UK Home Office guidance on the operation of the Animal (Scientific Procedures) Act 1986 and University of Cambridge Animal Welfare Policy under project licenses 70/8238, 70/7963 and 70/8239.

## Mitochondria targeted compounds

Both the design and chemical synthesis of mitochondria-targeted compounds including MitoPQ, MitoPQ control compound 1, MitoPQ control compound 2, MitoNeoD and MitoCDNB were performed by S. Caldwell and R. Hartley (WestChem School of Chemistry, University of Glasgow, UK). They were stored at -20 °C and dissolved in either ethanol or DMSO as indicated.

## i.v. injections

### Conscious mice

In conscious mice, the animal was placed in heat chamber at 40 °C for approximately 5 minutes and then transferred to a restrainer. A bolus injection was delivered into a lateral tail vein with a 29 G needle connected directly to the syringe. The concentration of solutions was altered to maintain the volume injected at 100 μL for a 25 g mouse, and where dosages were administered relative to bodyweight the volume injected was adjusted accordingly.

Due to the known diurnal changes in cellular glutathione (Blanco et al., 2007) mice for experiments involving MitoCDNB were all injected at the same time of the day.

### Anaesthetised mice

In anaesthetised mice, the tail was heated using a lamp and then a 4-0 silk suture tied tightly at the rostral end of the tail. A 27 G needle connected to fine bore polythene tubing and a syringe was inserted into a lateral tail vein. Presence of the needle in the vein was confirmed by the appearance of the blood in the tubing and/or through a low pressure upon injection. The 4-0 silk suture was then cut, and a single bolus of maximum volume 120 µL injected slowly. For i.v. infusions, a single syring infusion pump was used (Model 11, Harvard Apparatus).

In the same manner as for i.v. injections in conscious mice, the concentration of the solution injected was altered rather than the volume that was administered. This is of particular importance where mice were undergoing a surgical procedure as increases the volume of fluid within the circulatory system will increase venous load and thus impact upon the work performed by the heart due to for example intrinsic control mechanisms to the heart such as the Frank-Starling mechanism which describes the effect of increases in the preload of the heart upon cardiac work.

## ***in vivo*** **myocardial ischaemia reperfusion injury**

### Non-recovery model

An open chest mouse model of acute myocardial ischaemia reperfusion was used as has been described in detail elsewhere in the literature (Fisher and Marber, 2002). Mice were anaesthetised with 70 mg/kg i.p. sodium pentobarbital (Euthatal®). For experiments involving magnetic resonance spectroscopy, a combination of ketamine (75 mg/kg, Velatar®, Boehringer Ingelheim) and medetomidine (1 mg/kg, Domitor, Janssen Animal Health) was administered subcutaneously due to local animal regulations with additional anaesthesia administered after the start of the surgical protocol with gaseous isoflurane (IsoFlo®, 100 % w/w Inhalation Vapour, Abbott). The chest, neck and right leg were shaved, before transfer of the mouse to a warm heating pad where it was secured with tape. Body temperature was maintained at 37±0.5 °C using a rectal temperature probe and a temperature-controlled heating pad (MouseMonitor S, Indus Instruments, USA)). An oxygen saturation monitor (MouseMonitor S Pulse Oximeter, Indus Instruments, USA) was placed on the right thigh. Depth of anaesthesia was monitored using the withdrawal reflex, and additional sodium pentobarbital was administered i.p. throughout the procedure as necessary. Using a stereo dissection microscope (Mantis Compact,

Vision Engineering, UK) an incision was made in the midline of the neck, and the trachea exposed by blunt dissection before intubation using a cannula (73-2848, Harvard Apparatus). Intubation was confirmed visually by the presence of the cannula within the trachea (Figure 7). Mice were ventilated with oxygen at 3 cm $H_2O$ positive end expiratory pressure (150 µL tidal volume, 110 breaths per minute) using a rodent ventilator (Minivent Type 845, Harvard Apparatus, Germany). A left thoracotomy was performed using a small vessel cauteriser (18000-00, Fine Science Tools) and the ribs retracted using 6-0 sutures to expose the heart. The pericardium was stripped and the left anterior descending coronary artery (LAD) was surrounded using a 7-0 prolene suture. Both ends of this were passed through a small section of tubing to create a snare, and the snare was pulled tight against the heart and clamped using needle holders to occlude the LAD. Ischaemia was confirmed by a colour change from pink to off-white of the anterior wall of the left ventricle and elevation of the J-T segment in of the electrocardiogram. Reperfusion was then achieved by release of the needle holder and thus occluding tube, resulting in the reverse colour change of the heart.


**Figure 2.1 Images of the left anterior descending coronary artery occlusion surgery.**

**A.** After an incision is made in the midline of the neck and the tracheae exposed by blunt dissection, the mouse is intubated using a metal cannula. This may be confirmed visually by the presence of the cannula within the tracheae.

**B.** A length of 7-0 suture has been placed in the heart surrounding the LAD, with both ends passed through a small section of tubing to create a snare.

**C.** The snare has been pulled tight against the heart and clamped using needle holders to occlude the LAD.

Assessment of infarct size

After 2 hours of reperfusion, the thoracic cavity was further opened by two transverse cuts at the lower end of the existing opening to allow access to the thoracic aorta. This was stripped of fat, and a 4-0 silk suture was passed around it and tied loosely at the rostral end of the visible segment. A small incision was made in the aorta using fine spring scissors to allow insertion of fine bore (0.8 mm external diameter) polythene tubing. This was then secured by tightening the suture. 0.9 % saline was injected in a retrograde fashion into the heart until it was cleared of blood. The LAD was re-occluded permanently by means of a square knot and Evans blue dye (10 mg/ml in 0.9 % saline, Sigma-Aldrich) was injected in the same manner to allow visualisation of the area at risk. Hearts were excised and frozen at -20 °C to allow slicing into ~1 mm sections parallel to the atrioventricular groove from the apex of the heart to the point of ligation. Sections were then incubated in 1% (w/v) tripheyltetrazolium chloride (TTC) (T8877, Sigma-Aldrich) in phosphate buffered saline at 37 °C for 25 minutes, and compressed between two glass slides before fixing in 10% w/v formaldehyde for 24 hours to enhance the contrast between TTC-stained and unstained tissue. Images were then taken using a digital camera (Olympus μ-7040) or scanner (WF-3520, Epson) and analysed using image analysis software (ImageJ, National Institute of Health, USA).

Planimetry was performed by an independent researcher in a blinded fashion, as shown in Figure 2.2B-D. All tissue that is stained blue is scored as non-risk, as the fact that the Evans blue dye perfused it despite re-occlusion of the suture ligating the LAD means that it by definition cannot have been ischaemic when the suture was ligated by means of the snare during the previous ischaemic period(s). The remainder of the heart sections correspond directly to the area at risk. Within the area at risk, living tissue is stained red due to the incubation with TTC as various dehydrogenases (most notably lactate dehydrogenase) reduce the white TTC to the brick red product 1,3,5-triphenylformozan (Figure 2.2A). In infarcted tissue these enzymes have either been denatured or degraded and so the tissue remains white.

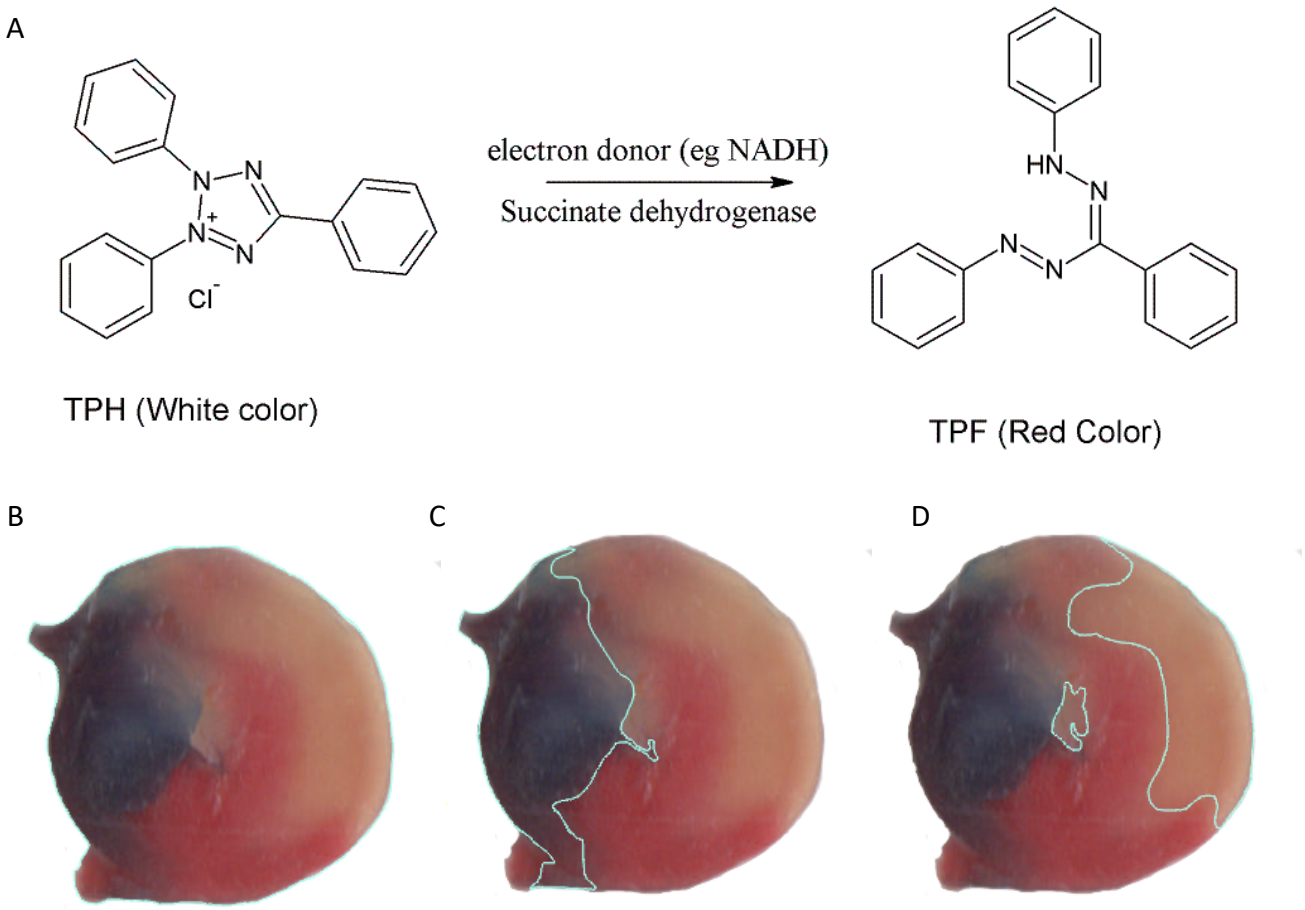


**Figure 2.2 Infarct size was determined using a double staining method.**

**A**. TTC is reduced in living tissue catalysed by a range of dehydrogenase enzymes, causing a colour change from white to brick red which enable viable heart tissue to be discriminated from infarcted tissue.

**B-D**. Planimetry was performed to determine the total heart area (B**)**, and would exclude any area inside the ventricles if these are still patent) and the non-risk tissue as all that which is perfused with Evans Blue after re-occlusion of the suture surrounding the LAD (C). The area at risk can then be calculated as the difference between these two measurements, corresponding to all tissue that was non stained blue. Infarct size is then all white tissue (D). This process is completed for all heart sections and areas are summed over the volume of the heart from the apex to the point at which occluding suture was placed.

Hearts in which the area at risk was outside of the range 30%-60% of total area were excluded from any further analysis, and the data showing the risk zone as a percentage of the total areas are always presented to demonstrate that it is invariant between experimental groups. A plot of

absolute infarct size against absolute risk zone produces a straight line as shown in Figure 2.3, indicative of the fact that the ischaemic insult is the key parameter in determining tissue death and infarct generation. However, in rodents the intercept is negative and so exceptionally low sizes of risk zones may skew the data towards reduced infarct sizes. Equally an exceptionally large area at risk may be indicative of technical problems during the surgery (such as an incomplete perfusion of the tissue by the Evans blue dye caused by an embolus) and so are likewise excluded.

Representative images have been edited to remove artefacts in the background.

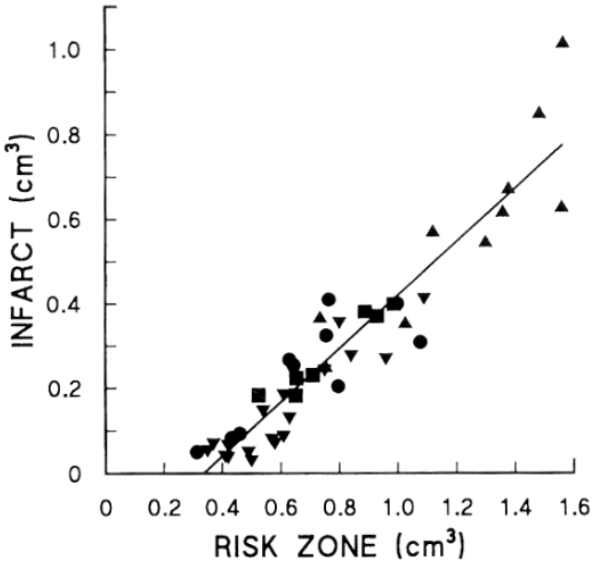


**Figure 2.3 Infarct volume has a linear relationship with risk volume, with a negative y-intercept.**

In rodents, plotting absolute infarct volume against the volume of the risk zone demonstrates a linear relationship which means that infarct size can informatively be expressed as a percentage of risk zone in order to control for small differences in the risk zone volume due to the heterogeneity of the coronary artery anatomy in the mouse (Chen et al., 2017). The negative y-intercept implies that at very small risk areas there is no tissue death and so we set a lower bound of risk area as part of our inclusion criteria to ensure that this does not confound our results.

Modified from (Ytrehus et al., 1994)

Recovery model

The recovery model of open chest acute myocardial infarction is largely similar to that described for the non-recovery model and unless otherwise noted details are the same as described in the previous section.

All necessary precautions were taken to ensure asepsis, according to the guidelines set out in Laboratory Animal Science Association guidelines (Guillen, 2012). Mice were anaesthetised an injectable combination of ketamine (100 mg/kg i.p, Velatar®, Boehringer Ingelheim) and xylazine (10 mg/kg i.p, Rompun® 2 %, Bayer), and the chest was then shaved whilst on a heated pad to help maintain body temperature. If additional anaesthesia was necessary, gaseous isoflurane (IsoFlo®, 100 % w/w Inhalation Vapour, Abbott) was administered but this was not usually required. The mouse was transferred to the surgical platform, and eye lubricant (Lacri-Lube Eye Ointment 5g, Allergan) was applied to prevent damage during the procedure. Mice were covered with a fenestrated sterile drape, allowing access to the chest area and neck area only. They were intubated in the same way as for the non-recovery model, but once the cannula was in place the incision was immediately sutured closed using absorbable suture (W9575, 6-0 Vicryl, Johnson & Johnson Medical). In order to avoid cutting muscles, a square opening to access the rib cage was created by displacing the major and minor pectoral muscles and kept open by four retractors (Single Blunt Hook Stay, 72-2595, Harvard Apparatus). A left thoracotomy was performed between the 2$^{nd}$ and 3$^{rd}$ ribs by blunt dissection to allow access to the heart. This opening was both enlarged and maintained by tension of sutures placed either side of it and secured to the surgical platform with tape. After creating a whole in the pericardium, the main branch of the left coronary artery was identified and permanently ligated with a 7-0 prolene suture and 6.5 mm needle. The thoracic incision was closed using a non-absorbable suture (W8711, 6-0 prolene, Johnson & Johnson), with care taken to re-inflate the lungs by temporarily increasing the pulmonary end expiratory pressure by pinching the outflow tube of the ventilator. The pectoral muscles were returned to their original positions, and the skin was again closed using the same absorbable vicryl suture as before. Once conscious, mice were placed in a cage containing only soft bedding and recovery gel and kept in an incubator at 37℃ for a few hours to aid in the maintenance of body temperature. Buprenorphine (0.10 mg/kg, Temgesic®) was given subcutaneously pre-op, immediately post-op and 24 hours, as well as additionally during the recovery period as required.

## Assessment of cardiac function

### Cardiac catheterisation

*Surgical procedure*

Anaesthesia was induced with 3% isoflurane in $O_2$ in a plexiglass chamber. Mice were transferred to a heated surgical platform, and sufficient isoflurane administered to maintain a surgical plane of anaesthesia as assessed by the pedal reflex. Body temperature was maintained at 37ºC using a rectal thermometer and temperature controller (TCAT-2LV, Physitemp, USA). The left ventricle was catheterized via the right carotid artery with a 1.2 French tetrapolar catheter (Transonic Scisense Inc, Canada) according to the method of (Pacher et al., 2008). In brief, a small midline incision was made in the neck in order to expose the carotid artery and isolate it from the vagus nerve. A 4-0 silk suture was tied tightly around the distal end of the artery, and two more sutures were placed loosely at the proximal end. Using a vascular clamp (0.4-1 mm) to minimize blood loss, a small incision was made in the carotid artery with microscissors and the catheter inserted and secured using the additional sutures. The catheter was the inserted along the carotid until it was located centrally within the left ventricle, as indicated by the phase signal and by the shape of the resultant pressure-magnitude loops.

The catheter senses pressure with a piezoelectric pressure sensor, for which the zero-offset is adjusted immediately prior to inserting the catheter into the mouse by placing it at the meniscus of a saline filled receptacle. The volume measurement is calculated based on the measured admittance, which changes in relation to the volume of the ventricle. Admittance is a measure of how easily a current is able to flow in an electrical circuit, and by applying an alternating current to two excitation electrodes on the section of the recording segment of the catheter that will be positioned at the top and bottom of the ventricle, an electrical field is applied. Changes in admittance are then measured by a similarly placed pair of sensing electrodes. The blood within the ventricle has purely resistive properties, but the muscle of the ventricle wall is both resistive and capacitive. This capacitive property means that a phase delay is introduced between the applied and measured signals, allowing the conductance to be calculated throughout the heartbeat despite changes in the geometry of the ventricle during systole and diastole (Figure 2.4). Volumes can then be calculated on dynamic basis using Wei's equation (Larson et al., 2013).

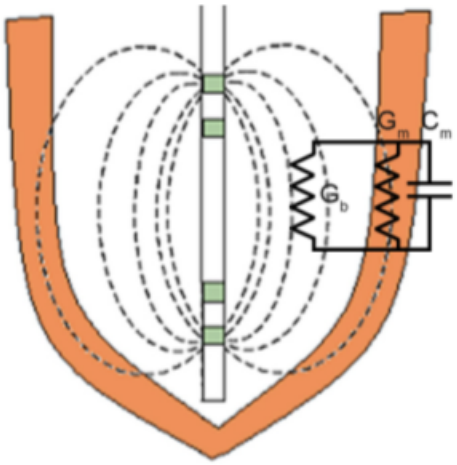


**Figure 2.4 Measurement of ventricular volume by admittance.**
The catheter is placed centrally within the ventricle, where it generates an alternating electrical field of known current with two excitation electrodes (green). The voltage measured by the sensing electrodes (blue) is affected not only by the resistance of both the blood within the ventricle ($G_b$) and muscle of the ventricle wall ($G_m$) but also by the capacitive properties of the muscle ($C_m$). From the current measured we are able to calculate the volume of the ventricular lumen on a dynamic basis (and without assuming linearity) using the method of Wei et al (Chia-Ling Wei et al., 2005).

At least 15 minutes were allowed for the measurements to stabilize. A 100 µL bolus containing either MitoPQ (100 pmol) or vehicle only (1.6 % v/v ethanol in saline) was then injected via the lateral tail vein. Data were recorded at 1000 Hz using the ADV500 PV system (Transonic Scisense Inc, Canada) and a multi-channel acquisition system (Powerlab, ADInstruments, UK) and were analysed in LabChart (ADInstruments, UK). Upon completion of the protocol all animals were killed via cervical dislocation.

*Analysis of pressure-volume data*

Three short sections of loops contained within one breathing cycle were examined at both baseline conditions and 5 minutes following injection. LabChart (AD Instruments) was used to calculate a comprehensive range of parameters of gross cardiovascular function. All of the parameters are dependent upon the cardiac pre- and after-load, which is itself greatly influenced by the depth of anaesthesia. For this reason, it was necessary to compare values before and after injection so that each animal could serve as its own control. Great care was taken to keep the anaesthesia consistent throughout the data collection period. To this end, average baseline values were calculated for each animal, and the data collected after administration of the compound are expressed relative to these. Reported errors therefore reflect the biological rather than technical variation.

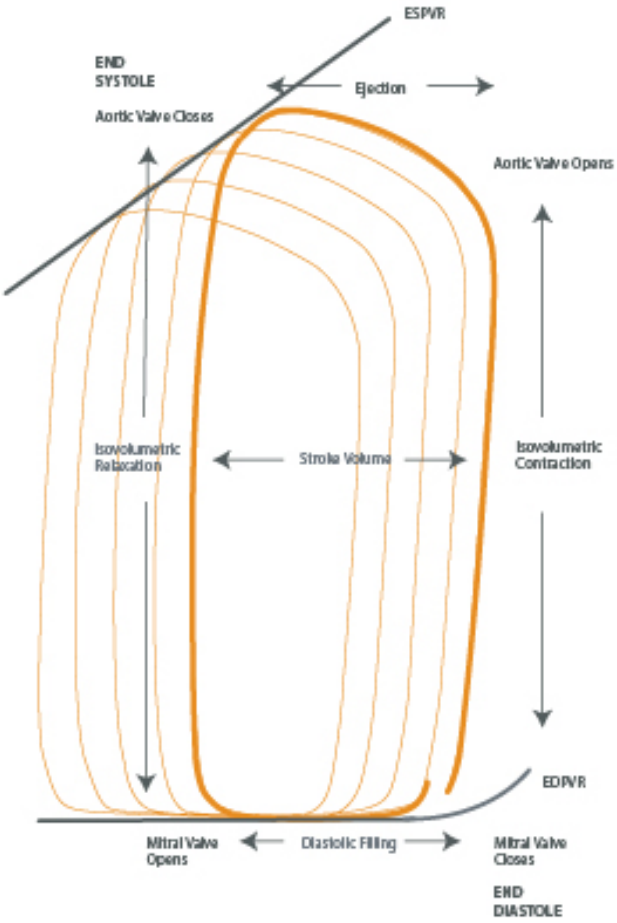


**Figure 2.5 Exemplar pressure-volume loops.**

Using a catheter inserted into the left ventricle, we are able to measure ventricular volume and pressure simultaneously and in real time. The range of parameters that we are able to derive from this are however dependent upon the preload at which blood enters the heart, due to processes that function to maintain cardiovascular function in a range of physiological

situations such as the Frank-Starling mechanism. Reproduced from (Millar.com, accessed 2019)

Further than those parameters which are measured directly, a range of cardiac indices can also be calculated, as presented in Table 2.1. A range of 19 parameters providing insight into cardiac function were chosen prior to the experiment. Due to the multiplicity of the statistical testing used it was important to control the family-wise error rate as detailed in the section on statistical analysis.

| **Parameter** | **Calculation** |
|---|---|
| Stroke volume | end diastolic volume – end systolic volume |
| Cardiac Output | stroke volume x heart rate |
| Ejection fraction | stroke volume / (stroke volume + end diastolic volume) |
| Developed pressure | end systolic pressure – end diastolic pressure |
| Stroke Work | stroke volume x developed pressure (i.e. the area enclosed within the pressure-volume loop) |
| dP/dt_max | maximum rate of change of pressure with respect to time |
| dP/dt_min | minimum rate of change of pressure with respect to time |
| dV/dt_max | maximum rate of change of volume with respect to time |
| dV/dt_max | minimum rate of change of volume with respect to time |

**Table 2.1 Calculation of cardiac parameters beyond those that were directly measured.**

Echocardiography

*Data acquisition*

Echocardiography allows for non-invasive, serial measurements of cardiac function to be made using ultrasound to determine tissue boundaries and motion in the heart. This was performed using a VisualSonics Vevo2100 (FujiFilm VisualSonics, Canada) in a manner that has been previous been validated against the gold standard technique of magnetic resonance imaging (Zhou et al., 2004). The mouse represents a significant challenge compared to performing echocardiography in humans due to its small size (~120 mg heart weight) and high hearts rates (~650 bpm in an unanaesthetised mouse), but recent advancements in the use of higher

frequency transducers (up to 70 mHz) have greatly improved both spatial and temporal resolutions (Lindsey et al., 2018).

Mice were anaesthetised with 1.5 % gaseous isoflurane (IsoFlo®, 100 % w/w Inhalation Vapour, Abbott) and attached to the imaging platform in a supine position with paws taped onto surface electrodes in order to obtain the electrocardiogram. This platform was warmed to approximately 40-42 °C in order to maintain the core temperature of the mouse at 37 °C as measured by a rectal temperature probe. The chest was first shaved and then the remaining hair was removed using hair removal cream and echo gel was applied. Images were obtained for the parasternal short axis, parasternal long axis and apical 4 chamber views.

Heart rate was maintained at 450 ± 50 bpm during these experiments. It is important that heart rate is kept constant as far as possible both within and between mice due to the dependence of systolic function on heart rate. Low heart rates (<400 bpm) normally correspond to too great a depth of anaesthesia, whereas high heart rates (>600 bpm) suggest either stress or activation of the autonomic nervous system, and thus measurements taken under these circumstances should be interpreted with caution (Pachon et al., 2015). Further, heart rates over 500 bpm are often accompanied with fusion of the E and A waves of LV filling and therefore an inability to assess diastolic dysfunction.

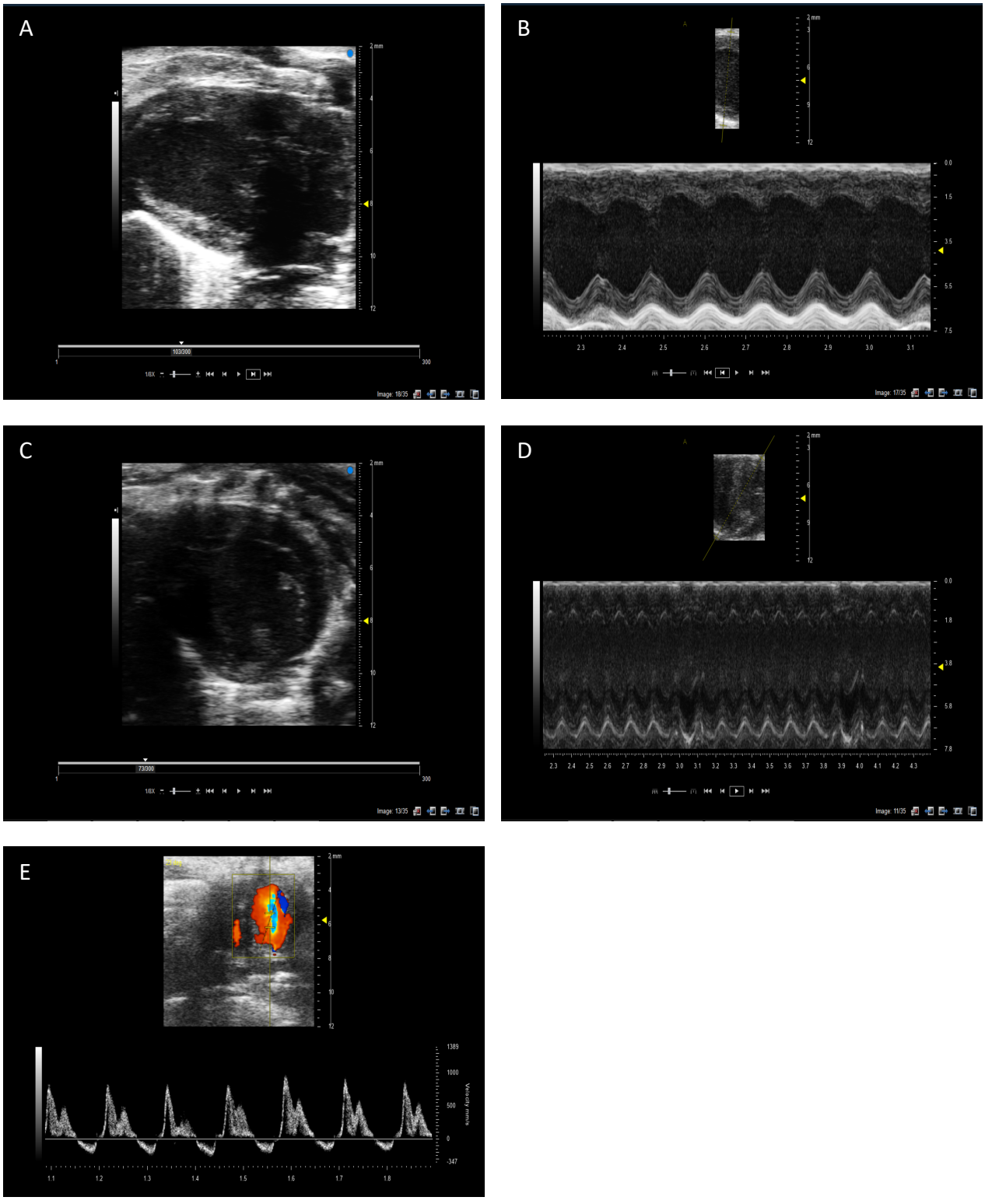


**Figure 2.6 Exemplar echocardiograms.**

Transthoracic echocardiography was used to obtain images in the parasternal long axis (**A-B**) and short axis (**C-D**) using brightness-mode (B-mode) and motion-mode (M-Mode) respectively. Flow velocity through mitral valve was measured using pulse wave doppler in the apical 4 chamber view (**E**).

*Analysis of echocardiograms*

The Vevo Strain software package (FujiFilm VisualSonics, Canada) was used to analyse echocardiograms. To measure systolic function, cardiac output, ejection fraction and fractional shortening were calculated using B- mode and M-mode images with parasternal long axis (PSLX) and short axis (PSAX) views. To measure LV mass, the endocardium and echocardiogram were traced from PSAX during diastole, and the LV length traced from PLAX in both systole and diastole. From these a volume is calculated as the difference between the volumes enclosed by the epicardial and endocardial surfaces and then converted into tissue mass by consideration of the average density of myocardial tissue.

The apical 4 chamber view was used to determine mitral valve flow velocity from which the E/A ratio can be calculated. The E or early wave represents blood flow velocity through the mitral valve during passive filling due to the relaxation of the left ventricle, which is affected by both its rate of relaxation as well as its compliance. The A or atrial wave represents blood flow through the mitral valve as the atrium contracts, and as diastolic dysfunction develops LV filling is increasingly dependent upon atrial contraction, corresponding to an increase in the E/A ratio.

**Volitional exercise of mice**

Mice were singly housed and given access to an exercise wheel to allow volitional running. Distance was measured using a wireless bicycle odometer (Wireless 546C, SunDing), measuring the number of revolutions of the wheel and reliant upon the assumption that mice were running in the middle of the track.

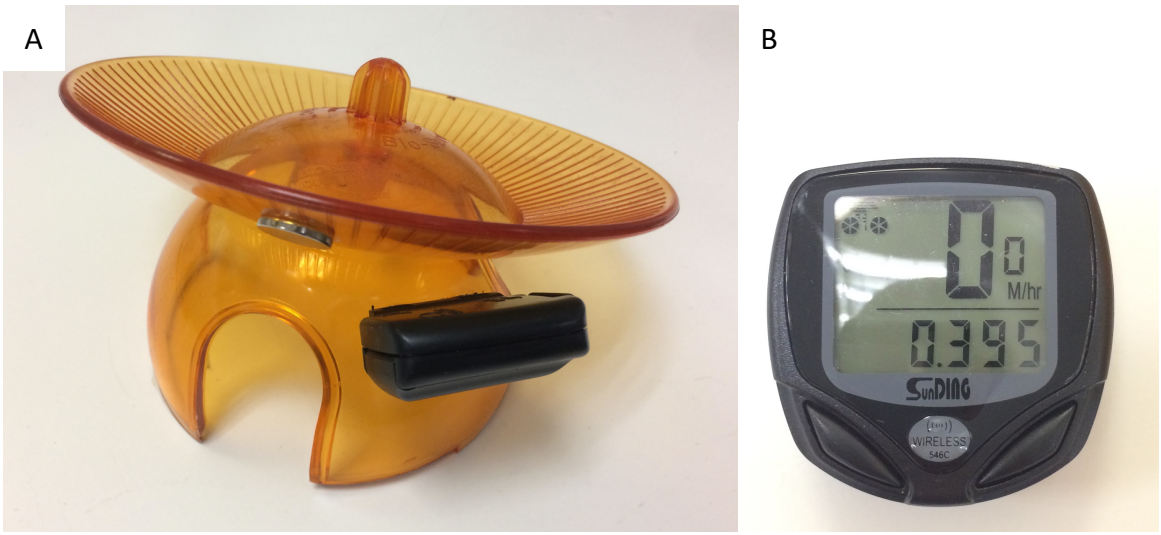


**Figure 2.7 Equipment used to allow volitional exercise and its monitoring.**
**A.** An exercise wheel was provided within the cages of certain mice to allow volitional exercise. **B.** A wireless bicycle computer was used to monitor running distance, with the magnetically operated sensor and magnet permanently fixed to the wheel. The head unit was mounted outside of the cage for ease of access.

## Cell culture

*Primary neonatal rat ventricular myocytes*

Neonatal rat ventricular myocytes (NRVMs) were isolated from 1-3 day old Wistar rats as reported previously (Kaludercic et al., 2013). Hearts were excised, cut with a razor blade into small pieces and incubated overnight at 4 °C in 2.5 % (v/v) trypsin 10X (Thermo Fisher Scientific) in HBSS (Sigma-Aldrich). The following day tissues were incubated with 0.75 mg/ml collagenase type II (Thermo Fisher Scientific) in HBSS for 10 min and cells separated by mechanical dissociation in a pipette. They were then centrifuged for 7 min at 300 *g*, resuspended in MEM (Invitrogen) and pre-plated for 2 hours to allow adherence of cardiac fibroblasts to the plastic surface. The non-adherent myocytes were plated in porcine gelatin coated plates (0.1%; Sigma-Aldrich) at variable density (at least $1x10^5$ cells/ml) in MEM supplemented with 10% FBS (Thermo Fisher Scientific), 1% penicillin/streptomycin (Thermo Fisher Scientific), 1% non-essential amino acids (Thermo Fisher Scientific) and 1 mM 5-Bromo-2-Deoxyuridine (Sigma-Aldrich) in order to inhibit proliferation of any non-myocytes present in the culture. 24 hours after plating the medium was changed to MEM supplemented

with 1% FBS, 1% penicillin/streptomycin and 1% non-essential amino acids. They were maintained in a humidified atmosphere (5% CO2/95% air) at 37 °C.

*C2C12*

C2C12 mouse myoblast cells were cultured in a humidified atmosphere (5% CO2/95% air) at 37 °C in standard DMEM/GlutaMAX medium: glucose 4.5 g/L; sodium pyruvate 100 mg/ml; supplemented with 10% (v/v) fetal bovine serum (FBS), 100 units/ml penicillin and 100 µg/ml streptomycin.

These experiments were performed by A. Hall (MRC Mitochondrial Biology Unit, University of Cambridge, UK).

Transfection

*C2C12*

Prior to experimentation, C2C12 cells were seeded at a density of $2x10^5$ cells on pre-coated glass coverslips in 6 well plates (Nunclon Delta Surface, Thermo Fisher Scientific). 24 hours after plating, cells were transfected using Lipofectamine 2000 according to manufacturer's instructions and 1 µg of a plasmid encoding either the cytoplasmic targeted roGFP2 ORP1 (addgene ID 64993) or the mitochondrial targeted roGFP2 ORP1 (addgene ID 64992) (Gutscher et al., 2009).

*NRVMs*

NRVMs at a density of $3x10^5$ cells/well in six-well plates were transfected with Lipofectamine 3000 reagent. For each transfection, 2.5 µg of MitoHyPer (Evrogen) was added to 125 µl of Opti-MEM medium (Thermo Fisher Scientific) and 5 µl of Lipofectamine 3000 (Life Technologies). The following day cells were washed with PBS and new MEM was added. Experiments were performed after a further 24 hours.

**Assessment of cell death**

Lactate dehydrogenase (LDH) enzyme activity was measured spectrophotometrically by the absorbance of nicotinamide adenine dinucleotide (Roche) at 340 nm, which is indicative of the reduction of lactate to pyruvate that is catalysed by this enzyme.

For experiments carried out in normoxia, NRVMs were seeded in 24 well plates at density of $10^5$ cells/well and cultured in MEM supplemented with 1% FBS, 1% penicillin/streptomycin and 1% non-essential amino acids.

For anoxia/reoxygenation experiments, NRVMs were seeded in 24 well plates at density of $10^5$ cells/well and incubated in 118 mM NaCl, 5 mM KCl, 1.2 mM $KH_2PO_4$, 1.2 mM $MgSO_4$, 2 mM $CaCl_2$, 25 mM MOPS (Bond et al., 1991). Anoxia was induced adding 20 mM 2-deoxy-D-glucose in order to inhibit glycolysis, reducing the pH to 6.4 and incubating in a BD GasPak™ EZ Anaerobe Gas-generating Pouch System with an indicator (BD Biosciences) at 37°C for 12 h. To induce reoxygenation, plates were removed from the GasPak™ pouch, 2-deoxy-D-glucose was replaced with 10 mM D-glucose, and the pH was restored at 7.4. The plates were then incubated for 1 hour in a humidified incubator at 37°C. Media aliquots were collected after 24 hours of normoxia, 12 hours of anoxia and 1 hour of reoxygenation.

**Measurement of mitochondrial membrane potential**

To measure mitochondrial membrane potential cells were incubated for 30 min at 37 °C with 25 nM tetramethylrhodamine (TMRM; Thermo Fisher Scientific) (Rowe and Boletta, 2013). This is a lipophilic cation and so accumulates within mitochondria according to the membrane potential in the same manner as described in chapter 1 for other mitochondria targeted compounds. This was conducted in presence of 1.6 μM cyclosporin H in order to inhibit multidrug resistance pumps for which TMRM is a known substrate and which thus would confound its loading into cells (Nicolli et al., 1996). It is worth noting the cyclosporin H has no effect upon the formation of the mitochondrial permeability transition pore. TMRM fluorescence intensity was then monitored with excitation at 535 nm and emission at 600 nm following addition of 4 μM oligomycin (Sigma-Aldrich) in order to inhibit ATP synthase. At the end of the protocol of 4 μM carbonyl cyanide-p-trifluoromethoxyphenylhydrazone (FCCP; Sigma-Aldrich) was added as a positive control to dissipate mitochondrial membrane potential.

Images were acquired using an inverted fluorescence microscope (Leica DMI6000B; DFC365FX camera) with PL APO 40x/1.25 oil objective. Fluorescence intensity was quantified using the Fiji distribution of ImageJ (Schindelin et al., 2012), with the background subtracted from the regions of interest analysed.

**Measurement of cytosolic calcium**

To measure cytosolic calcium dynamics, the cytosolic indicator Fluo-4 acetoxymethyl ester was used. The esterification of the Fluo-4 fluorophore enables its passive uptake across the cell membrane into the cytoplasm, where it undergoes hydrolysis catalysed by intracellular esterases to prevent its release from the cell.

Cells were incubated for 20 min at 37 °C with MEM supplemented with 5 μM Fluo-4 acetoxymethyl ester (Thermo Fisher Scientific), 0.01% w/v pluronic F-127 (to aid solvation of Fluo-4 acetoxymethyl in cell media; Sigma-Aldrich) and 250 μM sulfinpyrazone (Sigma-Aldrich). Sulfinapyrazone inhibits organic anion transport and so prevents leakage of the cleaved Fluo-4 dye from the cell (Di Virgilio et al., 1990). This was followed by a washout period of 20 min before imaging.

Excitation was at 490 nm and emission monitored at 520 nm. Images were acquired as described above. 10 mM caffeine was used to induce release of stored calcium from the sarcoplasmic reticulum into the cytosol. The peak analyzer tool of Origin Pro 9.1 (Origin Lab Corporation) was used to quantify the time-series data.

**Measurement of mitochondrial permeability transition pore opening**

To assay MPTP opening, cells were incubated for 15 min at 37 °C with 1 μM calcein acetoxymethyl (AM) ester (Thermo Fisher Scientific). This is taken up throughout the cell and its intracellular compartments but is then entrapped within the cell in the same manner as Fluo-4 due to hydrolysis of the acetoxylmethyl ester group. This is done in the presence of 1 mM cobalt chloride which is taken up into the cell but not the mitochondria, quenching any fluorescence signal outside the mitochondria. This incubation was followed by a washout period of 20 min in order to remove any unloaded dye. As the MPTP opens two events happen: calcein is lost from the mitochondria through the MPTP into the cytosol where its fluorescence

is quenched by colbalt, as well as entry of cobalt into the mitochondria from the cytoplasm which quenches the fluorescence from calcein remaining inside the mitochondria. MPTP opening is thus represented by a decrease in the calcein fluorescence signal (Petronilli et al., 1999). The calcium ionophore calcimycin is used as a positive control to induce MPTP opening and CsA is used as a negative control to inhibit MPTP opening.

Excitation was at 485 nm and emission monitored at 530 nm. Images were acquired as described above.

**Measurement of compartmentalised ROS production with roGFP**

Experiments were performed 48 hours after transfection. Images were captured every 30 seconds for 1 hour using a Zeiss LSM microscope. Compounds were added immediately prior imaging and remained present throughout. The roGFP was alternatingly excited at 405 nm and 488 nm and emission collected at 500-550 nm for both wavelengths. Images were analysed in ImageJ, with the channels split for the two excitation wavelengths. Regions of interest were manually drawn around cells, and fluorescence intensity measured across the full hour. The ratio of 405/488 fluorescence emitted was expressed relative to initial baseline values.

**Measurement of superoxide production by coelenterazine fluorescence**

Superoxide production was measured in bovine heart mitochondrial membranes was detected by measuring SOD-sensitive coelenterazine ( 2-(*p*-hydroxybenzyl)-6-(*p*-hydroxyphenyl)-8-benzyl-imidazo[1,2-a]pyrazin-3-(*7H*)-one) chemiluminescence (Lucas and Solano, 1992). This reaction is specific for superoxide (Rees et al., 1998). Bovine heart mitochondrial membranes are used rather than intact mitochondria so that uptake of compounds across a membrane is not required, but rather the reaction takes place in the bulk solution. Note also that since the matrix fraction which contains MnSOD has been discarded the coelenterazine does not have to compete which the more rapid kinetics of the dismutase reaction.

Bovine heart mitochondrial membranes (70 μg protein) were incubated in KCl buffer (120 mM KCl, 10 mM Hepes, 1 mM EGTA, pH 7.4) with 4 μg/ml rotenone, 2 μM coelenterazine (Calbiochem), 1 mM NADH and 1 μM MitoPQ, MitoPQ control compound 1 or MitoPQ control compound 2 in a final volume of 1 ml. Chemiluminescence was measured in a

luminometer (Berthold AutoLumatPlus LB 953) with 5 s cumulative readings taken every 30 s over 5 min incubations at 30 °C.

**Uptake of mitochondria-targeted compounds by HPLC**

Rat liver mitochondria (1 mg protein/mL) isolated as described previously were incubated at 30 °C in 4 mL KCl buffer (120 mM KCl, 10 mM Hepes, 1 mM EGTA) supplemented with 10 mM succinate, 4 μg/ml rotenone and the indicated compound (MitoPQ control compound 1, MitPQ control compound 2; 5 μM), either with or without *p*-trifluoromethoxyphenylhydrazone (FCCP; 500 nM). After 5 min the mitochondria were pelleted by centrifugation at 10000 *g* for 5 min. Mitochondrial pellets were extracted by vortexing in 250 μL 100% acetonitrile (ACN) with 0.1% trifluoracetic acid (TFA) and centrifuged again at 10000 *g* for 5 min. The supernatant was collected and was diluted with 750 μL 1% (v/v) TFA in water to give an total volume of approximately 1 mL.

The samples were then filtered through a 0.22 μm syringe-driven polyvinylidene difluoride filter (Millex, Millipore) and constituents separated by reverse phase-high performance liquid chromatography performed using a Gilson 321 pump fitted with a C18 column (Jupiter 300 A, Phenomenex) and a Widepore C18 guard column (Phenomenex). HPLC buffers A (0.1% TFA) and B (90% ACN and 0.1% TFA) were used to generate a gradient: 0–2 min, 5% B; 2–17 min, 5-100% B; 17–19 min, 100% B; 19–22 min 100–5% B with a flow rate of 1 mL/min. Peaks were detected by absorbance at 220 nm (UV/Vis 151; Gilson) and Chart 5 software (AdInstruments) was used to calculate peak areas.

**Cyclic voltametry**

In order to determine the ease with which MitoPQ and MitoPQ control compound 2 may be reduced, cyclic voltammetry was used. The reference electrode was Ag/AgCl, while the working electrode was a glassy carbon disk and the counter electrode was platinum wire. These experiments were conducted in pH 7.4 phosphate buffer, with the electrode potential ramped linearly between 0 V and -1.4 V and back again at a scan rate of 0.05 V/s.

**Glutathione measurement**

To precipitate proteins including glutathione and glutathione disulphide, samples containing 1 mg protein for isolated mitochondria or >1 mg protein for tissue homogenates were treated with 100 µL of 5 % (w/v) sulfosalicyclic acid and vortexed for 30 s. For tissue samples the sulfosalicyclic acid was supplemented with 0.1 % (v/v) Triton X100 detergent in order to permeabilise cells. They were then centrifuged for 10 min at 16000 *g* and the supernatant collected.

The total glutathione pool (comprising of both free glutathione and glutathione disulphide) in tissue was measured using a GSH recycling assay was used as has been previously described (Akerboom and Sies, 1981; Scarlett et al., 1996). This assay involves oxidation of GSH by the sulfhydryl reagent 2-nitrobenzoic acid (DTNB) to form the yellow derivative 5′-thio-2-nitrobenzoic acid (TNB) and oxidized glutathione–TNB adduct (GS–TNB). The rate of formation of TNB is therefore proportional to the concentration of GSH in the sample which can be measured by the change in absorbance at 412 nm. The addition of glutathione reductase (GR) in the presence of NADPH allows TNB to be regenerated from GS-TNB. However because GR also reduces GSSG into 2GSH, the amount of glutathione measured represents the total sum of reduced and oxidized glutathione in the sample (i.e. GSH + 2 x GSSG).

Solutions were prepared as follows:

0.1 M potassium phosphate buffer with 5 mM disodium EDTA salt, pH 7.5 (KPE)
40 µl of GR (250 units $ml^{-1}$) in 3 ml KPE
2 mg of β-NADPH in 3 ml KPE
2 mg of DTNB in 3 ml KPE

20 µL KPE, 20 µL sample, 60 µL DTNB and 60 µL GR were added to a well. After 30 seconds to allow conversion of GSSG to GSH, 60 uL of β-NADH was added and absorbance was read at 412 nm every 30 seconds for a total of 2 minutes. Data were normalised to total protein content as determined by a BCA assay.

**Measurement of TrxR activity**

Measurement of TrxR activity was based upon the assay reported by (Cunniff et al., 2013), measuring the decreased in absorbance as NADPH is consumed by the TrxR catalysed reduction of thioredoxin. Mitochondrial suspensions (1 mg protein) or >1 mg protein of tissue

homogenate was centrifuged at 16000 *g* for 10 min and the pellet resuspended in 100 µL NP-40 lysis buffer (150 mM NaCl, 1 % (v/v) NP-40, 50 mM Tris-Cl, pH 8.0) and left on ice for 10 min.

Samples were then centrifuged at 16000 *g* for 10 min again and the supernatant retained. Protein concentration was calculated by BCA assay and 25 µg protein used per replicate. In a 96-well plate, purified TrxR1 (Sigma; 400 µg/ml in PBS) was combined with 25 µg protein sample to a final volume of 60 µL. 40 µL of 1 mM NADPH and 2 mM selenocysteine in NP40-lysis buffer was added, and NADPH consumption measured at 340 nm (6.22 $mM^{-1}$ $cm^{-1}$) for 30 min using a SpectraMax plate reader (Molecular Devices). The background rate was determined from wells containing only NADPH and sample and was subtracted from the total activity measured.

**Western blotting**

After extraction, samples were resuspended in 4x loading buffer (200 mM Tris-Cl, pH 6.8, 8 % (w/v) SDS, 0.4 % (w/v) bromophenol blue, 40 % (v/v) glycerol), with 400 mM dithiothreitol as a reductant. 10-25 µg protein was loaded onto 12 % Tris-Glycine SDS-PAGE gels (BioRad) and run at 120 V for 45 min. Protein was transferred to polyvinylidene flouride membranes (BioRad Trans-Blot® Turbo™ Mini) by wet transfer in the presence of 25 mM Tris, 192 mM glycine, 20 % (v/v) methanol, pH 8.4) before blocking for 1 h at RT with Odyssey blocking buffer (LICOR). Primary antibody incubation was completed in 4 % (v/v) Odyssey buffer in PBS + 0.1 % (v/v) Tween-20 (PBST) for 1 h at RT. Membranes were then washed 3 x 15 min in PBST, followed by secondary incubation in 4 % Odyssey buffer in PBS for 1 h at RT, washed 2 x 15 min in PBST and 1 x 15 min in PBS. Membranes were visualised using a LICOR Odyssey CLx system and analysed using ImageStudio Lite.

Antibodies

| | **Manafacturer** | **Antibody ID** |
|---|---|---|
| glutathione synthetase antibody | Abcam | AB_2049703 |
| gamma-glutamylcysteine synthetase antibody | ThermoFisher | AB_2608691 |
| IRDye 800CW Donkey anti-Rabbit IgG | LICOR | AB_2715510 |

**Table 2.2 Antibodies used to determine protein expression levels in tissue samples isolated after administration of MitoCDNB *in vivo*.**

**Mass spectrometry of mitochondria-targeted compounds**

*MitoNeoD – tissue extraction*

For the determination of concentrations of MitoNeo compounds, 50 ± 5 mg tissue (wet weight) was added to 248 µL KCl buffer and 2 µL of 10 mM chloranil solution in acetone (Sigma-Aldrich). The deuterated internal standards (5 µM$d_{15}$-MitoNeoOH and 10 µM $d_{15}$-MitoNeo) were added to give a final concentration of 10 µM. Samples were homogenised in a bullet blender (Storm 24 (BBY24M), Next Advance) for 3 min at speed 10, using a volume of beads approximately equal to that of the tissue sample. For heart samples 0.9-2.0 mm diameter stainless steel beads were added, whilst for all other tissues 0.5 mm diameter zirconium oxide beads were used. Homogenates were then incubated at 37 °C for 30 min rotating at 1000 rpm. 1 mL butan-2-ol/methanol (3:1) was added and samples sonicated in a water bath (Branson 3800, Bransonic Ultrasonic Bath, CPX from Emerson Industrial Automation) for 1 hour at RT. They were centrifuged for 10 min at 16,000 *g* to aid phase separation and the upper phase transferred to a fresh 2 mL Eppendorf for drying under vacuum at 40°C (Genevac miVac Quattro concentrator). 400 µL of 40 % HPLC grade methanol/0.1 % formic acid/60 % HPLC grade water was added, and the samples vortexed for 15 min to resuspend them. A further centrifugation at 16,000 *g* for 10 min followed by vacuum filtration of the supernatant was performed to ensure sample purity. Finally 300 µL was transferred into mass spectrometry vials and stored at 4 °C until further analysis.

*MitoNeoD – mass spectrometry*

Samples and the relevant standards were placed in a refrigerated holder at 4 °C for introduction by the autosampler. LC was performed using an I-class Acquity LC with an Acquity UPLC BEH C18 1.7 µm, 1 × 50 mm column (Waters). This was run at a temperature of 30 °C and flow rate of 200 µL/min with 2 µL of sample volume introduced via a flow-through needle. An in-line divert valve was used to reroute eluent away from the mass spectrometer from 0-3 min and 7-10 min of the protocol. The mobile phase consisted of 5 % acetonitrile/0.1 % formic acid in water (buffer A) and 90 % acetonitrile/0.1 % formic acid (buffer B) which was delivered as a series of linear gradients: 0-0.3 min, 5 % B; 0.3-8 min, 5-100 % B; 8-9 min, 100% B; 9-9.1 min, 100-5 % B; 9.1-10 min, 5 % B.

MS was performed using a Xevo TQ-S triple quadrupole mass spectrometer (Waters) in positive ion mode with multiple reaction monitoring. Source spray voltage was 2.7 kV and the ion source temperature was 150 °C, while cone voltage and collision energy were optimised for each compound. The curtain gas as nitrogen and the collision gas argon. Peak area was determined using MassLynx 4.1 software (Waters).

Standard curves were prepared using the appropriate biological tissue spiked with known concentrations of $d_{15}$-MitoNeo and $d_{15}$-MitoNeoOH internal standards processed in parallel with experimental samples. These were highly linear over the range 1-1,000 pmol with $R^2$ routinely > 0.99 (Figure 2.8).

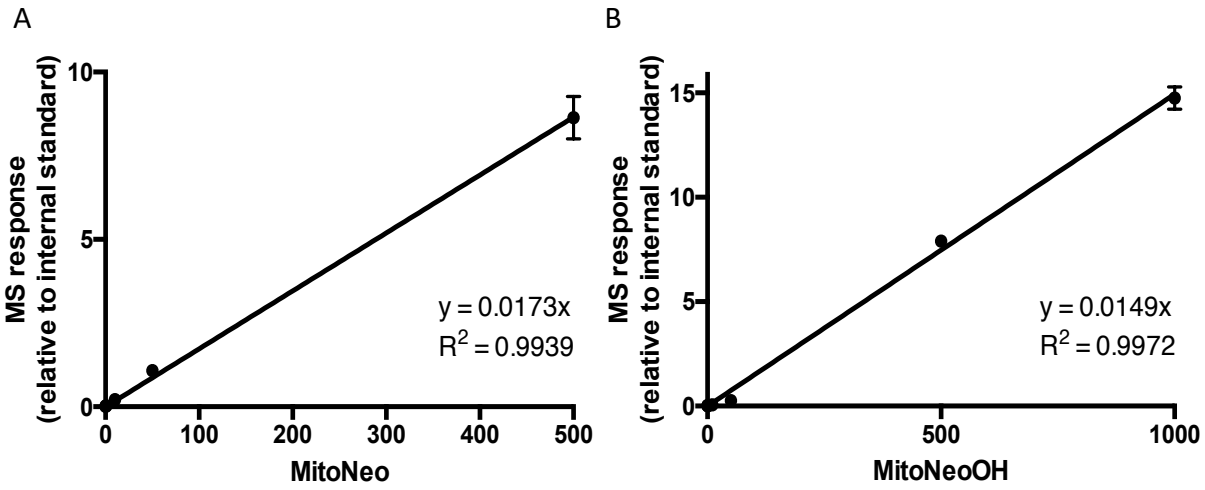


**Figure 2.8 Linearity of MS response over a wide range of concentrations of MitoNeo and MitoNeoOH**.

Standard curves were obtained by spiking pooled tissue samples with known concentrations of the deuterated internal standards $d_{15}$-MitoNeo and $d_{15}$-MitoNeoOH. These were highly linear between 1-500 pmol for MitoNeo ($R^2$ = 0.9939, **A**) and between 1-1000 pmol for MitoNeoOH ($R^2$ = 0.9972, **B**).

*MitoCDNB – tissue extraction*

Plasma was extracted from blood samples by centrifugation at 16,000 *g* for 5 min in 10 % (v/v) 5 mM EDTA solution. Tissue homogenates were prepared as for MitoNeo and these, urine or blood were mixed 1:1 with 95 % acetonitrile + 0.1 % formic acid. Samples were kept on ice

for 1 hour, followed by 3 centrifugation steps at 16,000 *g* for 10 min, with the supernatants collected and filtered through a 0.45 μm polyethylene filter plate (Porvair Sciences). They were then vacuum dried overnight. The resultant solid was resuspended in 200 μL of 20 % acetonitrile/0.1 % formic/80 % HPLC grade water, and vortexed for 15 min to ensure resuspension. A further centrifugation at 16,000 *g* for 10 min followed by vacuum filtration of the supernatant was performed to ensure sample purity.

*MitoCDNB – mass spectrometry*

LC-MS/MS analysis was carried out as for MitoNeo unless otherwise noted. Parameters were as follows: capillary voltage - 3.2 kV; cone voltage -79 V; ion source temperature – 150 °C; collision energy - 45 V. The LC mobile phase was delivered as the following series of linear gradients: 0–0.3 min, 5 % B; 0.3–3 min, 5–100 % B; 4–4.1 min, 100–5 % B; 4.1–4.6 min, 5 % B. The eluent was diverted at 0–1 and 4-4.6 min acquisition time. Multiple reaction monitoring in positive ion mode was used for compound detection. Transitions used were: MitoCDNB, 534>183; MitoGSDNB, 805>183, $d_{15}$-MitoB, 412>191, MitoCysDNB, 619>183. Standard curves were prepared using known amounts of MitoCDNB, MitoGSDNB or MitoCysDNB, spiked with internal standard of 10 pmol $d_{15}$-MitoB as a deuterated MitoCDNB was not available.

**Mass spectrometry of endogenous metabolites**

Extraction protocol

Tissue samples were snap frozen in liquid nitrogen immediately after excision and stored at -80 °C until further analysis.

To extract aqueous metabolites, 20-30 mg of tissue was placed in an eppendorf tube on dry ice, and an extraction solution (50 % Methanol, 30 % Acetonitrile, 20 % ultrapure water and *d*8-valine to give a final concentration 5μM) was added at a volume of 25 μL/mg tissue. This was then homogenised Bullet Blender (Next Advance) using a combination of Zirconium Oxide (ZrOBO5) and Stainless Steel (SSB148) beads to result in complete disruption of sample. Homogenates were then vortexed for 2 min at 4 °C. Samples were centrifuged at 16,000 *g* for

10 minutes at 4 °C, and the supernatant transferred to a separate tube. A further centrifugation step was performed to ensure all insoluble debris had been removed. The supernatant was then transferred to autosampler vials (1.5 ml silanised, Chromacol) and stored at -80 °C until analysis by mass spectrometry.

Targeted measurement of malonate and succinate

LC-MS/MS was used to measure malonate and succinate in a targeted manner using an LCMS-8060 mass spectrometer (Shimadzu, UK) with a Nexera UHPLC system (Shimadzu, UK). Samples were stored in a refrigerated autosampler at 4 °C until injection of 5 µl via a 15 µl flowthrough needle. Separation was achieved using a SeQuant ZIC-HILIC column (3.5 µm, 100 Å, 150 x 2.1 mm, 30 °C column temperature; Merck Millipore, UK) with a ZIC-HILIC guard column (200 Å, 1 x 5mm). Mobile phases were: A = 100 mM ammonium acetate (pH unaltered) and B = 100 % acetonitrile. The flow rate was 200 µl/min delivered as a series of linear gradients as follows. 0-0.1 min, 80 % B; 0.1-4 min, 20 % B; 10 min, 20 % B, 11 min, 80 % B; 15 min, 80 % B. The mass spectrometer was operated in negative ion mode with multiple reaction monitoring and spectra were acquired with Labsolutions software (Shimadzu, UK). Absolute quantitation was performed by calculation from relevant standard curves in MS extraction buffer (50 % (v/v) methanol, 30 % (v/v) acetonitrile, 20 % (v/v) MS-grade water) compared to 100 pmol of relevant standard. For endogenous malonate and succinate this was $^{13}C_3$-malonate and $^{13}C_4$-succinate respectively. For experiments involving the administration of $^{13}C$ labelled compounds, *d*8-valine was used.

## Measurement of succinate by magnetic resonance spectroscopy

Magnetic resonance spectroscopy refers to the application of nuclear magnetic resonance techniques to biological tissues in order to determine the molecules contained within them. In brief, certain atomic nuclei such as $^{1}H$ and $^{13}C$ possess spin such as that when placed in an external magnetic field the magnetic moments of the protons can align with the field in either a parallel or antiparallel fashion. Most will be aligned in a parallel fashion as this is the lower energy state. The application of a radio frequency pulse can excite protons into the higher energy antiparallel alignment, and then their relaxation back to parallel alignment can be measured due to their magnetic precession through the process of spin-lattice relaxation. The frequency of this signal depends upon the local magnetic properties of each proton, determined

by, for example, the molecules in which they are contained. This magnetic flux can be measured as a voltage in electromagnetic coils, and if required 2D fourier transforms used to reconstitute spatial information.

During scansion, body temperature was measured with a rectal thermometer, and maintained as best as possible with a flow of warm air. MR conditional neonatal electrodes (3M Red Dot) were used to measure ECG and a pressure sensor was placed underneath the animal to determine the rate of respiration. These two signals were combined in order to gate the magnetic resonance sequence to identical points of the cardiac and breathing cycle so as to ensure that the heart was in the same position in 3D space at all points of the acquisition protocol. A birdcage coil of 12 cm was used for signal excitation and a 2 cm surface coil for signal reception.

A purpose-built ventilator (MRI-1, CWE Inc) was used in order to avoid the compliance problems that result from the long lengths of tubing required if a traditional ventilator was used due to need to locate it outside of the magnet room. This ventilator contains pneumatically actuated valves to switch between inspiration and exhalation phases of the breathing cycle which are made of non-magnetic materials and thus can be located within the bore of the magnet.

Cine imaging

For mice, a spoiled gradient echo sequence was used to acquire a single slice measuring 36 mm x 36 mm in area and 2 mm thick axially through the mouse and the wall of the left ventricle. The images were acquired with 128 x 64 points, 300ms repetition time and 2.29ms echo time, a 20 degree flip angle and 20 frames capturing 1 cardiac cycle.

For rats, a spoiled gradient echo sequence was used to acquire a single slice axially through the heart with 60mm x 60mm in area and 2mm thick. Images were acquired with 128 x 128 points, a reptition time of 120 ms and 2.13 ms echo time. 20 CINE images were acquired over one cardiac cycle. Images were acquired with a 20mm send receive coil, but otherwise details were as for mice.

$^{1}$H NMR spectroscopy

For mice, a point resolved spectroscopy sequence (PRESS) was acquired with an echo time of 18ms and a repetition time of 3s. The voxel measured 1 mm x 2 mm x 2mm with a spectral width of 4006 Hz and 512 averages. Water suppression was with WET (Ogg et al., 1994) using a 200 Hz bandwidth.

For rats, a stimulated echo acquisition mode (STEAM) sequence was used. The voxel measured 6.2 mm x 6 mm x 3.2 mm localised to the left ventricular wall of the heart. The STEAM sequence had 4.95 ms echo time, 10 ms mixing time and 2.2s repetition time with 2000 points and 4006 Hz sweep width. Water suppression was achieved with a WET sequence at 250 Hz bandwidth.

## Mitochondrial function

### Rat heart mitochondria isolation

Mitochondria were isolated from Wistar rat hearts using the method of differential centrifugation described previously (Chappell and Hansford, 1972). Rats were killed by cervical dislocation, and the hearts excised and blotted to remove excess blood and quickly transferred into ice-cold STE-BSA buffer (250 mM sucrose, 5 mM Tris, 1 mM EGTA, 0.01% w/v fatty acid free BSA, pH 7.4). All tools and equipment were rinsed in MilliQ water followed by STE-BSA buffer in order to remove any contaminants such as detergents that might cause lysis of the mitochondria, and all steps were performed on ice. The tissue was rinsed in STE-BSA buffer and transferred to a petri dish where visible non-cardiac tissue was dissected and removed. The heart was thoroughly chopped using a razor blade and any further fat or blood clots removed. This tissue was then transferred to a beaker and rinsed several times with STE-BSA buffer, before complete homogenisation in an Ultra Turrax (IKA) homogeniser at setting 3 for 5 seconds. The homogenate was placed in a 50 ml Dounce homogeniser, and a further homogenisation performed with 4-5 strokes of a ‘tight’ plunger. The homogenate was centrifuged for 5 min at 4 °C and 700 *g* in order to remove large cellular debris. The supernatant was decanted through pre-soaked muslin into a second centrifuge tube, and a second centrifugation for 10 min at 4 °C at 10,000 *g* in order to obtain a pellet containing only mitochondria. This was then re-suspended in approximately 300 μL of STE-BSA buffer. The protein concentration of this sample was then measured using the bicinchonic acid (BCA) assay

(Smith et al., 1985) in order that the quantity of mitochondria could be normalised between different mitochondrial isolates in later experiments. Mitochondria were used as soon as possible after isolation.

High resolution respirometry

High resolution respirometry was performed using a two-chamber Oxygraph-2k (Oroboros Instruments, Austria). 2 ml of KCl respiration buffer (115 mM KCl, 5 mM $KH_2PO_4$, 1 mM EGTA, 10 mM HEPES) was added to the stirred reaction chamber, along with 10 μM amplex red (Thermo Fisher Scientific), 5 U/ml horseradish peroxidase (HRP), 50 U/ml SOD and 150 μg/ml fatty acid-free BSA and 500 μg of isolated rat heart mitochondria.

Complex II RET-dependent oxygen consumption and ROS generation was measured in order to prevent reliance upon complex I linked respiratory substrates. Respiration was initiated through the addition of 10 mM succinate while ROS generation was determined by monitoring the HRP dependent oxidation of amplex red to the fluorescent resofurin (Zhou et al., 1997). Mitochondrial oxygen consumption and ROS production were recorded using the Oroboros DatLab software, and ROS generation calculated to $H_2O_2$ equivalents by titration with $H_2O_2$ at the end of a run.

## Assessment of complex I function

Complex I activity assay

At the appropriate time point, tissue samples were quickly dissected from the hearts of mice undergoing IRI and immediately clamp frozen in liquid nitrogen using custom made Wollenberger tongs with a serrated profile.

Ice-cold 25 mM KPi buffer at pH 7.8 was added to the tissue sample in CK14 lysis tubes and they were homogenised for 15 seconds at an intensity of 6500 using a Bertin Instruments Precellys24 tissue-homogenizer. Samples were further diluted in KPi buffer to achieve a final concentration of 22.4 μg/ml protein. Also present were 100 μM decylubiquinone, 300 nM antimycin, 200 μM potassium cyanide and 0.025% DDM. They were maintained on ice for approximately 5 minutes. 200 μM nicotinamide adenine dinucleotide was added to initiate the assay, and the absorbance was monitored at 340 nm ($A_{340}$) and 380 nm ($A_{380}$) for 30 min at 30

˚C using a double wavelength UV-vis microplate reader (Molecular Devices SpectraMax Plus 384). The maximum linear rate ($A_{340}$-$A_{380}$) $s^{-1}$ was determined. The background rate after addition of 500 nM rotenone in an independent experiment was subtracted to give the values reported here.

Differential labelling of complex I active and deactive isoforms

In order to determine the relative proportion of the active and deactive isoforms of complex I a differential labelling strategy of cysteine residues by the alkylating agent iodoacetamide was used. Due to conformational changes between the isoforms the ND3 peptide is exposed differently and thus its labelling may be used to measure their relative proportions using light and heavy isotopes of iodoacetamide.

Frozen heart tissue (~5 mg) was homogenised for 15 seconds at intensity 6500 in 400µl of ice cold 50 mM KPi buffer (pH 7.5 - 7.8 at 37˚C) containing 20 mM of light iodoacetamide and 10 mM of tris(2-carboxyethyl)phosphine (TCEP), using a Precellys24 tissue homogeniser (Bertin Instruments) and in CK14 lysis tubes. Exposed cysteine residues were labelled for 5 min on ice before the reaction was quenched by adding 1 ml of KPi buffer and pelleting the membranous fraction at 17.000 *g* for 5 min at 4 ˚C. The pellets were washed with 1 ml of KPi buffer and a centrifuged again as before. All residual thiols were then labelled by resuspending the pellets in 45 µl of lysis buffer (4% SDS, 50 mM NaPi, pH 7.8) containing 20 mM of heavy ($^{13}C_2$, 2-$d_2$) iodoacetamide and 10 mM TCEP and incubating for 30 min at 37˚C.

5x Laemmli loading dye was added and samples were subjected to SDS-PAGE, followed by fixation in 50 % methanol and 10 % acetic acid. Coomassie staining was performed to visualise peptides. Gel sections between the 10 and 20 kDa marker bands (BioRad, Precision Plus Protein™ Dual Color Standard) were excised and proteins were digested in-gel using trypsin. The extracted peptides were desalted with C18 tips (Agilent, OMIX C18) used according to manufacturer's instructions and then dissolved in mass spectrometry sample buffer (20% acetonitrile, 0.1% formic acid).

The light and heavy iodoacetamide labelled tryptic ND3 peptides were analysed by LC-MSMS using a Xevo TQ-S triple-quadrupole mass spectrometer with the attached I-class Acquity LC system (Waters). Peptides were separated by revere-phase on an Acquity UPLC® BEH C18

column (Waters). MS buffer A (5% acetonitrile, 0.1% formic acid) and MS buffer B (90% acetonitrile, 0.1% formic acid) were used at a flow rate of 200 µl/min for the following LC gradient: 0-0.3 min, 5% buffer B; 0.3-3 min, 5%-100% buffer B; 3-4 min, 100% buffer B; 4.0-4.10, 100%-5% buffer B; 4.10-4.60 min, 5% buffer B; 4.60-5.00. Eluant was diverted to waste at 0-1 min and 4-5 min. The peptides were detected by multiple reaction monitoring (MRM) in positive ion mode. For quantification following transitions were used: light labelled ND3 peptide, 836 > 744; heavy labelled ND3 peptide, 838 > 746. The peak area of light and heavy labelled ND3 peptides was quantified using MassLynx 4.1 software in order to determine the relative proportion of the light and total labelled peptides.

**RNA extraction and sequencing**

To extract RNA from tissues, the medial lobe of the mouse liver was excised and stored in RNAlater (Invitrogen). After 2 hours 30 mg wet weight of tissue was added to PureLink RNA Mini Kit lysis buffer (Invitrogen) in a Precellys tube (Soft tissue homogenising CK14 – 2mL; Bertin Instruments) and homogenised twice using a Precellys 24 tissue homogeniser (6,500 rpm, 15 seconds: Bertin Instruments). A PureLink RNA Mini Kit (Invitrogen) was used to extract RNA, which was eluted into 80 µl RNA-free water and placed immediately on ice. The 260:280 and 260:230 UV absorption ratios were assessed using a NanoDrop spectrophotometer. The RNA concentration and RNA integrity number were determined using the Agilent 4200 TapeStation System and RNA ScreenTape (Agilent Technologies). Only samples with an RNA integrity number >8 were used for downstream analysis.
Subsequent RNA preparation and sequencing was done by Novogene. The mRNA was purified from total RNA using NEBNext Poly(A) mRNA Magnetic Isolation Module (New England Biolabs). First- and second-strand cDNA were synthesised using NEBNext synthesis modules (New England Biolabs) before purification using Agencourt AMPure XP beads (Beckman Coulter). RNA library preparation was done using NEBNext Ultra RNA Library Prep kit for Illumina (New England Biolabs). Libraries were pooled and sequenced on a HiSeq X Ten platform (Illumina) with paired-end 150 bp (PE 150) sequencing strategy by Novogene.

**Analysis of RNAseq data**

The resulting sequencing BCL files were demultiplexed with CASAVA to FASTQ files. TrimGalore! Was used remove low quality reads and adapter sequences and the quality of the

sequencing data was confirmed using FASTQC. Reads were aligned to the mm10 genome (*Mus musculus*; Dec 2011, Genome Reference Consortium GRCm38) using hisat2 and a count table produced using Featurecounts from RSubread. Normalisation and differential expression analysis was carried out using DESEQ2 within the R statistical environment (R Core Team).

## Statistical analysis

Data are shown as mean ± standard error of the mean.

Statistical analysis was performed by two-tailed Student's t-test or one-way ANOVA as appropriate using GraphPad Prism 6.0 (GraphPad, USA), R (R Core Team, 2013), or Microsoft Excel. Where ANOVA indicated a significant different between groups, Tukey's honest significant difference was used to determine which comparisons were statistically significant where sample sizes were equal among all groups. Where they were not, the Tukey-Kramer test was used. In both cases pairwise comparisons were made back to vehicle-only or other suitable control group as indicated. Since this procedure already attempts to control the family-wise error rate, no correction for multiple testing was necessary. Where the structure of the data necessitated that multiple t-tests were carried out, the Bonferroni-Šidák method has been used to correct for multiple testing.

On figures, signifiers (for example *) indicate significance at the level of $p < 0.05$ (prior to amending to control for family-wise error rate where applicable) which was the threshold used to determine statistical significance. For *in vitro* experiments, *n* refer to the number of independent experiments whereas for those conducted *in vivo* the *n* reported refer to individual animals.

## Collaborations and attributions

As this has been a collaborative project, some of the experiments presented in this thesis have been performed either in whole or in part by collaborators and where this is the case it has been indicated in the figure legend. Attribution and thanks are also given in full here. Unless it is explicitly indicated otherwise all work was performed by myself.

Mass spectrometry for measurement of tissue levels of mitochondria-targeted compounds was performed by A. Logan (MRC Mitochondrial Biology Unit, University of Cambridge, UK). T. Prime (MRC Mitochondrial Biology Unit, University of Cambridge, UK) is also thanked for her help with LC-MS/MS extractions for MitoNeoD, whilst those for MitoCDNB were performed by L. Booty (MRC Mitochondrial Biology Unit, University of Cambridge, UK). Mass spectrometry using LC-MS/MS for measurement of metabolites in a targeted methodology was performed under the supervision of H.Pragg (MRC Mitochondrial Biology Unit, University of Cambridge, UK). S. Costa (MRC Cancer Unit, Cambridge, UK) performed LC-MS spectroscopy using a semi-targeted approach. Magnetic resonance spectroscopy was carried out by A. Wright (CRUK-Cambridge Institute, UK).

Cyclic voltammetry of MitoPQ control compound 2 was performed by M. Cariello (University of Glasgow, UK). Assays to determine glutathione levels in either whole tissue or mitochondria were performed by L. Booty (MRC Mitochondrial Biology Unit, University of Cambridge, UK). F. Cvetko (MRC Mitochondrial Biology Unit, University of Cambridge, UK) performed the analysis of RNAseq data after MitoCDNB administration. S. Antonucci (University of Padua, Italy) performed the experiments presented here using NRVMs, including the measurements of ROS production, LDH release, mitochondrial membrane potential, MPTP opening and calcium dynamics as well as the anoxia-reoxygenation protocol. A. Hall (MRC Mitochondrial Biology Unit, University of Cambridge, UK) performed the experiments in C2C12 cells using the Orp fusion proteins to measure ROS production within both the cytosol and mitochondria. Complex I activity assays and differential labelling procedures were performed by N. Burger (MRC Mitochondrial Biology Unit, University of Cambridge, UK) using tissue samples that I generated during surgical procedures.

O. Souchanka (Department of Medicine, University of Cambridge, UK) is thanked for her surgical assistance during recovery procedures. Echocardiography was performed by T. Young (Department of Medicine, University of Cambridge, UK). Surgery for two experiments was performed in concert with other people: the pre-conditioning experiments were done in combination with V. Pell (Department of Medicine, University of Cambridge, UK) and the surgery examining the effect of disodium malonate upon infarct size was done in concert with D. Luping (Tianjin Medical University, China).

Much of the work presented here has already been published, and attribution is given in the relevant section of the appendix to these sources.

# Chapter 3 – Validation of novel tools for mitochondrial reactive oxygen species modulation and detection

## Introduction

### The need for a tool to generate reactive oxygen species within the mitochondria

In order to investigate the role of reactive oxygen species in the setting of IRI it is necessary to be able to modulate the dose of ROS within the mitochondria. This may be done through either an increase or a decrease in ROS above endogenous levels, but due to the fact that our situation of interest involves generation of ROS above baseline levels, we focus first on methods to increase ROS. As discussed in chapter 1 the concentration of ROS is a function of both sources and sinks, and so an intervention may either increase production or decrease breakdown in order to result in an increase in ROS levels. As with any drug or experimental compound, we must also aim for a high degree of specificity: that it has limited off target effects beyond its desired effect. In order to adequately mimic endogenous ROS production, an experimental manipulation should also ideally generate the same ROS species in the same cellular compartment and sub-compartmental location. There are a range of existing approaches, but all have significant drawbacks when judged against these criteria.

Decreasing ROS sinks is experimentally challenging. Most common amongst these approaches are genetic methods, such as either partial or complete knockdown or deletion (homo- or hetero-) of MnSOD. No genetic method allows much control over the extent of the modulation achieved, and further they have poor reproducibility from one experimental replicate to another. In addition, this approach allows us either no temporal control or in the case of inducible genetic systems only very coarse timing. There are few current methods to decrease endogenous levels of non-enzymatic antioxidants and thus this is also an area in which there is an unmet need.

A plethora of compounds have been used in experimental systems to increase ROS production but there are also questions here as to their experimental validity. Current approaches are still fairly crude, with both the effective cellular concentrations of ROS that result as well as their cellular location unclear. This is in stark contrast to the endogenous generation of ROS which as discussed is now appreciated to be a highly specific and regulated process (Chouchani et al., 2014).

The first method that is used is simply to expose a system to exogenous ROS, commonly in the form of hydrogen peroxide or a purine/xanthine oxidase radical generating system. This however relies on the uptake of ROS across membranes which introduces variability into the process, and also is agnostic to cellular location. Further, we are not elevating concentrations of the primary ROS species but those downstream of it.

Respiratory inhibitors such as rotenone and antimycin allow control over cellular location but have a range of off target effects, such as the disruption of mitochondrial membrane potential and synthesis of the small nucleotides ATP and NADH. Redox cyclers such as paraquat and menadione offer a better solution as they more closely mimic the production of superoxide as thought to occur at complex I in IRI. However high concentrations are required for sufficient uptake into the mitochondria.

What we require in order to better investigate this phenomenon then is a more specific tool, capable of generating a specific ROS species at a specific site within mitochondria, that also allows us a high degree of precision over the dose of ROS that we introduce. For this we shall utilise a mitochondria-targeted compound.

MitoParaquat

Mitoparaquat (MitoPQ) is a compound newly developed by Professor Michael Murphy and Professor Richard Hartley (Robb et al., 2015). In this case, the functional group of interest is the redox cycler paraquat (PQ). The PQ dication undergoes one electron reduction (Bus and Gibson, 1984) at the flavin site of complex I in mammalian mitochondria to generate the radical monocation $PQ^{\cdot+}$, which reacts rapidly with oxygen to produce superoxide ($k \sim 7.7 \times 10^8\ M^{-1}s^{-1}$) (Hassan, 1984). However its mitochondrial uptake is slow, with kinetics consistent with a mitochondrial membrane potential-dependent, ATP-independent transporter (Cochemé and Murphy, 2008). This means that high extracellular concentrations (~1 mM) are required in order to generate superoxide within the mitochondrion, and large amounts of the compound will also present in the cytosol and elsewhere.

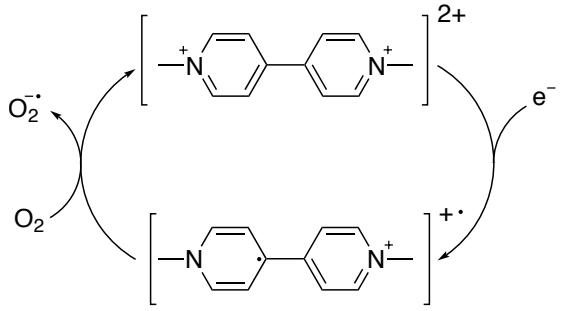


**Figure 3.1 The redox cycle of paraquat**.
The paraquat dication ($PQ^{2+}$) undergoes univalent reduction at complex I to generate the paraquat radical ($PQ^{2+}$). This then reacts rapidly with oxygen to produce superoxide and reform the dication. After Cochemé and Murphy (2008).

MitoPQ was developed in response to these issues and selected from a range of prospective compounds based on its ability to selectively generate superoxide within the mitochondria. Within mitochondrial membrane preparations (in which mitochondria are fragmented such that the matrix face of the inner mitochondrial is accessible to the bulk solution, and therefore do not require the uptake of a compound across a membrane for access to complex I) incubated with NADH and rotenone, MitoPQ caused superoxide production that was comparable to that caused by PQ (Robb et al. 2015). However, uptake by energised mitochondria was greatly enhanced compared with very low capacity uptake of PQ, as shown by the accumulation ratio in isolated mitochondria relative to the supernatant (Robb et al. 2015). MitoPQ thus represents an ideal tool to investigate the dose-response characteristic of mitochondrial ROS: precise and specific in both cellular location and the reactive species it generates.

Problems with traditional reactive oxygen species indicators

Concurrent with the need for a tool to accurately generate ROS in a physiological and controllable manner is the need for a tool to measure ROS within biological systems.
Measurement of ROS with current approaches is problematic – many commercially available indicators have now been shown to be riddled with confounding factors and thus to not measure that which they claim. Here we will explore hydroethidine (HE) and its mitochondria-targeted version MitoSox as a specific case due to their common use as superoxide and mitochondrial superoxide reporters respectively (Zielonka and Kalyanaraman, 2010), but many aspects are

generalisable to other indicators which have also been reported to not be what they are claimed (Kalyanaraman et al., 2012).

HE is the most popularly used intracellular superoxide probe used, and as MitoSox is a TPP conjugated version of the same molecule all the inherent properties of HE are also contained in the HE moiety present in MitoSox. Thus when discussing HE here, we are able to transfer the same arguments to MitoSox as well.

The complexity of the chemistry involved is indicated by the fact that whilst HE was initially concluded to be a non-specific indicator for ROS (Nethery et al., 1999), it was later described to react specifically with superoxide to give the product 2-hydroxyethidium. It is most commonly used as a fluorescent indictor due to the advantages of live measurements that gives, with 2-hydroxyethidium emitting red fluorescence that is used as a readout of superoxide levels. However, in addition to this specific oxidation by superoxide, HE may also be oxidised by either one- or two- electron oxidation to form the ethidium cation. Further, it will also dimerize to form fluorescent products. Due to the overlapping spectra of these products, dimers and their composites, to properly separate the specific product 2-hydroxyethidium HPLC or other destructive techniques must be used (Kalyanaraman et al., 2012).

The picture is further complicated by the fact that whilst HE lacks a positive charge and does not significantly intercalate with DNA, the ethidium cation will do so to an appreciable extent. Therefore if it is used fluorescence must be measured with an excitation wavelength of 396 nm in order to specifically excite the specific product 2-hydroxyethidium but not HE that has intercalated with DNA (Mailloux, 2015; Zielonka and Kalyanaraman, 2010).

In addition to reactions with any probe, superoxide reacts exceedingly rapidly with SODs as described in chapter 1, which are present both at high quantities and in the relevant cellular location. This means that they have a high capacity to neutralise any superoxide that is produced, and either this must be either exceeded or their rate outcompeted in order for a probe to function. Therefore there is likely a floor effect below which we cannot measure superoxide with HE before it is dismuted, and the concentration at which this occurs will depend on the concentration of HE used. Higher concentrations result in a theoretically lower limit of detection, but also increase the extent of any off-target effects. As discussed regarding other

mitochondria-targeted molecules such as MitoPQ this is however inherently less of a problem for a mitochondria-targeted molecule such as MitoSox due to its orders of magnitude greater accumulation in the compartment of interest compared with the rest of the cell.

This is not to say that HE and MitoSox cannot be used as superoxide indictors, rather that experiments using them must be very carefully designed with their weaknesses in mind. In particular, the scientific community needs to use great scrutiny in interpreting results where they have been used. Of course, an alternative approach is to design a probe that has fewer of the inherent problems that HE does.

Development of MitoNeoD: a mitochondrial probe for superoxide

In a similar fashion to the need for the development of MitoPQ as a better tool to generate ROS within the mitochondria, there is then also the need for a better tool to measure ROS. This lead Murphy and Hartley to design and synthesis the novel compound MitoNeoD. In a similar fashion to MitoSox, MitoNeoD is based on HE and also targeted to the mitochondria as described previously by conjugation to TPP cation and the same alkyl linker. However, its chemical properties have been modified in order to overcome some the limitations described before.

First, its oxidation product should not intercalate with DNA (so generating a fluorescent signal) which is achieved by the addition of two bulky neopentyl groups that sterically hinder this interaction. Secondly, a deuterium atom rather than hydrogen at C6 location increases its specificity to superoxide by modifying the reaction constant for the rate limiting step of non-specific (but not that specific to superoxide) oxidation. This also improves stability in the presence of air and light.

Detection of the specific reaction products with superoxide is then performed by mass spectrometry, similar to best practice when using HE or MitoSox. This is the same strategy utilised for the hydrogen peroxide probe MitoB/P. This has been demonstrated to be successful in a range of model organisms in vivo, in what has been described as an ‘exomarker’ approach (2015). It is worth noting that this strategy to allow its use *in vivo* provides a key advantage for a ROS probe: most experiments performed *in vitro* are at much higher oxygen tensions than

are present *in vivo*, and this will lead to a higher ROS production in these model systems than is present in reality. It is thus of considerable interest specifically in the case of a superoxide probe that we can use it *in vivo*, in addition to the usual drawbacks and differences that are present between *in vitro* and *in vivo* systems. It is also worth noting that by measuring the concentrations of both the original exomarker as well as its reaction products, we can use it as a ratiometric probe which provides an internal control for its own uptake.

Whilst we have to trade-off a large amount of the specificity for superoxide, it is also possible for MitoNeoD to be used in model systems *in vitro* as a fluorescent indicator to allow changes in ROS production to be visualised in real time – though bearing in mind the mechanisms and unsolved problems of HE and MitoSox discussed above, these results should be interpreted in a relative rather than absolute terms.

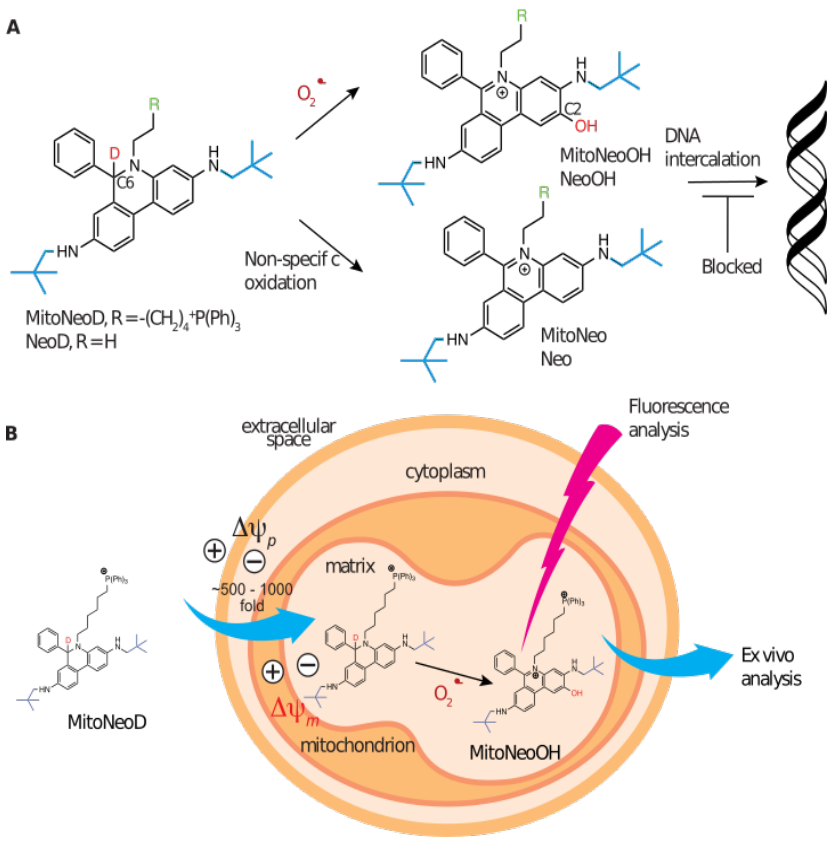


**Figure 3.2 Schematic of the actions of MitoNeoD.**

**A.** MitoNeoD may be specifically oxidised by superoxide to form MitoNeoOH. Non-specific oxidation results in the formation of MitoNeo. The neopentyl groups present in all of these compounds add bulk to hinder their intercalation with DNA.
**B.** Like other TPP conjugated compounds, uptake of MitoNeoD into cells and then mitochondria is driven by the respective membrane potentials. It may be analysed either quantitatively as an exomarker using mass spectrometry, or qualitatively by fluorescence to allow imaging of cells in real time.
Reproduced from Shchepinova…Mulvey… et al (2017)

Development of MitoCDNB: selective depletion of mitochondrial glutathione

So far, our focus has been upon modulating mitochondrial redox status through the generation of exogenous ROS, but we may also change ROS levels by altering the quantities of small molecule antioxidants: targeting sinks rather than sources. As discussed, direct interventions to increase these are problematic, and so we have developed an alternative approach to deplete them. The mitochondria-targeted compound MitoCDNB is presented for use as a tool to selectively deplete glutathione within the mitochondria, and thus alter mitochondrial redox balance towards a more reduced environment.

The glutathione (GSH) system is the dominant mitochondrial thiol redox system, playing a crucial role in protecting the mitochondria against ROS and other electrophiles. Within the mitochondria it functions independently from the rest of the cell, although since glutathione is not synthesised inside the mitochondria it must initially be imported from the cytosol. The glutathione pool is then coupled to the redox state of the $NADP^+$/NADPH pool in the matrix by the enzyme glutathione reductase, maintaining it in a reduced state under normal conditions.

The second major system in mitochondrial thiol regulation is the thioredoxin system, with thioredoxin reductase 2 (Trx2) functioning to reduce protein disulfides and is again coupled to the $NADP^+$/NADPH ratio. The thioredoxin system in turn is also coupled to peroxiredoxins that degrade hydrogen peroxide and methionine sulfoxide reductases that reverse methionine oxidation.

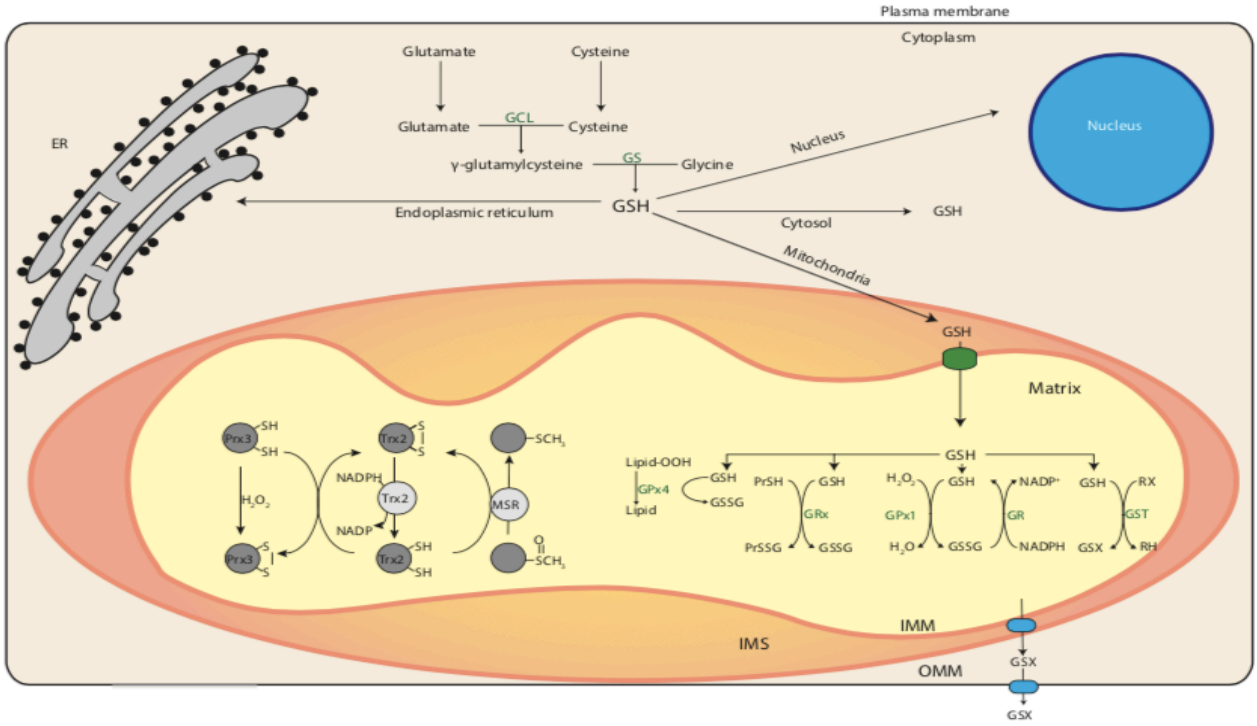


**Figure 3.3 The glutathione redox couple.**

Glutathione is synthesised in the cytosol by the enzymes glutamate cysteine ligase (GCL) and glutathione synthetase (GS). It may then remain in the cytosol or be imported into organelles such the as mitochondria, although the molecular nature of the mitochondrial transporter is not currently known. Within the mitochondria glutathione acts to maintain thiol redox state in several ways: through degradation of hydrogen peroxide (catalysed by glutathione peroxidases; GPXs), lipid peroxides (glutathione peroxidase 4; GPx4), reducing oxidised protein thiols (catalysed by glutaredoxin 2; Grx2) and detoxifying xenobiotics and other electrophiles (catalysed by glutathione-S-transferases; GST). If formed, glutathione disulfide (GSSG) may be recycled into glutathione by glutathione reductase (GR) which is coupled to the mitochondrial NADP/NADPH pool.

The Thioredoxin system acts similarly to maintain thiol redox homeostasis. Within the mitochondria, Trx2 re may reduce other protein dithiols – itself becoming oxidised as an intra-protein disulfide forms. This may be reduced by the reductase TrxR2 driven by the mitochondrial NADH pool. In addition, Trx2 is also couple to the peroxiredoxins (Prx3; that

degrade hydrogen peroxide) and methionine sulfoxide reductases (MSR; that reverse methionine oxidation).
Reproduced from Booty, …Mulvey… et al 2019.

Genetic approaches to modulate the thiol redox state in the mitochondria are currently untenable, since the identity of the transporter that shuttles glutathione across the mitochondrial membranes is unknown (Booty et al., 2015). Moreover, the knockout of different components of this system such as TrxR2 or GPx4 has been found to be embryonically lethal (Conrad, 2009).

Instead we have developed the small molecule MitoCDNB, which has been designed and synthesised by collaborators Murphy and Hartley. This utilises the same mitochondria-targeting strategy using the TPP cation described before, conjugated to the GST substrate 1-chloro-2,4-dinitrobenzene. It then acts as a competitive inhibitor of glutathione S-transferase, forming the redox silent product MitoGSDNB. The original intention behind this compound was that the membrane impermeable MitoGSDNB would be 'locked-in' within the mitochondria, enabling its use as a probe to measure mitochondrial volume. However testing *in vitro* revealed that is has pleiotropic effects due to mechanistic overlap in the multiple systems regulating mitochondrial thiol status: MitoCDNB also inhibits thioredoxin reductase 2 and peroxiredoxin 3. Taken together, the actual function of MitoCDNB is then to cause a widespread disruption of thiol redox status selectively within the mitochondria but not elsewhere in the cell.

Existing *in vitro* data from our collaboration with the lab of Mike Murphy has validated both the selective mitochondrial accumulation of MitoCDNB and its functions in depleting GSH and inhibiting TrxR2 in *in vitro* cell culture and in isolated mitochondria. However its use *in vivo* remains to be validated, in order that we can widen the range of model systems in which the effects of such a selective disruption of mitochondrial thiol redox status can be examined.

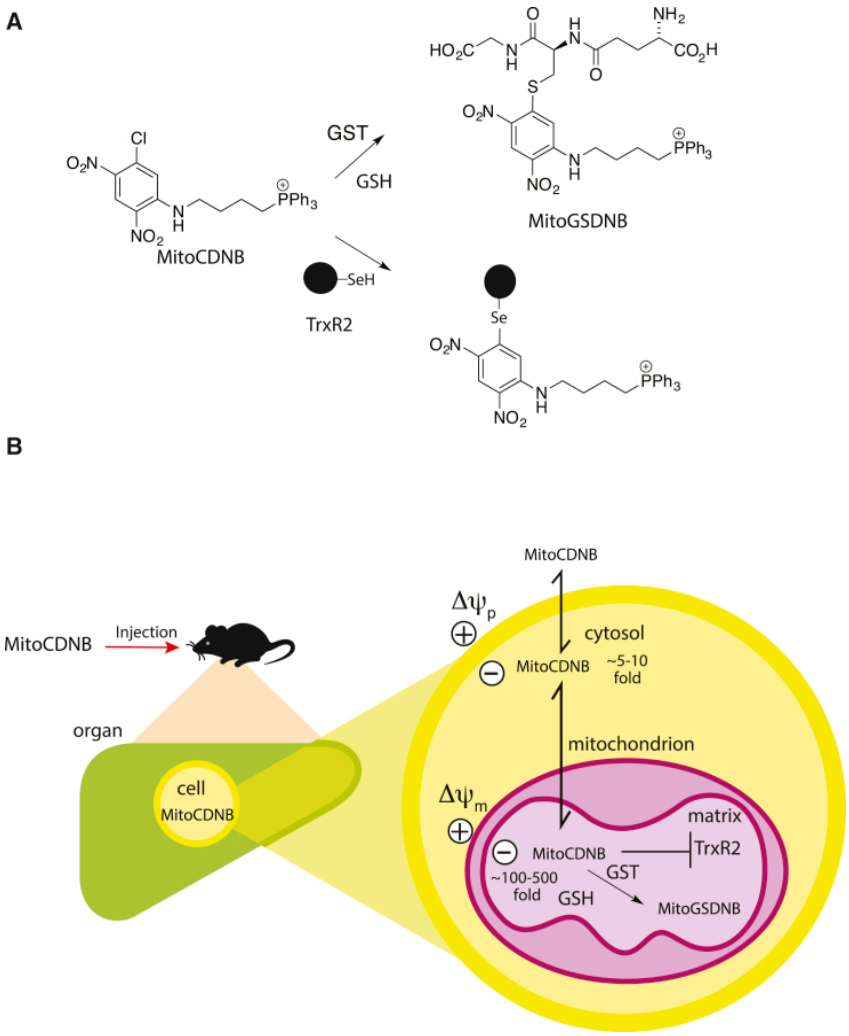


**Figure 3.4 Schematic of the actions of MitoCDNB.**

**A.** MitoCDNB may react with glutathione in a reaction catalysed by GST so as to deplete the levels of glutathione within the mitochondria. This forms the product MitoGSDNB. Inhibition of TrxR2 occurs as MitoCDNB is able to bond to a critical selenol in its active site.

**B**. As with other TPP-conjugated compounds, uptake of MitoCDNB occurs due to the inside negative membrane potentials of both the cell and the mitochondria. Here it depletes glutathione levels and inhibits the enzyme TrxR2, causing a disruption to mitochondrial thiol homeostasis.

Reproduced from Booty, …Mulvey… et al 2019.

Aims and objectives

- Validate the location of the ROS generated by MitoPQ as occurring within the mitochondria and not elsewhere within the cell
- Validate that ROS generation by MitoPQ occurs in a dose-dependent manner, in order to allow the assessment of dose-response relationships of ROS.
- Validate a 'MitoPQ control compound' so as to allow better experimental design that accounts specifically for any off-target effects
- Measure uptake, metabolism and distribution of MitoNeoD *in vivo*
- Validate MitoNeoD *in vivo* to demonstrate proof of principle of mitochondrial superoxide detection in a whole living organism
- Measure uptake, metabolism and distribution of MitoCDNB *in vivo*
- Validate MitoCDNB *in vivo* to demonstrate proof of principle of mitochondrial glutathione depletion in a whole living organism

## Results

### Design and *in vitro* testing of MitoParaquat control compound 1 and MitoParaquat control compound 2

The effects of the TPP moiety that causes the accumulation of MitoPQ within mitochondria is a well validated strategy used to target molecules to mitochondria (Smith et al., 2011). Whilst the off-target effects of the TPP cation have be shown to be minimal at commonly used doses of these compounds, it is desirable to have a more cogent negative control to which to compare experimental groups to than just the vehicle alone. For this reason, we developed and validated a MitoPQ control compound that as far as possible shares the same molecular properties apart from the ability to redox cycle and thus produce superoxide within the mitochondria. Richard Hartley and colleagues at the University of Glasgow designed several bespoke candidate control compounds, which aimed to retain a chemical structure and properties as similar as possible to MitoPQ but lack the ability to redox cycle at complex I. This was achieved through keeping the molecular structure of the TPP mitochondria targeting moiety and hydrocarbon linker, but causing a disruption of bipyridine structure so as to disfavour the acceptance of electrons at the FMN site of complex I.

*version 1*

The first version of this compound is shown in Figure 3.5B, where the distance between the two pyridine rings in the paraquat moiety is extended with the effect that electrons are no longer delocalised between the two rings. Like MitoPQ (shown in Figure 3.5A for comparison) it is a triply charged cation, has a similar molecular weight, similar separation between TPP and second charge, and a similar overall charge distribution. We thus hypothesised similar molecular properties and uptake into mitochondria but without the ROS producing capability of MitoPQ.

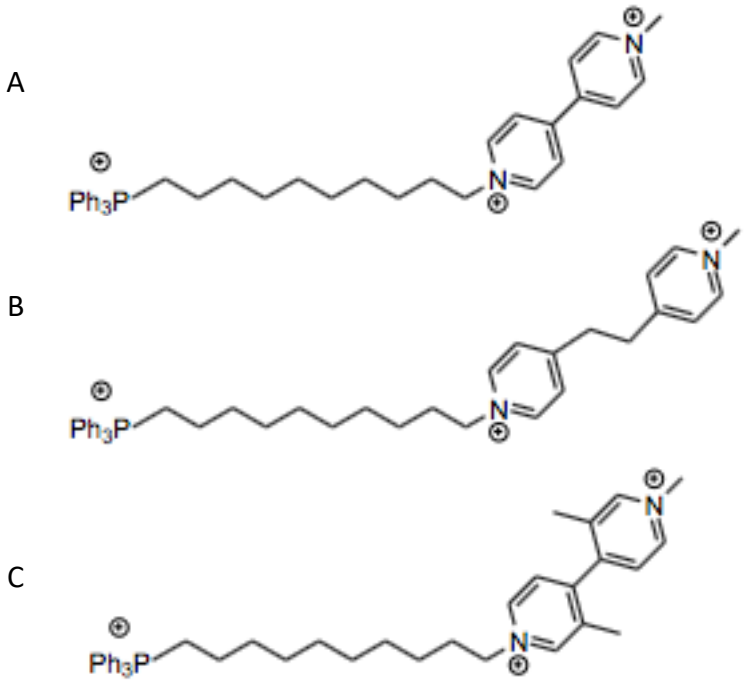


**Figure 3.5 Comparison of the structure of MitoParaquat, MitoParaquat control compound 1 and MitoParaquat control compound 2.**

**A.** MitoPQ consists of the paraquat moiety joined to the TPP cation by a 10 carbon linker.

**B.** MitoPQ control compound 1 was designed with a greater distance between the pyridine rings of the paraquat moiety, preventing electron dissociation between them with that rationale that this would remove its ability to accept an electron from complex I.

**C.** MitoPQ control compound 2 used an alternative strategy to prevent it accepting an electron at complex I: by the addition of methyl groups a twist is introduced between the two pyridine rings, disfavouring the acceptance of electrons at the FMN site of complex I.

The coelenterazine fluorescence assay for superoxide production in mitochondrial membranes confirmed that MitoPQ control compound 1 causes significantly less superoxide is comparison to MitoPQ itself (Figure 3.6A). This was performed using bovine heart mitochondrial membranes which are fragmented and therefore complex I is accessible to the bulk solution: meaning that the compound does not require uptake across membranes as would be the case if the mitochondria were intact.

However, experiments using HPLC to measure the uptake of MitoPQ control compound 1 in intact isolated mitochondria indicated that this is substantially different from MitoPQ (Figure 3.6B), with MitoPQ control compound 1 accumulating at approximately 4-fold higher

concentrations. As expected, the uptake of both compounds was dependent of mitochondrial membrane potential, demonstrated by the negative control experiments with the addition of FCCP (a protonophore which dissipates mitochondrial membrane potential).

Similarly, when ROS production was measured in intact C2C12 cells no difference was observed between MitoPQ control compound 1 and MitoPQ (Figure 3.6C). This was performed using MitoNeoD, which specifically detects superoxide within the mitochondria and for which a full validation is presented later in this chapter. Thus despite the results showing that MitoPQ control compound 1 was not able to produce superoxide in mitochondrial membrane fragments it was concluded that MitoPQ control compound 1 was not tenable for use in the desired manner as a non-redox active control.

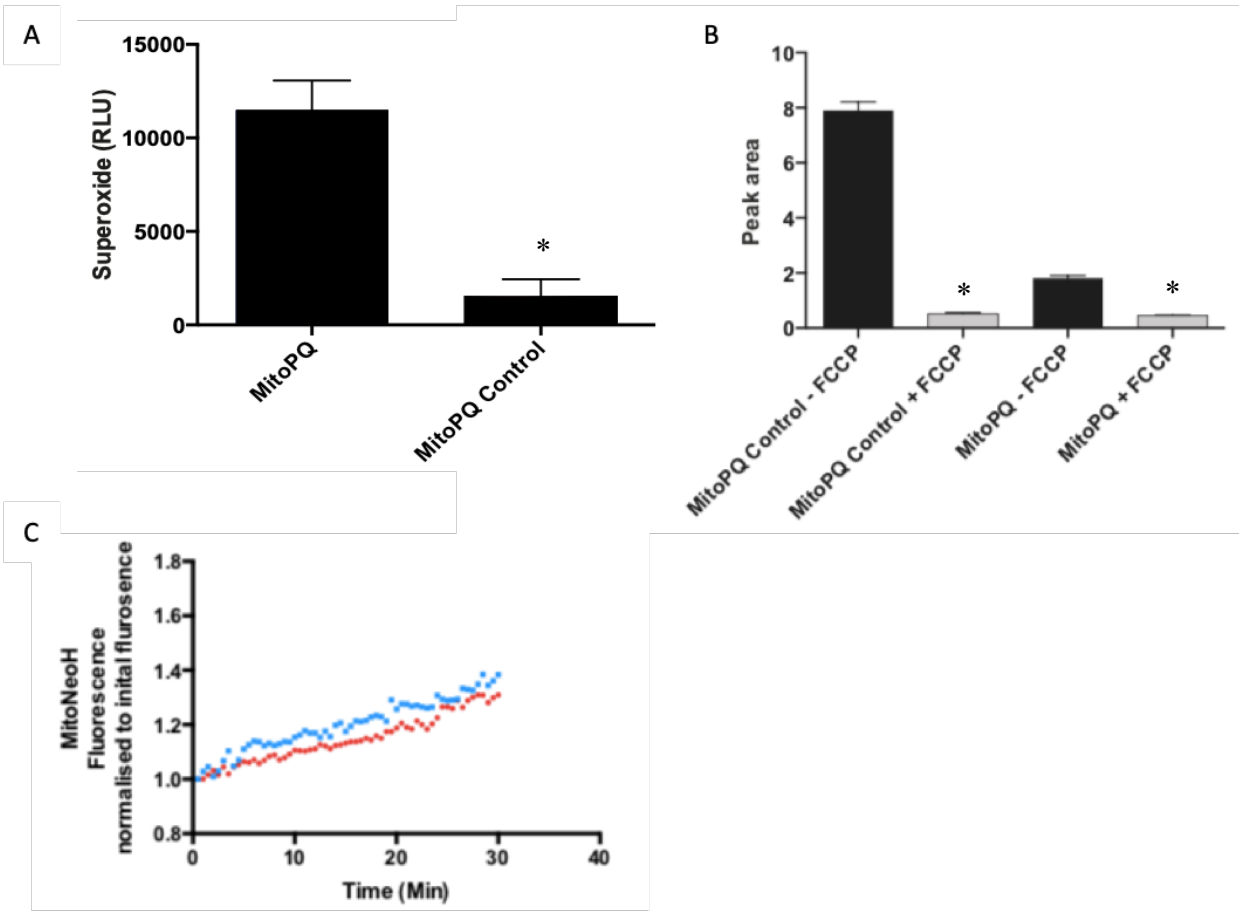


**Figure 3.6 Characterisation of MitoParaquat control compound 1.**

**A.** MitoPQ control compound 1 does not produce significant superoxide compared to MitoPQ. Bovine heart mitochondrial membranes were incubated for 5 min with MitoPQ control compound 1 or MitoPQ to give a final concentration of 1 μM, and cumulative superoxide production was assessed by coelenterazine fluorescence.

*n = 3, Student's t-test*

**B.** MitoPQ control compound 1 is taken up into mitochondria at approximately 4-times the extent of MitoPQ. Rat liver mitochondria were incubated with 5 μM MitoMPQ control compound 1 or MitoPQ for 5 min before pelleting of mitochondria from the bulk solution and analysis by RP-HPLC. The uptake of both compounds remains sensitive to dissipation of mitochondrial membrane potential by the ionophore FCCP (500 nM).

*n = 3, One-way ANOVA with Tukey-Kramer for pairwise comparisons. * indicates statistically significant difference between MitoPQ and MitoPQ control compound 1 conditions*

**C.** MitoPQ control compound 1 (blue) produces ROS in C2C12 cells at a comparable rate to MitoPQ (red), measured by MitoNeoD fluorescence. Compounds were administered at time=0 (5 μM) after incubation of cells with MitoNeoD for 10 minutes.
HPLC and coelenterazine fluorescence experiments were performed by T.Bright, (MRC-MBU). A. Hall (MRC-MBU) measured MitoNeoD fluorescence in C2C12 cells.

*Version 2*

We thus proceeded to assess version 2 of the control compound (MitoPQ control compound 2), whose synthesis is presented in Figure S1 of the appendix. Instead of extending the distance between the two pyridine rings, methyl groups were added which introduce a twist into the viologen unit with the same consequence that electron delocalisation around the bipyridine structure should be lost. This means that the formation of the intermediate radical is disfavoured, and thus it is less likely to accept an electron at complex I. This was experimentally confirmed by the cyclic voltammetry data of Figure 3.7A, with a redox potential of almost -1.0 V required in order to induce oxidation of MitoPQ control compound 2: almost double that required for MitoPQ to accept an electron. Whilst these experiments were performed under standard rather than physiological conditions, this is far beyond the redox potentials generated in the mitochondrial respiratory chain with NADH the most oxidising agent at -320 mV (Ramsay, 2019). As with MitoPQ control compound version 1, a coelenterazine fluorescence assay in mitochondrial membranes demonstrated that MitoPQ control compound version 2 caused significantly less superoxide production that MitoPQ (Figure 3.7B).

The altered charge distribution on the viologen moiety lead us to hypothesise that MitoPQ control compound 2 should remain more similar to MitoPQ than with MitoPQ control compound 1. Since charge density is a key parameter in determining membrane permeability and thus mitochondrial uptake, it was hoped the accumulation of MitoPQ control compound 2 in mitochondria would likewise be more similar to MitoPQ than the 4-fold increase observed with MitoPQ control compound 1.

Figure 3.7C shows the accumulation of MitoPQ control compound 2 in isolated mitochondria, which remains statistically different from MitoPQ but with a smaller difference than that of

MitoPQ control compound 1. Since the substitution of methyl groups in place of protons will make the compound more lipophilic, a slightly higher uptake into the mitochondria is in fact expected due to the importance of membrane permeability in the uptake of TPP-conjugated compounds (Ross et al., 2005). Indeed, since altering the electron delocalisation of the bipyridine structure necessarily changes the charge density of the molecule there is therefore inevitable that a trade-off must be made between the ROS producing capability and uptake of any control compound for MitoPQ. Despite this difference in uptake then, we accepted MitoPQ control compound 2 as possessing similar enough molecular properties to MitoPQ to justify its use as a control compound that does not produce ROS.

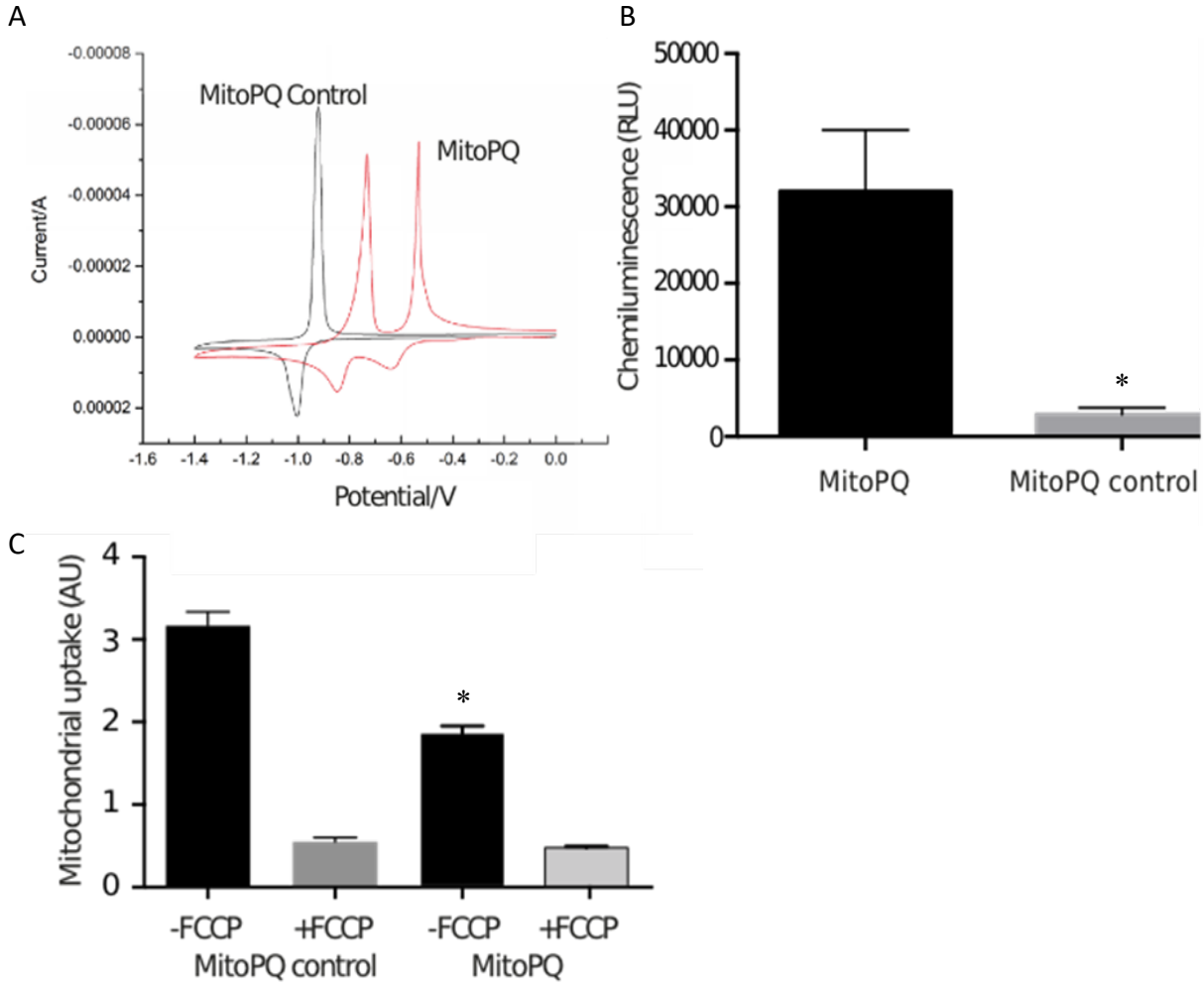


**Figure 3.7 Characterisation of MitoParaquat control compound 2.**

**A.** Cyclic voltametry confirms that MitoPQ control compound 2 is much more difficult to reduce than MitoPQ, with a reduction half potential of -0.97 V compared to that of -0.59 V for MitoPQ.

**B.** Uptake in isolated mitochondria, measured by RP-HPLC. Uptake of MitoPQ control compound 2 is higher than that of MitoPQ (both 5 μM), though the increase is less than that seen for MitoPQ control compound 1. The uptake of both compounds remains susceptible to membrane dissipation by the ionophore FCCP (500 nM), as expected for the uptake of TPP-conjugated compounds.

*n = 3, Student's t-test*

**C.** MitoPQ control compound 2 causes orders of magnitude less superoxide production than MitoPQ (both 1 μM) as measured by coelenterazine luminescence in bovine heart mitochondrial membranes.

*n = 3, One-way ANOVA with Tukey-Kramer for pairwise comparisons, * indicates statistically significant difference between MitoPQ and MitoPQ control compound 2 conditions*

Coelenterazine fluorescence and HPLC experiments were performed by T. Bright (MRC-MBU). Cyclic voltametry was performed by M. Cariello (University of Glasgow).

Data amended from Antonucci et al. (2019).

MitoParaquat – validation of reactive oxygen species production

In order to show that MitoPQ was suitable for use in investigating the dose-response characteristic of mitochondrial ROS, it was necessary to definitively validate that it produced ROS in a dose-dependent manner. Since the measurement of mitochondrial superoxide using current technologies is not straightforward, we present data here in both isolated mitochondria and in cultured cells using three orthogonal methods in order to show that this was the case.

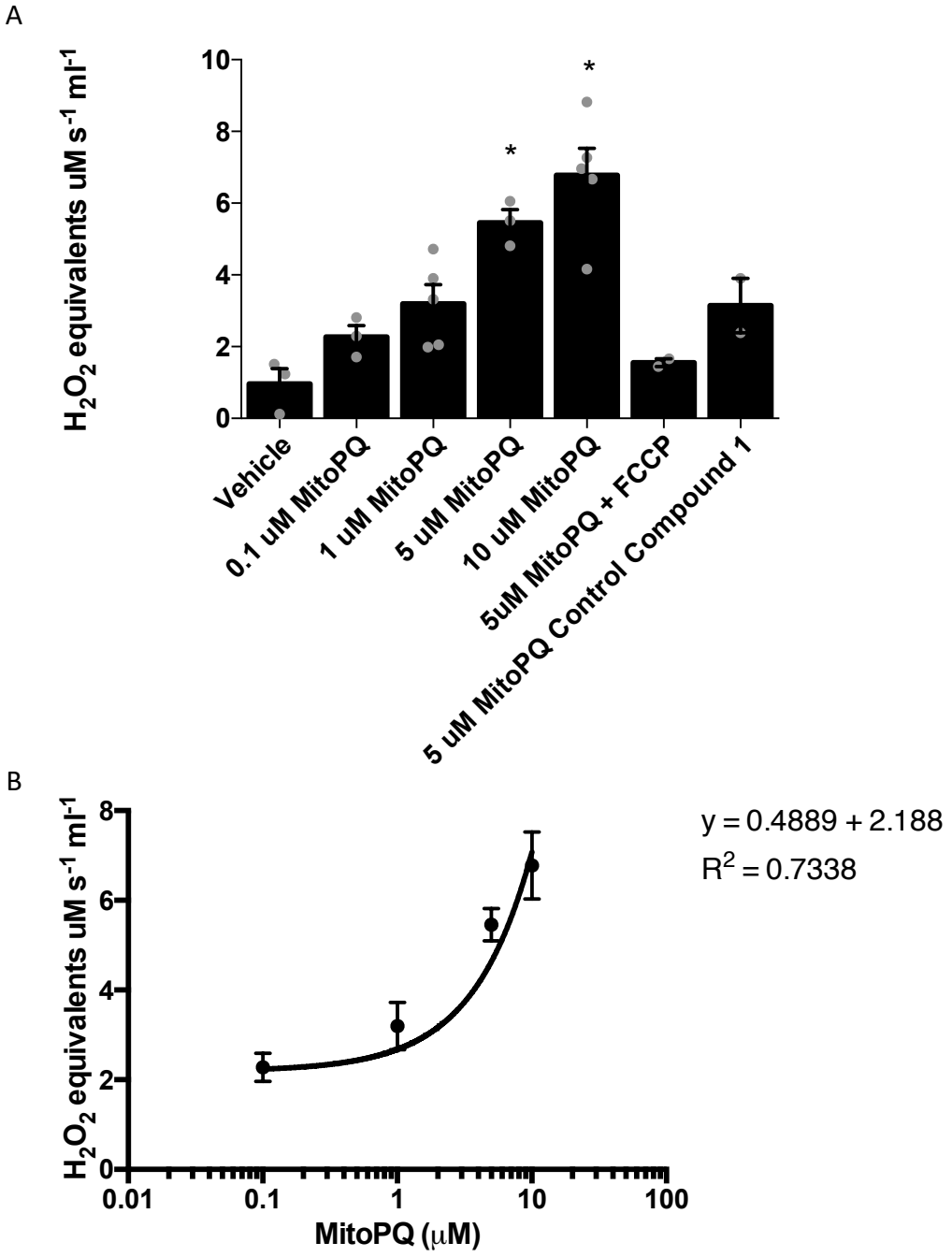


**Figure 3.8 Reactive oxygen species production by MitoParaquat in isolated mitochondria.**

**A.** Hydrogen peroxide production was measured with amplex red in isolated mitochondria for 3 min following compound addition, showing a dose dependent ROS production by MitoPQ. MitoPQ control compound 1 produces less ROS than MitoPQ itself at an equivalent concentration, but still significantly more than ethanol vehicle only control.

**B.** ROS production was linear over the range of 0.1 – 10 μM ($R^2$ = 0.73)

*n = 3-5, one-way ANOVA with Tukey-Kramer for comparisons to vehicle only control*

We first used amplex red fluorescence in isolated mitochondria (Figure 3.8A). In the presence of excess horse radish peroxidase, the conversion of amplex red to resorufin is proportional to the concentration of hydrogen peroxide present. This is formed as discussed by the rapid dismutation catalysed by SODs that are present at high concentrations. Here we see dose-dependent ROS production by MitoPQ, but also that whilst MitoPQ control compound 1 causes less ROS production than the active compound it is still greater than the vehicle only control (Figure 3.8A). Caution must be used in interpreting the statistical analysis of this combined dataset. A one-way ANOVA shows a significant effect of treatment group, but it should be noted that the use of post-hoc testing to differentiate between groups is misleading: since the dose of MitoPQ is a continuous rather than categorical variable, the smallest increase in dose that causes a significant increase in ROS production relative to control is dependent upon the sample size chosen for the experiment in addition to the number of different doses tested. Instead a linear regression of $H_2O_2$ production upon dose of MitoPQ provides a reasonable fit (Figure 3.8B; $y = 0.4489x + 2.188$, $R^2 = 0.73$).

Whilst amplex red fluorescence is a reliable, sensitive and robust method but it must be borne in mind that as we are measuring a downstream ROS species there may be a discontinuity in extrapolating these measurements to superoxide levels. Firstly, not all superoxide is necessarily converted to $H_2O_2$ as it may also react with other molecules, and there are also sources of $H_2O_2$ other than the dismutation of superoxide. Secondly, not all the $H_2O_2$ present in the mitochondria will necessarily survive efflux due for example to reaction with matrix peroxidases. It is also noteworthy that $H_2O_2$ flux across membranes occurs primarily not via diffusion across the membrane but is mediated by aquaporins and so is a potentially modifiable rather than consistent process.

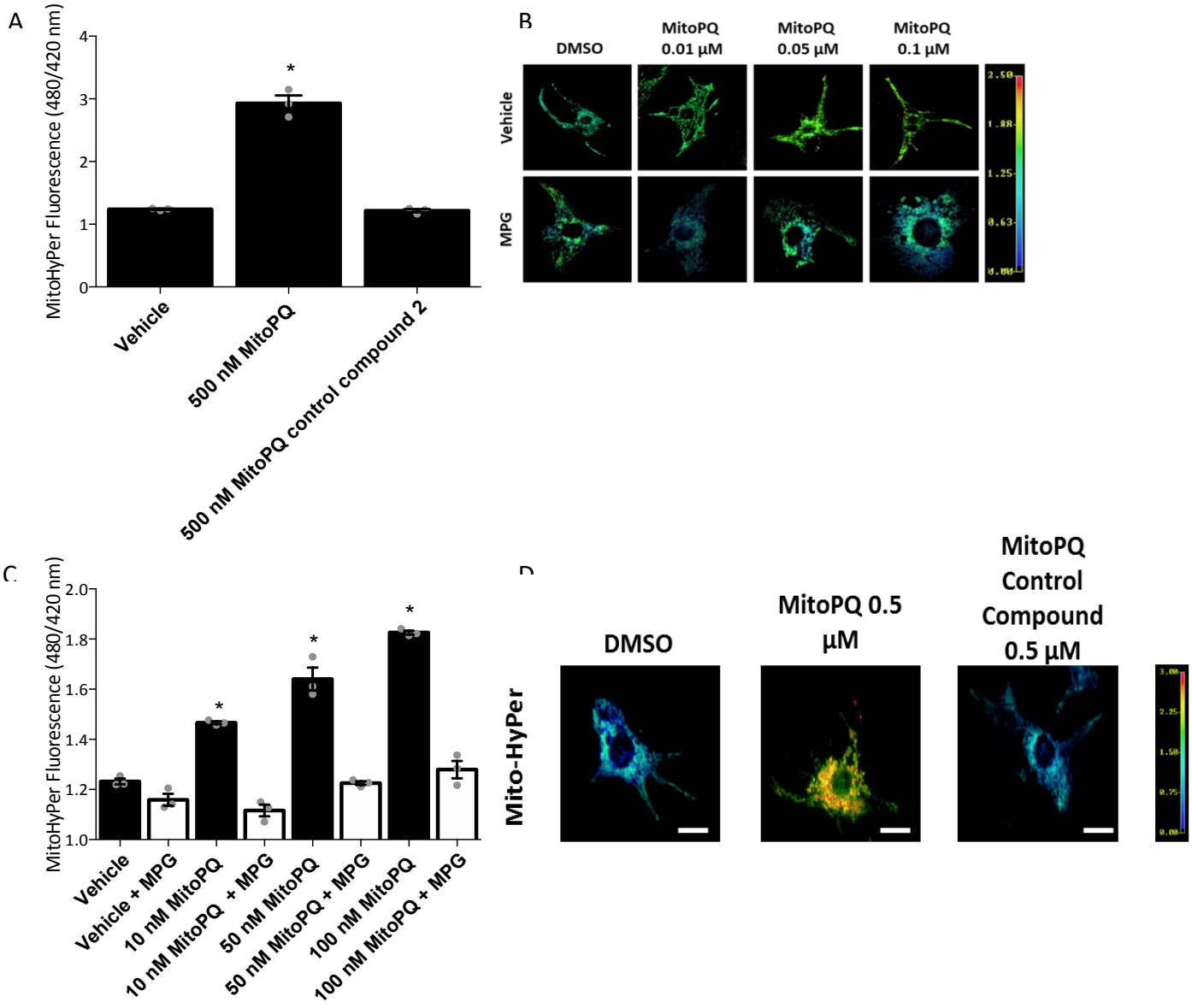


**Figure 3.9 ROS production by MitoParaquat in neonatal rat ventricular myocytes expressing MitoHyPer.**

**A-B.** Mitochondrial $H_2O_2$ formation was induced by MitoPQ as measured by MitoHyPer in isolated NRVMs. Cells were incubated with MitoPQ for 2 h, with or without pretreatment with 500 µM MPG for 30 minutes. Images show representative cells for each condition. *Scale Bar: 20 µm.*

**C-D.** Levels of mitochondrial ROS generation by MitoPQ control compound 2 are not significantly different from vehicle only control.

*n = 3 biological replicates, 20 cells measured per condition. One-way ANOVA with Tukey-Kramer for comparisons to vehicle only control.*

Experiments using NRVMs with MitoHyPer were performed by S. Antonucci.

We thus next sought to measure ROS levels within the mitochondria in order that $H_2O_2$ efflux across membranes was no longer a confounding factor. This was achieved using the genetically encoded indicator MitoHyPer in neonatal rat ventricular myocytes. MitoHyPer is based upon circularly permuted yellow fluorescent protein (cpYFP) that is inserted into the regulatory domain of the bacterial $H_2O_2$ sensing protein OxyR (Zhang et al., 2018b). By this coupling of the two proteins the reaction of $H_2O_2$ with OxyR induces a conformational change in the cpYFP domain, which corresponds to a change in the fluorescence spectrum and thus can be measured. These experiments showed that MitoPQ caused a dose dependent production of ROS within the mitochondria (Figure 3.9A-D). In addition, whilst MitoPQ caused a significant increase in hydrogen peroxide levels within the mitochondria relative to the vehicle-only control (Figure 3.9A), no difference was observed when cells were instead treated with MitoPQ control compound 2. This is visualised in the representative false-colour images which express an increase in the ratio of the oxidised to non-oxidised conformations of MitoHyPer (signal at 480 nm and 420 nm respectively) with increasingly warm colours (Figure 3.9B,D).

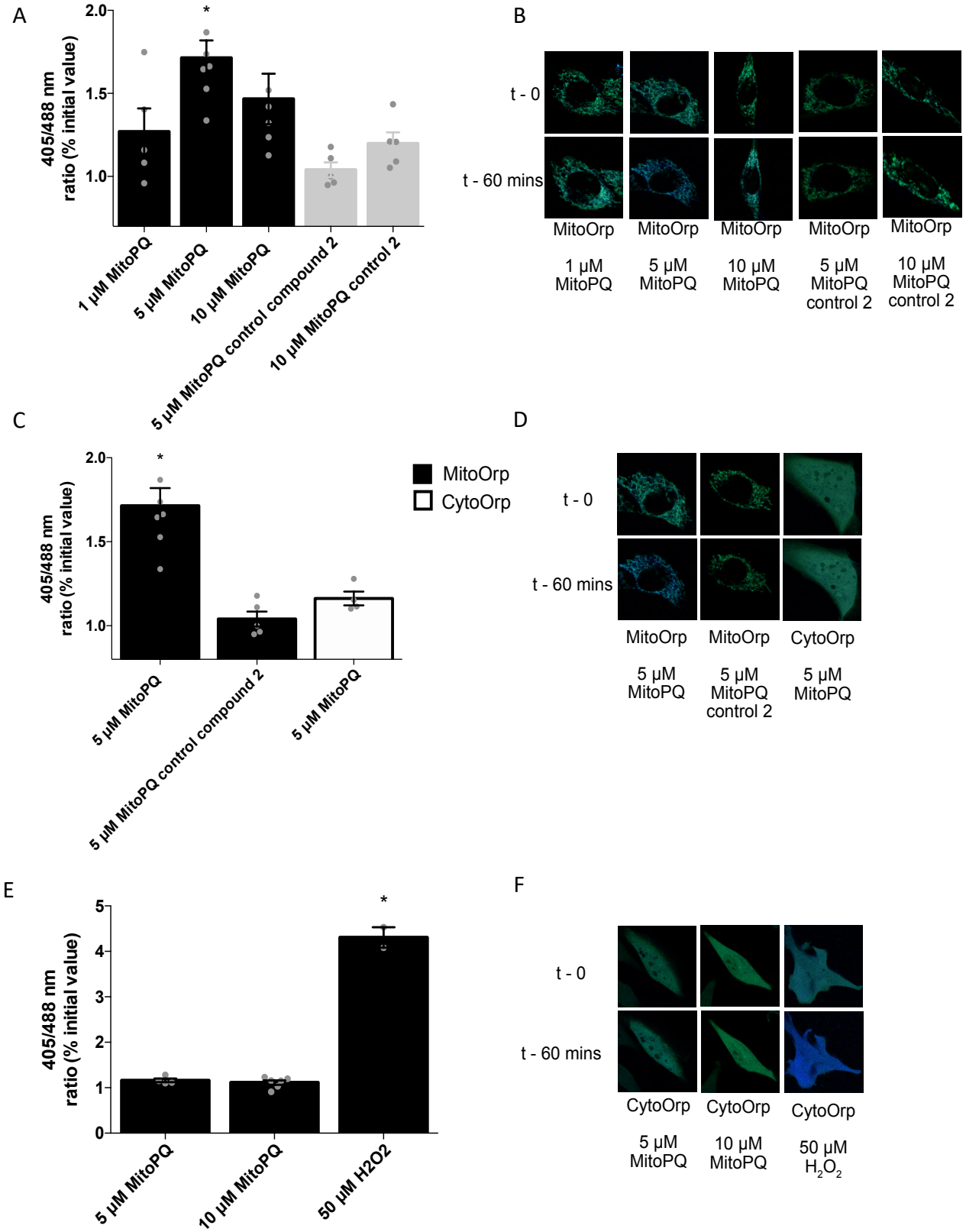


**Figure 3.10 ROS production by MitoParaquat in C2C12 myoblasts expressing roGFP.** **A-B**. MitoPQ control compound 2 does not oxidise the mitochondrial-targeted form of the redox sensor roGFP in C2C12 cells. Expression of roGFP was targeted to the mitochondria,

where oxidation by $H_2O_2$ causes a change in excitation from 488 nm to 405 nm, shown here by increasing levels of blue. Treatment with MitoPQ showed a dose dependent oxidation of the mitochondrial targeted roGFP with an acme at 5 μM, but treatment with MitoPQ control compound 2 did not oxidise the roGFP with little change from the baseline ratio.

**C-D.** MitoPQ specifically oxidises the mitochondrial targeted roGFP. C2C12 cells were transfected with either the mitochondrial or the cytosolic targeted roGFP. MitoPQ specifically oxidised the mitochondrial targeted roGFP, with no changes observed in the cytosolic targeted roGFP. No changes were also observed in the mitochondrial targeted roGFP when treated with MitoPQ control compound 2.

**E-F.** MitoPQ does not oxidise the cytosolic targeted roGFP**.** No significant difference was observed when cells expressed the cytosolic targeted construct were treated with MitoPQ, although it can be oxidised was observed when treated with 50 μM $H_2O_2$.

*n = 3-6, one-way ANOVA with Tukey-Kramer for comparisons to time zero*

Experiments using C2C12 myoblasts were performed by A. Hall (MRC-MBU).

MitoHyPer has rightly received some criticism, as a similar change in the fluorescence spectrum to that caused by oxidation by $H_2O_2$ may also occur due to changes in pH (Quatresous et al., 2012). We thus further used the genetically encoded roGFP-ORP1 protein as it has been described to be substantially less sensitive to pH changes. This functions by an analogous mechanism to the MitoHyPer technology, consisting of the redox sensitive roGFP fluorescence reporter domain which is coupled to the yeast peroxidase protein ORP1 in order to further increase its specificity towards $H_2O_2$ over other oxidising species (Dey et al., 2016). The expression of this construct can then be targeted to the mitochondria (MitoOrp) or the cytosol (CytoOrp), allowing us to also measure ROS production within both cellular compartments. Using C1C12 mouse myoblasts expressing MitoOrp we validated that MitoPQ produces ROS within the mitochondria (Figure 3.10A-B). Representative images (Figure 3.10B, D, E) are visualised by overlaying the signals of the 405 nm (blue; oxidised conformation) and 488 nm (green; baseline conformation) channels, with an increase in hydrogen peroxide therefore appearing as increasingly blue. In contrast, cells treated with MitoPQ control compound 2 do not show any difference from baseline values indicating that it does not produce ROS within the mitochondria to any great extent (Figure 3.10C-D).

Whilst our data indicated that MitoPQ causes an increase in ROS within the mitochondria, we were not able to detect an increase in ROS within the cytosol with no change observed after 60 mins incubation with even high doses of MitoPQ relative to baseline levels (Figure 3.10E-F). This is in contrast to the positive control of the extracellular application of hydrogen peroxide which induced a large increase in the 405/488 nm ratio of the cytosolic targeted sensor CytoOrp.

Taken together, we therefore conclude from this body of evidence that both MitoPQ and MitoPQ control compound 2 are fit for purpose as tools with which to investigate the roles of mitochondrial superoxide levels.

MitoNeoD tissue uptake for *in vivo* validation

In order that we can use MitoNeoD to assess mitochondrial superoxide levels *in vivo*, it is necessary that we can measure the levels of both the original compound and its products so that we can normalise for differing levels of uptake. In initial experiments this was not possible due to variable oxidation during the extraction procedure, and so after optimisation of the method we performed the extraction in the presence of chloranil. This is a mild oxidising agent and so will oxidise any remaining MitoNeo to MitoNeoD whilst leaving the specific superoxide reaction product MitoNeoOH unchanged. We then normalise the quantity of MitoNeoOH detected to the sum of MitoNeoD and MitoNeoOH, which corresponds to the total quantity of MitoNeoD that was taken up into the mitochondria under the assumption that excretion is negligible.

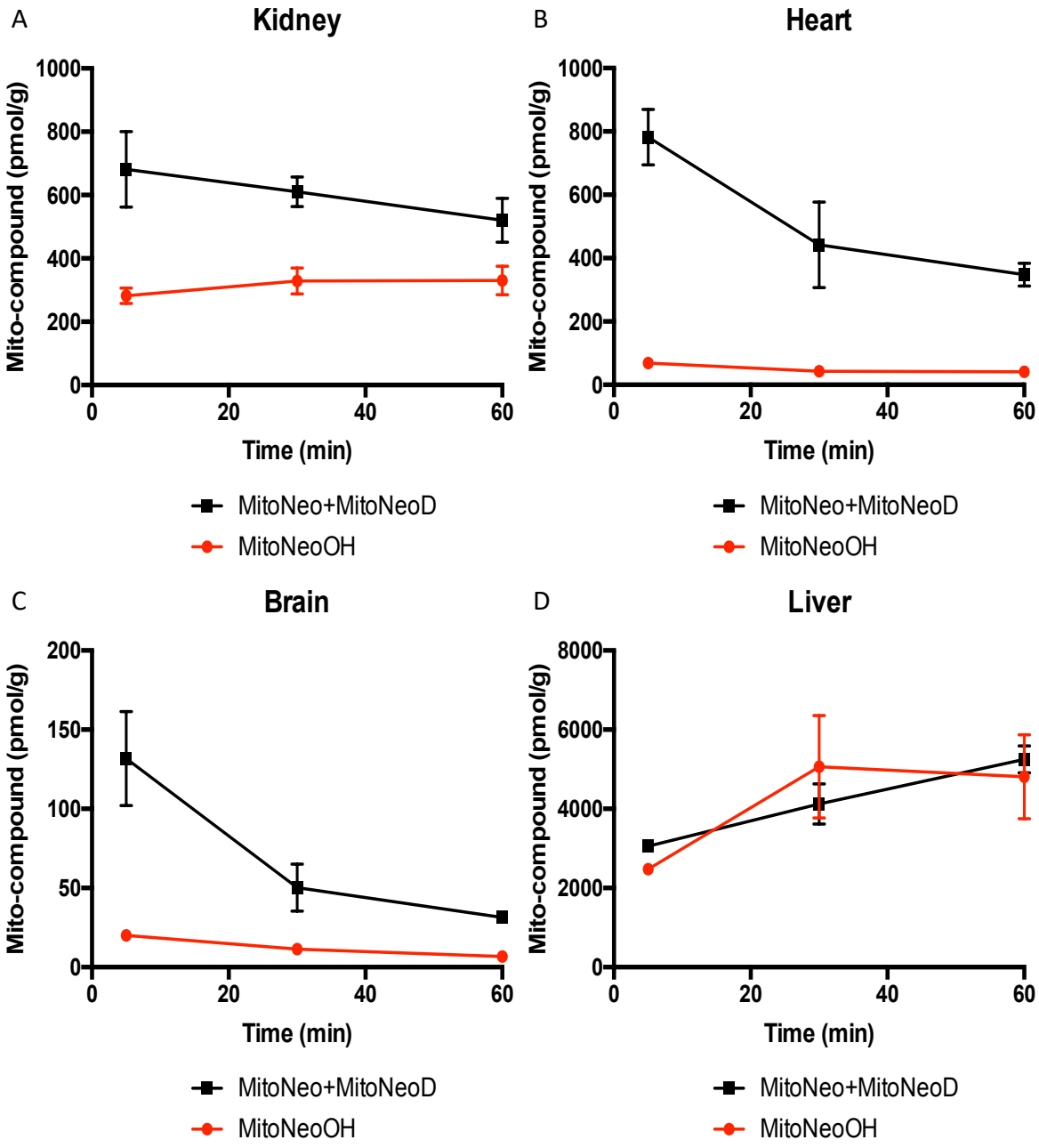


**Figure 3.11 MitoNeoD is taken into tissues *in vivo* following i.v. injection.**

Mice were injected with 25 nmol MitoNeoD into a lateral tail vein and were euthanized for collection of tissues at the indicated timepoints. These were snap frozen in liquid nitrogen in order to quench any further reaction. MitoNeo and its derivative compounds are observed in the kidney (**A**), heart (**B**), brain (**C**) and liver (**D**).

*n = 3*

T. Prime (MRC-MBU) is thanked for her help with the mass spectrometry extractions of the tissue samples. Mass spectrometry was performed by A. Logan (MRC-MBU).

Following i.v. injection into a lateral tail vein, we saw rapid uptake of MitoNeoD into all of the tissues assessed, which is then lost slowly over time with a half life of ~1 hour (Figure 3.11A-D). The quantities of MitoNeoD and its derivative compounds was observed to be markedly different between different tissues (for example after 5 min there is 850 ± 100 pmol/g of all MitoNeo compounds in the heart compared to 5536 ± 162 pmol/g in the liver). In part this variation reflects physiological differences in uptake – most notably in the brain where capillaries lack fenestrations and therefore the compound must travel through epithelial cells in order to move between the circulation and the tissue environment. Similarly since uptake is driven by the inside negative membrane potentials of the mitochondria, higher uptake was also expected in tissues containing a higher volume of mitochondria, such as the liver and the heart. However extraction efficiency also varies between tissues which makes interpretation of these comparisons problematic, with a greater loss of the compounds expected in fibrous tissues such as the heart (Figure 3.11B) compared to softer tissues such as the liver (Figure 3.11D) which fits with the data observed here.

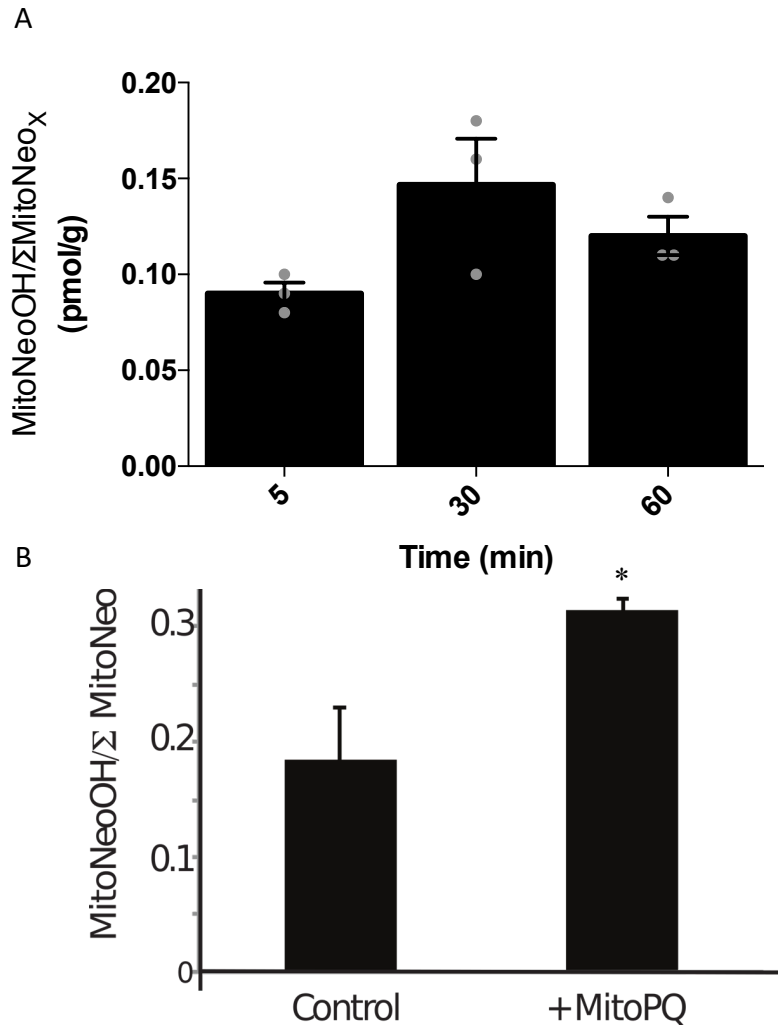


**Figure 3.12 Measurement of superoxide formation by MitoNeoD after administration *in vivo.***

**A.** Shows data from the same experiment as in Figure 3.11B, with the ratio of MitoNeoOH/MitoNeo+MitoNeoD corresponding to the quantity of superoxide produced within the mitochondria. However the fact that this decreases between 30 – 60 min indicates that the compound is lost from the tissue since the reaction to form MitoNeoOH should not be reversible under biological conditions.

**B.** Mice were injected with a solution containing 2.5 nmol MitoNeoD along with 2.5 nmol MitoPQ to cause exogenous production of superoxide within the mitochondria. Compared to vehicle only control, co-injection with the mitochondrial superoxide generator MitoPQ causes a significant increase in superoxide production which is detectable by MitoNeo).

*n = 3, one-way ANOVA and Student's t-test.*

T. Prime (MRC-MBU) is thanked for her help with the mass spectrometry extractions of the tissue samples for panel A. Mass spectrometry was performed by A. Logan (MRC-MBU).

Superoxide production under endogenous conditions was assessed in the heart after MitoNeoD administration, however we did no observe a significant increase in superoxide production (Figure 3.12A), perhaps indicating that the quantity of superoxide produced under normal physiological conditions was insufficient for a positive control. We therefore co-administered MitoNeoD with MitoPQ to mice to determine if exogenous superoxide specifically within the mitochondria by MitoPQ can be detected using MitoNeoD. MitoNeoOH (and thus mitochondrial superoxide) levels were low in hearts of mice treated with vehicle only control, but we detected a marked increase in the ratio of MitoNeoOH over all MitoNeo compounds within heart tissue (Fig 3.12B). This indicated that MitoNeoD can be successfully used *in vivo* as a probe to measure mitochondrial superoxide levels.

MitoCDNB *in vivo* validation

MitoCDNB was administered to mice as a bolus injection into a lateral tail vein in order to assess the viability of its use as a tool to disrupt mitochondrial thiol homeostasis *in vivo*.

Our data confirm that when administered to a living animal MitoCDNB was taken up into a range of tissues, including the liver, kidney, and heart measured here. In a similar fashion to other TPP conjugated compounds (Chouchani et al., 2013) within 60 min the majority of MitoCDNB and its glutathione reacted product MitoGSDNB was cleared from the blood (Figure 3.13B). The breakdown product MitoCysDNB accumulated in the blood more slowly, which is consistent with its excretion from tissues after uptake and metabolism of MitoCDNB. MitoCysDNB then appeared to be removed from the body in the urine, and was observed in spot urine samples collected at the 24 hour time point (Figure 3.13C).

**Figure 3.13 Uptake of MitoCDNB into tissues *in vivo.***

Mice were injected i.v. with 5 mg/kg MitoCDNB, culled at the time points indicated and tissues were collected to determine the accumulation of MitoCDNB and its derivative compounds by LC-MS/MS. **A.** Liver **B.** Blood. **C.** Urine at 24 hours **D.** Liver mitochondria levels **E.** Kidney **F.** Heart.

*n = 4*

Mass spectrometry was performed by A. Logan (MRC-MBU).

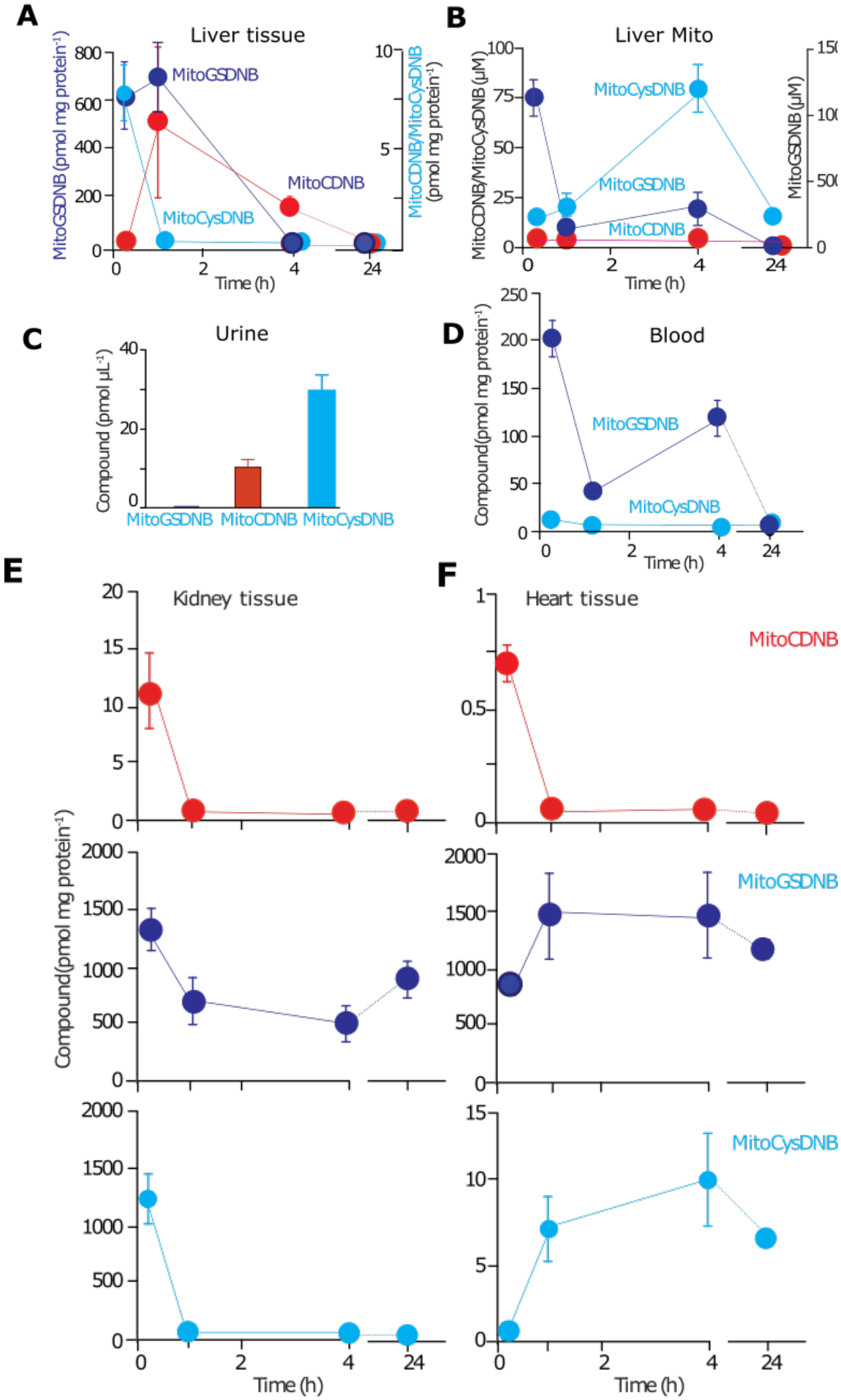
A
Liver tissue
MitoGSDNB (pmol mg protein⁻¹)
MitoCDNB/MitoCysDNB (pmol mg protein⁻¹)
MitoGSDNB
MitoCDNB
MitoCysDNB
Time (h)
B
Liver Mito
MitoCDNB/MitoCysDNB (µM)
MitoGSDNB (µM)
MitoCysDNB
MitoGSDNB
MitoCDNB
Time (h)
C
Urine
Compound (pmol µL⁻¹)
MitoGSDNB MitoCDNB MitoCysDNB
D
Blood
Compound(pmol mg protein⁻¹)
MitoGSDNB
MitoCysDNB
Time (h)
E
Kidney tissue
Compound(pmol mg protein⁻¹)
Time (h)
F
Heart tissue
MitoCDNB
MitoGSDNB
MitoCysDNB
Time (h)

The kinetics of the uptake of MitoCDNB and its conversion to MitoGSDNB and then MitoCysDNB were surprisingly heterogeneous in different tissue types. Analogously to MitoNeoD it is not possible to compare the absolute values measured between different tissues due to differing extraction efficiencies depending on the tissue makeup, but their relative time courses may still provide insight. The liver was slow to accumulate MitoCDNB with peak levels observed at 1 hour post injection (Figure 3.13A), whereas both for the kidney (Figure 3.13E) and the heart (Figure 3.13F) MitoCDNB had reached its zenith 5 minutes after injection.

In both the kidney and the heart, we observed an accumulation of MitoGSDNB at all time points up to 24 hours. This is consistent with the fact that once within cells, MitoCDNB is rapidly converted to MitoGSDNB by reaction with GSH. Unlike MitoCDNB this is membrane impermeant, and so remains within the mitochondria until it is excreted from the cell. In contrast to the other tissues, MitoGSDNB levels in the liver had greatly decreased by 4 hours compared to the 5 minute time point (Figure 3.13A). This is likely to be mediated by the glutathione S-conjugate export pump (Ishikawa, 1992), and is consistent with significant expression of these transporters in hepatocytes due to their function in allowing the removal of oxidants and other electrophilic compounds after detoxification by glutathione (Lee et al., 1997).

Further conversion to breakdown product MitoCysDNB may then occur outside the cell catalysed by enzymes on the extracellular face of the plasma membrane (Zhang et al., 2005). Intriguingly, unlike the time course in the liver or kidney these data show that there is no initial accumulation of MitoCysDNB in the heart (Figure 3.13F). Data from Booty and colleagues (2019) show that a similar accumulation of MitoGSNB is seen *in vitro* in C2C12 muscle myotubes but not in HepG2 hepatocytes. Using LC-MSMS a product scan was performed on culture media from these cell types to examine for precursor ion that gave rise to a fragment of 188 m/z, which is diagnostic of the TPP cation and thus indicates a metabolite of MitoCDNB. The analysis of these compounds suggested that MitoGSDNB is metabolised as shown in Figure 3.14. This first step of this is catalysed by a γ-glutamyl transpeptidase, (GGT) which interestingly are found to be highly expressed on the extracellular membrane face of liver cells (Zhang et al., 2005) and were shown to be necessary for that conversion of MitoGSDNB to MitoCysDNB by the use of an inhibitor (Booty et al., 2019). Further work is required in order to confirm if there is a relative lack of expression of GGTs in the heart that could also account

for the comparative lack of accumulation of MitoCysDNB in the heart that we observed in the heart in our experiments.

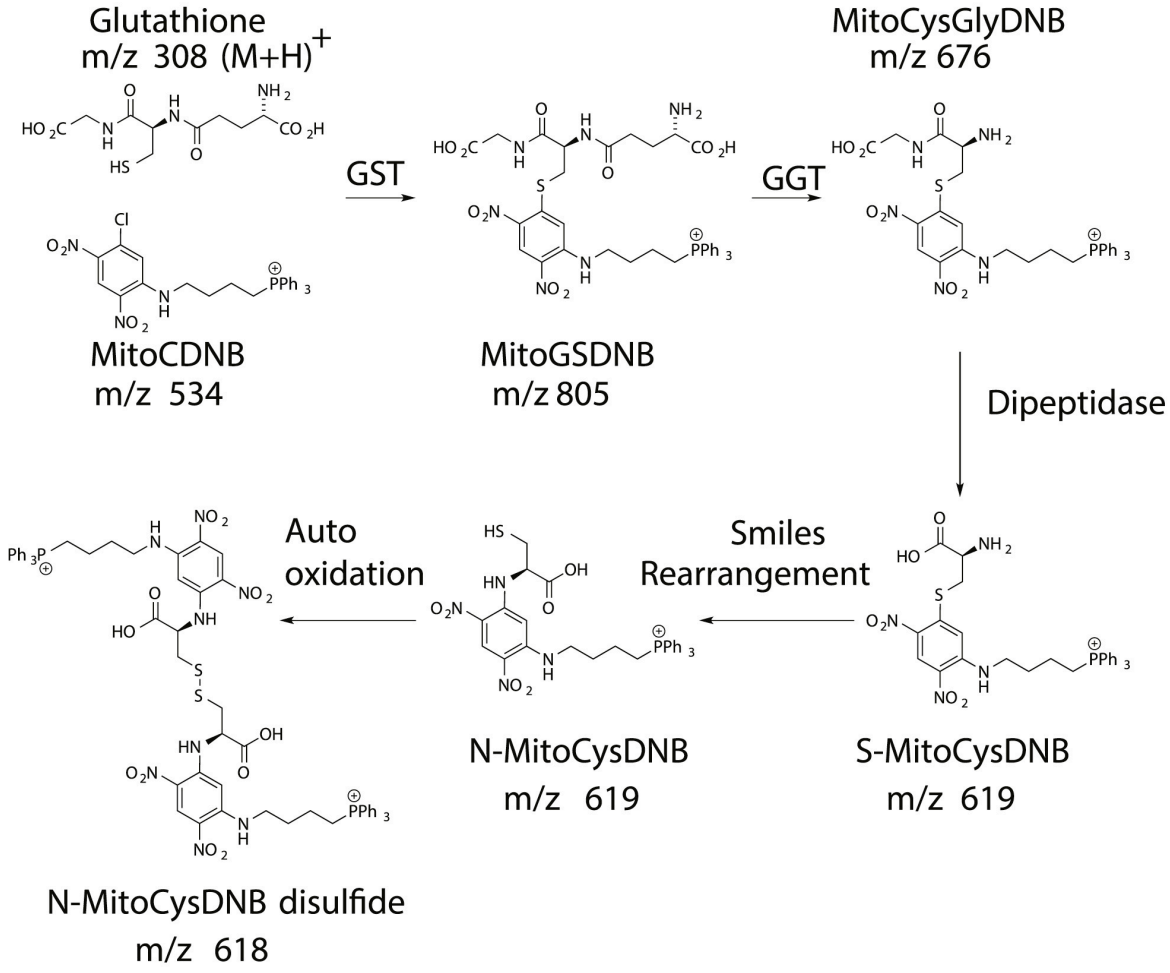


**Figure 3.14 Schematic of MitoCDNB metabolism.**

Within the cell, MitoCDNB reacts with glutathione, catalysed by glutathione-S-tranferase (GST) to form MitoGSDNB. This is membrane impermeant, and so remains within the cell unless it is actively excreted. In the extracellular space, MitoGSDNB has a glutamyl unit removed by a γ-glutamyl transpeptidase (GGT) which are abundant in the extracellular face of hepatocytes but not in all other tissue types. A dipeptidase then removes a glycine unit from MitoCysGlyDNB to form S-MitoCysDNB. This then undergoes spontaneous Smiles rearrangement to form the N-MitoCysDNB which contains a free thiol. As such this can then auto-oxidate to give the corresponding disulphide N-MitoCysDNB disulfide.

After Booty et al. (2019)

Consequences of MitoCDNB Uptake

The accumulation of MitoCDNB within tissue of the liver and kidney was shown to result in depletion of GSH within the mitochondrial fraction (but not whole tissue extracts) within 24 hours, which had returned to baseline levels by 7 days (Figure 3.15A and B respectively). Glutathione measurements were expressed relative to time of day matched controls to account for the diurnal variations in glutathione levels in both the wider cell and in the mitochondria specifically (Blanco et al., 2007). The time course of glutathione depletion in the heart was considerably slower, with mitochondrial GSH only showing depletion after 7 days (Figure 3.13C), which suggests that MitoCDNB metabolism may be different in the heart compared with other tissues.

In addition to causing depletion of mitochondrial glutathione, MitoCDNB also acts to inhibit TrxR. We were able to measure a significant decrease in TrxR activity in mitochondria isolated from liver tissue at 1 hour, 4 hours and 24 hours compared to baseline values (Figure 3.15E) which had with normal TrxR activity re-established by 7 days. It is interesting that inhibition was still seen at 24 hours since by this timepoint we could only detect very small quantities of MitoCDNB and its derivative compounds remaining in the tissue (Figure 3.13A). We can speculate that this may therefore reflect the relative stability of the MitoCDNB adduct on the active site selenol of TrxR. No difference in TrxR activity was measured in whole tissue extracts at any of the time points measured (Figure 3.15E).

The fact that mitochondrial glutathione levels had returned to baseline by 7 days in the liver and kidney suggest that there is an orchestrated compensatory response from the rest of the cell. For this reason, we measured both protein and mRNA levels of glutamate cysteine ligases (the rate limiting enzyme in the glutathione synthesis pathway) and found that they were both elevated at 24 hours (Figure 3.15D). We similarly observed increased level of glutathione synthetase (Figure 3.15D). Since these are both nuclear encoded genes, such an increase in expression levels is indicative of a retrograde signal from the mitochondria to the nucleus.

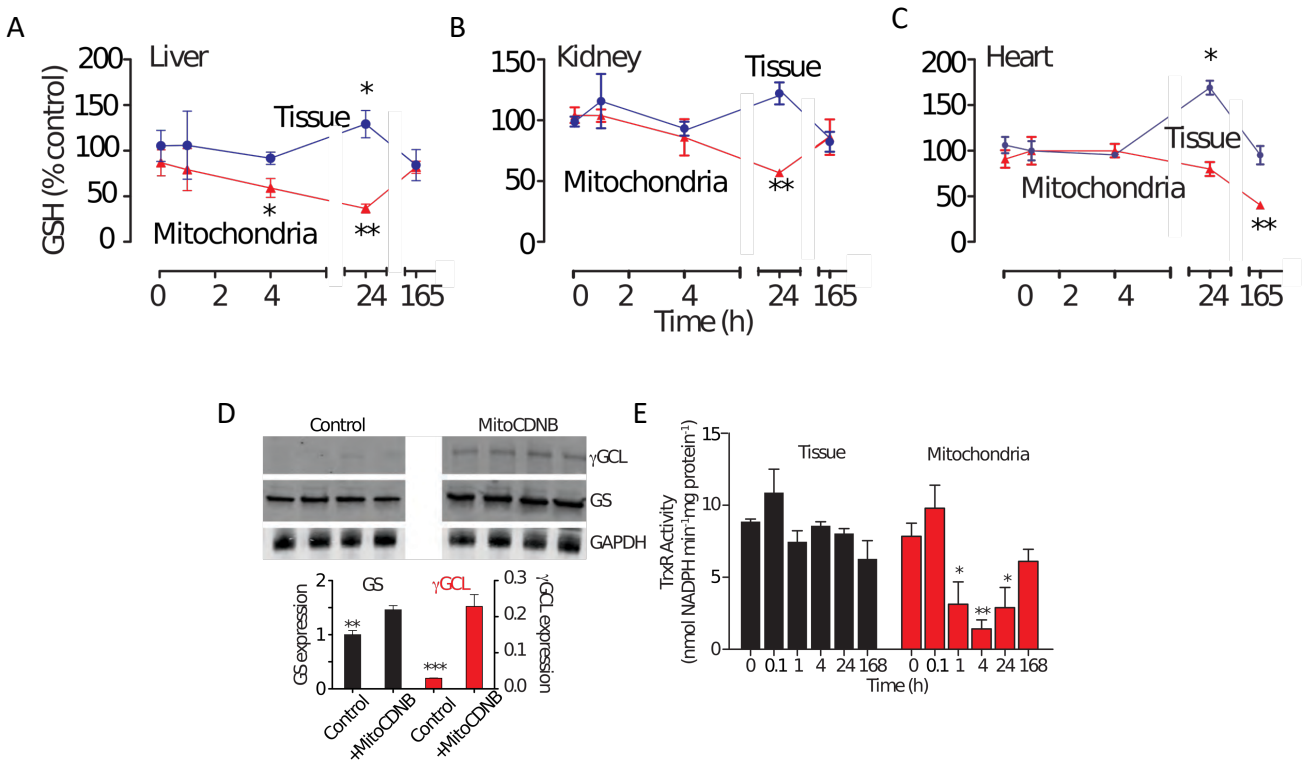


**Figure 3.15 Consequences of *in vivo* administration of MitoCDNB upon redox balance.** Mice were administered with 5 mg/kg MitoCDNB. **A-C.** Either whole cell or mitochondrial GSH was measured in liver, kidney and heart tissue collected from mice culled at the times indicated, expressed relative to time of day matched uninjected controls. **D**. Expression levels of γ-glutamylcysteine ligase (γGCL) and glutathione synthetase (GS) in liver at 24 hours post injection. Each lane is a separate biological replicate. This data is quantified relative to GAPDH. **E.** Effect on TrxR activity in liver tissue and mitochondria.
*n = 5 (A-C) or 4 (D-E). One-way ANOVA performed separately for mitochondrial and tissue measurements, with Tukey-Kramer used for comparisons to the time zero baseline.*
These assays were performed by L. Booty (MRC-MBU, University of Cambridge)

In order to examine this in more detail, we performed a proof of principle experiment using RNAseq to identify the response of the transcriptome following administration of MitoCDNB. We identified a rapid and widespread transcriptional response to an acute disruption of mitochondrial thiol redox state as demonstrated by the volcano plot (Figure 3.16A). This is much more marked at 1 hour compared to 4 hours post injection, particularly so for the 20 most up- or down-regulated genes shown in the heatmap (Figure 3.16B). Multivariate statistics also indicated an orchestrated acute transcriptional response from the nucleus, with clear separation

of the 1 hour MitoCDNB treated mice from all other groups along component 1 in a principal component analysis (Figure 3.16C).

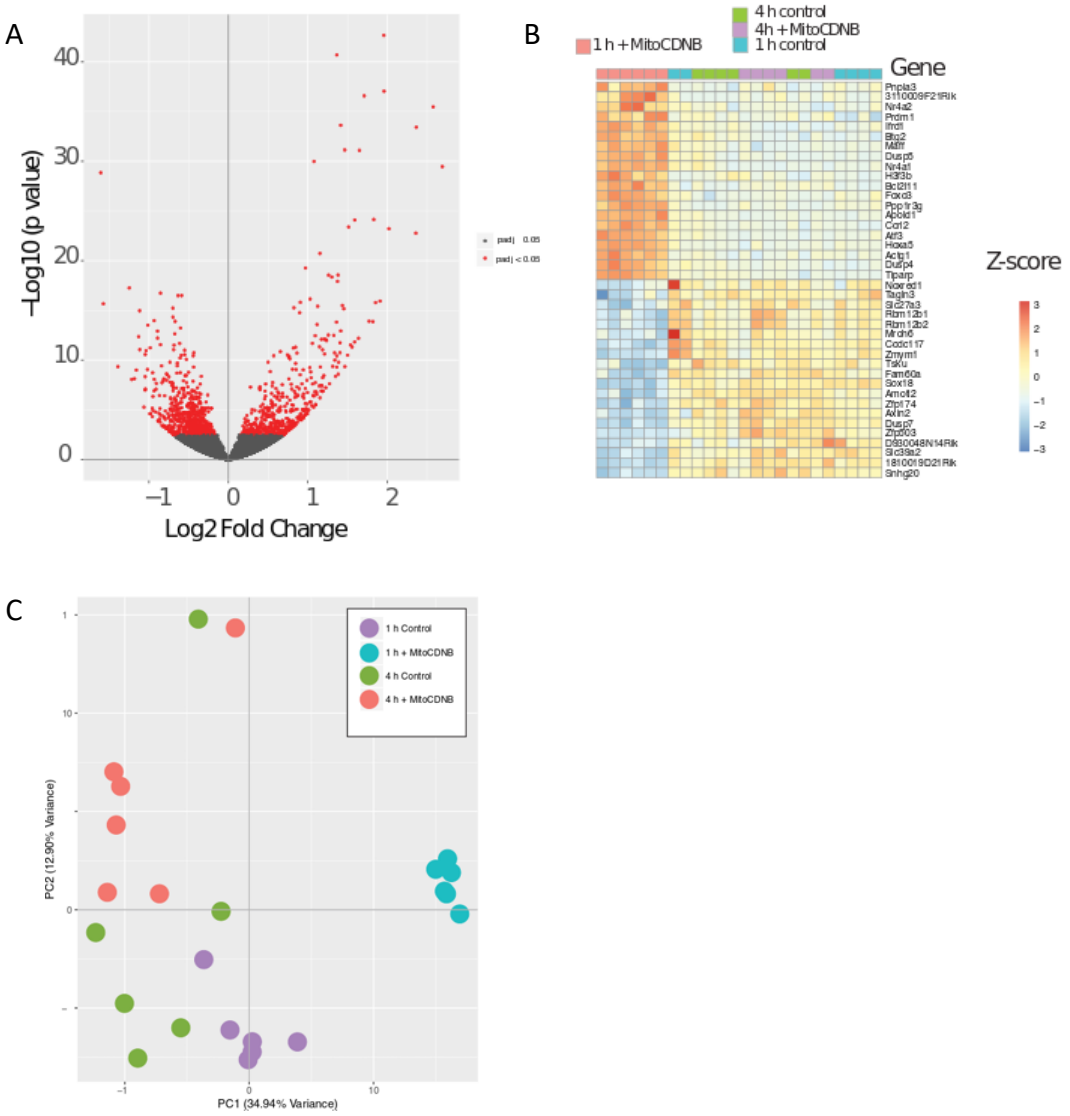


**Figure 3.16 Consequences of MitoCDNB upon the transcriptome.**

Mice were administered with MitoCDNB or vehicle only control and at the times indicated mice were culled and the liver collected for whole transcriptome analysis by RNAseq. **A**. Volcano plot showing a significant change in gene transcription induced by MitoCDNB at 1 hour after injection relative to vehicle only control. **B.** Heatmap showing the change in expression of the 20 most up- and down-regulated genes induced by MitoCDNB at 1 hour after injection relative to vehicle only control. **C**. Principal Component Analysis showing the effect of treatment with MitoCDNB or vehicle at both 1 hour and 4 hour post injection, performed using the 500 genes whose expression was most altered.

*n = 5*

Data analysis was performed by F. Cvetko (MRC-MBU, University of Cambridge)

## Discussion

### Dose dependent production of reactive oxygen species by MitoParaquat

The data that we present here validate with a high degree of confidence that MitoPQ causes a dose-dependent production of ROS within the mitochondria but not the cytosol. As discussed when introducing MitoNeoD, current technologies that we can use to measure ROS levels are not without their disadvantages but the use of multiple orthogonal methods which all demonstrate that ROS production by MitoPQ is dose-dependent suggests that we can have a high degree of confidence that this is actually the case.

### Validation of a bespoke control compound

Despite their established use as a method of targeting molecules to the mitochondria TPP-linked compounds have been shown to have a small degree of off-target effects. They have for example been found to increase mitochondrial calcium in some *in vitro* experiments through inhibition of the $Na^+$(or $H^+$)/$Ca^{2+}$ exchanger (Leo et al., 2008), although this effect was smaller with the conjugated molecule than with TPP alone. Inhibition of this antiporter results in reduced efflux of calcium from mitochondria and thus passive accumulation due to the negative membrane potential and actions of the MCU, as summarised in Figure 3.17. TPP linked molecules may also increase mitochondrial uncoupling by increasing proton leak: either directly by cycling between the matrix and the intermembrane space, or by interaction with proteins in the inner mitochondrial membrane (Smith et al., 2011). There are also reports of a direct effect of TPP on cellular bioenergetics by inhibition of oxidative phosphorylation by both the TPP moiety and the alkyl chain (Reily et al., 2013).

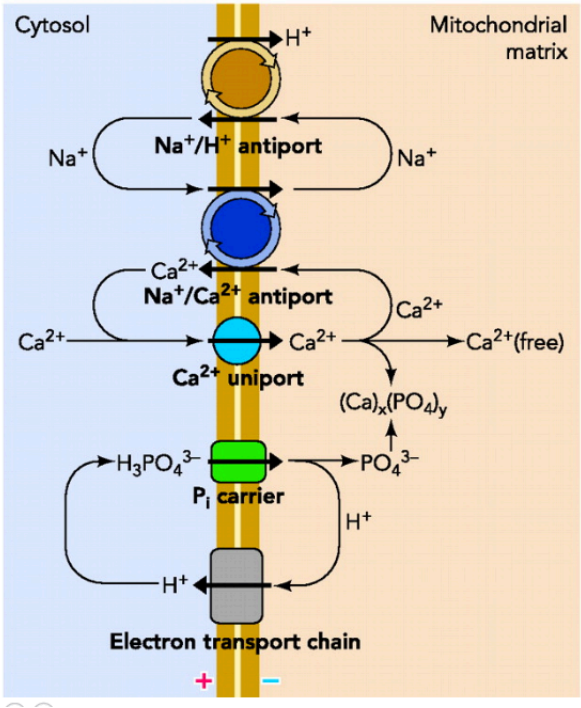


**Figure 3.17 Role of the sodium/calcium antiporter in mitochondrial calcium homeostasis.** TPP has been reported to inhibit the $Na^+/Ca^{2+}$ antiporter. Such an effect reduces calcium efflux from the mitochondrial matrix, allowing its passive accumulation through the mitochondrial $Ca^{2+}$ uniporter due to the electrochemical gradient. Reproduced from (Szabadkai and Duchen, 2008).

The magnitude of these effects is minimal where they have been reported, but nevertheless it is desirable to compare the effect of MitoPQ to a control compound possessing chemical properties as close as possible to those of MitoPQ but without the ability to redox cycle. Previous approaches have used either the TPP cation alone or conjugated just to an alkyl linker.

MitoPQ control compound 2 is validated in cells and in isolated mitochondria as a bespoke negative control that accumulates to similar levels within the mitochondria but does not produce ROS to any significant extent. This means that implicit assumptions that off-target effects are either non-existent or insignificant no longer have to be made.

Data shown here indicate that MitoPQ control compound 1 still causes significantly more ROS production than vehicle only controls. Both MitoPQ control compound 1 and MitoPQ control

compound 2 do not redox cycle at complex I which is the location where MitoPQ produces superoxide. We unexpectedly found however that MitoPQ control compound 1 does cause a degree of ROS production in the mitochondria. The mechanism by which MitoPQ control compound 1 produces ROS is unknown, and to determine this is beyond the scope of this project. It may however act as a fortuitous control for non-specific mitochondrial ROS production (i.e. not occurring by superoxide generation at complex I) rather than its intended role as a non-ROS producing control compound. This property is utilised in chapter 4 when investigating the role of ROS in IRI.

The uptake into mitochondria was found to be significantly higher for both MitoPQ control compound 1 and MitoPQ control compound 2 than MitoPQ, but it seems that this is an inevitable consequence of the structural alterations required to prevent redox cycling. It is interesting to note is that the uptake of MitoPQ itself in the first place is not Nernstian – an unexpected finding reported by Robb et al. (2015) - and instead has kinetics consistent with uptake as a monocation rather than the dication that it is. This is unusual for TPP conjugated compounds and suggests that MitoPQ may be transported across the membrane complexed with an anion: most likely to be chloride due to its quantitative dominance in biological fluids. It is a distinct but unexplored possibility that this hypothesised ion pairing is altered in MitoPQ control compound 1 and 2 due to the additional separation between the pyridine rings and that this could account for its greater uptake, but again to explore this further is beyond the scope of this work.

Inability to measure tissue levels of MitoParaquat

The uptake of mitochondria-targeted compounds like MitoPQ into cells and then mitochondria is dependent upon membrane potential and other factors which must be assumed to remain constant between experimental replicates. It was therefore desirable to directly measure the mitochondrial concentrations of compounds in order to further the precision with which we can deliver exogenous ROS. Paraquat is however difficult to detect by mass spectrometry, and so the same is true for MitoPQ. We have been unable to solve this either by reduction of the PQ moiety or by the use of an inclusion compound (data not shown). These are designed to cage the PQ moiety and so prevent it from reacting with other small molecules in the mass spectrometer. This would allow detection of the compound via the TPP moiety and

hydrocarbon linker. Tissue levels could then be compared to a known concentration of a deuterated internal standard added to samples prior to extraction in order to allow absolute quantitation. Similarly we were unable to assess mitochondrial levels directly within tissues, as TPP-conjugated compounds are lost during mitochondrial isolation protocols. Nevertheless the extensive set of control experiments carried out here in order to validate ROS production both inside and outside the mitochondria by a range of different methods still allows a high degree of confidence in the ability to precisely titrate additional exogenous ROS using MitoPQ.

MitoNeoD *in vivo* validation

MitoNeoD was developed to address the unmet need for a method to specifically measure mitochondria superoxide. This followed on from the development of MitoB/MitoP as an exomarker to measure mitochondrial hydrogen peroxide; an approach that is now widely used. Similar to the need for MitoPQ, it is worth stressing the utility provided by MitoNeoD in measuring superoxide as the proximal ROS species rather than estimating its effects from downstream markers.

Our experiments here successfully demonstrate proof of principle for the use of MitoNeoD *in vivo*, successfully detecting an increase in superoxide production following injection with MitoPQ. The dose of MitoPQ used here was higher than that reported elsewhere in this thesis. We speculate here that the requirement for the high dose of MitoPQ is likely to reflect the conceptual difficulties described in the introduction to this chapter of detecting a species that is so rapidly scavenged: an inherent problem for all probe-based approaches used to detect superoxide. Future experiments might use a higher concentration of MitoNeoD in order to aid its competition with SODs.

It is worth highlighting two inherent drawbacks of the use of MitoNeoD *in vivo*. First, the mass spectrometry-based approach involves destruction of tissue and so prevents serial measurements being taken in small animals such as mice where biopsy is impractical. As discussed it can and has also been used as a fluorescent indicator (Shchepinova et al., 2017) though with the trade-off that specificity towards superoxide is reduced. Secondly, the mass spectrometry approach also entails that we time-average superoxide levels between the point at which MitoNeoD is taken up into the relevant tissues and the point at which we cull the

animal in order to collect tissue. The kinetics of TPP-conjugated compounds between the point of injection and their uptake into tissues are rapid, especially in mitochondria rich tissues such as the heart and liver, but nonetheless make the use of MitoNeoD in this way unsuitable for studying particularly acute changes such as are commonly investigated in settings like ischaemia reperfusion injury where rapid ROS production is occurring within the first few seconds of reperfusion.

A limitation of the protocol used to harvest organs during the experiments reported here is that we are unable to distinguish between the intracellular pool of the compound, that in the extracellular fluid and that in the blood perfused within the tissue. Since the reaction between MitoNeoD and superoxide occurs rapidly, a trade-off must be made between quenching any further reactions by freezing tissues as soon as possible and using methods such as *ex vivo* perfusion of organs in order to remove any blood that is present in their circulatory systems. It is worth noting that the kinetics of loss of MitoNeoD from the intracellular pool in such situations are unexplored, but is expected to be not insignificant given that TPP conjugated compounds including MitoNeoD are generally observed to be lost from tissues over time and appear in the urine as demonstrated in this chapter for MitoCDNB. An alternative approach might be to attempt to measure the level of MitoNeoD and its derivative compounds in the extracellular fluid directly such that tissue levels can be experimentally corrected for. One potential method to do this would be using a microdialysis catheter, which are widely used in the brain and have been reported to allow metabolite concentrations to be determined in the heart (Kavianipour et al., 2003).

MitoCDNB *in vivo* validation

MitoCDNB was originally conceived as a ‘lock in’ compound for mitochondria in order allow the measurement of mitochondrial volume, with the rationale that it would be modified by glutathione within the mitochondria to form a membrane impermeable product. However testing soon showed that MitoCDNB was not an inert ‘bio-orthogonal’ compound, but rather had a range of consequences within the mitochondria. MitoCDNB therefore has pleiotropic effects due to the similarity of the chemistry involved in a range of glutathione regulating systems. As reported here this allows its use *in vivo* to investigate acute changes to mitochondrial redox state brought about by disruption of the glutathione and thioredoxin

systems. Work is currently underway for the design and validation of a control compound for MitoCDNB, which in a similar vein to MitoPQ control compound 2 will aim to act as a control for any potential off-target effects of both the 1-chloro-2,4-dinitrobenzene and mitochondrial targeting moieties.

Does MitoCDNB have potential for translation to a therapy?

In addition to the development of a tool for general use, MitoCDNB is also interesting from the perspective of the heart in and of itself, as disruption of mitochondrial thiol redox state has been implicated in the development and progression of cardiomyopathy. Mutation in TrxR2 has been described in patients with dilated cardiomyopathy (Sibbing et al., 2011), and thioredoxin1 has been shown to regulate cardiac hypertrophy in small animal models (Ago et al., 2008; Liu et al., 2015; Yamamoto et al., 2003; Yang et al., 2011). It is thus of specific interest to the pathology of heart disease as well as in a range of other conditions (Murphy, 2012).

There is also a growing interest in targeting the glutathione system in anti-cancer therapy. TrxR expression has been shown to be elevated in many types of cancer (Urig and Becker, 2006), and is suggested to play a major role in drug resistance including the mitochondrial Trx2 isoform (Coronnello et al., 2005) that is inhibited by MitoCDNB. Elevated glutathione levels have also been reported in many tumours, and this has been shown in interfere with the action of many existing cancer drugs (Balendiran et al., 2004). For example glutathione has also been shown to modify platinum containing drugs such as cis-platin that are commonly used in chemotherapy: by either binding directly to the drug or to the platinum-DNA adducts (Britten et al., 1992; Winter et al., 2000). Furthermore, using a combination of glutathione depletion and exposure to chemotherapeutic drugs has been shown to achieve differential responses in normal and malignant cells (Chen et al., 1998; Russo et al., 1986). These data therefore suggest that MitoCDNB might potentially be of interest to be used in combination with other cytotoxic drugs either in order to either increase their efficacy or to increase their selectively in inducing death tumour cells over healthy cells.

**Summary**

We present data validating the use of two different strategies with which we can alter redox balance specifically within the mitochondria *in vivo*. First, MitoPQ is shown to produce ROS within the mitochondria in a dose-dependent manner which will allow its use to investigate the paradoxical roles of ROS in myocardial IRI. MitoCDNB is also presented as a tool with which to bring about the opposite change of a decrease in mitochondrial redox state by disruption of the glutathione and thioredoxin systems.

MitoNeoD is also presented as a probe with which to specifically measure mitochondrial superoxide concentrations, representing a key development over existing strategies that commonly do not do what they are claimed to do.

# Chapter 4 – Paradoxical reactive oxygen species in ischaemia reperfusion injury

## Introduction

### Role of reactive oxygen species in ischaemia reperfusion injury: a therapeutic opportunity?

As discussed in the general background, the damaging role of ROS in IRI is robust and well investigated. Given that we have a plethora of compounds available that are known to act as antioxidants, the hypothesis logically presents itself that the administration of these compounds might abrogate the damage caused during IRI, thus leading to better clinical outcomes.

This hypothesis would also seem to be supported by epidemiological data. Firstly, dietary fruit and vegetable consumption is well described to have large positive effects upon both the risk and mortality of cardiovascular disease (Aune et al., 2017). The mechanism by which the consumption of fruit and vegetables brings about these benefits is less clear, but the most common hypothesis is that their beneficial effect is at least in part due to their high content of bioactive compounds such as vitamin C, vitamin E and beta-carotene which may act as antioxidants to counter the known role of ROS in the pathology of cardiovascular disease.

The use of antioxidants to counter heart disease would also seem to be supported by epidemiological correlations between antioxidant levels and mortality due to ischaemic heart disease in patients (Nagel et al., 1997). Both this evidence and that from other fields such as cancer (Toyokuni et al., 1995) and aging (Harman, 1992) has lead to the simplistic idea that ROS are bad and antioxidants are good permeating into popular culture, but yet the scientific validity of the concept remains an open question.

### Antioxidants as therapy in myocardial IRI?

The use of dietary antioxidant supplements in an attempt to improve the outcome of major cardiovascular events has been tested in large-scale clinical trials. Several such large-scale placebo-controlled intervention studies have now been conducted with the majority finding no beneficial effect. Ye et al. (Ye et al., 2013) conducted a recent meta-analysis on the effect of supplementation with vitamin E, beta-carotene or vitamin C on major cardiovascular outcomes. Using data regarding >12,000 major cardiovascular events from 188209 patients they find no significant effect compared with placebo on any reported outcome. Likewise Fortman *et al.*

found no evidence that supplementation with vitamins including the antioxidants vitamin C, vitamin E and vitamin A has any beneficial effect upon cardiovascular disease, and indeed showed that beta-carotene actually increased cancer risk in smokers (Fortmann et al., 2013).

Despite a seemingly sound theoretical basis, the data on the use of antioxidants against IRI are equivocal. Several possible explanations have been suggested for the failure of antioxidants to improve cardiovascular or other health outcomes. First, it does remain a possibility that the antioxidants used in these trials were not administered in such a way as to adequately counteract the ROS produced during a pathology such as IRI. The antioxidant compounds used in these trials (all of which are already found as naturally occurring antioxidant compounds) have a very little specificity with regard to the particular ROS that they detoxify. Similarly, they are not targeted to a specific cellular location meaning that their ability to, for example, nullify ROS generated within the mitochondria at reperfusion may be limited. There could also be an issue with the timing with which they are applied, with most being administered on a chronic and not acute basis.

A more intriguing possibility that has increasing support from the basic science literature is that effective scavenging of ROS might exactly be the problem itself. ROS are increasingly being understood to play a role in not just pathology but also in normal physiology. Under such a paradigm, low levels of ROS might be actively beneficial despite their damaging effects at high concentrations and thus effective scavenging will also prevent these beneficial effects in addition to counteracting the detrimental ones.

"Good" versus "bad" roles of reactive oxygen species

A diverse range of cellular processes have now been shown to involve or be effected by redox signalling, including for example but by no means limited to the cell cycle (Sauer et al., 2001), cell proliferation (Kim et al., 2001), apoptosis (Li et al., 2003), and intercellular communication (Liang, 2018). Viewed through this lens the application of an untargeted antioxidant is likely to result in widescale dysregulation of these processes, and thus appears a much less enticing proposition. The evolutionary conservation of ROS signalling throughout multiple taxa also adds credence to the theory that it is a mechanism of plausible importance (Imlay, 2008; Wong and Shimamoto, 2009).

The current position in the field is well summed up by Holstrom and Finkel in their 2014 review, highlighting the apparent complexity and lack of understanding that we currently possess:

*'...from a biological point of view, it is beginning to look as if ROS are neither cellular heroes nor villains—but instead something that occupies that always entertaining, captivating and fertile middle ground.'* (Holmström and Finkel, 2014)

Further, there is some existing evidence that ROS might play a beneficial role in IRI specifically. Firstly, the protection conferred by ischaemic preconditioning has been shown to be blocked by the application of sufficient antioxidants (Dost et al., 2008). This has led to experiments showing that protection in cell models of anoxia/reoxygenation could be conferred by the addition of exogenous oxidants (Hoek et al., 1998). There are a few disparate reports of the addition of ROS being cardioprotective in isolated heart preparations (Tullio et al., 2013), although in one of these the authors explicitly note that they were unable to find a dose that was protective in an *in vivo* surgical model (Ytrehus et al., 1995).

Whilst the damaging effects of the high concentrations of ROS that are generated during reperfusion are well characterised and uncontroversial, it remains an open question whether low doses of ROS are actively beneficial *in vivo* and in particular this has yet to be determined in the setting of acute myocardial IRI. The development and validation of MitoPQ and its improved characteristics over other methods of ROS generation gives the opportunity for new insight into these processes.

<u>Aims and objectives</u>

- Validate that protection can be conferred by ROS in a model system of ischaemia/reperfusion injury
- Replicate this *in vivo*, and characterise the dose-response relationship
- Explore the role of timing in the ability of ROS to confer cardioprotection by administering MitoPQ either before ischaemia (analogous to ischaemic preconditioning) or at reperfusion (analogous to ischaemic postconditioning)

## Results

Protection in anoxia/reoxygenation

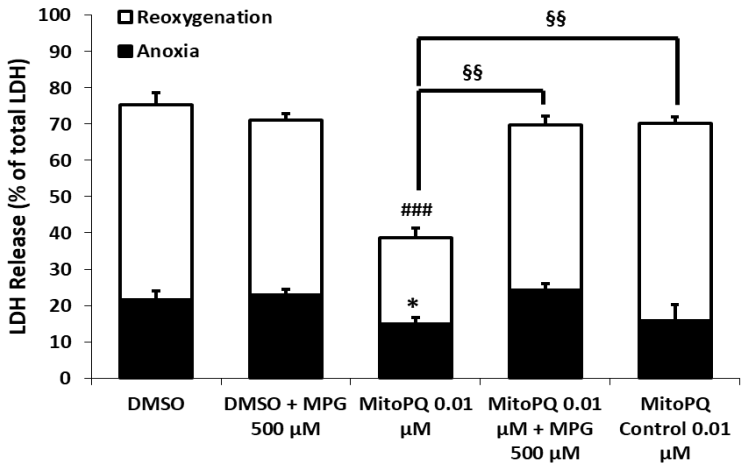


**Figure 4.1 Cell death in neonatal rat ventricular myocytes undergoing anoxia/reoxygenation.**

Cell death was measured by LDH release in NRVM cells treated for 2 hours with either 0.01 µM MitoPQ or 0.01 µM MitoPQ control compound 2, with or without the addition of 500 µM MPG**.**

*n = 3 biological replicates, each with 4-6 technical replicates*

**vs DMSO Anoxia, # vs DMSO Reoxygenation, § vs MitoPQ, one-way ANOVA with Tukey's HSD*

These experiments were performed by S Antonucci (University of Padua)

Reproduced from Antonucci, Mulvey et al 2019.

To determine proof of principle that the application of exogenous ROS by MitoPQ could be protective in IRI, we used a model of anoxia/reoxygenation in primary cultured neonatal rat ventricular myocytes. In this procedure, cells are subjected to 12 hours of anoxia in the presence of 2-deoxy-D-glucose and at reduced pH in order to mimic the conditions experienced by cardiomyoctyes in the heart when it undergoes ischaemia. We saw that compared to the vehicle-only control treatment, 0.01 µM MitoPQ decreased cell death at the end of anoxia as measured by LDH release (Figure 4.1; 21.6 ± 2.3 % total LDH and 14.8 ± 1.3 % total LDH respectively). This difference was much more dramatic after 1 hour of reoxygenation (Figure 4.1; 53.5 ± 3.3 % total LDH released after control treatment but only

23.7 ± 1.8 % total LDH with 0.01 μM MitoPQ), where similar to IRI the majority of cell death is found to occur. This protective effective could be abrogated either with great excess of the antioxidant N-(2-mercaptopropionyl)-glycine (MPG) present or when cells were treated with MitoPQ control compound 2 rather than MitoPQ, neither of which were significantly different from vehicle-only control. We therefore concluded that this protective effect was due to the superoxide production driven by the redox cycling of MitoPQ.

Protection in an *in vivo* model of acute myocardial infarction

Based upon these data we then used an *in vivo* surgical model of acute myocardial infarction in the mouse to examine if the effect could be recapitulated *in vivo*. In anaesthetised mice the thorax was opened to expose the heart and a snare placed around the left anterior descending coronary artery. This was then pulled tight in order to occlude the vessel and subject a large proportion of the left ventricular to a period of ischaemia: mimicking the tissue ischaemia found in STEMI patients in the clinic. By releasing the snare we were then able to reperfuse the tissue and use a double staining method to make acute measurements of the infarct size, expressed as a percentage of the area at risk.

First and foremost, it is noteworthy that MitoPQ delivered prior to the onset of ischaemia (mimicking the protocol of ischaemic preconditioning) reduced infarct size in a mouse model of acute myocardial IRI compared to vehicle-only control (Figure 4.2, 23 ± 2 % after 10 pmol MitoPQ and 41 ± 4 % with ethanol vehicle control). This protection was not seen if MitoPQ control compound 2 was administered instead (infarct size of 45 ± 3 % risk area), confirming that this protection was due to the capacity of MitoPQ to produce ROS within the mitochondria. Intriguingly MitoPQ control compound 1 was also found to not significantly different to the vehicle-only control (35 ± 2 %), despite the fact that this compound was shown to produce ROS within the mitochondria – albeit not by redox cycling at complex I. This suggests that the specific mode of ROS production might be of importance.

We further characterised the dose-response relationship of MitoPQ upon infarct size in myocardial IRI. MitoPQ was found to be lethal to mice undergoing the surgery at 10 nmol, 5 nmol and 2.5nmol, but protective at 1 nmol, 100 pmol and 10 pmol with infarct size reduced to 28 ± 4 %, 24 ± 3 % and 23 ± 2 % respectively. At an even lower the concentration of 1 pmol

MitoPQ, no protective effect was observed with infarct size not significantly different from vehicle only control (35 ± 8 %).

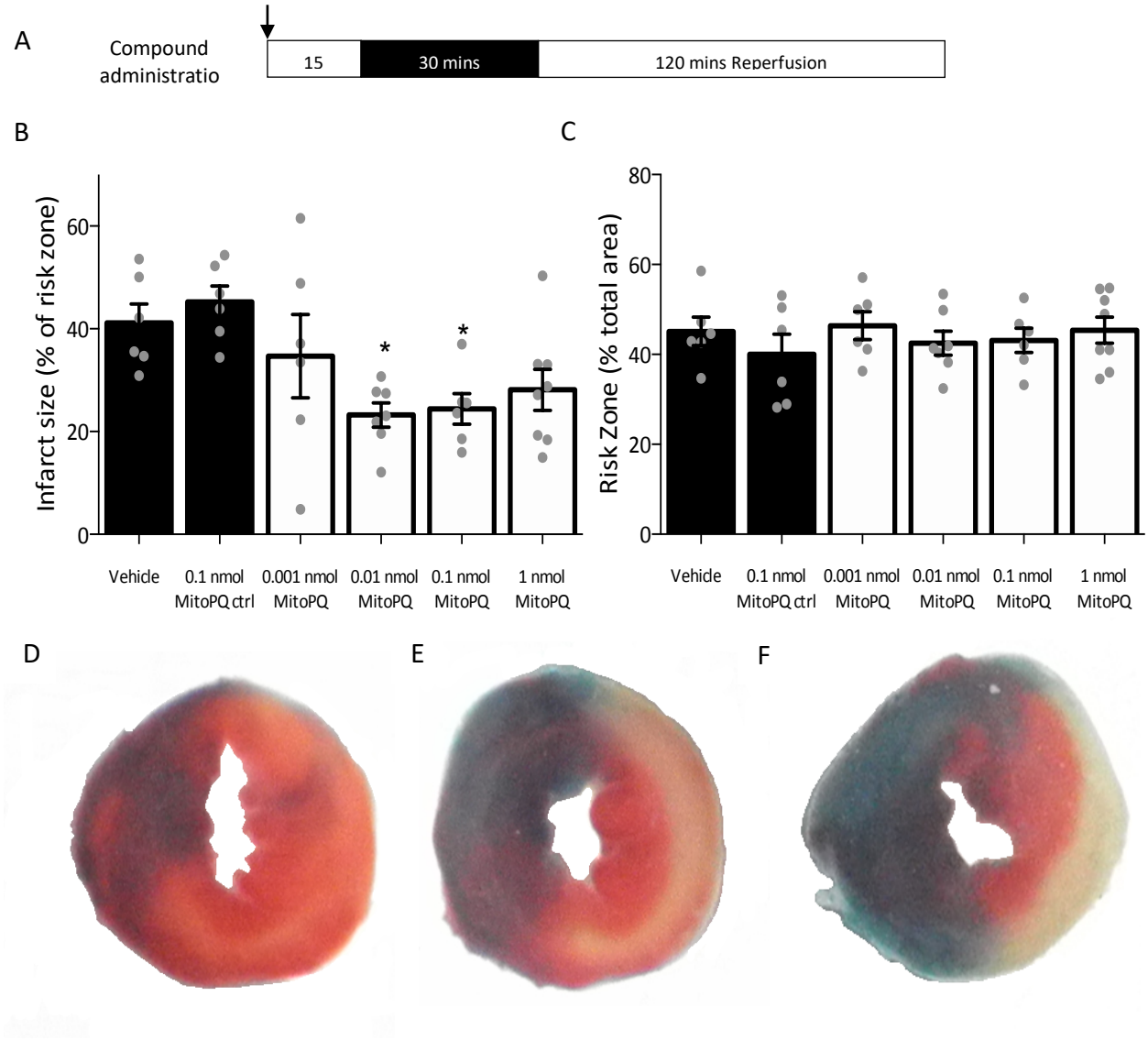


**Figure 4.2 Dose-response characterisation during *in vivo* acute ischaemia reperfusion injury.**

**A.** Experimental protocols. Mice underwent 30 minutes of ischaemia by LAD occlusion followed by 120 minutes reperfusion. In all groups an i.v. injection of a 100 µL bolus was administered 15 minutes prior to the onset of the index ischaemic period, containing either ethanol vehicle only control or the indicated compound.

**B.** Infarct size, shown as a percentage of the risk area. One-way ANOVA shows a significant effect of treatment, with 10 pmol MitoPQ and 100 pmol MitoPQ groups significantly different from the vehicle only control in post hoc testing with Tukey-Kramer.

**C.** The risk zone as a percentage of total area heart area below the point of ligation is not significantly different between any of the groups.
**D-F.** Representative infarct slices from the 100 pmol MitoPQ, vehicle and MitoPQ control compound 2 groups respectively are shown with other groups omitted for clarity.
*n = 6-8*

Figure 4.2B shows that throughout this experiment the size of the risk zone expressed as a percentage of total area was not significantly different between groups. This is an important control for the quality of the surgery since the anatomy of the mouse coronary circulation is variable and therefore producing a repeatable risk zone is technically challenging and indicative of the repeatable nature of the surgery that is being performed. As discussed in greater detail in the methods section, it is also important that as far as possible it is invariant between groups given its role as a potentially confounding variable.

Similarly, an experiment was performed using the well validated cardioprotective strategy of ischaemic postconditioning (a staccato reperfusion consisting here of 6 cycles of 10 seconds reperfusion and 10 seconds ischaemia), in order to validate the acute open-chest model of IRI in my hands. The LAD occlusion surgery is a technically challenging procedure to perform in a small animal such as the mouse, and there a multitude of opportunities to unintentionally protect the heart through the activation of pre-conditioning pathways. The small body mass and blood volume mean that even short periods of hypoxia (such as might occur during intubation) or small amounts of bleeding have proportionally large effects. Ischaemic postconditioning (22 ± 3 % of risk area) was shown to cause a statistically significantly smaller infarct size than the time-matched control group (Figure 4.3, 41 ± 4 % of risk area), whilst the risk zone was again invariant (54 ± 2 % of risk area and 48 ± 2 % of total area respectively). Furthermore, infarct sizes for both the vehicle only control group and the group which received the postconditioning procedure are in line with results previously produced by our laboratory (Methner et al., 2014).

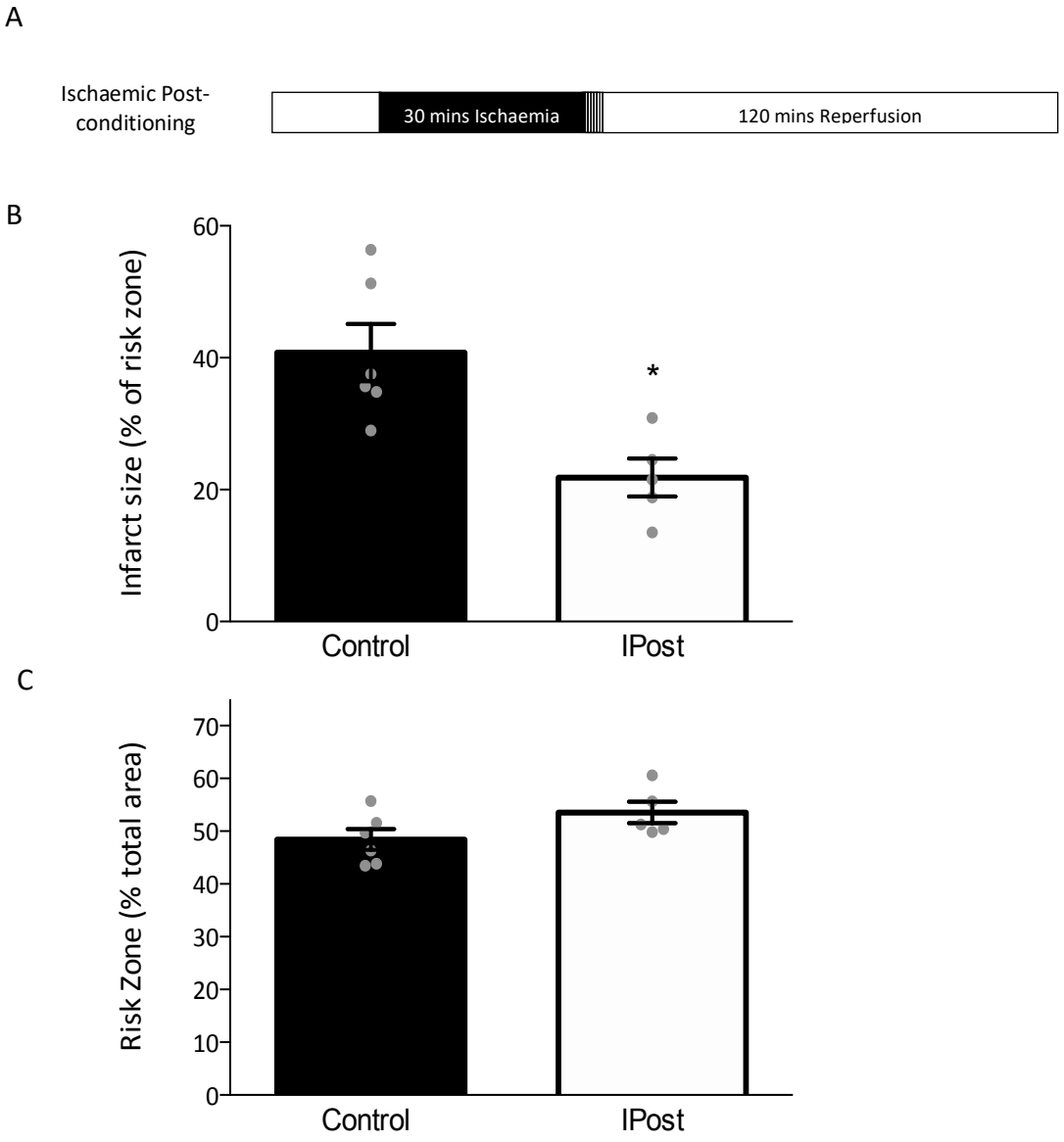


**Figure 4.3 Validation of the temporary LAD occlusion surgical model of acute myocardial infarction in the mou**se.

In order to validate the temporary LAD occlusion model in my hands, mice were subject to 30 min index ischaemia followed either directly by 120 min reperfusion (control group) or by 6 cycles of 10 s reperfusion, 10 s ischaemia and then 118 min reperfusion (IPost) such that total time after the index ischaemia was equal between groups. **A.** IPost caused a significant reduction in infarct size compared to the control group **B**. The risk area (a potentially confounding variable) was not significantly different between groups.

*n = 5-6, Students t-test*

Assessment of gross cardiovascular function after MitoParaquat administration

In order to confirm that the protection conferred by MitoPQ was not simply due to a reduction in cardiac work during the ischaemic period, left ventricular catheterisation was performed in a closed chest experimental model to assess the effect of MitoPQ on gross cardiovascular function. A catheter using admittance technology to measure volume and piezoelectric pressure sensing was inserted into the left ventricle via the right carotid artery in anaesthetised animals. Due to the number of parameters of cardiovascular function measured during these experiments, correction was applied to account for multiple testing using the Bonferroni-Sidák method. No significant difference was found in the fold change of any of the parameters measured following i.v. injection compared to before injection, compared between the most efficacious dose of MitoPQ in the infarct experiments (100 pmol) or vehicle only control solution (Table 4.1).

| | Vehicle | | MitoParaquat | |
|---|---|---|---|---|
| | mean fold change | SEM | mean fold change | SEM |
| Cardiac output | 1.17 | 0.15 | 1.13 | 0.22 |
| Heart rate | 1.00 | 0.00 | 0.98 | 0.00 |
| Ejection fraction | 1.00 | 0.04 | 0.99 | 0.05 |
| Stroke volume | 1.17 | 0.15 | 1.15 | 0.23 |
| End systolic volume | 1.15 | 0.17 | 1.23 | 0.16 |
| End diastolic volume | 1.10 | 0.13 | 1.12 | 0.18 |
| End systolic pressure | 1.01 | 0.03 | 0.98 | 0.02 |
| End diastolic pressure | 1.32 | 0.34 | 1.30 | 0.28 |
| Stroke work | 1.13 | 0.14 | 1.06 | 0.23 |
| Mean pressure | 1.05 | 0.05 | 1.02 | 0.04 |
| Developed pressure | 0.99 | 0.00 | 0.97 | 0.01 |
| dP/dt_max | 0.91 | 0.05 | 0.86 | 0.03 |
| dP/dt_min | 0.98 | 0.05 | 0.88 | 0.03 |
| dV/dt_max | 1.27 | 0.30 | 1.24 | 0.25 |
| dV/dt_min | 1.34 | 0.27 | 1.10 | 0.25 |
| Pressure at dV/dt_max | 1.03 | 0.23 | 1.08 | 0.28 |
| Pressure at dP/dt_max | 0.97 | 0.01 | 0.93 | 0.01 |
| Volume at dP/dt_max | 1.17 | 0.12 | 1.15 | 0.21 |
| Volume at dP/dt_min | 1.19 | 0.18 | 1.24 | 0.16 |

**Table 4.1 Effect of MitoParaquat upon gross cardiovascular function.**

A closed chest experimental model was used to assess the gross effect of MitoPQ upon gross cardiovascular function *in vivo*. An admittance pressure-volume catheter was inserted into the left ventricle via the right carotid artery, and following equilibration measurements were taken before and 5 minutes following injection of 100 pmol MitoPQ into a lateral tail vein. No significant difference is observed in the fold change of any parameters following i.v. injection, compared between MitoPQ or vehicle only.

*n = 4, Student's t-test with Bonferroni-Šidák correction for multiple comparisons.*

Complex I activity

Complex I has recently been shown to be the key site of ROS production at reperfusion, with a critical cysteine residue modulating the re-activation of the complex from the deactive state that it enters whilst it is inactive during ischaemia (Chouchani et al., 2014). Previous experiments identified that this residue can be subject to range of oxidative modifications, with the nitrosylating compound MitoSNO conferring protection to the heart by slowing the re-activation of the complex in this way. We thus hypothesised that this might be the mechanism by which MitoPQ acts. Heart tissue samples were collected from mice undergoing IRI using the LAD occlusion model, which were snap frozen and then examined *in vitro*. Complex I activity was found to be reduced after 30 minutes compared to baseline values (Figure 4.4A), with an increase seen after 5 minutes of reperfusion. Using a differential labelling method to determine the state of the complex, we determined that this decrease in function is due in part to an increase in the proportion of complex I in the deactive state during the ischaemic period (Figure 4.4B). Quantitatively however it seems unlikely that this is the major mechanism for the large difference in the activity of the complex that we observed. Administration of MitoPQ during the IRI protocol however caused no significant difference in complex I activity at any of the time points measured compared to vehicle only control (Figure 4.4A). Similarly, experiments using bovine heart mitochondrial membranes which induced the deactive conformation with a period of metabolic inactivity showed that incubation with MitoPQ caused no difference in the activity of the complex in either the active or deactive states (Figure 4.4B). We thus conclude that this is not the mechanism by which MitoPQ confers protection against IRI to the heart.

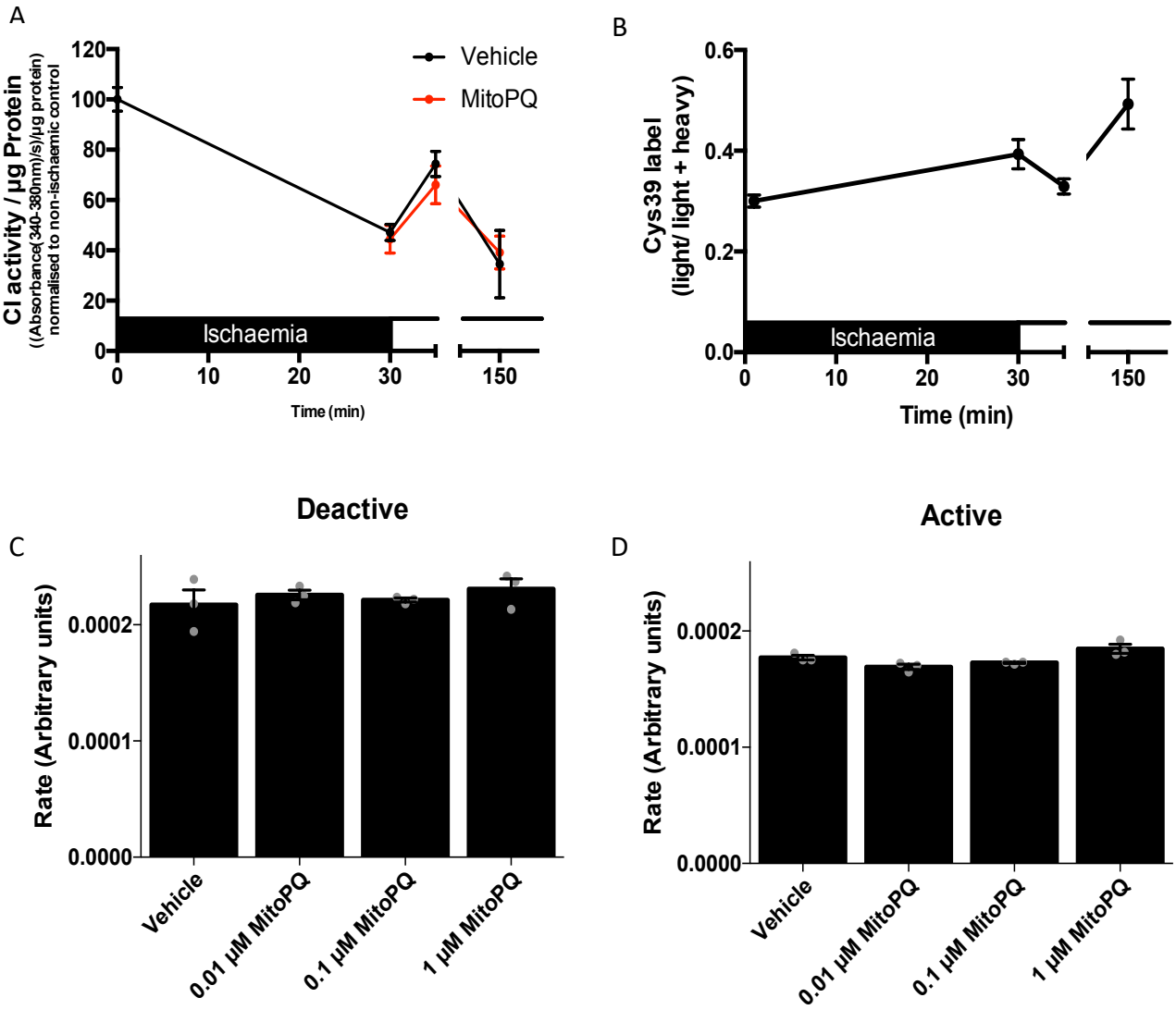


**Figure 4.4 Effect of MitoParaquat upon complex I activity in heart tissue samples from mice undergoing ischaemia/reperfusion injury.**

**A.** Complex I activity was measured via NAD fluorescence in tissue collected from the area at risk of ischaemia in hearts from mice undergoing acute myocardial IRI. Either 100 pmol MitoPQ or vehicle only control was administered i.v. 15 mins before the onset of ischaemia, with tissue clamp frozen for subsequent analysis.

*2-way ANOVA non-significant for both treatment (± MitoPQ) and risk vs non-risk factors and any interaction at both 30 min and 35 min timepoints.*

**B.** The same control samples were examined for complex I activity state using a differential labelling method for the Cys39 residue that is only exposed in the deactive complex. The changes in the activity assay are found to correlate inversely with the proportion of the compound in the active state.

**C-D**. Complex I activity was measured via NAD fluorescence in bovine heart mitochondrial membranes in which the complex was in an active (C) or deactive (D) states were induced by the presence or absence of respiratory substrates during 5 min pre-incubation.
*n = 3 biological replicates, each with 2 technical replicates*
These assays were performed by N. Burger (MRC-MBU)

MitoParaquat administered at reperfusion

Administering MitoPQ prior to the onset of ischaemia mimics ischaemic preconditioning, but previously published data also implicates the generation of ROS in the signal transduction pathways of ischaemic postconditioning (Cohen and Downey, 2015a). We therefore examined if MitoPQ administered immediately prior to reperfusion was able to protect the heart against IRI using the mouse model of LAD occlusion. MitoPQ was again seen to be able to generate a reduction in infarcts compared to vehicle only control (Figure 4.5B), albeit at different concentrations than that required for protection when given prior to the onset of ischaemia. Both the 10 pmol MitoPQ (17 ± 7 %) and the 1 nmol MitoPQ (26 ± 9 %) groups showed smaller infarcts compared to the vehicle only control (46 ± 2 %), while the 100 pmol group did not (35 ± 5 %). These experiments showed an increased variation in infarct size relative to the other reported here, which may be hypothesised to be due to the experimental protocol: MitoPQ was administered 1 minute prior to reperfusion. There is therefore a very short window between reperfusion of the tissue which allows uptake of MitoPQ into the area at risk, and the opening of the MPTP on a timescale of seconds to minutes which determines cell fate (Andrienko et al., 2016). This might be expected to amplify the effects of any errors in the delivery and uptake of the compound.

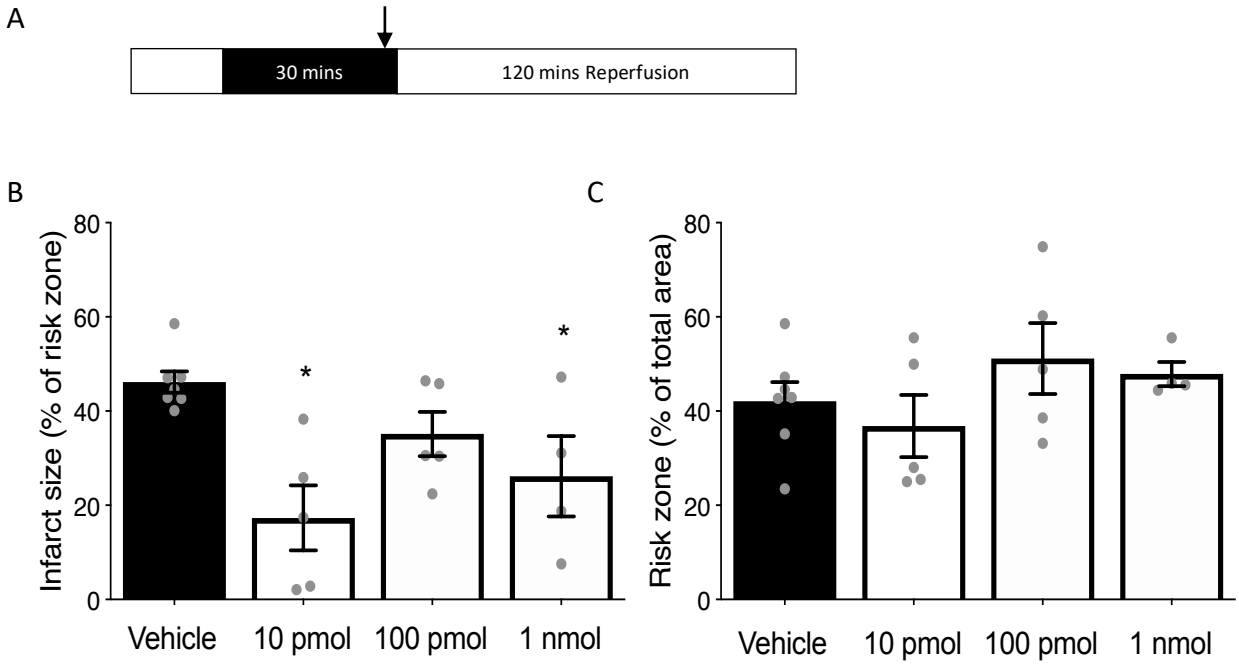


**Figure 4.5 MitoParaquat at reperfusion during *in vivo* acute ischaemia reperfusion injury.**

**A.** MitoPQ at the indicated dose or ethanol vehicle only were injected as a 100 µL bolus 1 minute prior to initiating reperfusion in mice undergoing a surgical model of regional cardiac IRI, before infarct size was assessment after 120 min reperfusion by a TTC and Evan's blue staining method to demarcate infarcted tissue and tissue that was non subject to ischaemia respectively.

**B.** Infarct size expressed relative to the risk zone was significantly different from the vehicle only control in both the 10 pmol and 1 nmol MitoPQ groups. It is of note that no difference was detected in 100 pmol group, which protected the heart against IRI when MitoPQ was administered prior to the onset of ischaemia as in Figure 4.2B.

**C.** The risk zone was not significantly different between any of the groups.

*n = 4-6, one-way ANOVA with Tukey-Kramer*

Effect of MitoParaquat upon cellular function

In order to elucidate the mechanism by which MitoPQ was able to protect the heart *in vivo* when administered at the correct dosage we conducted a range of experiments to measure its effects upon cellular function using primary NRVMs. Increasing doses of MitoPQ were found

to progressively decrease the mitochondrial membrane potential measured using TMRM (Figure 4.6A). Loss of membrane potential is well described as a consequence of MPTP opening (Hausenloy and Yellon, 2003) and ROS are known to play a role in its induction.

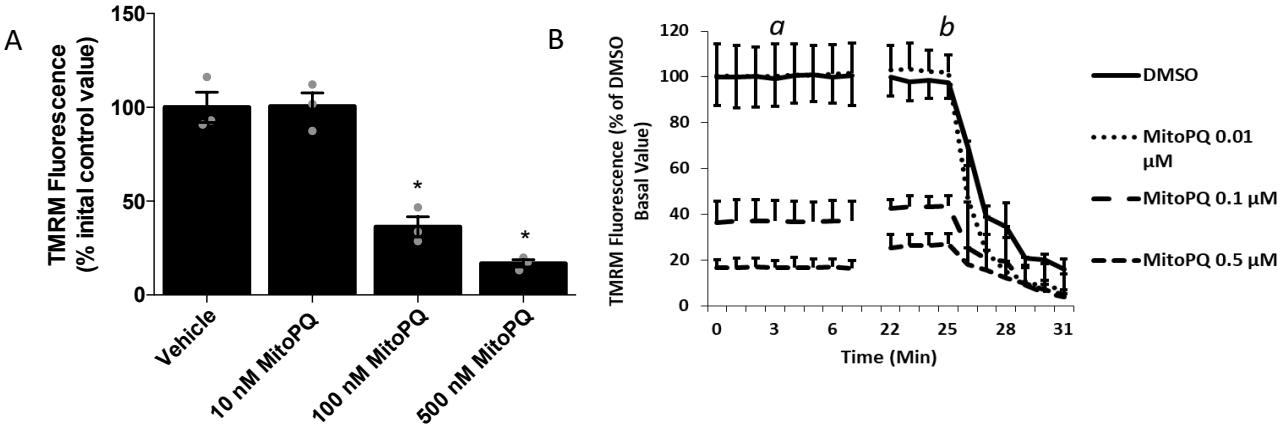


**Figure 4.6 Effect of MitoParaquat upon mitochondrial membrane potential.**

**A.** The effect of MitoPQ upon mitochondrial membrane potential was assessed via TMRM fluorescence following incubation of NRVMs for 2 hours with different concentrations of MitoPQ. **B**. Example traces, with 4 µM Oligomycin added at *a* in order to inhibit dissipation of membrane potential by reversal of the ATP synthase and 4 µM FCCP at *b* as a positive control to show the dissipation of membrane potential as the membrane is made permeable to protons.

*n = 3 biological replicates, each with 3 technical replicates and 6-10 cells measured per condition*

We thus hypothesised that MitoPQ might act upon the MPTP, which furthermore is a well identified cardioprotective target in the heart undergoing IRI (Bernardi and Di Lisa, 2015). We first measured LDH release to assay for cell death and found that whilst MitoPQ caused cell death at high concentrations, this could be blocked by treatment with the MPTP inhibitor cyclosporin A (CsA; Figure 4.7B). Similar protection against MitoPQ were achieved with an excess of the antioxidant molecule N-(2-mercaptopropionyl)-glycine (MPG), demonstrating the cell death induced was due to the ROS generated by MitoPQ (Figure 4.7A).

The induction of the MPTP by MitoPQ was also demonstrated by a direct assay for MPTP opening. Cells were loaded with calcein which fluoresces within the mitochondria, and so opening of the MPTP was measured as a decrease in signal due to its loss from the mitochondria

through the pore. We observed that MitoPQ induced MPTP opening, and that once more this could be abrogated by either inhibition of pore formation with CsA or treatment with excess MPG (Figure 4.7C). The ROS generated by MitoPQ therefore might act either directly upon the MPTP to induce opening of the pore or somewhere upstream of it.

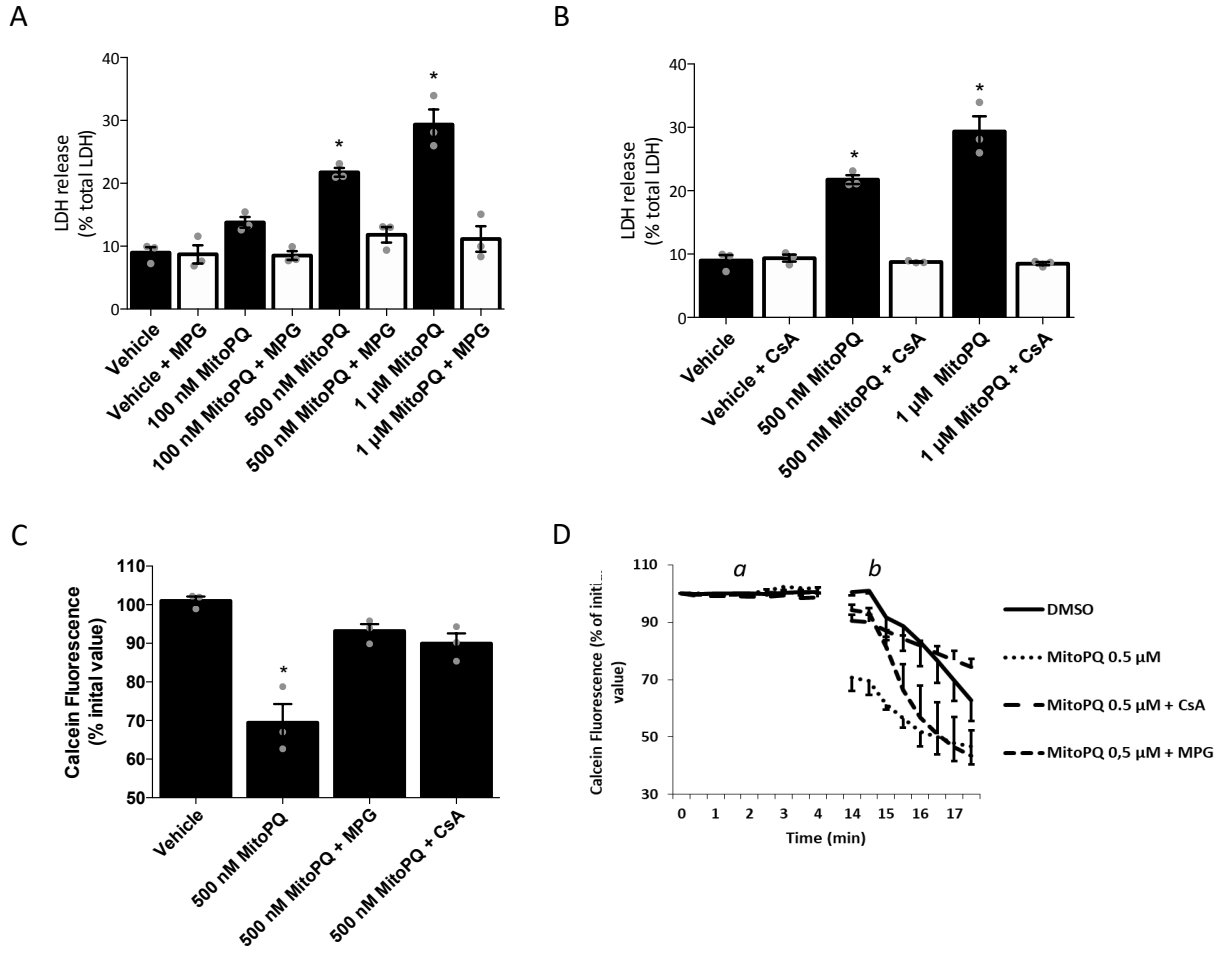


**Figure 4.7 Effect of MitoParaquat upon cellular viability in neonatal rate ventricular myocytes.**

**A-B.** Cell viability of NRVMs was monitored by LDH release in cells incubated for 24 hours with different concentrations of MitoPQ, both with and without the 500 µM of the antioxidant MPG or 1 µM of the mitochondrial permeability transition pore inhibitor Cyclosporin A (CsA). *n = 3 biological replicates, each with 4-6 technical replicates*

**C**. Mitochondrial Permeability transition pore opening was assayed, utilising a decrease in calcein fluorescence in cells when the pore opens which is then quenched in the cytosol. Measurements were taken 12 minutes after treatment with MitoPQ, following 30 min preincubation with or without the presence of 1 µM CsA or 500 µM MPG.

*n = 3 biological replicates, each with 3 technical replicates and 6-10 cells measured per replicate*

**D.** Representative traces showing the time course of changes in calcein fluorescence. *a*: addition of vehicle only control DMSO or 0.5 μM MitoPQ; *b*: 5 μM Calcimycin (a calcium ionophore) is added to as a positive control to induce MPTP opening

** vs vehicle only control*

These experiments were performed by S Antonucci (University of Padua)

There is a close interplay between ROS and calcium, with alternations in cellular calcium dynamics sufficient to drive IRI (Garcia-Dorado et al., 2012). We therefore measured the effect of treatment with MitoPQ upon cytosolic calcium homeostasis using the fluorescent dye Fluo-4. The first point of interest is that despite MitoPQ producing no ROS that we are able to detect within the cytosol (Figure 3.10), it does cause notable changes in calcium dynamics, both at baseline and following stimulation with caffeine (Figure 4.8A). Stimulation with caffeine induces transient calcium release by sensitising the ryanodine receptor and so allowing calcium-induced-calcium-release (Kong et al., 2008).

Low doses of MitoPQ (0.01 μM) caused an increase in the amplitude (Figure 4.8B) and area under the curve (corresponding to the total quantity of calcium released during each oscillation; Figure 4.8C) of spontaneous oscillations under unstimulated conditions, but had no effect on their frequency (Figure 4.8D). Medium doses of MitoPQ (0.05 μM) similarly increase the amplitude and area under the curve, but in contrast significantly reduce the frequency. Both caused an increase in the total quantity of calcium released into the cytoplasm from intracellular stores compared to the vehicle only control (158 ± 30 % vehicle control for the lose dose MitoPQ and 214 ± 32 % for the medium dose respectively). High doses of MitoPQ (0.1 μM) caused a loss of spontaneous calcium oscillations at baseline compared to the vehicle only control (Figure 4.8A). The small magnitude of the transient following caffeine stimulation suggests that caffeine sensitive calcium stores have been depleted (Figure 4.8B-C; amplitude of 31 ± 7 % of vehicle only control and area under curve of 44 ± 10 % control values). These deficits in calcium regulation are consistent with the data in Figure 4.6 which demonstrated that 0.1 μM MitoPQ induced significant loss of mitochondrial membrane potential and significant difference in cell death measured in the LDH release assay: consistent with widespread cellular dysfunction. Taken together, these data indicate that ROS originating

within the mitochondria have considerable effects beyond the mitochondria on the wider functioning of the cell.

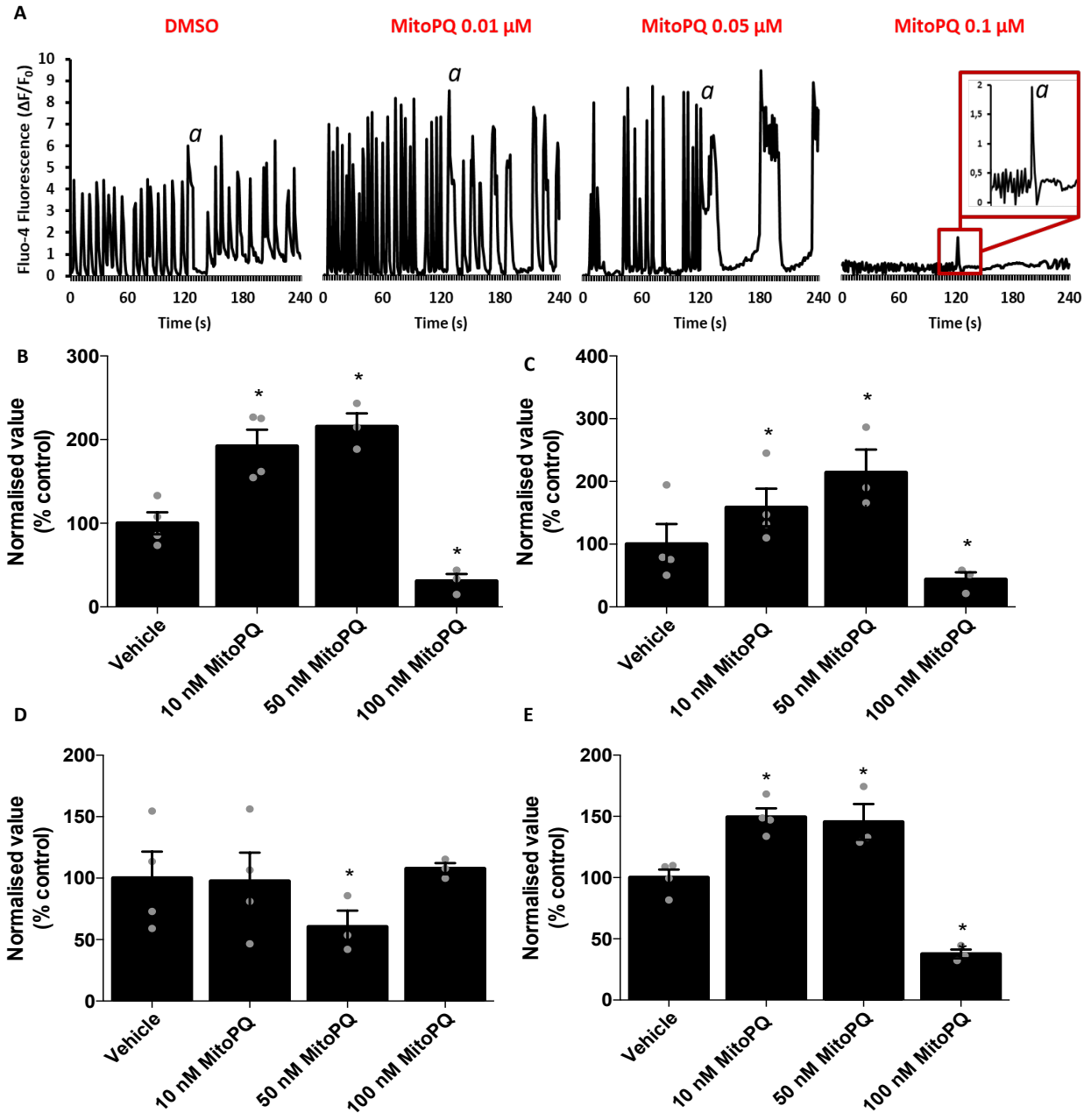


**Figure 4.8 Effect of a primary change in mitochondrial ROS caused by MitoPQ upon cytosolic calcium dynamics.**

Neonatal rat ventricular myocytes were loaded with the fluorescent indicator Fluo-4 AM and pre-treated for 4 hours with the indicated concentrations of MitoPQ. **A**. Example oscillatory patterns both at rest and following stimulation of intracellular calcium stores with 10 mM caffeine (*a*). These oscillations in the basal condition may be quantified by their **B**. amplitude **C.** area under curve **D**. frequency and **E.** the amplitude of the peak following caffeine stimulation. All data are expressed relative to the DMSO vehicle only control condition.

*n = 3-4 biological replicates, each with 3 technical replicates, * vs DMSO control*

These experiments were performed by S Antonucci (University of Padua)

## Discussion

### Cardioprotection by exogenous ROS

The data I present here show that the generation of small amounts of exogenous superoxide generated within the mitochondria by the bespoke compound MitoPQ can protect the heart against IRI, although only within a narrow dose range.

A considerable amount of work has been put in over the past few decades in order to establish a protocol of anoxia/reoxygenation in a cell system that successfully recapitulates the cellular milieu occurring during ischaemia/reperfusion injury. The system used here with NRVMs has been published several times, but there remain differences compared with what happens to the tissue *in vivo*. Most notably, cardiomyocytes are present as isolated cells rather than the situation in tissue where they are embedded within the extracellular matrix and can communicate with multiple cell types. These experiments in isolated myocytes therefore provide direct evidence that this effect is due the actions of ROS on the cardiomyocyte rather than other cell types within the heart, as we show that a cardiomyocyte only preparation is sufficient to replicate the results seen in the whole heart *in vivo*. This is important as there is evidence that ROS have effects on multiple cell types, including for example those in the microvasculature (Yu et al., 2019). Indeed the importance of non-cardiomyocyte cell types in the heart is an area which is receiving increasing amounts of attention (Wojtovich et al., 2013). There are also other differences between our *in vitro* system and the whole heart. In particular the ROS generated in cultured cells might be expected to be quantitatively different compared to similar doses of MitoPQ *in vivo*. The cells are cultured in an incubator with almost atmospheric oxygen levels, whereas the distribution of oxygen tensions within tissue (whilst technically challenging to measure) are significantly lower (Mik et al., 2009). The cells are also not beating, and thus the energetic requirements are vastly lower than in the ischaemic heart. Additionally, they are neonatal rather than adult cells and thus tend to be more plastic and able to adapt to environmental changes. Taken together, this means that in order to introduce a reasonable amount of damage our cell model requires 12 hours of anoxia (after which some 20% of cells remain living), whereas our *in vivo* model 30 mins of regional ischaemia is sufficient to cause a large amount of damage. Nevertheless we see here the same patterns of protection at low but not high doses of MitoPQ recapitulated in both systems despite

these differences, adding credence to our hypothesis that the protection by low doses of ROS is a robust phenomenon.

*Impact of MitoPQ upon cardiac functional parameters*

We note that treatment with MitoPQ caused no significant change in any of the parameters measuring gross cardiovascular function, which is sufficient to rule out that protection is due to changes in the work performed by the heart and thus its energetic needs during the IRI protocol. This is of particular importance given the known role of ROS in modifying muscle function. For example  show that in skeletal muscle exogenous ROS (there in the form of hydrogen peroxide) may either stimulate or inhibit contractile function depending upon the dose administered. In the IRI heart *in vivo*, heart rate has also been described as a key factor in the protective effects of lowering myocardial work during ischaemia (Heusch and Schulz, 2001).

The magnitude of the protection observed here is unlikely to be explained by small and not statistically significant changes shown here. Due to the format of this data with 19 parameters measured in 2 different experimental conditions, it is necessary to use statistical methods to control for multiple testing. Methods to control the false discovery rate rely upon an assumption that all the parameters are independent. This is not the case here, as many are interdependent due to intrinsic control mechanisms as described by the Frank-Starling relationship. As such, we control for the family wise error rate using the Sidak correction for to modify the alpha level for each of the t-tests that are performed in parallel.

It is also noting that we only examined for acute changes in gross cardiovascular function, with measurements collected approximately 5 minutes after administration of MitoPQ. This protocol was chosen due to wanting to measure load-independent parameters (e.g. end systolic elastance and preload recruitable stroke work) which can be derived from pressure-volume loops collected during transient decreases in preload such as be occlusion of the inferior vena cava. However technical problems prevented this data from being gathered in a repeatable manner. The catheter technology used here calculates volume of the ventricle based on changes in admittance and this means that (unlike the pressure measurements from the piezoelectric transducer) volume measurements are exquisitely sensitive to changes in the position of the

catheter within the left ventricle. If this is unable to be precisely replicated between experiments upon different animals, this changes the relative admittance contributions of the muscle and blood and thus alters volume measurements. Future experiments could use echocardiography derived volume measurements, which also gives the advantage of allowing direct visualisation of the catheter position within the ventricle.

Unfortunately, at the time of the experiments our home office licence did not allow the administration of an ionotrope such as the beta adrenergic receptor agonist dobutamine as a positive control, or for use as a stress agent administered in conjunction with MitoPQ. Examining heart function under conditions were the cardiac work is high often allows smaller differences in functional changes to be observed due to the fact that ejection fraction increases with increasing cardiac output (Ehsani et al., 1978), and is why stress echo tests are commonly used for diagnosis in humans. For the experiments presented here this is compounded by the fact that since the technology required a catheter to be inserted into the ventricle in an invasive procedure the animals needed to be maintained in a surgical plane of anaesthesia, which depresses the function of the cardiovascular system. Administration of an ionotrope would then have theoretically increased our power to detect differences, but since the aim of these experiments was to determine if there was a direct effect of MitoPQ on gross cardiovascular function in a similarly anaesthetised surgical model the presented methodology is sufficient for our purposes here.

It is somewhat difficult to reconcile these findings of no effect of MitoPQ upon gross cardiovascular function with the changes in cytosolic calcium dynamics observed in isolated NRVMs loaded with a cytosolic calcium indictor. There may be a variety of explanations that we can speculate may account for this unexpected difference. Most likely is the difference between the neonatal nature of the NRVMS compared with the mature cells in the adult mouse heart, but it is also possible that there could be influence of other cell types found in the myocardium or that the lack of an external contractile stimulus in the NRVMs might be responsible.

Evidence from the existing literature

In the existing literature there is a small body of evidence regarding a cardioprotective effect of exogenous ROS in IRI. Attempts to synthesise this research into a coherent theory are problematic due to the variety in experimental models, protocols and compounds, but a discussion of previous studies is nevertheless instructive.

Exposure to ROS before ischaemia (in a manner analogous to preconditioning) via either hydrogen peroxide (Ambrosio et al., 1992; Hegstad et al., 1997; Saotome et al., 2009; Tritto et al., 1997; Wang et al., 2014; Yaguchi et al., 2003) or a xanthine oxidase radical generating system (creating hydrogen peroxide and potentially superoxide under certain circumstances) in the isolated heart has been reported to be protective, in addition to evidence from isolated cardiomyocytes (Hoek et al., 1998). Others such as Baines et al. (Baines et al., 1997) find no effect of ROS applied likewise before ischaemia, and due to the publication bias against negative studies likely many more have found no effect. There is scarce data regarding the *in situ* heart, although (Tritto et al., 1997) report that they were unable to identify a protocol of ROS application that was protective following their positive *ex vivo* experiments. Our contribution shows for the first time *in vivo* that low doses of exogenous ROS may be cardioprotective.

The development and validation of MitoNeoD for us *in vivo*, represents an important technological development that can be used in future experiments in order to aid in the interpretation of such experiments by measuring the dose of mitochondrial superoxide directly. Work is already underway in our laboratory to measure superoxide production during IRI using mouse LAD surgical model with MitoNeoD, both with and without the administration of MitoPQ in order to determine the quantity of ROS generated by different doses of MitoPQ. Some care is needed in experimental design since MitoNeoD effectively integrates the amount of superoxide generated within the mitochondria between the time that it is taken up into a tissue and when the organ is harvested. This is especially relevant in the case of IRI, as the tissue is inaccessible to compounds administered via the blood until the moment of reperfusion – at which point changes occur rapidly.

Principles of biological signal transduction

In order to have a beneficial effect upon the heart, this exogenous ROS must be acting as a signal since it does not have inherent beneficial properties. In order to understand the

characteristics of the signal, it is necessary to be aware of the inherent properties required in such a process. Firstly, it must contain information: here the signalling of cardioprotective changes. There are several domains that biological information is commonly coded in: quantity, space and time. Next we must have the ability to turn a signal on, to turn it off, and ideally the ability to amplify it if required. Lastly, the signal must be able to be detected in order that the information contained within it can be decoded and acted on as appropriate.

These properties of signal transduction are all possessed by ROS, with its production via a number of potential mechanisms allowing the signal to be initiated. Similarly the scavenging of ROS would allow it to be switched off. Amplification of ROS has also been described, with 'ROS-induced ROS-release' now an accepted phenomenon (Zorov et al., 2000). We therefore now focus on the domain in which the ROS signal encoding the protection conferred on the heart by MitoPQ is encoded.

Signal coding in the dose domain: hormesis

Coding of the protective signal in the quantity of the ROS present is an attractive hypothesis as it is strongly suggested by the discrepancy between the protective effect of low doses of MitoPQ which is lost at higher concentrations. Such a phenomenon might also be used to explain the disparate findings in the literature that we have discussed: the direct application of ROS into the extracellular milieu is highly imprecise and the effective ROS concentration in the intracellular compartment is unknown, and as such it may be impossible to consistently deliver a precise enough dose to be able to observe statistically significant cardioprotection. MitoPQ however allows the dose of ROS applied to be controlled much more tightly than by any other methodology.

There are several different models that have, either implicitly or explicitly been used in previous literature to rationalise of the dose-response characteristic of ROS.

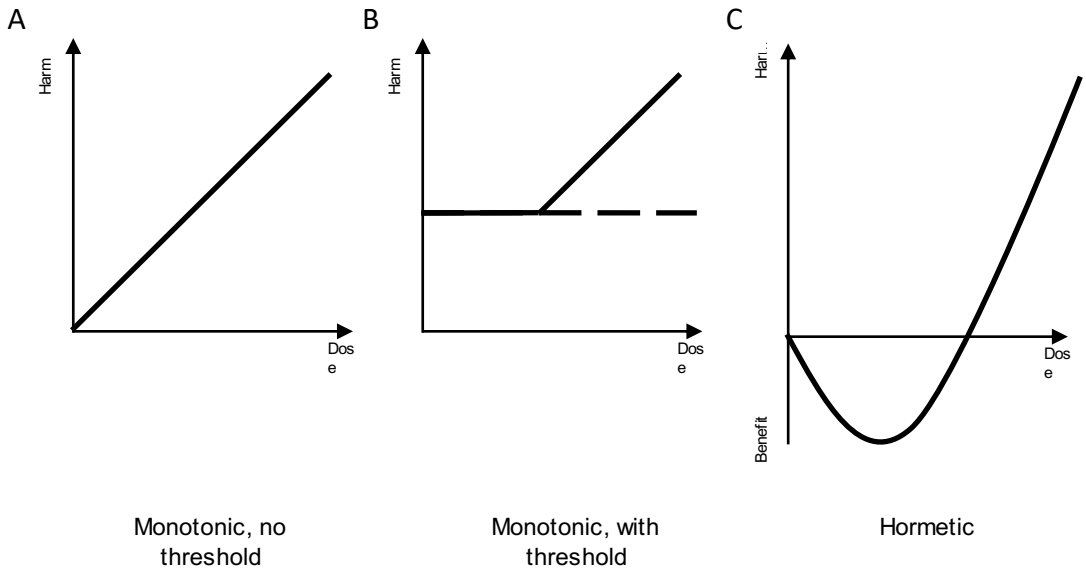


**Figure 4.9 Models for dose-response relationships.**

**A.** Traditionally the dose-response relationship of ROS has been considered to be monotonic, as exemplified by the 'monotonic, no threshold' model in which increasingly more ROS always cause increasingly more harm. This is shown here as a linear relationship for the sake of simplicity, but it could be any monotonic function. **B.** The floodgate hypothesis suggests that at low levels ROS will be buffered by endogenous antioxidant systems, such that there is a threshold below which ROS will cause no harm. **C.** The concept of hormesis proposes that the dose-response relationship is biphasic, with actively beneficial effects observed at low doses and harm at high doses.

The 'monotonic no threshold' model is no longer supported by the literature, given the well described role of ROS in physiology that we have already discussed. The 'monotonic with threshold' model is still commonly held, and is often discussed as the 'floodgate hypothesis' in which there is a basal level of antioxidant tone that must be exceeded in order for ROS to have any consequence (Toledano et al., 2010).

The dose-response relationship that characterises the hormetic model is relatively loosely defined, but is commonly described as biphasic or J-shape (Calabrese and Baldwin, 2001) with actively beneficial effects at low doses and harm at high ones. The central characteristic is that it is non-monotonic in nature. It is worth noting that hormesis refers to a phenomenon rather than a specific mechanistic process, and unfortunately that it is a term that is used with disparate meanings in the literature, referring to both adaptive processes occurring over time (perhaps better called adaptive homeostasis: 'the non-damaging process by which an apparent toxicant

can activate biological signal transduction pathways to increase expression of protective genes, by mechanisms that are completely different from those by which the same agent induces toxicity at high concentrations' (Davies et al., 2017) as well as an inherent property of the dose-response curve when measured at a single time point.

This hormetic relationship effectively describes the coding of the cardioprotective signal in the quantity of ROS that are present, and offers a good framework for rationalising the data presented here in which cardioprotection is conferred by a low concentration of MitoPQ but not by higher ones.

Altering the dose-response relationship

*MitoParaquat at reperfusion*

Rather than administering MitoPQ as a bolus prior to the onset of ischaemia, we have also administered it shortly before reperfusion. The area at risk is obviously inaccessible to blood based methods of delivery until the moment of reperfusion, but by administering it shortly beforehand we hoped to target the crucial first minutes during which MPTP opening occurs and thus cell fate is determined (Andrienko et al., 2017). The experiments here show that the most efficacious dose when given prior to the onset of ischaemia is no longer protective when given immediately prior to reperfusion, but that slightly lower doses remain cardioprotective. From this we can hypothesise that there is a left-right shift in the dose-response curve, which fits with existing literature that the external milieu may shift hormetic responses (Fadda et al., 1990). Data from a wider range of doses administered at reperfusion would allow this to be investigated more thoroughly.

It is likely that such a shift may also correspond to the induction of a different protective pathway. In addition to their role in ischaemic preconditioning as we have discussed, ROS have also been described to have a role in facilitating ischaemic postconditioning – as determined by similar experiments showing that protection from postconditioning can be blocked by the infusion of an antioxidant such as NAC, though it must be applied during the staccato postconditioning cycles and not at reperfusion proper following the completion of the protocol (Dost et al., 2008). This difference is mechanistically intriguing, and fits with the evidence

presented here that a different dose of MitoPQ must be used in order to confer protection to the heart.

Relation of hormesis to the failure of promising treatments in clinical trials

Taken together, these data presented here on the quantitative relationship between the dose of ROS and cardiac outcome provide a theoretical framework in which we can interpret the failure of antioxidant treatments to show beneficial effects upon patients mortality and morbidity in clinical trials (Fortmann et al., 2013; Ye et al., 2013). Rather than ROS being something that needs to be 'detoxified', these data suggest that there is a small efficacious window of oxidant dose that must be targeted for beneficial outcomes. As discussed there are numerous problems with targeting this window in the experimental setting, and these exact same considerations would apply if designing a therapeutic strategy. The differing doses of MitoPQ required to confer protection when given either before ischaemia or at the start of reperfusion suggest that the efficacious dose also depends upon the time that it is administered.

The framework of hormesis can not only offer a lens through which to interpret the failure of these treatments, but also to guide in the selection of which future therapeutics to select for further investigation.

Signal coding in the space and/or species domain

Another possibility that these data raise is that the exact location within the mitochondria or the species produced might encode the cardioprotective signal.

MitoPQ, as used here, represents a key development in the investigation of ROS due to its improved mitochondrial uptake. The technical advantages of this tool discussed in chapter 3 allow us to place greater confidence in these results that would have been possible with conventional methodologies, but also allow further conclusions to be drawn due to the specific nature in which ROS are produced. The failure of MitoPQ control compound 1 to lack ROS producing abilities allows its use as a fortuitous control, in that it results in ROS production through an unknown mechanism, but not from complex I in the mitochondria. This adds

credence to the theory that either the exact location or specific mode of ROS production is crucial to the effects that it has as a signal.

It is worth noting that despite the data presented here showing changes in both cytosolic and cellular function, we are not able to detect any ROS within the cytosol. This would suggest that the signal is transferred to the cytosol by some mechanism other than by ROS, but also does not rule out the possibility that it is acting locally within the mitochondria to cause cardioprotection.

What is the output of the reactive oxygen species signal?

In order to be classified as a signal that conveys information, this ROS must also be able to be detected. In most biological systems this occurs by the modification of a protein, which in order to be functional beyond a single use must happen in a reversible manner. We must therefore attempt to understand the direct output of the ROS signal, hypothesised to occur by the post-translational modification of a protein.

As determined by chemical reactivity, ROS are most commonly found to modify proteins on thiol residues due to the ability of the sulfur atom to donate electrons. This is a thermodynamically favourable process but has a high activation energy, and so the rate of reaction will determine when and how they occur. Cysteine residues are by far the most common site of modification, and indeed also represent the dominant thiol group within the mitochondria (Requejo et al., 2010). Methionine residues will also react with ROS but at a much slower rate: for example the rate of reaction with $H_2O_2$ is ~2 orders of magnitude slower than a comparable cysteine (Winterbourn and Metodiewa, 1999).

We must also note that not all cysteines respond equally. The local protein environment may dramatically alter the $pK_a$ of a cysteine residue, with those with a lower $pK_a$ more ionized at physiological pH and thus are more reactive towards $H_2O_2$. This may also create different responsiveness during different physiological conditions, as for example intracellular pH is significantly lowered during ischaemia. Further, protein structure is not static and so a particular residue may have differing accessibility depending upon the conformation of a protein. Therefore there is also the possibility that a reaction may only occur under a specific

set of circumstances, with the consequence that the specificity of a ROS signal be greatly increased. Proof of concept is shown by the fact that S-nitrosation of cysteine residues has been shown to occur endogenously in both pre- (Kohr et al., 2011) and post- (Tong et al., 2014) conditioning.

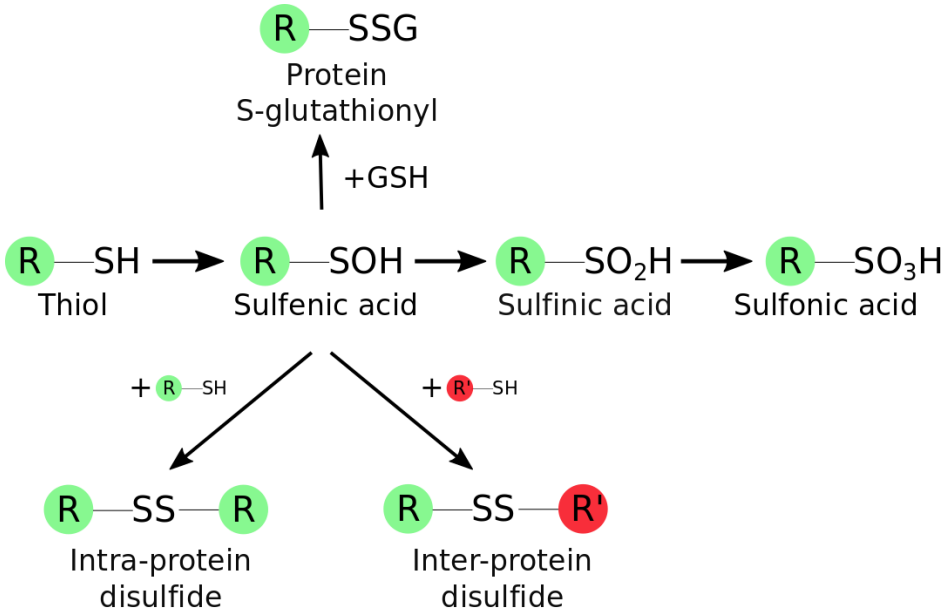


**Figure 4.10 Oxidative modifications of protein thiols.**

Protein thiols may be oxidised to sulfenic acid by 2 electron donation. This is a transient modification, and unless stabilised by the local protein environment will react with other thiols on the same protein (intra-protein disulfide), another protein (inter-protein disulfide), or with gluathione in a process called glutathionylation. Alternatively, it may undergoe further 2 electron oxidation to form sulfinic acid and sulfonic acids sequentially.

After Yuan et al (Yuan et al., 2015)

The ROS species that acts directly to modify a protein is also currently an open question. The rate constant for the (non-enzymatic) reaction of superoxide with thiols is insignificant at pH 7 compared to that with intracellular dismutases, which favours the dismuation reaction over and above all others. However microdomains have been reported to play a role in calcium signalling, and it is possible that such a phenomenon may also be in play here, with the possibility that microdomains of high concentrations in combination with thiols in particular local environments could even further increase the specificity of a signal.

It is however generally considered more common that ROS signals be transduced through $H_2O_2$ as it better fits the criteria for a second messenger. Firstly, $H_2O_2$ generally has a higher reactivity with thiols. The persistence of $H_2O_2$ is much greater than that of superoxide due to the relative concentrations and rate constants of SODs and peroxidases respectively. It is therefore also possible that the local ROS signal within the mitochondria may act via $H_2O_2$ rather than superoxide.

We must emphasise that the cardioprotection observed here is an acute process, with the *in vivo* IRI experiments lasting only 2.75 hours at most after the administration of the compound. Such acute cardioprotective changes are generally considered to occur independent of transcriptional or translational changes, canonically occurring via post-translational signalling cascades. This has been shown by experiments with inhibitors of protein synthesis which do not alter the beneficial effects of cardioprotective treatments such as ischaemic preconditioning (Thornton et al., 1990). Whilst it is highly probable that the ROS signal generated by MitoPQ will result in transcriptional changes as has been described by retrograde signalling from the mitochondria to the nucleus (Yun and Finkel, 2014), they are therefore unlikely to be responsible for the data presented here.

*Hypothesis of modifying the active/deactive transition of complex I*

Considerable work has been carried out recently regarding the mechanism by which the ROS burst at reperfusion occurs, which then goes on to trigger MPTP formation and thus determine cell fate. The current consensus is that the most likely mechanism of ROS production at reperfusion is via RET at complex I (Chouchani et al., 2016). This is of particular relevance, as ROS production by RET is known to be dramatically altered by a conformational change that has been termed the active/deactive transition (Babot et al., 2014). When complex I is not active – not oxidising NADH and pumping protons across the IMM – it slowly converts into the deactive state, with a half-life of around 10-12 minutes in ischaemia (Ciano et al., 2013; Galkin et al., 2009). At reperfusion, it then rapidly reactivates and thus can support superoxide production by RET (Gorenkova et al., 2013) as described previously. The deactive structure exposes what has been found to be a crucial cysteine residue (Cys39 in the ND3 subunit in the mammalian complex) that is normally occluded in the active complex. This residue may be covalently modified to alter the reactivation kinetics of the complex: temporarily locking it in

the deactive state. If this can be timed so that the complex is prevented from reactivating at reperfusion, then ROS production by RET and the subsequent tissue damage may be prevented. This has been shown to be occur with *S*-nitrosation (Burwell et al., 2006; Chouchani et al., 2013; Methner et al., 2014; Prime et al., 2009), in which case the modification is reversed by endogenous thiol reduction mechanisms with a half-life of ~5 minutes. Complex I is thus inactive and unable to generate ROS for the crucial first few minutes of reperfusion only, by which time the electrons stored in the pool of succinate accumulated during ischaemia will have been dissipated by other mechanisms.

Most notably for the development of a therapy, modifying the re-activation of complex I via Cys39 represents an excellent target as unless tissue is ischaemic and thus complex I is in the deactive state, the therapy should have no effect upon the patient as the modification cannot occur in the active complex. Better understanding of this process is thus a key priority in our basic research.

However not only *S*-nitrosation can modify Cys39, but like many cysteine residues it can undergo a range of redox post-translational modifications (Chung et al., 2013). Of note here is that it can be oxidised to a sulfenic acid and/or to a glutathione mixed disulphide by oxidative stressors including hydrogen peroxide (Gorenkova et al., 2013; Yaguchi et al., 2003), which could be reversed by reductants such as the glutathione and thioredoxin systems (Chouchani et al., 2013).

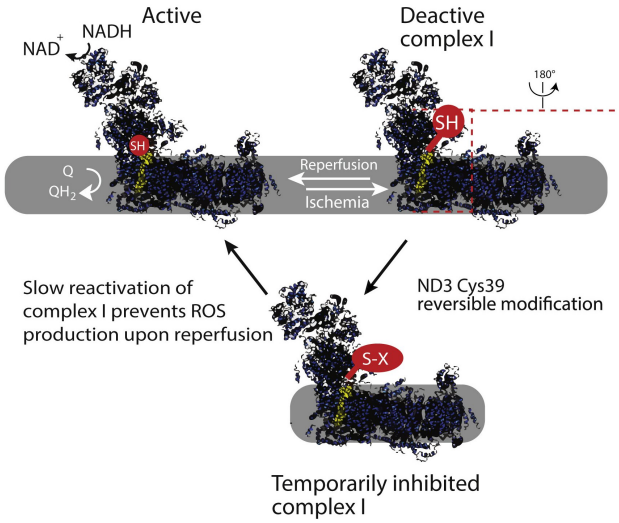


**Figure 4.11 The active/deactive transition of complex I in ischaemia reperfusion injury.** During ischaemia, the lack of respiratory substrates causes complex I to enter the deactive state. Modification of a critical cysteine residue (ND3 Cys39) may cause the complex to be temporarily inhibited by slowing its reactivation at reperfusion and thus reducing ROS production at this point. Figure reproduced from Chouchani et al. (2016).

Here the working hypothesis was that MitoPQ confers its protection via this mechanism, but this has been found to not be the case. Complex I activity assays using tissue samples collected from hearts undergoing *in situ* ischaemia reperfusion injury find no difference in activity between control mice and those treated with MitoPQ. We therefore reject the hypothesis that the protection conferred by MitoPQ is due to alterations in the re-activation of complex I at reperfusion and it must therefore be occurring by other means.

Other potential effectors

There are several other plausible effectors that could be the output of the ROS signal, which would be an interesting avenue for further work. Over the past three decades since the discovery of ischaemia preconditioning (Murry et al., 1986), considerable efforts have been undertaken to characterise the molecular pathways involved such that a chemical mimetic could be produced to target these pathways. Ischaemic preconditioning was found to be blocked by the addition of antioxidants at great excess, such as NAC (Chen Weina et al., 1995) or MPG (Baines et al., 1997). This clearly showed that ROS played a role in these signalling

pathways. Notably protein kinase C has be oxidatively modified by ROS during the preconditioning signalling cascade (Korichneva et al., 2002). However most research has studied the effect of cytosolic ROS which has been shown to cause mitochondrial targeting of the kinase (Majumder et al., 2001), rather than the effect of mitochondrial ROS. Further work is clearly required here given the fact that we are not able to detect ROS within the cytosol after treatment with MitoPQ.

Our *in vitro* data which show that ROS generated by MitoPQ are sufficient to induce MPTP opening, which may be a direct target responsible for cardioprotection. This is consistent with previous reports that ROS may act directly upon the MPTP in order to modualte its opening (Vercesi et al., 2018). In contrast to normal opening of the MPTP which leads to cell death, it has been shown that the pore can also open transiently or in a low conductance state (Saotome et al., 2009). Hausenloy and colleagues (Hausenloy et al., 2004) describe how the induction of transient MPTP opening may protect the heart against IRI, which is plausible as a mechanism given the known role of ROS in promoting MPTP formation described in the seminal work on 'ROS-induced ROS-release' by Zorov et al (Zorov et al., 2000). Further investigations are hampered by the disputed molecular nature of the MPTP (Bernardi and Di Lisa, 2015), but the availability of MitoPQ as a tool respresents a key development to enable the research. For example, it could be administered in combination with CsA in the mouse surgical model of AMI in order to examine if the combination of these agents reduces infarct size below that achieved by either agent alone. This would be suggestive that MitoPQ was acting via a mechanism of action other than those which converge on opening of the MPTP at reperfusion.

However as increasing amounts of research are conducted on the topic there are an increasing number of proteins that are implicated in the ROS response. Advancing methodologies in redox proteomics (Kumar et al., 2013; Leichert et al., 2008) will provide a logical pipeline for analysis of the responsible proteins in an unbiased manner. The measurement of post-translational modifications (such including redox modifications) in proteomics is an area of rapid technological progress, and techniques such as OxICAT (Kumar et al., 2013) now enable this to be done with reasonable coverage of both the whole cell and in particular the mitochondrial proteome (Topf et al., 2018). After screening candidate effectors can then be confirmed using conventional techniques. It is also worth noting that since we were not able to detect ROS within the cytosolic compartment, the ROS signal must be transduced and one or more intermediary messengers must be mediating these changes.

Interplay between reactive oxygen species and calcium

There is a close intertwinement of ROS and calcium in the heart. Calcium regulates contraction of myocytes through myofilament cross-bridge formation (Eisner David A. et al., 2017). ROS production from the mitochondrial reparatory chain is linked to the rate of metabolism, which is in turn determined by cardiac workload and the cross-bridge cycle (Balaban, 2009). This is at least in part achieved directly through regulation of multiple metabolic steps by calcium including pyruvate dehydrogenase (the key rate limiting enzyme in glycolysis) α-ketoglutarate–, and isocitrate dehydrogenases in the citric acid cycle, complex III in the ETC and the $F_1F_0$-ATPase directly (Balaban, 2002). Using conventional experimental methods it is difficult to interpret the primacy between mitochondrial ROS and calcium events due to this synergistic relationship. The ability of MitoPQ to selectively generate ROS within the mitochondria is therefore an important technological develop to allow investigation into these processes.

The interplay between ROS and calcium is a point of particular interest to this work given the synergistic role that the two play in the opening of the MPTP. With conventional methods it has been very hard to tease apart the primacy of the changes that occur, but with MitoPQ we are able to generate a stimulus specifically within the mitochondria. We then observe downstream changes in cytosolic calcium homeostasis and opening of the MPTP at high concentrations of exogenous ROS generated by MitoPQ. It is worth noting that since we are not able to detect cytosolic ROS using a compartmentalised ROS sensor, this signal transduction from the mitochondria to cytosol must happen by some other mechanism. How this occurs is naturally a point of interest but is outside the scope of this work. It would also be instructive to directly measure mitochondrial calcium levels in order to explore the possibility that the protective mechanism occurs via alterations in this.

**Summary**

The data we present here show that MitoPQ is able to create a cardioprotective signal at low doses, resulting in smaller infarct size in a mouse model of acute myocardial IRI. However, this is not seen at higher doses which is suggestive of hormesis: that the dose of ROS is the crucial factor in determining the outcome. This would also seem to be a highly specific process, with the exact location and/or species of ROS apparently also crucial in conferring protection. These changes are likely to be occurring within the cardiomyocyte, where we can observe downstream changes in cytosolic and cellular function following a primary disturbance in mitochondrial ROS.

# Chapter 5 – Measuring and modulating the metabolism of succinate during ischaemia reperfusion injury

## Introduction

Since succinate metabolism has been shown to have a causative role in IRI, there is translational potential for it to be used both as a biomarker for ischaemia and as a therapeutic target in order to decrease the extent of damage at reperfusion.

### Measuring the succinate accumulation

Previous work in preclinical models has used invasive methods to measure succinate concentration in tissues, mainly using mass spectrometry based approaches (Chouchani et al., 2014; Valls-Lacalle et al., 2015). Non-invasive methodologies to measure succinate would allow increasing flexibility in experimental design and a reduction in animal numbers, but more importantly there is a clinical application in measuring succinate levels as a marker of ischaemia.

Currently cardiac specific troponins I and T are used as the standard diagnostic marker prior to angiography (Bertrand et al., 2000; Braunwald Eugene et al., 2000), but since troponin is a downstream indicator of cell death rather than of ischaemia itself it is inherently less sensitive as a diagnostic marker for ischaemia and further may not always be detected until up to 4 hours after the onset of ischaemia (Sharma et al., 2004). A study using the OxAMI patient cohort obtained blood samples from the coronary artery, the coronary sinus and from a peripheral vein in patients undergoing either PPCI for an acute STEMI or control patients undergoing nonemergency coronary angiography or percutaneous coronary intervention for stable angina or non-STEMI. Succinate was found to be the only metabolite with net release from the heart during ischaemia (by comparison of blood leaving the coronary circulation in the coronary sinus with that entering it in the coronary artery). The cardiac release of succinate was also shown to correlate with the extent of AMI injury assessed by the standard practice of late gadolinium enhanced cardiac magnetic resonance imaging (Kohlhauer et al., 2018).

In addition to approaches measuring succinate that is released into the systemic circulation, succinate might also be measured directly within tissues. Magnetic resonance spectroscopy (MRS) has been used to measure a range of metabolites within cardiac tissue, both in patients in the clinic (Qureshi and Nasir, 2017) as well as in a range of pre-clinical animal models

(Bakermans et al., 2015). It has however not yet been applied to measure succinate levels during ischaemia, which we aim to do here.

Do established cardioprotective strategies act via a decreased accumulation of succinate during ischaemia?

The interest in the effect of ischaemic preconditioning (IPC) upon ischaemic metabolism is twofold: firstly, it is unknown whether decreases in the accumulation of succinate during ischaemia are necessary or merely sufficient to protect the heart against injury. The latter is overwhelmingly likely due to the extent of work that has been done to understand the signalling pathways involved in IPC (such as the RISK and SAFE pathways), but being mechanistically separate from the activation of these signalling cascades would mean that by combination of a therapy targeting succinate with a therapy targeting a protective signalling pathway we may achieve an additive effect – conferring greater protection than with either strategy alone. This is an approach that it is increasingly hoped will underly the successful translation of a therapy into the clinic (Hausenloy Derek J. and Yellon Derek M., 2017). This has been an overwhelmingly failure of the field, that despite the discovery of ischaemic preconditioning over 30 years ago and a host of other cardioprotective strategies that have since been demonstrated to work in pre-clinical models and in small phase 2 trials, there is as yet nothing that can be administered to a patient to decrease the extent of injury in AMI.

Tissue succinate decreases at reperfusion: metabolism

The ultimate aim of elucidating mechanisms of damage in pathologies such as IRI is to generate insight that may be used to treat the condition. Since succinate metabolism has been shown to drive ROS production and damage at reperfusion, it can be targeted in two ways: either by inhibition of SDH during ischaemia to decrease the extent to which succinate accumulates, or by inhibition of SDH at reperfusion in order to slow the rate at which succinate is metabolised. The former has been achieved with the use of the membrane permeable malonate analogue dimethyl malonate administered prior to the onset of ischaemia (Chouchani et al., 2014). The utility of this in the clinic is however limited outside of a few specific scenarios, as patients with AMI present to medical services only after the onset of symptoms and ischaemia. The inhibition of succinate metabolism at reperfusion has been reported in the isolated heart by the

infusion of the malonate salt disodium malonate (Valls-Lacalle et al., 2015), but this finding has not been confirmed *in vivo*. The efficacy of the membrane impermeable malonate salt is also surprising, since there is a common assumption in the literature that membrane permeable prodrugs are required for uptake of carboxylates such as malonate into the cell (Ehinger et al., 2016).

**Aims and objectives**

- Determine if the existing cardioprotective strategy of ischaemic preconditioning decreases the accumulation of succinate during ischaemia
- Measure succinate accumulation *in vivo* using MRS as a non-invasive method
- Investigate the use of malonate as a competitive inhibitor of SDH to inhibit its metabolism during the crucial first seconds of reperfusion as a cardioprotective strategy

## Results

Does ischaemic preconditioning affect succinate accumulation during ischaemia?

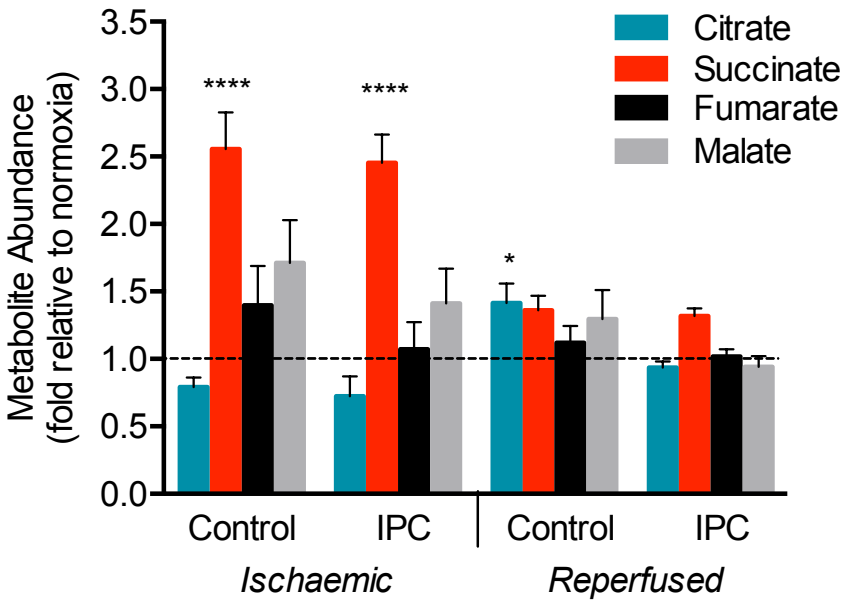


**Figure 5.1 Ischaemic preconditioning does not impact the accumulation of succinate in the mouse heart undergoing ischaemia reperfusion injury.**

Mice were subjected to 30 min regional myocardial ischaemia by occlusion of the LAD coronary artery, with or without a preconditioning protocol consisting of 3 cycles of 5 min ischaemia, 5 min reperfusion followed by 10 min washout. Tissues were collected either at the end of the ischaemic period or following 5 min reperfusion and the levels of the citric acid cycle intermediates citrate, succinate fumarate and malate were measured by LC-MS.

Statistical significance was assessed for each metabolite separately using a 2-way ANOVA with factors defined as ischaemia/reperfusion and IPC/control and the Tukey-Kramer test used for post hoc comparisons.

*n = 7-8*

LC-MS was performed by S. Costa (MRC Cancer Unit, Cambridge), surgery was performed in concert with V. Pell (University of Cambridge).

In order to determine if IPC altered the accumulation of succinate during IRI, a surgical model of AMI in the mouse was used. The concentrations of key citric acid cycle metabolites were measured by LC-MS in tissue collected from mice that had been subject to an ischaemic preconditioning protocol consisting of 3 cycles of 5 min ischaemia, 5 min reperfusion followed

by 10 min washout that has been previously shown to reduce infarct size in our laboratory (unpublished observations). Consistent with previously reported data, at the end of 30 min ischaemia there was a significant elevation in succinate compared to samples collected after reperfusion (Figure 5.1, $p < 0.0001$, 2-way ANOVA). However, the quantity of succinate was not different between control and IPC conditions (2-way ANOVA, $p = 0.70$). The protection that may be afforded by alteration in succinate metabolism is therefore mechanistically distinct from that of IPC, which does not alter succinate accumulation during ischaemia. Thus there is potential for these two pathways to be targeted in a combined therapy aimed at reducing infarct size after AMI.

We also observed a significant difference in the quantity of citrate present in tissue between ischaemic and reperfused tissue (Figure 5.1, $p < 0.001$, 2-way ANOVA), with an increase in citrate abundance in reperfused tissue. The significance of this finding is unclear, since it has not been found in previous experiments reported by ourselves (Chouchani et al., 2014) or others (Zhang et al., 2018a). The reasons for this discrepancy should be investigated in further work, though it should be noted that the magnitude of this change is much smaller (~1.5 fold relative to normoxia) than that observed for succinate (~2.5 fold). Similar to the dynamics of succinate, no difference was observed between the control and IPC conditions ($p = 0.178$) for citrate. All other factors and interactions for fumarate and malate were similarly non-significant (Figure 5.1, 2-way ANOVA).

Succinate MRS pilot experiments

We also performed a series of pilot experiments in order to assess the viability of MRS as a method measure succinate in the ischaemic heart using the LAD ligation model of AMI in the mouse.

In order to acquire the MR spectrum, we must first specify the positions and dimensions of the voxel within which this spectrum will be acquired. This was performed anatomically using T1 weighted MR images captured serially through the thorax along the rostral-caudal axis.

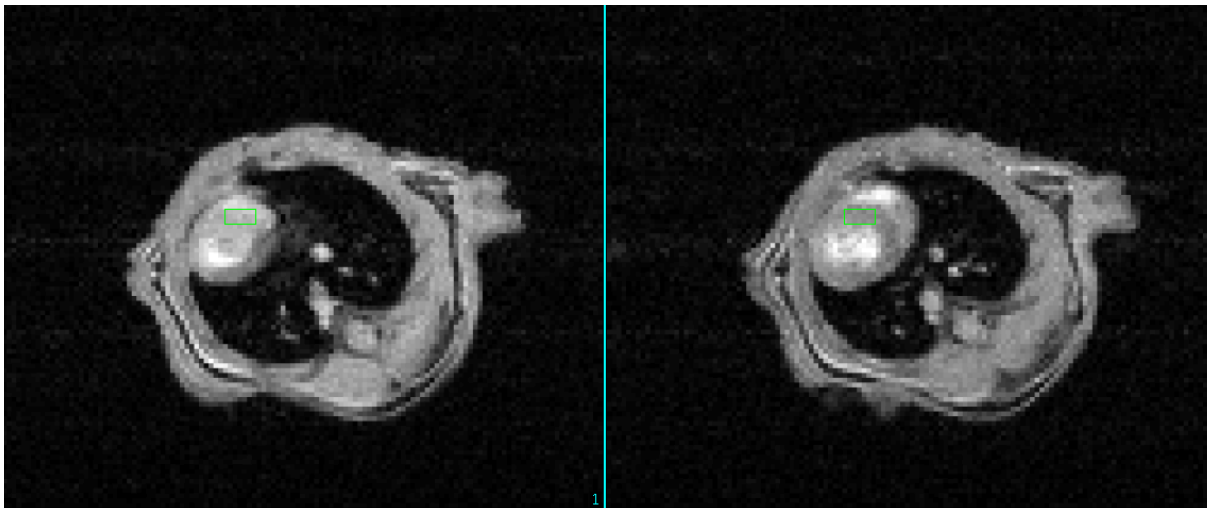

**Figure 5.2 Voxel placement in the mouse by T1 weighted MR imaging.**

Representative cine-flash images taken 2 mm apart along the rostral-caudal axis showing voxel placement in green during diastole. Blood in the ventricles of the heart can be visualised by the strong white signal.

MR imaging was performed by A. Wright (Cancer Research UK Cambridge Institute).

After specification of the voxel in 3D-space, the homogeneity of magnetic field generated within the voxel was adjusted in a processing known as shimming in order to maximise the signal-to-noise ratio. A spectrum was then acquired using a PRESS sequence. Since the heart of the mouse moves in space during both the cardiac and breathing cycles, acquisition was gated using the both the ECG signal (to ensure the data collection at the same point of the cardiac cycle) and that of the respirator using a pressure sensor placed underneath the thorax. Both of these signals required some optimisation, with best results achieved using 3M neonatal electrodes placed directly onto the chest of the mouse and the respiratory pressure sensor approximately mid thorax in the rostral/caudal axis. The double gating of acquisition substantially lengthened the experimental time required to obtain spectra, and was further found to be highly variable between experimental replicates. This extended experimental time compounded problems in maintaining body temperature in the mouse within the bore of the magnet. This factor in particular decreased the signal-to-noise ratio achievable as drift in the temperature within the voxel reduces the homogeneity of the magnetic field. We were unable to reliably observe any signal corresponding to succinate, which should give a relatively sharp singlet peak at 2.42 ppm (Fig 5.3, indicated by the red arrow).

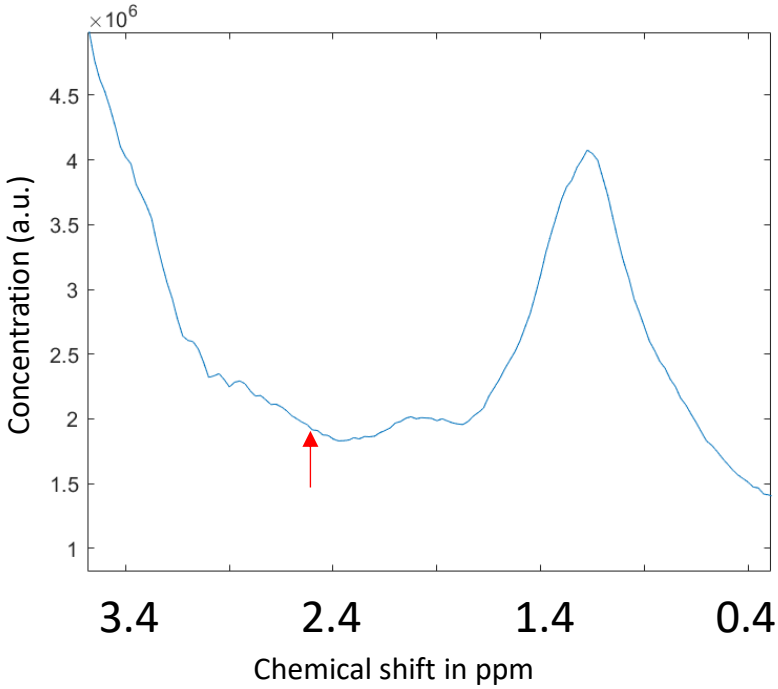


**Figure 5.3 An example MRS spectrum collected from the regionally ischaemic mouse heart.**

The large lipid peak is visible at ~1.2 ppm, and another from choline and taurine beginning ~3.4 ppm. The location of the expected succinate singlet peak is shown by the red arrow at 2.42 ppm, at which we observe no measurable signal. A 4 µL voxel was specified as indicated in Figure 5.2.

MR imaging was performed by A. Wright (Cancer Research UK Cambridge Institute).

Signal-to-noise ratios are in MR spectra are intrinsically worse in small animals such as the mouse due to the low absolute magnitude of the signal that results from the small tissue volume. We therefore performed this same experiment in the rat, whose body mass is ~1 order of magnitude greater than that of mice. This allowed the use of a voxel with an area of 19.84 $mm^3$ compared to 4 $mm^3$ used for the mouse. The decreased surface area to volume ratio of the rat also mitigated some of the issues we had with regards to maintenance of body temperature.

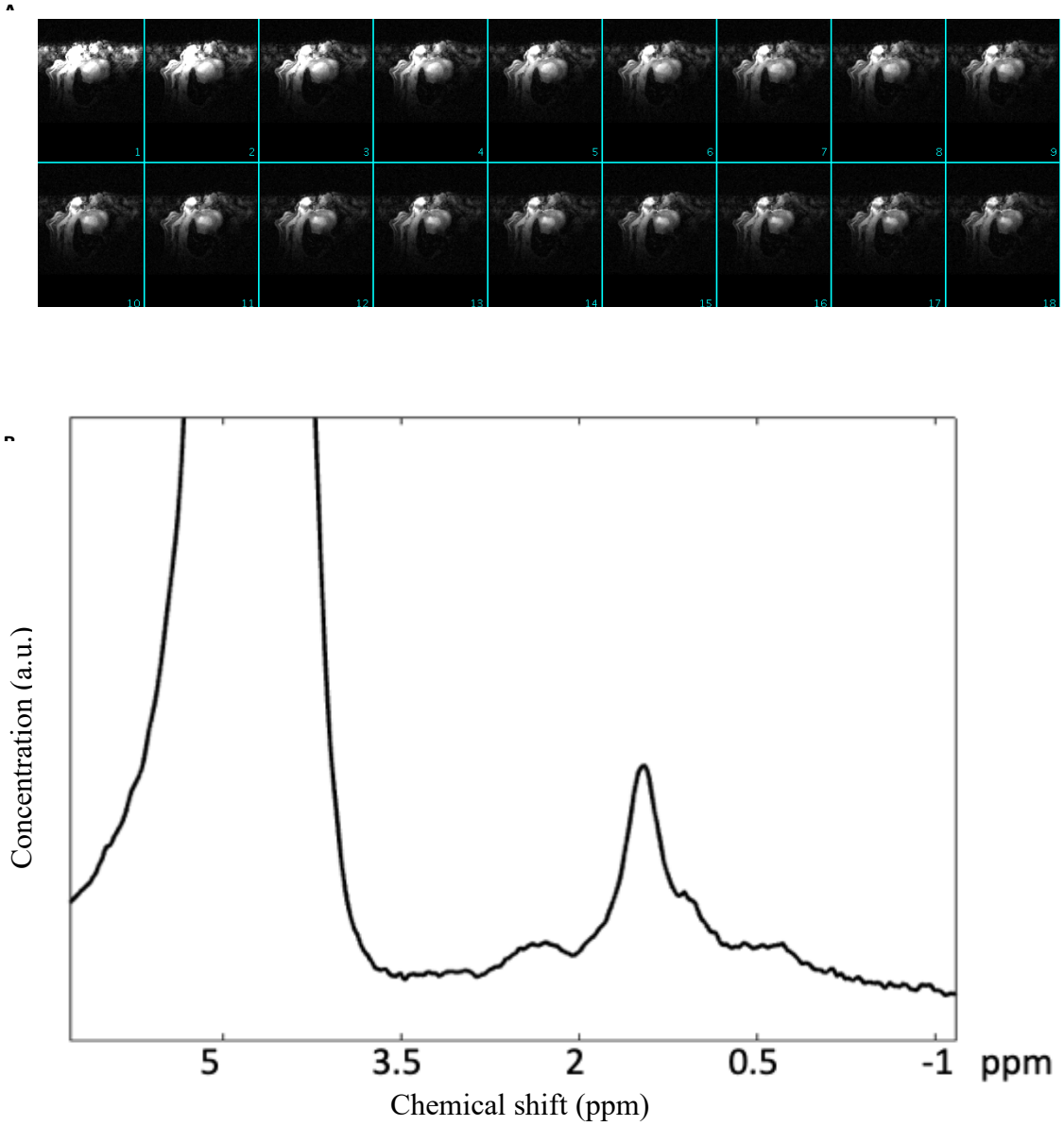


**Figure 5.4 Voxel placement and MR spectrum in the regionally ischaemic rat heart.** **A.** Representative cine-flash images taken through the cardiac cycle were used to guide voxel placement **B.** Example spectrum achieved, showing no distinct succinate peak at 2.4 ppm. MR imaging was performed by A. Wright (Cancer Research UK Cambridge Institute).

However, the experimental outcome remained similar to that of the mouse, with no succinate signal reliably seen (Figure 5.4B). We therefore concluded that within our resource constraints it is not feasible to quantitatively measure succinate in the rodent heart undergoing IRI using MR spectroscopy.

Preventing succinate metabolism at reperfusion

Previous work has shown that the membrane permeable malonate ester DMM protects the heart against IRI when administered prior to the onset of ischaemia, acting to reduce the quantity of succinate accumulated by ischaemic metabolism. However for translation to the clinic it is necessary to have a therapy which can be administered at or after reperfusion. Despite sound mechanistic reasoning by decreasing the rate of ROS production by RET which is driven by the metabolism of succinate early in reperfusion, the protective effect of succinate dehydrogenase inhibition during reperfusion *in vivo* has not been tested.

Administration of the membrane permeable malonate pro-drug dimethyl malonate at reperfusion was however found not to protect the heart (D. Kulaveerasingam, unpublished observations). We hypothesised that this was due to insufficient delivery of malonate to the mitochondria, with the esterified DMM requiring cleavage by intracellular esterases before malonate can inhibit succinate dehydrogenase. To assess the kinetics of malonate delivery we therefore measured malonate levels in heart tissue of mice undergoing LAD occlusion using targeted LC-MS/MS. Relative to the saline control (6.3 ± 0.7 pmol $mg^{-1)}$, administration of DMM before ischaemia but not at reperfusion caused a significant increase in malonate levels within the heart after 1 min of reperfusion (11.6 ± 3.0 pmol mg-1; Figure 5.5A). Inhibition of succinate dehydrogenase during ischaemia would be expected to decrease the succinate present in the heart at 1 min reperfusion due to a reduction in its accumulation, which was what was observed in Figure 5.5B (309 ± 40 pmol $mg^{-1}$ in baseline conditions compared to 191 ± 30 pmol $mg^{-1}$ after DMM administration). Were DMM inhibiting the metabolism of succinate when administered during reperfusion, we would expect to see an elevation in succinate relative to the saline control when measured at 1 min reperfusion, whereas as consistent with no elevation in malonate levels we observe no difference in succinate (Figure 5.5B). It therefore appears that DMM does not release malonate sufficiently quickly to inhibit succinate metabolism during the crucial early phase of reperfusion.

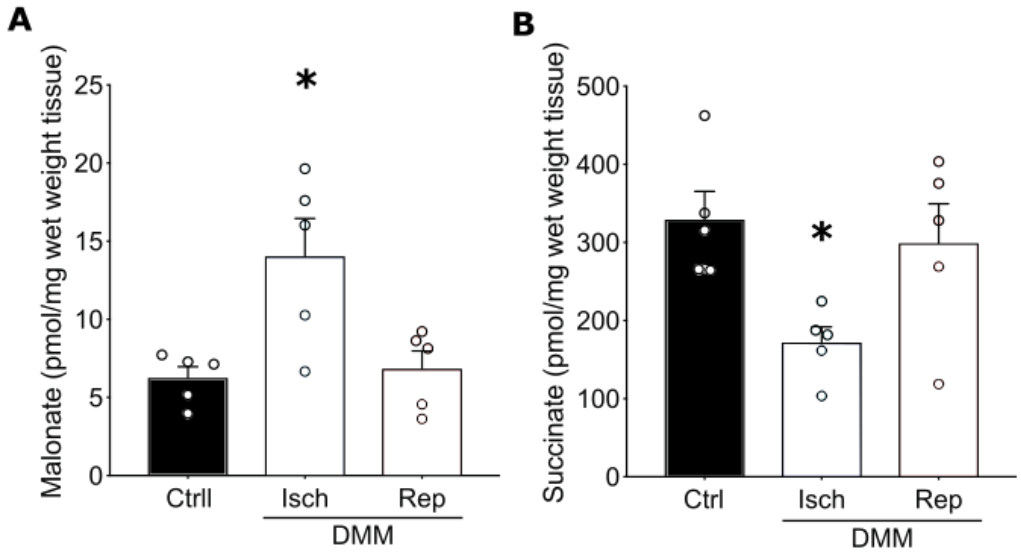


**Figure 5.5 Consequences of dimethyl malonate administration during reperfusion upon myocardial malonate and succinate concentrations.**

Mice undergoing regional cardiac IRI were administration with an i.v. infusion of DMM (8 mg/kg/min), beginning 5 min before reperfusion and continuing until tissues were collected either at the end of ischaemia or after 1 min of reperfusion. Tissue levels of **A.** malonate and **B.** succinate were measured using a targeted LC-MS/MS assay.

*n = 5, One-way ANOVA, Dunnett's multiple comparisons*

Due to reports that the disodium malonate salt could be protective when administered to *ex vivo* organs at reperfusion, we therefore characterised its uptake into tissues *in vivo*. The kinetics of disodium malonate uptake into tissues *in vivo* was assessed by i.v. injection of disodium malonate into mice and the quantity of malonate in heart, liver and brain tissues that were collected at various time points (Figure 5.6) was measured by LC-MS/MS. Substantial elevations in malonate were measurable in all tissues within 5 minutes compared to baseline conditions (two-way ANOVA). Malonate was then lost from the tissue over the next ~30 min, presumably due to metabolism through malonyl-CoA. The kinetics of malonate delivery are therefore highly suited for the prevention of IRI in the heart, facilitating a transient inhibition of succinate dehydrogenase during the early phase of reperfusion and thereafter a restoration of normal mitochondrial function.

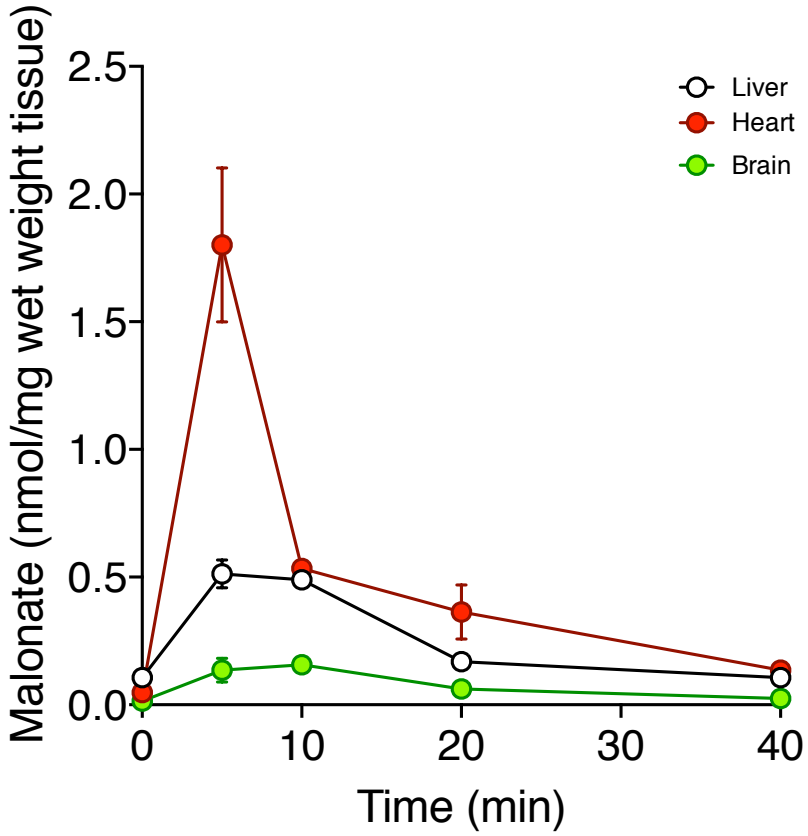


**Figure 5.6 Uptake of disodium malonate in the mouse in vivo.**

160 mg/kg disodium malonate was administered to conscious mice as a ~100 µL bolus into the lateral tail vein. Mice were killed and tissues snap frozen in liquid nitrogen at the indicated time points, before quantification of malonate by LC-MS/MS.

*n = 3-5, Statistical significance was assessed by two-way ANOVA with factors defined as timepoint and tissue.*

LC-MS/MS was performed by H. Pragg (MRC-MBU, University of Cambridge)

The uptake of disodium malonate was also validated using uniformly labelled $^{13}C$ disodium malonate, which was administered to mice undergoing the LAD occlusion model of cardiac IRI. The presence of the stable isotope label allows using to distinguish between malonate that is exogenously administrated and that which is endogenously present within tissues. When administered as an i.v. infusion beginning 5 min before reperfusion and continuing throughout the duration of these experiments, $^{13}C$ labelled malonate was detected in heart tissue at both 15 s and 60 s of reperfusion (Figure 5.7A-B). This suggests that using this administration protocol dimethyl malonate can be delivered to the heart rapidly enough to inhibit the metabolism of succinate by succinate dehydrogenase that has been shown to drive ROS production and thus IRI (Chouchani et al., 2014). Uptake did however show significant variability between biological replicates, which is hypothesised to be due to magnifications in experimental error when introducing the cannula into the tail vein and verifying its location by the small volumes infused (flow rate 5 µL/min) during this short interval. This experiment also allowed a comparison to be made between ischaemic risk tissue and the non-risk tissue, which showed no difference in the quantity of labelled malonate during the early phase of reperfusion (Figure 5.7A, one-way ANOVA).

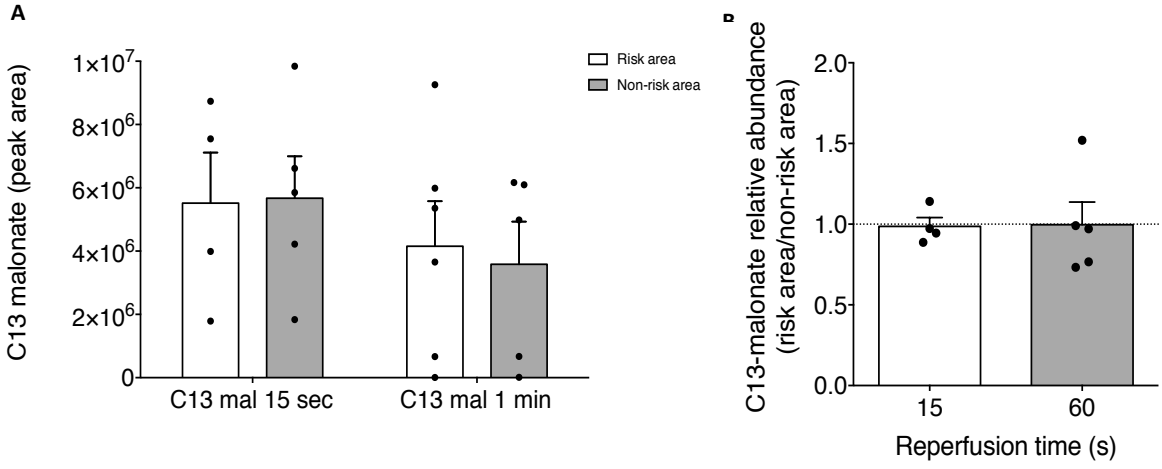


**Figure 5.7 Malonate uptake and metabolism during IRI.**

Mice undergoing regional cardiac IRI using the LAD occlusion model were administered with uniformly labelled $^{13}C$ 8 mg/kg/min disodium malonate (DSM) as an infusion into a lateral tail starting 5 min before reperfusion and continuing throughout the rest of the experiment. Tissue

from both the area at risk of ischaemia and the non-risk area was snap frozen in liquid nitrogen and the abundance of $^{13}C$ labelled malonate was measured using targeted LC-MS/MS. **A.** No significant difference was observed between levels of labelled malonate at 15s and 60 s in either tissue at risk of ischaemia or non-risk tissue (one-way ANOVA). **B.** $^{13}C$ labelled malonate is not significantly reduced after 60 s reperfusion compared to 15 s (Student's t-test). *n = 4-5*

Having determined that disodium malonate is taken up into heart tissue sufficiently quickly to act during the critical first few minutes of reperfusion, we then assessed whether by inhibition of SDH by malonate during this time could protect the heart against IRI which has not previously been shown.

Disodium malonate was administered during reperfusion to mice undergoing the LAD occlusion model of AMI at a range of concentrations, and was found to have a significant effect upon infarct size, with a significant reduction compared to the vehicle only control in the 160 mg/kg group (Figure 5.8A-B, one-way ANOVA). It must be noted that in these experiments the risk zone – a potentially confounding variable – was found to be different between the treatment groups (Figure 5.8C, one-way ANOVA). However post-hoc testing indicated that only the 16 mg/kg group was different to the vehicle only control group, and combined with the small magnitude of the effect (11% difference) this is unlikely to account for the effect of disodium malonate on infarct size that was observed.

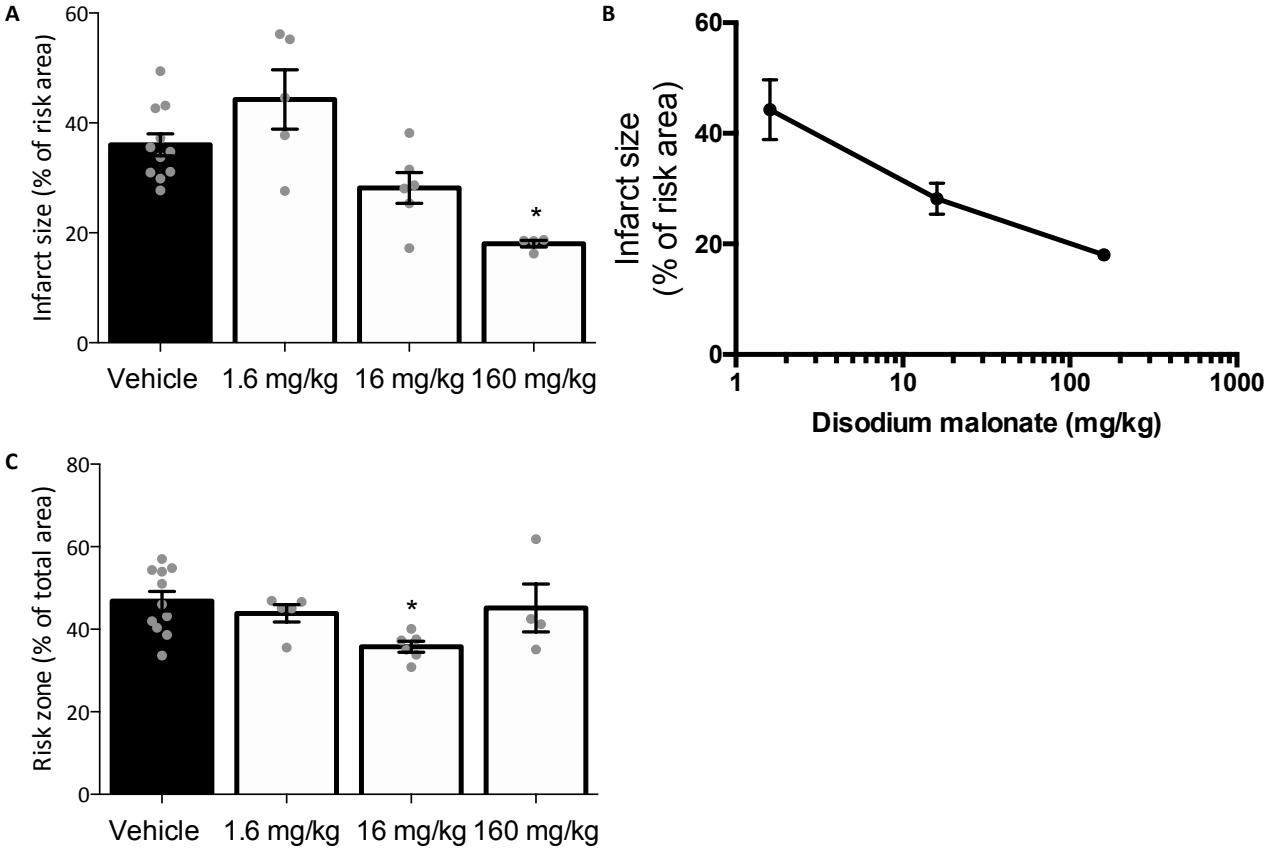


**Figure 5.8 Effect of disodium malonate administered during reperfusion upon infarct size.**

Mice undergoing IRI to the heart using the LAD occlusion model were administered either disodium malonate (1.6 mg/kg, 16 mg.kg, 160 mg/kg) or vehicle only saline control as an infusion into the lateral tail starting 5 min before reperfusion and continuing for a total of 20 min. Infarct size was then determined using an Evans blue/TTC double staining method. **A-B.** Infarct size was found to be dependent upon the dose of disodium malonate administered (one-way ANOVA, $p < 0.05$). **C.** The risk zone was significantly lower in the 16 mg/kg group compared to the vehicle-only control (one-way ANOVA, $p < 0.05$), however the magnitude of this difference (11%) was unlikely to account for the difference in infarct size observed.

*n = 4-8*

## Discussion

### Measuring ischaemic succinate using MRS

We were ultimately unable to reliably detect a succinate signal in the heart. There is no theoretical limit on the sensitivity of NMR spectroscopy as one can always improve signal-to-noise by performing additional acquisition scans. However, realistic detection limits are in the low-micromolar to high-nanomolar range (Emwas et al., 2019) leading us to be hopeful before conducting experiments that the elevations in succinate typically seen during ischaemia would be measurable using MRS. However for our experiments here, the limit of detection was likely much higher for a number of reasons.

#### *Effect of temperature on magnetic field homogeneity*

Temperature drift during these experiments prevented a good 'shim' (i.e. a high level of homogeneity in the magnetic field within the region of interest) which is required in order to maximise the signal-to-noise ratio. This is partially a limitation of the equipment available, as the animal could only be warmed by a hot air steam. This had been adequate for previous experiments conducted by our collaborators using isoflurane anaesthesia, but the combination of ketamine and xylazine used for these experiments is described to depress the circulatory system much more severely which would result in further problems with maintenance of body temperature. This is of particular importance for small rodents which are prone to heat loss due to their high surface area to volume ratios. Thermoneutrality for mice is reported to be around 30 degrees, and in normal conditions they are highly reliant upon movement to generate sufficient body heat to maintain their temperature. Future experiments could use a heated water jacket which might give better results.

Once the animal was placed into the scanner, the only monitoring that could be performed was by the measured signals (heart rate, rectal temperature) as in order to maximise signal-to-noise ratio the door to the MR room must be closed throughout the procedure to form a Faraday cage. Due to the decreased frequency of monitoring some experiments animals died during the imaging acquisition protocol: whilst this would not diminish the extent of succinate

accumulation (Martin et al., 2019) it compounded the problems regarding the maintenance of body temperature.

*ECG gating of the acquisition protocol*

In order to measure metabolites within the heart, we must gate the acquisition sequence to the ECG signal such that it always triggers at the same point of the cardiac cycle, in order that the ischaemic area is always in the same position relative to the voxel whose position is specified in 3D space. We also gate to a particular period of the breathing cycle in order prevent motion artefacts during movement of the thorax, and the combination of these factors mean that acquisition times are very long. Furthermore the ECG gating algorithm used also functioned poorly during ischaemia, with changes in the mouse ECG (J-wave inversion and T wave elevation) preventing reliable triggering with the consequence of increased acquisition times. This compounded the problems regarding maintenance of body temperature discussed above.

*Determining voxel size and position*

For these experiments, the voxel position was specified based upon anatomical landmarks using cine images. Ideally the ischaemic area could instead be determined directly by the administration of a contrast agent (containing for example gadolinium) in order to delineate perfused vs ischaemic tissue on contrast MRI. This would allow not only more precise positioning of the voxel but also adjustment of its size in order to maximise the magnitude of the succinate signal and therefore the signal-to-noise ratio.

Future experiments

A major problem encountered during these experiments was the motion of the heart. For this reason, I suggest that future experiments should address ischaemia in a static tissue. Ischaemic stroke in the brain is the obvious clinically relevant candidate, for which there are surgical models such as occlusion of the middle cerebral artery that can be performed in animals including the mouse or rat (Chiang et al., 2011). This is technically challenging due to the extent of collateral flow around the circle of Willis, but provides an advantage in that ischaemia is only induced in one hemisphere of the brain and so the contralateral side can be used as a negative control to measure baseline succinate levels in tissue with normal perfusion. It is

suggested that these be performed in that rat rather than the mouse to maximise the chance of successfully measuring a succinate signal, with the bore size of the magnet that we have access to precluding the use of larger animals.

Alternatively, a relatively recent advance to increase signal-to-noise ratios in MRI that might be utilised here is the use of hyperpolarised substrates. Hyperpolarisation methods such as dynamic nuclear polarisation increase the nuclear spin polarisation in a magnetic field well beyond the thermal equilibrium values described by the Boltzmann distribution that are normally observed, meaning a greater number of nuclei that can be detected by MRS. This is of particular utility for low abundance nuclei such as $^{13}C$, and results in an improvement of signal-to-noise ratios by ~4 orders of magnitude (Bhattacharya et al., 2009). Hyperpolarised MRI has been used in both small animal preclinical models (O h-Ici et al., 2015) as well as in patients as it is non-invasive and generally as safe as conventional MRI (Rider and Tyler, 2013). Proof of principle is provided by the fact that this has been used to probe succinate metabolism in cancers containing mutations in succinate dehydrogenase in both mice and in humans (Day et al., 2007; Lussey-Lepoutre et al., 2015). Preliminary experiments we have conducted encountered problems inducing the glass transition required during dynamic nuclear polarisation in potential esterified substrates, and the literature also reports mixed results (Billingsley et al., 2014; Lussey-Lepoutre et al., 2015; Zacharias et al., 2012).

Succinate accumulation in existing cardioprotective strategies

Ischaemic preconditioning was found not to have any affect upon the accumulation of succinate during the index ischaemia, which suggests that the molecular pathways underlying protection from IPC and by alterations in succinate metabolism are separate – and thus potentially additive. This result has since been replicated by the laboratory of Halestrap (Andrienko et al., 2017), although they incorrectly conclude from this finding that because decreases in succinate accumulation are not necessary to induce cardioprotection that they cannot be sufficient. Indeed the potentially additive nature of strategies targeting succinate metabolism to the range of preconditioning mimetics that have been developed (Hausenloy and Yellon, 2011) increases the potential benefit for translation with increasing moves in the field towards combining two or more therapies with different modes of action (Davidson et al., 2019).

Inhibition of succinate metabolism at reperfusion with disodium malonate

The finding of Valls-Lacalle et al. (2015) that disodium malonate administered at reperfusion could protect the *ex vivo* heart against IRI was unexpected since the malonate anion (which is formed by disodium malonate in aqueous solution) is membrane impermeable and is thus not expected to cross the plasma membrane. For this reason, there has been a widespread use of esterification in previous research to make dicarboxylates and monocarboxylates membrane permeable (Chouchani et al., 2014; Ehinger et al., 2016). The fact that we demonstrate that disodium malonate is taken up into heart tissue means and thence can inhibit SDH means that its uptake across both the plasma and mitochondrial membranes must be carrier mediated. The dicarboxylate carrier in the inner mitochondrial membrane is likely to be responsible for transport into the mitochondria (Palmieri et al., 1971), but the molecular identity of the plasma membrane transporter responsible is not known. Further work that is beyond the scope of this thesis is required to characterise the plasma membrane carrier, with a number of putative dicarboxylate carriers reported but whose affinities for malonate transport have not been characterised.

We show here in the mouse *in vivo* that, similar to reports previously published in the isolated organ, disodium malonate administered at reperfusion in order to inhibit the metabolism of succinate by complex II reduces infarct size. In terms of translation to the clinic, it is worth cautioning that there are potential toxicity issues using inhibitors of mitochondrial respiration such as malonate. Whilst this may be beneficial during IRI, it can nevertheless still be toxic and high doses and is likely undesirable at any concentration outside of this clinical scenario. No adverse effects were observed at the doses used here in the mouse, and since complex II is not obligatory for mitochondrial respiratory chain function, complex I linked respiration may still occur. We also show that the effects of administration of DSM upon malonate levels are transient, and its safety should also be aided by the fact that malonate is a competitive rather than non-competitive inhibitor.

**Summary**

During a series of pilot experiments, we were unable to reliably measure succinate in the rodent heart *in vivo* using magnetic resonance spectroscopy.

We also explored the therapeutic potential of modulating succinate metabolism during IRI. Ischaemic preconditioning was found not to alter the accumulation of succinate in ischaemic heart tissue, despite its efficacy as a cardioprotective strategy. We characterised the use of malonate to inhibit the metabolism of succinate by SDH during reperfusion. The esterified prodrug dimethyl malonate was found to not deliver malonate into heart tissue rapidly enough to prevent succinate metabolism when administered at reperfusion. However the disodium malonate salt is taken up into tissues despite being membrane impermeant, such that it protects against cardiac IRI in a surgical mouse model.

# Chapter 6 – The effect of exercise upon heart function after myocardial infarction: a pilot study

## Introduction

### Heart failure as a disease

As discussed in chapter 1, the development of heart failure is a common consequence of AMI and unlike the decrease in the mortality of AMI itself the prognosis of patients with heart failure has remained virtually unchanged over time (Hellermann et al., 2002). Preventing the development of heart failure and thus the costs associated with its treatment is therefore area of intense interest to the research community.

Current treatment recommendations following AMI involve a cocktail of drugs: beta-blockers, angiotensin-converting enzyme inhibitors (or alternatively angiotensin receptor blockers to achieve an equivalent effect), antiplatelet therapy (commonly either aspirin or dual therapy with aspirin and a $P2Y_{12}$ ADP receptor inhibitor), aldosterone antagonists and lipid lowering therapy such as statins (Reed et al., 2017). Whilst there is evidence that some of these have either direct or indirect effects upon myocardial remodelling, their use is largely targeted at secondary prevention. Similarly, lifestyle changes such as smoking cessation and switching to a 'heart-healthy' diet are advocated, along with increased levels of exercise (O'Gara et al., 2013). The benefits of exercise are multifactorial, but there is increasing evidence that as well as aiding secondary prevention it may have direct effects upon myocardial remodelling. It is therefore salient that we can understand the underlying mechanistic processes in order to guide the prescription and evaluation of exercise in cardiac rehabilitation programs.

### Exercise protocols in preclinical studies

There is a great disparity in clinical studies regarding exercise protocols: when to start, what duration to exercise for, how often and at what intensity (Ismail et al., 2013). This is similarly the case in the basic science research, with a wide variety of protocols reported that is further compounded by the use of differing models of heart failure. Unsurprisingly, there are also a variety of outcomes reported in these studies, with many not showing beneficial effects upon heart function (van Deel et al., 2018). There is therefore a need to validate if the effects of a given exercise protocol to cause beneficial changes in heart function can be replicated before conducting further experiments designed to generate mechanistic insight.

**Aims and objectives**

- Confirm that the exercise protocol reported by Duncker and colleagues can cause beneficial changes in heart function measured by echocardiography after permanent ligation of the LAD in our laboratory.

## Results

Volume of volitional exercise performed

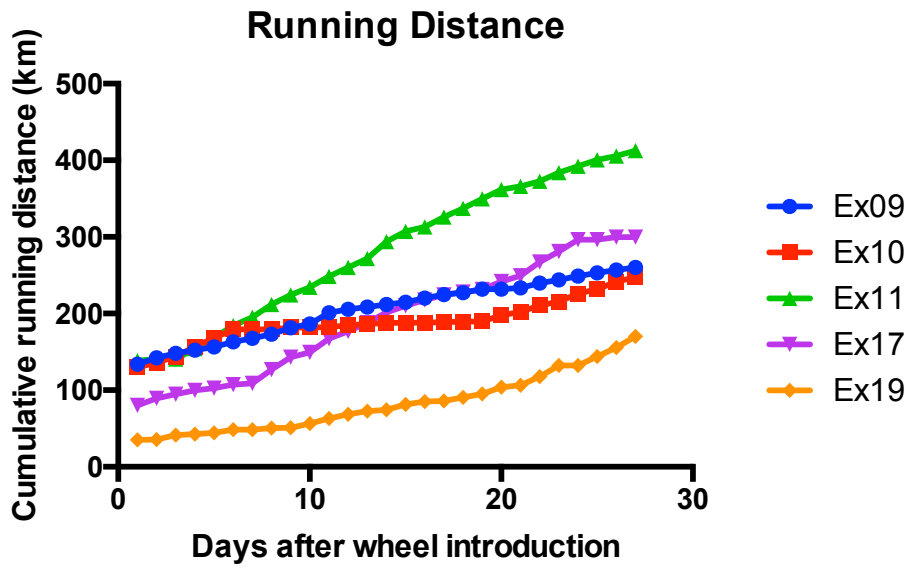


**Figure 6.1 Volitional running behaviour in mice after myocardial infarction.**
Mice were subject to a large myocardial infarction by permanent ligation of the LAD coronary artery, and 2 days later were supplied with a wheel to allow volitional running. Distance was monitored using a wireless odometer containing a reed switch that was magnetically activated once per wheel revolution.

For this study, we chose to use a modified version of the exercise protocol of the Duncker laboratory (Duncker et al., 2014) for volitional exercise after AMI using C57BL/6J mice. These have been previously reported to perform well during volitional exercise (Avila et al., 2017; De Bono et al., 2006; Lerman et al., 2002). The Duncker group provide access to a wheel to allow volitional exercise immediately post surgery, however we introduced the wheel from 2 days post surgery in order to avoid any potential effect upon recovery from the surgery.

Considerable heterogeneity was observed in running behaviour between mice (Fig 6.1, range 170–260 km), but most importantly all mice are found to run considerable distance. Average daily running distance was 7.13 ±0.37 km.

Assessment of cardiac function

Due to the experimental design involving two independent variables, these data were analysed by 2-way ANOVA with factors defined as the time after surgery (hereafter 'time factor') and the volitional exercise provision or not ('treatment factor'). Our data confirm that a large infarct induced by permanent ligation of the LAD coronary artery causes decreases systolic heart function which validates the permanent ligation surgery is being performed properly and consistently with an average decrease in ejection fraction from 63 ± 2.6 % (pooled) pre-surgery to 42 ± 2.1 % (pooled) 2 weeks post-surgery (Fig 6.2A, 2-way ANOVA time factor $p < 0.0001$). Fractional shortening has been suggested to be a more reliable indicator of systolic function than ejection fraction in mice post MI occlusion (Lindsey et al., 2018) as it does not require the assumption to be made that ventricular remodelling is uniform around the ventricle. This similarly showed a decrease following the surgery (Figure 6.2B, 2-way ANOVA time factor $p < 0.0001$). However observed no significant difference between sedentary and exercised mice at any of the time points measured here in either ejection fraction (Fig 6.2A, 2-way ANOVA treatment factor $p = 0.55$, interaction effect $p = 0.81$) or fractional shortening (Fig 6.2B, 2-way ANOVA treatment factor $p = 0.28$, interaction effect $p = 0.89$) was observed, indicating that contrary to the findings of Duncker and colleagues our exercise intervention had no effect upon systolic heart function.

We observed an acute increase in LV mass at 2 weeks post surgery (Figure 6.2E, 2-way ANOVA time factor $p < 0.0001$, 2 weeks significantly different from pre-surgery baseline) from a pre-surgery baseline of pooled row stats. However at 4 weeks this was not significantly difference from the pre-surgery levels. There was no statistical evidence for a change in either stroke volume ((Figure 6.2C, 2-way ANOVA time factor $p = 0.45$) or cardiac output (Figure 6.2D, 2-way ANOVA time factor $p = 0.07$), or in the E/A ratio (Figure 6.2F, 2-way ANOVA time factor $p = 0.55$) which is indicative of diastolic heart function. Similarly no significant effect of the treatment factor or interaction between factors was demonstrated.

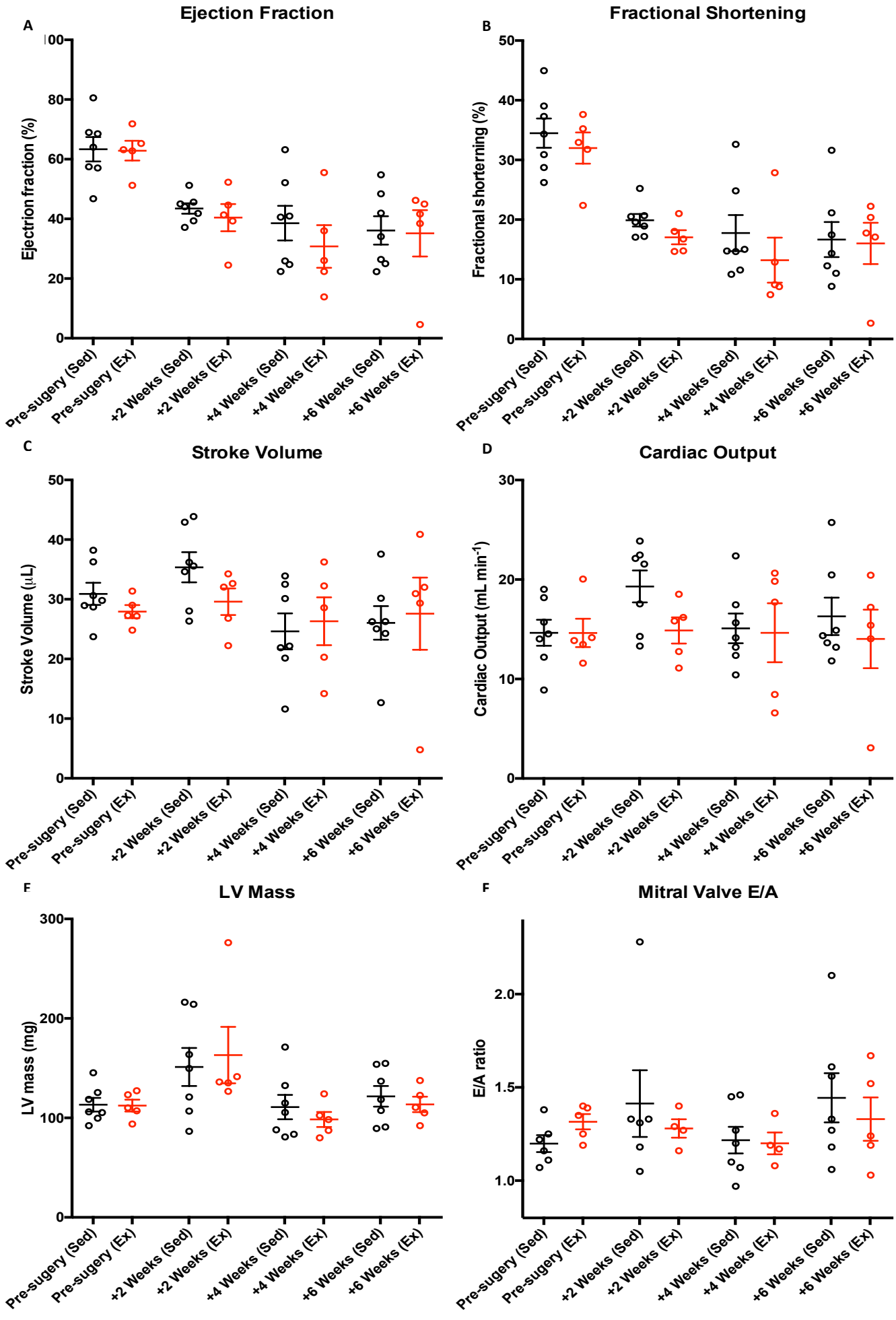
A
Ejection Fraction
Ejection fraction (%)
B
Fractional Shortening
Fractional shorterning (%)
C
Stroke Volume
Stroke Volume (µL)
D
Cardiac Output
Cardiac Output (mL min-1)
F
LV Mass
LV mass (mg)
F
Mitral Valve E/A
E/A ratio
Pre-sugery (Sed)
Pre-sugery (Ex)
+2 Weeks (Sed)
+2 Weeks (Ex)
+4 Weeks (Sed)
+4 Weeks (Ex)
+6 Weeks (Sed)
+6 Weeks (Ex)

**Figure 6.2 Assessment of heart function by echocardiography in exercised or sedentary mice after surgical induction of myocardial infarction.**

Mice were subjected to a large myocardial infarction by permanent ligation of the LAD coronary artery during a surgical procedure. 2 days after the surgery, an exercise wheel was provided to mice in the exercised group (Ex, shown in red; n = 5) in order to allow volitional running. Sedentary animals (Sed, shown in black) were housed in an equivalent environment with the exception that a wheel was not provided (n = 7). Heart function was assessed serially during the procedure by echocardiography under isoflurane anaesthesia.

*2-way ANOVA was performed with factors defined as treatment group and time. Post hoc comparisons were performed relative to pre-surgery baseline values and Šidák correction applied to account for multiplicity of testing.*

Echocardiography was performed by T. Young (Department of Medicine, University of Cambridge).

## Discussion

### Induction of heart failure following AMI

All animals in our experiments subject to permanent ligation of the coronary artery showed decreases is systolic heart function, consistent with the induction of heart failure. Unfortunately, at the time that these experiments were undertaken our home office licence did not include authority to perform sham surgery, and so we are only able to make comparisons relative to baseline levels before the surgery rather than against a non-infarcted control group.

It is worth emphasising the differences between permanent ligation and temporary occlusion model used in an acute setting as earlier in this thesis. Since blood will never be restored to the ischaemic area when the ligation is permanent, all tissue that is functionally ischaemic will become infarcted and so cardioprotective changes are not relevant to these experiments. We are instead interested in looking at the changes that occur in the tissue following infarct generation, and if these processes can be modulated by exercise in order to cause beneficial changes in heart function.

### Effect of volitional exercise upon systolic heart function after AMI

The effects of exercise on LV function and remodelling remain incompletely understood, as highlighted by our failure to replicate beneficial effects using the protocol of de Waard et al that they have published several times with consistent results (de Waard Monique C. et al., 2007; van Deel et al., 2018; de Waard et al., 2010). The reason for this discrepancy is unclear.

Other groups using alternative protocols of volitional exercise after AMI in mice have reported similar findings to ours of exercise not inducing beneficial effects on measures of heart function, but have seen changes in surrogate measures of remodelling such as attenuation of the inflammatory response, decreased scar thinning and fibrosis (Puhl et al., 2015). Others do however show benefit of moderate exercise in the rat (Liao et al., 2019). Similarly in humans the data are equivocal. For example there is mixed evidence for the large exercise component of cardiac rehabilitation programs which have been taken up as standard practice in many

countries including the UK (West et al., 2012). A number of possible explanations may be suggested for this lack of consensus.

Reasons for failing to observe beneficial effects of exercise upon heart function

*When should the exercise occur?*

In order to attempt to keep mortality levels low, the ability to exercise by provision of a wheel in our experiments was only provided after the LAD ligation surgery had been performed. Mice need to habituate to exercising on a wheel but after this period they show regular running behaviour. Therefore, even when a wheel is provided immediately after surgery only a small quantity of exercise is performed in the first few days during this habituation period (de Waard Monique C. et al., 2007). Provision of a wheel before the surgery in order to allow prior habituation might be hypothesised to increase the beneficial effects of the exercise intervention upon the heart, with current data in patients suggesting that the exercise intervention should take place as early as possible after MI (Haykowsky et al., 2011). This is however at odds with current clinical recommendations are to avoid exertion for the first 7 days after MI. Similarly in the mouse model there is likely to be a trade-off between starting exercise early in order to maximise the efficacy of the interventions and increased mortality due to the increased cardiac workload during exercise increasing the chance of rupture of the infarcted ventricle wall.

*Is the magnitude of the exercise stimulus enough?*

There are a multitude of different ways to design an exercise intervention – with different modalities (e.g. swimming vs running), volitional or forced exercise, and regimes that differ in duration, intensity and frequency. These factors may be proposed to account for some of the disparity seen in the literature on the effect of exercise upon heart function after AMI. Zhao et al. for example report that 15 minutes of continuous swimming induced beneficial increases in left ventricular ejection fraction after AMI, but 60 minutes of continuous swimming did not (Zhao et al., 2018). It is however difficult to reconcile such differences in the effects of different quantities of exercise to what is known about the benefits of exercise outside the setting of AMI. A systematic review of the available evidence suggested that the majority of the benefit may be achieved from a very small amount of exercise in humans, with increasingly higher quantities providing increasingly small benefits to health (Warburton and Bredin, 2017). On

the other hand this means that it would seem unlikely that the 'dose' of exercise here is too small. It is also worth noting that particularly given the current pandemic of inactivity in humans, rodents already volitionally perform high amounts of exercise. (De Bono et al., 2006) report ~4 hours of running per day in comparison with typically cardiac rehabilitation programs for patients which typically involve no more that 2.5 hours of exercise per week (Tucker et al., 2019). This creates additional difficultly in drawing comparisons between human and animal studies.

Another reason that the exercise intervention could have been insufficient to induce beneficial changes upon the heart could be that the exercise was at too low an intensity. Due to the motivational theory of exercise performance (Marcora, 2008), volitional exercise such as the protocol we used here will in most cases be performed at a lower intensity than forced exercise protocols. Even forced exercise protocols vary considerably in their intensity. Abad et al. (2017) however show that similar benefit in heart function in mice subject to MI is caused by both moderate intensity continuous exercise (MICT) and intermittent bouts of high intensity and during interval training (high intensity interval training; HIIT). A similar result is also found in human patients with systolic heart failure, where exercise interventions during rehabilitation programs effectively attenuate remodelling of the left ventricle but no differences observed between MICT and HIIT (Tucker et al., 2019). Consistent with this a recent meta-analysis has shown that the transcriptional changes induced by different forms of exercise are more similar than they are different when compared against inactivity (Pillon et al., 2020). It is worth noting however that the benefits of exercise upon heart function post AMI seem to apply to aerobic exercise only, with the addition of resistance training (such as weight lifting) conferring no additional benefit to remodelling indices in heart failure patients (Haykowsky et al., 2007) or in infarcted rats (Grans et al., 2014).

*Is our protocol to determine changes in heart function insufficiently sensitive?*

In this experiment we assessed heart function using echocardiography under sufficient anaesthesia for restraint of the animal. Stress echocardiography is often performed in patients with heart failure (Agricola et al., 2004), due to the increased diagnostic power that it provides compared to echocardiography at rest. Increases in cardiac output are achieved with either the infusion of a beta adrenergic receptor agonist such as dobutamine or exercise (such as when

patients are being prescribed beta adrenergic receptor blockers). Parameters of systolic heart function such as ejection fraction are not independent of changes in cardiac output (Cingolani and Kass, 2011) and so it is likely that increasing the demands placed upon the heart (and in particular when cardiac function is already depressed when the animal is restrained under anaesthesia) may unveil differences in function. It is suggested that this be used for future experiments, even with the trade-off against the ability to discern E/A ratios at high heart rates (Pachon et al., 2015).

Was statistical power sufficient in this pilot study?

Due to the fact that this was intended as a pilot study, group sizes were small. We had not previously conducted a study using echocardiography to measure functional changes after permanent occlusion of the LAD coronary artery, and so did not have our own data available for power calculations: the purpose of this study was in part to collect these data. As such, our ability to detect type 2 errors ($\beta$) is likely to be low and so it cannot be ruled out that our inability to replicate the results of Duncker and colleagues is simply a statistical occurrence. Since we now have an estimate for the observed variation in systolic parameters like ejection fraction, future studies can be properly powered to detect a difference in this endpoint.

Preclinical research and failures to replicate

It is worth noting that we are far from alone in being able to replicate previous findings. There is a growing body of evidence to suggest that perhaps even the majority of preclinical research (either in the published literature or in the private sector) cannot be replicated (Begley and Ellis, 2012; Prinz et al., 2011). This is a problem not only from the point of view of scientific progress, but in particular for translational research that might spawn clinical trials there is an ethical imperative to ensure that findings are true before potentially subjected patients to clinical trials of treatment regimens that are highly unlikely to work. There is therefore a need for the incentive structures for scientists to change such that both the replication of previously published work as well as the publication of ‘negative’ data should be encouraged.

## Summary

The finding that volitional exercise after AMI can cause beneficial changes in heart function was not replicated in our hands using a replication of the protocol published by Duncker and colleagues. Mice were subjected to myocardial infarction by permanent ligation of the LAD coronary artery, and then allowed to perform volitional exercise. All mice developed systolic heart failure, but no difference in heart function was observed between exercised and sedentary animals.

# Chapter 7 – General Discussion

## Summary of work

### Generation of tools

This thesis presents work providing further validation of the ROS production by MitoPQ, and also demonstrates the use of several novel mitochondria-targeted compounds *in vivo* for the first time in order to ratify their use. MitoPQ control compound 2 is a bespoke control compound for use as a negative control in experiments utilising MitoPQ. MitoNeoD is a probe to specifically measure superoxide within the mitochondria: this is important due to its position as the proximal ROS species. MitoCDNB in contrast brings about the opposite change in the redox state of the mitochondria by depletion of glutathione only within this cellular compartment, along with wider disruption of the mitochondrial thioredoxin and peroxiredoxin systems. It is hoped that these tools will be taken up and utilised by the research community at large in order to drive forward our understanding of the role that mitochondrial redox state plays in both physiology and pathology. To this end all of these compounds are free of intellectual property and both MitoNeoD and MitoCDNB are already available to purchase online at the time of writing.

### Mechanistic insights

MitoPQ is also used in the research presented here in order to investigate the role of mitochondrial ROS in the pathology of IRI. Moderate doses of ROS are found to protect the heart against IRI, whilst this effect is not observed at either low or high doses. The phenomenon of hormesis (referring to biphasic dose-response relationships) may be responsible, but further work is needed to unpick whether the cardioprotective signal is encoded in the dose, the species of ROS or the location at which they are generated.

Importantly the ROS generated by MitoPQ at the matrix face of complex I in the mitochondrial respiratory chain are demonstrated to have effects upon the function of the wider cell, including the demonstration for the first time that ROS originating within the mitochondria can alter cytosolic calcium dynamics. There has been significant interest in the interplay between these two species, in particular due to their combined actions in facilitating opening of the MPTP, but it has not previously been possible to delineate the causal relationship between them.

Towards diagnostic markers and therapies

Work is also presented on the role of the mitochondrial metabolite succinate in IRI. Ultimately unsuccessful attempts are made to non-invasively measure this in the ischaemic mouse heart by magnetic resonance spectroscopy, but this remains an open interest due to the potential of succinate as a marker of ischaemia. Disodium malonate is also used to inhibit the metabolism of succinate at reperfusion, which is shown to protect the heart against IRI. Data is also presented to characterise its kinetics of uptake in the heart, which are found to be sufficiently fast to allow its administration as an i.v. infusion during reperfusion.

The therapeutic potential of a protocol of volitional exercise in mice that has previously reported to be beneficial during the development of heart failure after AMI is also assessed, but in our hands this caused no difference in systolic heart function between exercised and sedentary animals.

## Limitations

Much of the work presented in this thesis is based heavily upon the use of a mouse model of AMI which is induced surgically by either temporary occlusion or permanent ligation of the LAD coronary artery. This is known to reproduce the ischaemia seen in many STEMI patients excellently in some respects (particular in comparison to *ex vivo* heart perfusion or cell models of anoxia/reoxygenation) but as will all models it is a simplification of the real scenario and is therefore a less accurate mimic of the clinical situation in other respects. This has been a point of much discussion in the field due to the collective failure to produce any therapy to protect the heart against IRI that has been successfully translated from basic science to produce beneficial outcomes for patients in large scale clinical trials (Downey and Cohen, 2009). The ultimate cause is almost definitely multifactorial, but the use of surgical mouse models such as used here has also been implicated. The animals used here are both young and healthy: this is a practical decision taken to reduce both costs and animal numbers given that both age and clinically relevant co-morbidities both reduce mortality and there is an ethical and legal imperative in undertaking animal experiments to reduce the numbers used. Experiments not reported on here are currently underway using the BKS.Cg-Dock7$^{m}$ *Lepr*$^{db}$/J (db/db) mouse

model which due to a deficient leptin receptor is both obese and has type 2 diabetes mellitus by the time it reaches maturity (Guest and Rahmoune, 2019). These animals are not without their issues for surgery however, with the large fat mass making the control of anaesthesia difficult since almost all anaesthetics are lipophilic and thus accumulate within fatty tissues (Casati and Putzu, 2005). This is a particular issue for the non-recovery protocol of AMI used here which necessitates the mouse be anaesthetised for a long period of time in order to allow sufficient reperfusion for infarct size to be accurately assessed with TTC (Andreas Redel et al., 2008; Pitts et al., 2007). Furthermore the use of sodium pentobarbital as an anaesthetic requires slow and careful titration due to its low therapeutic index, with preliminary experiments suggesting that other 'safer' anaesthetics (such as a ketamine/xylazine combination) should be explored despite the need for increased monitoring due to a significant reduction in the time at a surgical plane of anaesthesia (Flecknell, 2015).

There is another key difference between the means of LAD occlusion in the model used here and the clinical scenario, in that a clean and sterile suture is used to occlude the vessel by external constriction rather than occlusion happening internally by thrombosis after rupture of an atherosclerotic plaque (Libby, 2013). It may thus be hypothesised that from an immunological viewpoint they are two very distinct situations. A vulnerable plaque that ruptures with the ultimate consequences of embolising a coronary artery releases thrombogenic contents which cause platelet activation to initiate the coagulation cascade and form the thrombus in conjunction with other atherosclerotic debris. This is also a highly inflammatory event, as vulnerable plaques also contain high amounts of inflammatory cells such as lipid laden macrophages that will also be released into the circulation (Huo et al., 2003). In addition a vast number of pro-inflammatory molecules are released directly from plaque rupture, from activated platelets and from the endothelium of the vascular wall (Badimon et al., 2012). This milieu is not captured in the LAD occlusion model, and is likely to be highly relevant particularly in studying myocardial remodelling after AMI due to the role of immune cells in this process (O'Rourke et al., 2019).

A second major difference between the LAD occlusion model used here and the clinical scenario is the lack of other drugs that are administered as standard practice in patients undergoing AMI. For the experiments utilising disodium malonate which ultimately has potential for translation into the clinic, it would also be of interest to administer the mouse

undergoing AMI with these very same compounds. Ultimately our aim is to produce a therapy that has better outcomes than current standard best practice, and not to treat the disease in isolation of these confounding factors. This is of particular importance in light of the hypothesis proposed by Jim Downey and colleagues regarding the use of $P2Y_{12}$ ADP receptor inhibitors (such as clopidogrel and ticagrelor) that inhibit platelet activation and aggregation. These are given to patients in order to prevent further thrombosis formation (commonly occurring within a stent) after PPCI, but have also been found to also act directly on the heart to activate protective signalling cascades: acting as a pharmacological mimetic of preconditioning (Cohen and Downey, 2015b).

All the work presented here has been conducted in C56BL/6J mice, and ideally key findings should be repeated in another strain. In particular because this strain has accumulated a mutation in the nicotinamide nucleotide transhydrogenase (NNT) gene which results in a lack of NNT activity (Ronchi et al., 2013). This has been reported to result in several mitochondrial redox abnormalities, including higher rates of $H_2O_2$ release, a higher susceptibility to undergo $Ca^{2+}$-induced mitochondrial permeability transition and an increased ration of oxidised to reduced glutathione compared to mice of an NNT-wildtype C57BL/6 substrain. No difference has been observed between the results presented here in mice and tissues of various other animal origins, and so whilst there is no direct cause to think that this may have confounded the experimental results presented here it remains an unaddressed limitation of this work and something that may be worthwhile addressing by repeating key findings in another mouse strain.

Lastly, I only report data from male mice. It would be instructive to examine female mice as well, and this is of particular importance given that AMI is the disease of interest since there is a growing body of evidence regarding the sex differences in both the presentation and outcomes of AMI in patients, with women having a poorer prognosis (British Heart Foundation, 2019). This is a particular problem in the field with the female gender underrepresented at all stages of the research process from basic research (Ramirez F., Daniel et al., 2017) to clinical trials (Nguyen, Quoc Dinh et al., 2018) and with women also having worse outcomes following AMI (Jackson et al., 2019).

## Clinical Significance

Measurement and modulation of mitochondrial redox state

A large proportion of the work presented here is not intended to be targeted towards future translation, but rather to provide tools to equip basic researchers to investigate the molecular mechanisms underlying IRI, and indeed work to this end is presented here in chapter 4.

It is hoped that further work will elucidate the molecular mechanisms by which the addition of exogenous ROS during IRI may decrease infarct size in the heart, thereby generating novel therapeutic targets. Of particular note is that the protective effect upon the heart of exogenous ROS is recapitulated when administering MitoPQ at reperfusion, as outside a few specific scenarios (for example organ transplantation and some elective surgeries) patients only present once tissue has become ischaemic and thus (given the efficacy of the current strategy of minimising ischaemic time by minimising door to balloon times) the only opportunity to deliver an intervention is either at reperfusion or immediately prior to it. It is worth noting explicitly that despite being able to protect the heart against IRI, MitoPQ itself is not of clinical interest due to the narrow dose range in which it is protective, but rather is used here as a tool to demonstrate the paradoxical effects of ROS in IRI. Its therapeutic index is also low (in our mouse experiments of LAD occlusion, 2.5 nmol was lethal whilst the most efficacious dose was 100 pmol) and in the mouse studies presented here animals undergoing IRI seem particularly vulnerable to it – being killed by doses which appeared well tolerated in normal conscious mice. There is some evidence that it may be arrhythmogenic (Maack et al, unpublished observations) which may offer an explanation for this, and which would be another factor disfavouring its translation into the clinic.

There are however important clinical implications of a biphasic dose-response relationship between the addition of exogenous ROS to the heart during IRI and infarct size. It may be hypothesised that such a relationship might be involved in the failure of interventions that are reproducibly protective in pre-clinical models to show beneficial outcomes in large scale clinical trials as discussed in chapter 4. The biphasic nature of the dose-response means that simple increases in the dose may be effective in some situations (Ferdinandy et al., 1998), but that in other situations increasing the dose cannot be relied upon to have a beneficial outcome

(Przyklenk, 2011). Depending of the internal milieu of a particular patient (determined by factors such as age and co-morbidities along with their genetic background) this dose-response relationship could be shifted, meaning that reliably targeting the dose-range that results in beneficial outcomes is a theoretically difficult problem.

Measurement and modulation of succinate

The measurement and modulation of succinate during IRI are however both things that are ripe for translation into the clinic in the future.

Patients may be suspected of having an AMI due to the location and onset of chest pain, along with characteristic abnormalities on a 12-lead resting ECG (NICE, 2010). A blood sample is concurrently collected in order to measure either cardiac troponin I or troponin T, which are released into the circulation following damage to cardiomyocytes (Rottbauer et al., 1996). However whilst the sensitivity and specificity of troponin measurements are excellent, its temporal resolution is poor as is indicated by the fact that definitions to confirm AMI require that cardiac troponin levels be raised on at least one occasion in the first 24 hours after the onset of chest pain. Its diagnostic utility is therefore limited when viewed in the context of the need to minimise the time from the onset of ischaemia until reperfusion. There is therefore potential for succinate to be used as a new biomarker of IRI with a greater temporal resolution. This has recently been shown in principle in human patients using an MS approach to measure metabolite concentration in blood samples collected in either AMI or control patients, which found that succinate was the only metabolite showing net release from the heart (Kohlhauer et al., 2018). If technically feasible, measuring elevated succinate levels by MRS provides a key advantage over blood samples in that succinate can be measured directly within the ischaemic tissue rather than indirectly following its release into the blood. This is particularly salient given that the ‘cardiac release ratio’ (calculated from blood samples collected at the coronary artery and the coronary sinus) provided a much better correlation to infarct area than the succinate levels measured in peripheral blood samples. It is also of note that the rather than being released in proportion to myocardial damage like cardiac troponins, succinate will be elevated in proportion to the amount of tissue that is ischaemic. Thus it can also provide greater insight since there are no other existing biomarkers for ischaemia itself. In addition to its utility in AMI it may also be of particular utility in ischaemic stroke (i.e. IRI occurring in the brain)

since clinicians do not currently have a biomarker at all to distinguish between this and other differential diagnoses.

Since succinate metabolism at reperfusion has been demonstrated to have a causal role in driving ROS production and thus downstream damage (Chouchani et al., 2014), the opportunity to modulate succinate metabolism during IRI presents itself as a therapeutic target with translational potential. It is noteworthy that the inhibition of complex II within the mitochondria to slow succinate metabolism at reperfusion (such as by the use of disodium malonate presented here) is suitable for translation on a practical level due to the fact that disodium malonate is protective when applied immediately prior to reperfusion. This is in contrast to the multitude of interventions which must be applied before the onset of ischaemia which is an impossibility in a patient undergoing AMI as symptoms will only develop after ischaemia occurs. There is also an increasing move towards combination therapies in order to develop treatment strategies that will be effective in the clinic (Davidson et al., 2019; Hausenloy Derek J. and Yellon Derek M., 2017), and so future experiments should determine if the reduction in infarct size achieved by administering disodium malonate at reperfusion is additive with other cardioprotective strategies such as ischaemic postconditioning, cooling and remote ischaemic conditioning.

There are obviously a number of steps between a potential therapy showing benefit in a small animal model and small phase 2 clinical trials being conducted. In light of the failure of the field of cardioprotection to generate effective drugs despite a multitude of positive preclinical findings, it is important that these occur in a robust and reproducible manner. Consortia such as CAESAR have been founded to test interventions in a rigorous manner, using multiple centres and investigators even for the preclinical experimentation in order to ensure that ineffective therapies may be identified as earlier in the drug discovery process as possible (Jones et al., 2015). Similarly, any potential new therapy should be testing in a range of different preclinical models including those with ageing and other clinically relevant comorbidities as discussed before. Whilst the protective effects of disodium malonate administered at reperfusion have now been demonstrated by at least one other independent laboratory and in two species (Valls-Lacalle et al., 2015), these would be worthwhile experiments to perform.

## Future Directions

As is inevitable with almost any set of experiments, the work presented here raises many questions which would be particularly interesting or important to explore. Where specific experiments suggest themselves, these have been discussed in the relevant chapters. However the tools validated here and the insight into mitochondrial ROS and metabolism generated also have implications beyond the setting of myocardial IRI.

Work was begun in chapter 6 of this thesis to investigate the mechanisms involved in the development of heart failure. This was identified in chapter 1 as a significant contributor to morbidity and mortality following AMI, and an area in which little to no improvement in clinical outcomes has been made during the preceding decades. We have a particular interest in two potential mechanisms through which exercise might confer its benefit to the heart, that relate directly to other work reported on in this thesis.

### *Reactive oxygen species*

Exercise is well known to cause ROS production in skeletal muscle tissue which is known to be involved in adaptive signalling processes that bring about beneficial changes in both exercise capacity as well as other related changes in skeletal muscle (Merry and Ristow, 2016; Radak et al., 2017). Mitochondrial ROS have been shown to increase during contraction of skeletal muscle (Sakellariou et al., 2013; Zuo et al., 2011), which is expected since as detailed in chapter 1 their formation is proportional to mitochondrial respiratory chain flux which increases relative to increase work demands (Gibala et al., 1998). Their involvement in signalling adaptive changes can then be demonstrated by administering large doses of exogenous antioxidants like Vitamin C and E which prevent beneficial changes from occurring (Gomez-Cabrera et al., 2008; Sharman et al., 1971). There is less known about the response to exercise in the heart muscle itself, but an increase in the myocardium was also be expected by analogy to that observed in skeletal muscle due to the increase in cardiac workload during exercise. Moreover, exercise has been shown to also cause an increase in ROS in remote tissue such as the liver (Davies et al., 1982). The tools reported on in chapter 3 to measure and modulate mitochondrial ROS levels equip us to investigate a potential role for ROS in the

failing or remodelling myocardium with a level of specificity that has not previously been possible.

*Succinate*

Exercise is also known to bring about increases in succinate, both locally in skeletal muscle tissue (Gibala et al., 1998; Huffman et al., 2014; Yuan et al., 2017) as well as in the systemic circulation (Hochachka and Dressendorfer, 1976; Lewis et al., 2010). A recent systematic review identifies that succinate is one of the TCA cycle metabolites most increased in the blood after intense exercise (Schranner et al., 2020). Elevated levels of succinate in the systemic circulation have been recently showed to play a role in a variety of physiological processes, including the regulation of thermogenesis in brown fat (Mills et al., 2018) and in the polarisation of macrophages (Mills et al., 2016). In both of these situations succinate has been demonstrated to act via its G-protein coupled receptor GPR91 (alternatively known as Succinate Receptor 1; SCNR1), whose expression has also been reported in the heart (de Castro Fonseca et al., 2016). Indeed this pathway has been shown to be pathologically relevant, with reports that GPR91 is involved in pressure overload induced right ventricular hypertrophy (Aguiar et al., 2014; Yang et al., 2016), aberrant mitochondrial fission (Lu et al., 2018) and in metabolic reprogramming (Li et al., 2017) within the cardiomyocyte as have all been associated with the failing heart. There is therefore reasonable cause to hypothesise that succinate resulting from skeletal muscle metabolism may play a mechanistic role in exerting the beneficial effects of exercise upon the heart. To our knowledge, levels of succinate within the myocardium have not been measured during exercise but this could also be mechanistically relevant.

**Bibliography**

Abad, C.C.C., Nascimento, A.M. do, Santos, L.E. dos, Figueroa, D., Ramona, P., Sartori, M., Scapini, K.B., Albuquerque, O., Moraes-Silva, I.C., Coelho-Júnior, H.J., et al. (2017). Interval and continuous aerobic exercise training similarly increase cardiac function and autonomic modulation in infarcted mice. J. Exerc. Rehabil. *13*, 257–265.

Ago, T., Liu, T., Zhai, P., Chen, W., Li, H., Molkentin, J.D., Vatner, S.F., and Sadoshima, J. (2008). A redox-dependent pathway for regulating class II HDACs and cardiac hypertrophy. Cell *133*, 978–993.

Agricola, E., Oppizzi, M., Pisani, M., and Margonato, A. (2004). Stress echocardiography in heart failure. Cardiovasc. Ultrasound *2*, 11.

Aguiar, C.J., Andrade, V.L., Gomes, E.R.M., Alves, M.N.M., Ladeira, M.S., Pinheiro, A.C.N., Gomes, D.A., Almeida, A.P., Goes, A.M., Resende, R.R., et al. (2010). Succinate modulates Ca2+ transient and cardiomyocyte viability through PKA-dependent pathway. Cell Calcium *47*, 37–46.

Aguiar, C.J., Rocha-Franco, J.A., Sousa, P.A., Santos, A.K., Ladeira, M., Rocha-Resende, C., Ladeira, L.O., Resende, R.R., Botoni, F.A., Barrouin Melo, M., et al. (2014). Succinate causes pathological cardiomyocyte hypertrophy through GPR91 activation. Cell Commun. Signal. CCS *12*.

Akerboom, T.P.M., and Sies, H. (1981). [48] Assay of glutathione, glutathione disulfide, and glutathione mixed disulfides in biological samples. In Methods in Enzymology, (Academic Press), pp. 373–382.

Ambrosio, G., Santoro, G., Tritto, I., Elia, P.P., Duilio, C., Basso, A., Scognamiglio, A., and Chiariello, M. (1992). Effects of ischemia and reperfusion on cardiac tolerance to oxidative stress. Am. J. Physiol. - Heart Circ. Physiol. *262*, H23–H30.

Andreas Redel, Virginija Jazbutyte, Thorsten M. Smul, Markus Lange, Tobias Eckle, Holger Eltzschig, Norbert Roewer, and Franz Kehl (2008). Impact of Ischemia and Reperfusion Times on Myocardial Infarct Size in Mice In Vivo. Exp. Biol. Med. *233*, 84–93.

Andrienko, T., Pasdois, P., Rossbach, A., and Halestrap, A.P. (2016). Real-Time Fluorescence Measurements of ROS and [Ca2+] in Ischemic / Reperfused Rat Hearts: Detectable Increases Occur only after Mitochondrial Pore Opening and Are Attenuated by Ischemic Preconditioning. PLOS ONE *11*, e0167300.

Andrienko, T.N., Pasdois, P., Pereira, G.C., Ovens, M.J., and Halestrap, A.P. (2017). The role of succinate and ROS in reperfusion injury – A critical appraisal. J. Mol. Cell. Cardiol. *110*, 1–14.

Antonucci, S., Mulvey, J.F., Burger, N., Di Sante, M., Hall, A.R., Hinchy, E.C., Caldwell, S.T., Gruszczyk, A.V., Deshwal, S., Hartley, R.C., et al. (2019). Selective mitochondrial superoxide generation in vivo is cardioprotective through hormesis. Free Radic. Biol. Med. *134*, 678–687.

Ashrafian, H., Czibik, G., Bellahcene, M., Aksentijević, D., Smith, A.C., Mitchell, S.J., Dodd, M.S., Kirwan, J., Byrne, J.J., Ludwig, C., et al. (2012). Fumarate Is Cardioprotective via Activation of the Nrf2 Antioxidant Pathway. Cell Metab. *15*, 361–371.

Aune, D., Giovannucci, E., Boffetta, P., Fadnes, L.T., Keum, N., Norat, T., Greenwood, D.C., Riboli, E., Vatten, L.J., and Tonstad, S. (2017). Fruit and vegetable intake and the risk of cardiovascular disease, total cancer and all-cause mortality—a systematic review and dose-response meta-analysis of prospective studies. Int. J. Epidemiol. *46*, 1029–1056.

Avila, J.J., Kim, S.K., and Massett, M.P. (2017). Differences in Exercise Capacity and Responses to Training in 24 Inbred Mouse Strains. Front. Physiol. *8*.

Avkiran, M., and Marber, M.S. (2002). Na(+)/H(+) exchange inhibitors for cardioprotective therapy: progress, problems and prospects. J. Am. Coll. Cardiol. *39*, 747–753.

Babot, M., Birch, A., Labarbuta, P., and Galkin, A. (2014). Characterisation of the active/de-active transition of mitochondrial complex I. Biochim. Biophys. Acta BBA - Bioenerg. *1837*, 1083–1092.

Badimon, L., Padró, T., and Vilahur, G. (2012). Atherosclerosis, platelets and thrombosis in acute ischaemic heart disease. Eur. Heart J. Acute Cardiovasc. Care *1*, 60–74.

Baines, C.P., Goto, M., and Downey, J.M. (1997). Oxygen radicals released during ischemic preconditioning contribute to cardioprotection in the rabbit myocardium. J. Mol. Cell. Cardiol. *29*, 207–216.

Bakermans, A.J., Abdurrachim, D., Moonen, R.P.M., Motaal, A.G., Prompers, J.J., Strijkers, G.J., Vandoorne, K., and Nicolay, K. (2015). Small animal cardiovascular MR imaging and spectroscopy. Prog. Nucl. Magn. Reson. Spectrosc. *88–89*, 1–47.

Balaban, R.S. (2002). Cardiac Energy Metabolism Homeostasis: Role of Cytosolic Calcium. J. Mol. Cell. Cardiol. *34*, 1259–1271.

Balaban, R.S. (2009). Domestication of the cardiac mitochondrion for energy conversion. J. Mol. Cell. Cardiol. *46*, 832–841.

Balaban, R.S., Nemoto, S., and Finkel, T. (2005). Mitochondria, oxidants, and aging. Cell *120*, 483–495.

Balendiran, G.K., Dabur, R., and Fraser, D. (2004). The role of glutathione in cancer. Cell Biochem. Funct. *22*, 343–352.

Begley, C.G., and Ellis, L.M. (2012). Raise standards for preclinical cancer research. Nature *483*, 531–533.

Bernardi, P., and Di Lisa, F. (2015). The mitochondrial permeability transition pore: Molecular nature and role as a target in cardioprotection. J. Mol. Cell. Cardiol. *78*, 100–106.

Bertrand, M.E., Simoons, M.L., Fox, K. a. A., Wallentin, L.C., Hamm, C.W., McFadden, E., de Feyter, P.J., Specchia, G., and Ruzyllo, W. (2000). Management of acute coronary syndromes: acute coronary syndromes without persistent ST segment elevation. Recommendations of the Task Force of the European Society of Cardiology. Eur. Heart J. *21*, 1406–1432.

Bhattacharya, P., Ross, B.D., and Bünger, R. (2009). Cardiovascular Applications of Hyperpolarized Contrast Media and Metabolic Tracers. Exp. Biol. Med. *234*, 1395–1416.

Bienert, G.P., and Chaumont, F. (2014). Aquaporin-facilitated transmembrane diffusion of hydrogen peroxide. Biochim. Biophys. Acta BBA - Gen. Subj. *1840*, 1596–1604.

Billingsley, K.L., Josan, S., Park, J.M., Tee, S.S., Spielman-Sun, E., Hurd, R., Mayer, D., and Spielman, D. (2014). Hyperpolarized [1,4-13C]-Diethylsuccinate: A Potential DNP Substrate for In Vivo Metabolic Imaging. NMR Biomed. *27*, 356–362.

Blanco, R.A., Ziegler, T.R., Carlson, B.A., Cheng, P.-Y., Park, Y., Cotsonis, G.A., Accardi, C.J., and Jones, D.P. (2007). Diurnal variation in glutathione and cysteine redox states in human plasma. Am. J. Clin. Nutr. *86*, 1016–1023.

Bond, J.M., Herman, B., and Lemasters, J.J. (1991). Protection by acidotic pH against anoxia/reoxygenation injury to rat neonatal cardiac myocytes. Biochem. Biophys. Res. Commun. *179*, 798–803.

Booth, F.W., and Laye, M.J. (2009). Lack of adequate appreciation of physical exercise's complexities can pre-empt appropriate design and interpretation in scientific discovery. J. Physiol. *587*, 5527–5539.

Booty, L.M., King, M.S., Thangaratnarajah, C., Majd, H., James, A.M., Kunji, E.R.S., and Murphy, M.P. (2015). The mitochondrial dicarboxylate and 2-oxoglutarate carriers do not transport glutathione. Febs Lett. *589*, 621–628.

Booty, L.M., Gawel, J.M., Cvetko, F., Caldwell, S.T., Hall, A.R., Mulvey, J.F., James, A.M., Hinchy, E.C., Prime, T.A., Arndt, S., et al. (2019). Selective Disruption of Mitochondrial Thiol Redox State in Cells and In Vivo. Cell Chem. Biol. *26*, 449-461.e8.

Brand, M.D. (2016). Mitochondrial generation of superoxide and hydrogen peroxide as the source of mitochondrial redox signaling. Free Radic. Biol. Med. *100*, 14–31.

Braunwald, E., Maroko, P.R., and Libby, P. (1974). Reduction of infarct size following coronary occlusion. Circ. Res. *35 Suppl 3*, 192–201.

Braunwald Eugene, Antman Elliott M., Beasley John W., Califf Robert M., Cheitlin Melvin D., Hochman Judith S., Jones Robert H., Kereiakes Dean, Kupersmith Joel, Levin Thomas N., et al. (2000). ACC/AHA Guidelines for the Management of Patients With Unstable Angina and Non–ST-Segment Elevation Myocardial Infarction: Executive Summary and Recommendations. Circulation *102*, 1193–1209.

British Heart Foundation (2019). Bias and Biology.

Britten, R.A., Green, J.A., and Warenius, H.M. (1992). Cellular glutathione (GSH) and glutathione S-transferase (GST) activity in human ovarian tumor biopsies following exposure to alkylating agents. Int. J. Radiat. Oncol. *24*, 527–531.

Burwell, L.S., Nadtochiy, S.M., Tompkins, A.J., Young, S., and Brookes, P.S. (2006). Direct evidence for S-nitrosation of mitochondrial complex I. Biochem. J. *394*, 627–634.

Cadenas, E., and Davies, K.J.A. (2000). Mitochondrial free radical generation, oxidative stress, and aging1. Free Radic. Biol. Med. *29*, 222–230.

Cadenas, E., Boveris, A., Ragan, C.I., and Stoppani, A.O.M. (1977). Production of superoxide radicals and hydrogen peroxide by NADH-ubiquinone reductase and ubiquinol-cytochrome c reductase from beef-heart mitochondria. Arch. Biochem. Biophys. *180*, 248–257.

Calabrese, E.J., and Baldwin, L.A. (2001). U-Shaped Dose-Responses in Biology, Toxicology, and Public Health. Annu. Rev. Public Health *22*, 15–33.

Casati, A., and Putzu, M. (2005). Anesthesia in the obese patient: Pharmacokinetic considerations. J. Clin. Anesth. *17*, 134–145.

de Castro Fonseca, M., Aguiar, C.J., da Rocha Franco, J.A., Gingold, R.N., and Leite, M.F. (2016). GPR91: expanding the frontiers of Krebs cycle intermediates. Cell Commun. Signal. *14*, 3.

Chance, B., Sies, H., and Boveris, A. (1979). Hydroperoxide metabolism in mammalian organs. Physiol. Rev. *59*, 527–605.

Chappell, J.B., and Hansford, R.G. (1972). 4 - PREPARATION OF MITOCHONDRIA FROM ANIMAL TISSUES AND YEASTS. In Subcellular Components (Second Edition), G.D. Birnie, ed. (Butterworth-Heinemann), pp. 77–91.

Chareonthaitawee, P., Christian, T.F., Hirose, K., Gibbons, R.J., and Rumberger, J.A. (1995). Relation of initial infarct size to extent of left ventricular remodeling in the year after acute myocardial infarction. J. Am. Coll. Cardiol. *25*, 567–573.

Chen, J., Ceholski, D.K., Liang, L., Fish, K., and Hajjar, R.J. (2017). Variability in coronary artery anatomy affects consistency of cardiac damage after myocardial infarction in mice. Am. J. Physiol.-Heart Circ. Physiol. *313*, H275–H282.

Chen, X., Carystinos, G.D., and Batist, G. (1998). Potential for selective modulation of glutathione in cancer chemotherapy. Presented at the International Conference on Glutathione and Glutathione-Linked Enzymes in Human Cancer and Other Diseases, Hilton Head, SC, USA, November 1996.1. Chem. Biol. Interact. *111–112*, 263–275.

Chen W., Gabel S., Steenbergen C., and Murphy E. (1995). A Redox-Based Mechanism for Cardioprotection Induced by Ischemic Preconditioning in Perfused Rat Heart. Circ. Res. *77*, 424–429.

Chia-Ling W., Valvano, J.W., Feldman, M.D., and Pearce, J.A. (2005). Nonlinear conductance-volume relationship for murine conductance catheter measurement system. IEEE Trans. Biomed. Eng. *52*, 1654–1661.

Chiang, T., Messing, R.O., and Chou, W.-H. (2011). Mouse Model of Middle Cerebral Artery Occlusion. J. Vis. Exp. JoVE.

Chinopoulos, C. (2013). Which way does the citric acid cycle turn during hypoxia? The critical role of α-ketoglutarate dehydrogenase complex. J. Neurosci. Res. *91*, 1030–1043.

Chinopoulos, C. (2019). Succinate in ischemia: Where does it come from? Int. J. Biochem. Cell Biol. *115*, 105580.

Chouchani, E.T., Methner, C., Nadtochiy, S.M., Logan, A., Pell, V.R., Ding, S., James, A.M., Cochemé, H.M., Reinhold, J., Lilley, K.S., et al. (2013). Cardioprotection by S-nitrosation of a cysteine switch on mitochondrial complex I. Nat. Med. *19*, 753–759.

Chouchani, E.T., Pell, V.R., Gaude, E., Aksentijević, D., Sundier, S.Y., Robb, E.L., Logan, A., Nadtochiy, S.M., Ord, E.N.J., Smith, A.C., et al. (2014). Ischaemic accumulation of succinate controls reperfusion injury through mitochondrial ROS. Nature *515*, 431–435.

Chouchani, E.T., Pell, V.R., James, A.M., Work, L.M., Saeb-Parsy, K., Frezza, C., Krieg, T., and Murphy, M.P. (2016). A Unifying Mechanism for Mitochondrial Superoxide Production during Ischemia-Reperfusion Injury. Cell Metab. *23*, 254–263.

Chung, H.S., Wang, S.-B., Venkatraman, V., Murray, C.I., and Eyk, J.E.V. (2013). Cysteine Oxidative Posttranslational Modifications Emerging Regulation in the Cardiovascular System. Circ. Res. *112*, 382–392.

Ciano, M., Fuszard, M., Heide, H., Botting, C.H., and Galkin, A. (2013). Conformation-specific crosslinking of mitochondrial complex I. FEBS Lett. *587*, 867–872.

Cingolani, O.H., and Kass, D.A. (2011). Pressure-volume relation analysis of mouse ventricular function. Am. J. Physiol. - Heart Circ. Physiol. *301*, H2198–H2206.

Cochemé, H.M., and Murphy, M.P. (2008). Complex I is the major site of mitochondrial superoxide production by paraquat. J. Biol. Chem. *283*, 1786–1798.

Cochemé, H.M., Logan, A., Prime, T.A., Abakumova, I., Quin, C., McQuaker, S.J., Patel, J.V., Fearnley, I.M., James, A.M., Porteous, C.M., et al. (2012). Using the mitochondria-targeted ratiometric mass spectrometry probe MitoB to measure H2O2 in living Drosophila. Nat. Protoc. *7*, 946–958.

Cohen, M.V., and Downey, J.M. (2015a). Signalling pathways and mechanisms of protection in pre- and postconditioning: historical perspective and lessons for the future. Br. J. Pharmacol. *172*, 1913–1932.

Cohen, M.V., and Downey, J.M. (2015b). Status of P2Y12 treatment must be considered in evaluation of myocardial ischaemia/reperfusion injury. Cardiovasc. Res. *106*, 8–8.

Conrad, M. (2009). Transgenic mouse models for the vital selenoenzymes cytosolic thioredoxin reductase, mitochondrial thioredoxin reductase and glutathione peroxidase 4. Biochim. Biophys. Acta BBA - Gen. Subj. *1790*, 1575–1585.

Coronnello, M., Mini, E., Caciagli, B., Cinellu, M.A., Bindoli, A., Gabbiani, C., and Messori, L. (2005). Mechanisms of Cytotoxicity of Selected Organogold(III) Compounds. J. Med. Chem. *48*, 6761–6765.

Crompton, M., Costi, A., and Hayat, L. (1987). Evidence for the presence of a reversible Ca2+-dependent pore activated by oxidative stress in heart mitochondria. Biochem. J. *245*, 915–918.

Cunniff, B., Snider, G.W., Fredette, N., Hondal, R.J., and Heintz, N.H. (2013). A direct and continuous assay for the determination of thioredoxin reductase activity in cell lysates. Anal. Biochem. *443*, 34–40.

Davidson, S.M., Ferdinandy, P., Andreadou, I., Bøtker, H.E., Heusch, G., Ibáñez, B., Ovize, M., Schulz, R., Yellon, D.M., Hausenloy, D.J., et al. (2019). Multitarget Strategies to Reduce Myocardial Ischemia/Reperfusion Injury: JACC Review Topic of the Week. J. Am. Coll. Cardiol. *73*, 89–99.

Davies, K.J.A. (2016). The Oxygen Paradox, Oxidative Stress, and Ageing. Arch. Biochem. Biophys. *595*, 28–32.

Davies, J.M.S., Cillard, J., Friguet, B., Cadenas, E., Cadet, J., Cayce, R., Fishmann, A., Liao, D., Bulteau, A.-L., Derbré, F., et al. (2017). The Oxygen Paradox, the French Paradox, and age-related diseases. GeroScience *39*, 499–550.

Davies, K.J.A., Quintanilha, A.T., Brooks, G.A., and Packer, L. (1982). Free radicals and tissue damage produced by exercise. Biochem. Biophys. Res. Commun. *107*, 1198–1205.

Day, S.E., Kettunen, M.I., Gallagher, F.A., Hu, D.-E., Lerche, M., Wolber, J., Golman, K., Ardenkjaer-Larsen, J.H., and Brindle, K.M. (2007). Detecting tumor response to treatment using hyperpolarized 13C magnetic resonance imaging and spectroscopy. Nat. Med. *13*, 1382–1387.

De Bono, J.P., Adlam, D., Paterson, D.J., and Channon, K.M. (2006). Novel quantitative phenotypes of exercise training in mouse models. Am. J. Physiol.-Regul. Integr. Comp. Physiol. *290*, R926–R934.

de Waard Monique C., van der Velden Jolanda, Bito Virginie, Ozdemir Semir, Biesmans Liesbeth, Boontje Nicky M., Dekkers Dick H.W., Schoonderwoerd Kees, Schuurbiers Hans C.H., Crom Rini de, et al. (2007). Early Exercise Training Normalizes Myofilament Function and Attenuates Left Ventricular Pump Dysfunction in Mice With a Large Myocardial Infarction. Circ. Res. *100*, 1079–1088.

van Deel, E.D., Octavia, Y., de Waard, M.C., de Boer, M., and Duncker, D.J. (2018). Exercise Training Has Contrasting Effects in Myocardial Infarction and Pressure Overload Due to Divergent Endothelial Nitric Oxide Synthase Regulation. Int. J. Mol. Sci. *19*, 1968.

DeWood, M.A., Spores, J., Notske, R., Mouser, L.T., Burroughs, R., Golden, M.S., and Lang, H.T. (1980). Prevalence of Total Coronary Occlusion during the Early Hours of Transmural Myocardial Infarction. N. Engl. J. Med. *303*, 897–902.

Dey, S., Sidor, A., and O'Rourke, B. (2016). Compartment-specific Control of Reactive Oxygen Species Scavenging by Antioxidant Pathway Enzymes. J. Biol. Chem. *291*, 11185–11197.

Di Virgilio, F., Steinberg, T.H., and Silverstein, S.C. (1990). Inhibition of Fura-2 sequestration and secretion with organic anion transport blockers. Cell Calcium *11*, 57–62.

Dost, T., Cohen, M.V., and Downey, J.M. (2008). Redox signaling triggers protection during the reperfusion rather than the ischemic phase of preconditioning. Basic Res. Cardiol. *103*, 378–384.

Downey, J.M., and Cohen, M.V. (2009). Why Do We Still Not Have Cardioprotective Drugs? Circ. J. *73*, 1171–1177.

Duncker, D.J., Deel, E.D. van, Waard, M.C. de, Boer, M. de, Merkus, D., and Velden, J. van der (2014). Exercise training in adverse cardiac remodeling. Pflüg. Arch. - Eur. J. Physiol. *466*, 1079–1091.

Ehinger, J.K., Piel, S., Ford, R., Karlsson, M., Sjövall, F., Frostner, E.Å., Morota, S., Taylor, R.W., Turnbull, D.M., Cornell, C., et al. (2016). Cell-permeable succinate prodrugs bypass mitochondrial complex I deficiency. Nat. Commun. *7*, 1–8.

Ehsani, A.A., Hagberg, J.M., and Hickson, R.C. (1978). Rapid changes in left ventricular dimensions and mass in response to physical conditioning and deconditioning. Am. J. Cardiol. *42*, 52–56.

Eisner David A., Caldwell Jessica L., Kistamás Kornél, and Trafford Andrew W. (2017). Calcium and Excitation-Contraction Coupling in the Heart. Circ. Res. *121*, 181–195.

Emwas, A.-H., Roy, R., McKay, R.T., Tenori, L., Saccenti, E., Gowda, G.A.N., Raftery, D., Alahmari, F., Jaremko, L., Jaremko, M., et al. (2019). NMR Spectroscopy for Metabolomics Research. Metabolites *9*.

Ertracht, O., Malka, A., Atar, S., and Binah, O. (2014). The mitochondria as a target for cardioprotection in acute myocardial ischemia. Pharmacol. Ther. *142*, 33–40.

Fadda, G.Z., Akmal, M., Lipson, L.G., and Massry, S.G. (1990). Direct effect of parathyroid hormone on insulin secretion from pancreatic islets. Am. J. Physiol. *258*, E975-984.

Ferdinandy, P., Szilvassy, Z., and Baxter, G.F. (1998). Adaptation to myocardial stress in disease states: is preconditioning a healthy heart phenomenon? Trends Pharmacol. Sci. *19*, 223–229.

Fisher, S.G., and Marber, M.S. (2002). An in vivo model of ischaemia–reperfusion injury and ischaemic preconditioning in the mouse heart. J. Pharmacol. Toxicol. Methods *48*, 161–169.

Flecknell, P. (2015). Laboratory Animal Anaesthesia - 4th Edition (Academic Press).

Fortmann, S.P., Burda, B.U., Senger, C.A., Lin, J.S., and Whitlock, E.P. (2013). Vitamin and Mineral Supplements in the Primary Prevention of Cardiovascular Disease and Cancer: An Updated Systematic Evidence Review for the U.S. Preventive Services Task Force. Ann. Intern. Med. *159*, 824–834.

Frangogiannis, N.G. (2006). Targeting the inflammatory response in healing myocardial infarcts. Curr. Med. Chem. *13*, 1877–1893.

Galkin, A., Abramov, A.Y., Frakich, N., Duchen, M.R., and Moncada, S. (2009). Lack of Oxygen Deactivates Mitochondrial Complex I IMPLICATIONS FOR ISCHEMIC INJURY? J. Biol. Chem. *284*, 36055–36061.

Garcia-Dorado, D., Ruiz-Meana, M., Inserte, J., Rodriguez-Sinovas, A., and Piper, H.M. (2012). Calcium-mediated cell death during myocardial reperfusion. Cardiovasc. Res. *94*, 168–180.

Gibala, M.J., MacLean, D.A., Graham, T.E., and Saltin, B. (1998). Tricarboxylic acid cycle intermediate pool size and estimated cycle flux in human muscle during exercise. Am. J. Physiol.-Endocrinol. Metab. *275*, E235–E242.

van Gilst, W.H., Herre Kingma, J., Peels, K.H., Dambrink, J.-H.E., and Sutton, M.St.J. (1996). Which patient benefits from early angiotensin-converting enzyme inhibition after

myocardial infarction? Results of one-year serial echocardiographic follow-up from the captopril and thrombolysis study (CATS). J. Am. Coll. Cardiol. *28*, 114–121.

Gomez-Cabrera, M.-C., Domenech, E., Romagnoli, M., Arduini, A., Borras, C., Pallardo, F.V., Sastre, J., and Viña, J. (2008). Oral administration of vitamin C decreases muscle mitochondrial biogenesis and hampers training-induced adaptations in endurance performance. Am. J. Clin. Nutr. *87*, 142–149.

Gorenkova, N., Robinson, E., Grieve, D.J., and Galkin, A. (2013). Conformational Change of Mitochondrial Complex I Increases ROS Sensitivity During Ischemia. Antioxid. Redox Signal. *19*, 1459–1468.

Grans, C.F., Feriani, D.J., Abssamra, M.E.V., Rocha, L.Y., Carrozzi, N.M., Mostarda, C., Figueroa, D.M., Angelis, K.D., Irigoyen, M.C., and Rodrigues, B. (2014). Resistance training after myocardial infarction in rats: its role on cardiac and autonomic function. Arq. Bras. Cardiol. *103*, 60–68.

Guest, P.C., and Rahmoune, H. (2019). Characterization of the db/db Mouse Model of Type 2 Diabetes. In Pre-Clinical Models: Techniques and Protocols, P.C. Guest, ed. (New York, NY: Springer), pp. 195–201.

Guillen, J. (2012). FELASA Guidelines and Recommendations. J. Am. Assoc. Lab. Anim. Sci. JAALAS *51*, 311–321.

Gutscher, M., Sobotta, M.C., Wabnitz, G.H., Ballikaya, S., Meyer, A.J., Samstag, Y., and Dick, T.P. (2009). Proximity-based protein thiol oxidation by H2O2-scavenging peroxidases. J. Biol. Chem. *284*, 31532–31540.

Halestrap, A.P. (1991). Calcium-dependent opening of a non-specific pore in the mitochondrial inner membrane is inhibited at pH values below 7. Implications for the protective effect of low pH against chemical and hypoxic cell damage. Biochem. J. *278*, 715–719.

Harman, D. (1992). Free radical theory of aging. Mutat. Res. *275*, 257–266.

Hassan, H.M. (1984). Exacerbation of superoxide radical formation by Paraquat. B.-M. in Enzymology, ed. (Academic Press), pp. 523–532.

Hausenloy, D.J., and Yellon, D.M. (2003). The mitochondrial permeability transition pore: its fundamental role in mediating cell death during ischaemia and reperfusion. J. Mol. Cell. Cardiol. *35*, 339–341.

Hausenloy, D.J., and Yellon, D.M. (2011). The therapeutic potential of ischemic conditioning: an update. Nat. Rev. Cardiol. *8*, 619–629.

Hausenloy, D., Wynne, A., Duchen, M., and Yellon, D. (2004). Transient Mitochondrial Permeability Transition Pore Opening Mediates Preconditioning-Induced Protection. Circulation *109*, 1714–1717.

Hausenloy, D. J., and Yellon, D. M. (2017). Combination Therapy to Target Reperfusion Injury After ST-Segment–Elevation Myocardial Infarction. Circulation *136*, 904–906.

Haykowsky, M., Scott, J., Esch, B., Schopflocher, D., Myers, J., Paterson, I., Warburton, D., Jones, L., and Clark, A.M. (2011). A meta-analysis of the effects of exercise training on left ventricular remodeling following myocardial infarction: start early and go longer for greatest exercise benefits on remodeling. Trials *12*, 92.

Haykowsky, M.J., Liang, Y., Pechter, D., Jones, L.W., McAlister, F.A., and Clark, A.M. (2007). A meta-analysis of the effect of exercise training on left ventricular remodeling in heart failure patients: the benefit depends on the type of training performed. J. Am. Coll. Cardiol. *49*, 2329–2336.

Hegstad, A.C., Antonsen, O.H., and Ytrehus, K. (1997). Low concentrations of hydrogen peroxide improve post-ischaemic metabolic and functional recovery in isolated perfused rat hearts. J. Mol. Cell. Cardiol. *29*, 2779–2787.

Hellermann, J.P., Jacobsen, S.J., Gersh, B.J., Rodeheffer, R.J., Reeder, G.S., and Roger, V. éronique L. (2002). Heart failure after myocardial infarction: a review. Am. J. Med. *113*, 324–330.

Heusch, G., and Schulz, R. (2001). Perfusion-contraction match and mismatch. Basic Res. Cardiol. *96*, 1–10.

Hirst, J., Sucheta, A., Ackrell, B.A.C., and Armstrong, F.A. (1996). Electrocatalytic Voltammetry of Succinate Dehydrogenase: Direct Quantification of the Catalytic Properties of a Complex Electron-Transport Enzyme. J. Am. Chem. Soc. *118*, 5031–5038.

Hochachka, P.W., and Dressendorfer, R.H. (1976). Succinate accumulation in man during exercise. Eur. J. Appl. Physiol. *35*, 235–242.

Hoek, T.L.V., Becker, L.B., Shao, Z., Li, C., and Schumacker, P.T. (1998). Reactive Oxygen Species Released from Mitochondria during Brief Hypoxia Induce Preconditioning in Cardiomyocytes. J. Biol. Chem. *273*, 18092–18098.

Holmström, K.M., and Finkel, T. (2014). Cellular mechanisms and physiological consequences of redox-dependent signalling. Nat. Rev. Mol. Cell Biol. *15*, 411–421.

Honda, H.M., and Ping, P. (2006). Mitochondrial Permeability Transition in Cardiac Cell Injury and Death. Cardiovasc. Drugs Ther. *20*, 425–432.

Huffman, K.M., Koves, T.R., Hubal, M.J., Abouassi, H., Beri, N., Bateman, L.A., Stevens, R.D., Ilkayeva, O.R., Hoffman, E.P., Muoio, D.M., et al. (2014). Metabolite signatures of exercise training in human skeletal muscle relate to mitochondrial remodelling and cardiometabolic fitness. Diabetologia *57*, 2282–2295.

Huie, R.E., and Padmaja, S. (1993). The reaction of no with superoxide. Free Radic. Res. Commun. *18*, 195–199.

Huo, Y., Schober, A., Forlow, S.B., Smith, D.F., Hyman, M.C., Jung, S., Littman, D.R., Weber, C., and Ley, K. (2003). Circulating activated platelets exacerbate atherosclerosis in mice deficient in apolipoprotein E. Nat. Med. *9*, 61–67.

Imlay, J.A. (2008). Cellular Defenses against Superoxide and Hydrogen Peroxide. Annu. Rev. Biochem. *77*, 755–776.

Ishikawa, T. (1992). The ATP-dependent glutathione S-conjugate export pump. Trends Biochem. Sci. *17*, 463–468.

Ismail, H., McFarlane, J.R., Nojoumian, A.H., Dieberg, G., and Smart, N.A. (2013). Clinical Outcomes and Cardiovascular Responses to Different Exercise Training Intensities in

Patients With Heart Failure: A Systematic Review and Meta-Analysis. JACC Heart Fail. *1*, 514–522.

Jackson, A.M., Zhang, R., Findlay, I., Robertson, K., Lindsay, M., Morris, T., Forbes, B., Papworth, R., McConnachie, A., Mangion, K., et al. (2019). Healthcare disparities for women hospitalized with myocardial infarction and angina. Eur. Heart J. - Qual. Care Clin. Outcomes.

Jackson, B.M., Gorman, J.H., Moainie, S.L., Guy, T.S., Narula, N., Narula, J., John-Sutton, M.G., Edmunds, L.H., and Gorman, R.C. (2002). Extension of borderzone myocardium in postinfarction dilated cardiomyopathy. J. Am. Coll. Cardiol. *40*, 1160–1167; discussion 1168-1171.

Jennings, R.B., Sommers, H.M., Smyth, G.A., Flack, H.A., and Linn, H. (1960). Myocardial necrosis induced by temporary occlusion of a coronary artery in the dog. Arch. Pathol. *70*, 68–78.

Jones, S.P., Tang, X.-L., Guo, Y., Steenbergen, C., Lefer, D.J., Kukreja, R.C., Kong, M., Li, Q., Bhushan, S., Zhu, X., et al. (2015). The NHLBI-sponsored Consortium for preclinicAl assESsment of cARdioprotective therapies (CAESAR): a new paradigm for rigorous, accurate, and reproducible evaluation of putative infarct-sparing interventions in mice, rabbits, and pigs. Circ. Res. *116*, 572–586.

Kaludercic, N., Carpi, A., Nagayama, T., Sivakumaran, V., Zhu, G., Lai, E.W., Bedja, D., De Mario, A., Chen, K., Gabrielson, K.L., et al. (2013). Monoamine Oxidase B Prompts Mitochondrial and Cardiac Dysfunction in Pressure Overloaded Hearts. Antioxid. Redox Signal. *20*, 267–280.

Kalyanaraman, B., Darley-Usmar, V., Davies, K.J.A., Dennery, P.A., Forman, H.J., Grisham, M.B., Mann, G.E., Moore, K., Roberts, L.J., and Ischiropoulos, H. (2012). Measuring reactive oxygen and nitrogen species with fluorescent probes: challenges and limitations. Free Radic. Biol. Med. *52*, 1–6.

Kavianipour, M., Wikström, G., Ronquist, G., and Waldenström, A. (2003). Validity of the microdialysis technique for experimental in vivo studies of myocardial energy metabolism. Acta Physiol. Scand. *179*, 61–65.

Kim, K.-H., Rodriguez, A.M., Carrico, P.M., and Melendez, J.A. (2001). Potential Mechanisms for the Inhibition of Tumor Cell Growth by Manganese Superoxide Dismutase. Antioxid. Redox Signal. *3*, 361–373.

Kohlhauer, M., Dawkins, S., Costa, A.S.H., Lee, R., Young, T., Pell, V.R., Choudhury, R.P., Banning, A.P., Kharbanda, R.K., Oxford Acute Myocardial Infarction (OxAMI) Study, et al. (2018). Metabolomic Profiling in Acute ST-Segment-Elevation Myocardial Infarction Identifies Succinate as an Early Marker of Human Ischemia-Reperfusion Injury. J. Am. Heart Assoc. *7*.

Kohr, M.J., Sun, J., Aponte, A., Wang, G., Gucek, M., Murphy, E., and Steenbergen, C. (2011). Simultaneous Measurement of Protein Oxidation and S-Nitrosylation During Preconditioning and Ischemia/Reperfusion Injury With Resin-Assisted Capture. Circ. Res. *108*, 418–426.

Kong, H., Jones, P.P., Koop, A., Zhang, L., Duff, H.J., and Wayne Chen, S.R. (2008). Caffeine Induces Ca2+ Release by Reducing The Threshold for Luminal Ca2+ Activation of the Ryanodine Receptor. Biochem. J. *414*, 441–452.

Konstam, M.A., Kramer, D.G., Patel, A.R., Maron, M.S., and Udelson, J.E. (2011). Left Ventricular Remodeling in Heart Failure: Current Concepts in Clinical Significance and Assessment. JACC Cardiovasc. Imaging *4*, 98–108.

Korichneva, I., Hoyos, B., Chua, R., Levi, E., and Hammerling, U. (2002). Zinc release from protein kinase C as the common event during activation by lipid second messenger or reactive oxygen. J. Biol. Chem. *277*, 44327–44331.

Kumar, V., Kleffmann, T., Hampton, M.B., Cannell, M.B., and Winterbourn, C.C. (2013). Redox proteomics of thiol proteins in mouse heart during ischemia/reperfusion using ICAT reagents and mass spectrometry. Free Radic. Biol. Med. *58*, 109–117.

Larson, E.R., Feldman, M.D., Valvano, J.W., and Pearce, J.A. (2013). Analysis of the Spatial Sensitivity of Conductance/Admittance Catheter Ventricular Volume Estimation. IEEE Trans. Biomed. Eng. *60*, 2316–2324.

Lee, T.K., Li, L., and Ballatori, N. (1997). Hepatic glutathione and glutathione S-conjugate transport mechanisms. Yale J. Biol. Med. *70*, 287–300.

Leichert, L.I., Gehrke, F., Gudiseva, H.V., Blackwell, T., Ilbert, M., Walker, A.K., Strahler, J.R., Andrews, P.C., and Jakob, U. (2008). Quantifying changes in the thiol redox proteome upon oxidative stress in vivo. Proc. Natl. Acad. Sci. *105*, 8197–8202.

Leo, S., Szabadkai, G., and Rizzuto, R. (2008). The Mitochondrial Antioxidants MitoE2 and MitoQ10 Increase Mitochondrial Ca2+ Load upon Cell Stimulation by Inhibiting Ca2+ Efflux from the Organelle. Ann. N. Y. Acad. Sci. *1147*, 264–274.

Lerman, I., Harrison, B.C., Freeman, K., Hewett, T.E., Allen, D.L., Robbins, J., and Leinwand, L.A. (2002). Genetic variability in forced and voluntary endurance exercise performance in seven inbred mouse strains. J. Appl. Physiol. *92*, 2245–2255.

Lewis, G.D., Farrell, L., Wood, M.J., Martinovic, M., Arany, Z., Rowe, G.C., Souza, A., Cheng, S., McCabe, E.L., Yang, E., et al. (2010). Metabolic Signatures of Exercise in Human Plasma. Sci. Transl. Med. *2*, 33ra37-33ra37.

Li, J., Yang, Y.-L., Li, L.-Z., Zhang, L., Liu, Q., Liu, K., Li, P., Liu, B., and Qi, L.-W. (2017). Succinate accumulation impairs cardiac pyruvate dehydrogenase activity through GRP91-dependent and independent signaling pathways: Therapeutic effects of ginsenoside Rb1. Biochim. Biophys. Acta BBA - Mol. Basis Dis. *1863*, 2835–2847.

Li, N., Ragheb, K., Lawler, G., Sturgis, J., Rajwa, B., Melendez, J.A., and Robinson, J.P. (2003). Mitochondrial Complex I Inhibitor Rotenone Induces Apoptosis through Enhancing Mitochondrial Reactive Oxygen Species Production. J. Biol. Chem. *278*, 8516–8525.

Liang, D. (2018). A Salutary Role of Reactive Oxygen Species in Intercellular Tunnel-Mediated Communication. Front. Cell Dev. Biol. *6*.

Liao, Z., Li, D., Chen, Y., Li, Y., Huang, R., Zhu, K., Chen, H., Yuan, Z., Zheng, X., Zhao, H., et al. (2019). Early moderate exercise benefits myocardial infarction healing via improvement of inflammation and ventricular remodelling in rats. J. Cell. Mol. Med. *23*, 8328–8342.

Libby, P. (2013). Mechanisms of Acute Coronary Syndromes and Their Implications for Therapy. N Engl J Med *23,* 368(21):2004-13

Liberman, E.A., and Skulachev, V.P. (1970). Conversion of biomembrane-produced energy into electric form. IV. General discussion. Biochim. Biophys. Acta *216*, 30–42.

Liberman, E.A., Topaly, V.P., Tsofina, L.M., Jasaitis, A.A., and Skulachev, V.P. (1969). Mechanism of Coupling of Oxidative Phosphorylation and the Membrane Potential of Mitochondria. Nature *222*, 1076–1078.

Lindsey, M.L., Kassiri, Z., Virag, J.A.I., de Castro Brás, L.E., and Scherrer-Crosbie, M. (2018). Guidelines for measuring cardiac physiology in mice. Am. J. Physiol.-Heart Circ. Physiol. *314*, H733–H752.

Liu, T., Wu, C., Jain, M.R., Nagarajan, N., Yan, L., Dai, H., Cui, C., Baykal, A., Pan, S., Ago, T., et al. (2015). Master redox regulator Trx1 upregulates SMYD1 & modulates lysine methylation. Biochim. Biophys. Acta *1854*, 1816–1822.

Logan, A., Cochemé, H.M., Li Pun, P.B., Apostolova, N., Smith, R.A.J., Larsen, L., Larsen, D.S., James, A.M., Fearnley, I.M., Rogatti, S., et al. (2014). Using exomarkers to assess mitochondrial reactive species in vivo. Biochim. Biophys. Acta BBA - Gen. Subj. *1840*, 923–930.

Logan, A., Pell, V.R., Shaffer, K.J., Evans, C., Stanley, N.J., Robb, E.L., Prime, T.A., Chouchani, E.T., Cochemé, H.M., Fearnley, I.M., et al. (2016). Assessing the Mitochondrial Membrane Potential in Cells and In Vivo using Targeted Click Chemistry and Mass Spectrometry. Cell Metab. *23*, 379–385.

Lu, Y.-T., Li, L.-Z., Yang, Y.-L., Yin, X., Liu, Q., Zhang, L., Liu, K., Liu, B., Li, J., and Qi, L.-W. (2018). Succinate induces aberrant mitochondrial fission in cardiomyocytes through GPR91 signaling. Cell Death Dis. *9*, 1–14.

Lucas, M., and Solano, F. (1992). Coelenterazine is a superoxide anion-sensitive chemiluminescent probe: Its usefulness in the assay of respiratory burst in neutrophils. Anal. Biochem. *206*, 273–277.

Lussey-Lepoutre, C., Bellucci, A., Morin, A., Buffet, A., Amar, L., Janin, M., Ottolenghi, C., Zinzindohoué, F., Autret, G., Burnichon, N., et al. (2015). In Vivo Detection of Succinate by Magnetic Resonance Spectroscopy as a Hallmark of SDHx Mutations in Paraganglioma. Clin. Cancer Res.

Maessen, M.F., Eijsvogels, T.M., Stevens, G., van Dijk, A.P., and Hopman, M.T. (2017). Benefits of lifelong exercise training on left ventricular function after myocardial infarction. Eur. J. Prev. Cardiol. *24*, 1856–1866.

Mailloux, R.J. (2015). Teaching the fundamentals of electron transfer reactions in mitochondria and the production and detection of reactive oxygen species. Redox Biol. *4*, 381–398.

Majumder, P.K., Mishra, N.C., Sun, X., Bharti, A., Kharbanda, S., Saxena, S., and Kufe, D. (2001). Targeting of protein kinase C delta to mitochondria in the oxidative stress response. Cell Growth Differ. Mol. Biol. J. Am. Assoc. Cancer Res. *12*, 465–470.

Maklashina, E., Berthold, D.A., and Cecchini, G. (1998). Anaerobic Expression of Escherichia coli Succinate Dehydrogenase: Functional Replacement of Fumarate Reductase in the Respiratory Chain during Anaerobic Growth. J. Bacteriol. *180*, 5989–5996.

Marcora, S.M. (2008). Do we really need a central governor to explain brain regulation of exercise performance? Eur. J. Appl. Physiol. *104*, 929.

Martin, J.L., Costa, A.S.H., Gruszczyk, A.V., Beach, T.E., Allen, F.M., Prag, H.A., Hinchy, E.C., Mahbubani, K., Hamed, M., Tronci, L., et al. (2019). Succinate accumulation drives ischaemia-reperfusion injury during organ transplantation. Nat. Metab. *1*, 966–974.

McCord, J.M., and Day, E.D. (1978). Superoxide-dependent production of hydroxyl radical catalyzed by iron-EDTA complex. FEBS Lett. *86*, 139–142.

McKay R G, Pfeffer M A, Pasternak R C, Markis J E, Come P C, Nakao S, Alderman J D, Ferguson J J, Safian R D, and Grossman W (1986). Left ventricular remodeling after myocardial infarction: a corollary to infarct expansion. Circulation *74*, 693–702.

McMullen, J.R., and Jennings, G.L. (2007). Differences Between Pathological and Physiological Cardiac Hypertrophy: Novel Therapeutic Strategies to Treat Heart Failure. Clin. Exp. Pharmacol. Physiol. *34*, 255–262.

Merry, T.L., and Ristow, M. (2016). Mitohormesis in exercise training. Free Radic. Biol. Med. *98*, 123–130.

Methner, C., Chouchani, E.T., Buonincontri, G., Pell, V.R., Sawiak, S.J., Murphy, M.P., and Krieg, T. (2014). Mitochondria selective S-nitrosation by mitochondria-targeted S-nitrosothiol protects against post-infarct heart failure in mouse hearts. Eur. J. Heart Fail. *16*, 712–717.

Mik, E.G., Ince, C., Eerbeek, O., Heinen, A., Stap, J., Hooibrink, B., Schumacher, C.A., Balestra, G.M., Johannes, T., Beek, J.F., et al. (2009). Mitochondrial oxygen tension within the heart. J. Mol. Cell. Cardiol. *46*, 943–951.

Mills, E.L., Kelly, B., Logan, A., Costa, A.S.H., Varma, M., Bryant, C.E., Tourlomousis, P., Däbritz, J.H.M., Gottlieb, E., Latorre, I., et al. (2016). Succinate Dehydrogenase Supports Metabolic Repurposing of Mitochondria to Drive Inflammatory Macrophages. Cell *167*, 457-470.e13.

Mills, E.L., Pierce, K.A., Jedrychowski, M.P., Garrity, R., Winther, S., Vidoni, S., Yoneshiro, T., Spinelli, J.B., Lu, G.Z., Kazak, L., et al. (2018). Accumulation of succinate controls activation of adipose tissue thermogenesis. Nature *560*, 102–106.

Mitchell, P. (1961). Coupling of Phosphorylation to Electron and Hydrogen Transfer by a Chemi-Osmotic type of Mechanism. Nature *191*, 144–148.

Morris, J.N., Heady, J.A., Raffle, P.A., Roberts, C.G., and Parks, J.W. (1953). Coronary heart-disease and physical activity of work. Lancet Lond. Engl. *262*, 1111–1120; concl.

Murphy, M.P. (2009). How mitochondria produce reactive oxygen species. Biochem. J. *417*, 1–13.

Murphy, M.P. (2012). Mitochondrial thiols in antioxidant protection and redox signaling: distinct roles for glutathionylation and other thiol modifications. Antioxid. Redox Signal. *16*, 476–495.

Murry, C.E., Jennings, R.B., and Reimer, K.A. (1986). Preconditioning with ischemia: a delay of lethal cell injury in ischemic myocardium. Circulation *74*, 1124–1136.

Nagel, E., Meyer zu Vilsendorf, A., Bartels, M., and Pichlmayr, R. (1997). Antioxidative vitamins in prevention of ischemia/reperfusion injury. Int. J. Vitam. Nutr. Res. Int. Z. Für Vitam.- Ernährungsforschung J. Int. Vitaminol. Nutr. *67*, 298–306.

Nethery, D., Stofan, D., Callahan, L., DiMarco, A., and Supinski, G. (1999). Formation of reactive oxygen species by the contracting diaphragm is PLA(2) dependent. J. Appl. Physiol. Bethesda Md 1985 *87*, 792–800.

Neubauer, S. (2007). The Failing Heart — An Engine Out of Fuel. N. Engl. J. Med. *356*, 1140–1151.

Nguyen, Quoc Dinh, Peters, Eric, Wassef, Andreanne, Desmarais, Philippe, Rémillard-Labrosse, Delphine, and Tremblay-Gravel, Maxime (2018). Evolution of Age and Female Representation in the Most-Cited Randomized Controlled Trials of Cardiology of the Last 20 Years. Circ. Cardiovasc. Qual. Outcomes *11*, e004713.

NICE (2010). Recommendations | Recent-onset chest pain of suspected cardiac origin: assessment and diagnosis | Guidance | NICE.

Nicolli, A., Basso, E., Petronilli, V., Wenger, R.M., and Bernardi, P. (1996). Interactions of Cyclophilin with the Mitochondrial Inner Membrane and Regulation of the Permeability Transition Pore, a Cyclosporin A-sensitive Channel. J. Biol. Chem. *271*, 2185–2192.

O h-Ici, D., Wespi, P., Busch, J., Wissmann, L., Krajewski, M., Weiss, K., Sigfridsson, A., Messroghli, D., and Kozerke, S. (2015). Hyperpolarized Metabolic MR Imaging of Acute Myocardial Changes and Recovery after Ischemia-Reperfusion in a Small-Animal Model. Radiology *278*, 742–751.

O'Gara, P.T., Kushner, F.G., Ascheim, D.D., Casey, D.E., Chung, M.K., Lemos, J.A. de, Ettinger, S.M., Fang, J.C., Fesmire, F.M., Franklin, B.A., et al. (2013). 2013 ACCF/AHA Guideline for the Management of ST-Elevation Myocardial Infarction: A Report of the American College of Cardiology Foundation/American Heart Association Task Force on Practice Guidelines. J. Am. Coll. Cardiol. *61*, e78–e140.

Ogg, R.J., Kingsley, P.B., and Taylor, J.S. (1994). WET, a T1- and B1-insensitive water-suppression method for in vivo localized 1H NMR spectroscopy. J. Magn. Reson. B *104*, 1–10.

O'Rourke, S.A., Dunne, A., and Monaghan, M.G. (2019). The Role of Macrophages in the Infarcted Myocardium: Orchestrators of ECM Remodeling. Front. Cardiovasc. Med. *6*.

Pacher, P., Nagayama, T., Mukhopadhyay, P., Bátkai, S., and Kass, D.A. (2008). Measurement of cardiac function using pressure–volume conductance catheter technique in mice and rats. Nat. Protoc. *3*, 1422–1434.

Pachon, R.E., Scharf, B.A., Vatner, D.E., and Vatner, S.F. (2015). Best anesthetics for assessing left ventricular systolic function by echocardiography in mice. Am. J. Physiol.-Heart Circ. Physiol. *308*, H1525–H1529.

Palmieri, F., Prezioso, G., Quagliariello, E., and Klingenberg, M. (1971). Kinetic Study of the Dicarboxylate Carrier in Rat Liver Mitochondria. Eur. J. Biochem. *22*, 66–74.

Pedersen, B.K., and Saltin, B. (2006). Evidence for prescribing exercise as therapy in chronic disease. Scand. J. Med. Sci. Sports *16*, 3–63.

Petronilli, V., Miotto, G., Canton, M., Brini, M., Colonna, R., Bernardi, P., and Di Lisa, F. (1999). Transient and long-lasting openings of the mitochondrial permeability transition pore can be monitored directly in intact cells by changes in mitochondrial calcein fluorescence. Biophys. J. *76*, 725–734.

Pfeffer M A, and Braunwald E (1990). Ventricular remodeling after myocardial infarction. Experimental observations and clinical implications. Circulation *81*, 1161–1172.

Pillon, N.J., Gabriel, B.M., Dollet, L., Smith, J.A.B., Puig, L.S., Botella, J., Bishop, D.J., Krook, A., and Zierath, J.R. (2020). Transcriptomic profiling of skeletal muscle adaptations to exercise and inactivity. Nat. Commun. *11*, 1–15.

Pitts, K.R., Stiko, A., Buetow, B., Lott, F., Guo, P., Virca, D., and Toombs, C.F. (2007). Washout of heme-containing proteins dramatically improves tetrazolium-based infarct staining. J. Pharmacol. Toxicol. Methods *55*, 201–208.

Prime, T.A., Blaikie, F.H., Evans, C., Nadtochiy, S.M., James, A.M., Dahm, C.C., Vitturi, D.A., Patel, R.P., Hiley, C.R., Abakumova, I., et al. (2009). A mitochondria-targeted S-nitrosothiol modulates respiration, nitrosates thiols, and protects against ischemia-reperfusion injury. Proc. Natl. Acad. Sci. *106*, 10764–10769.

Prime, T.A., Forkink, M., Logan, A., Finichiu, P.G., McLachlan, J., Li Pun, P.B., Koopman, W.J.H., Larsen, L., Latter, M.J., Smith, R.A.J., et al. (2012). A ratiometric fluorescent probe

for assessing mitochondrial phospholipid peroxidation within living cells. Free Radic. Biol. Med. *53*, 544–553.

Prinz, F., Schlange, T., and Asadullah, K. (2011). Believe it or not: how much can we rely on published data on potential drug targets? Nat. Rev. Drug Discov. *10*, 712–712.

Przyklenk, K. (2011). Efficacy of Cardioprotective 'Conditioning' Strategies in Aging and Diabetic Cohorts. Drugs Aging *28*, 331–343.

Puhl, S.-L., Müller, A., Wagner, M., Devaux, Y., Böhm, M., Wagner, D.R., and Maack, C. (2015). Exercise attenuates inflammation and limits scar thinning after myocardial infarction in mice. Am. J. Physiol. Heart Circ. Physiol. *309*, H345-359.

Quatresous, E., Legrand, C., and Pouvreau, S. (2012). Mitochondria-targeted cpYFP: pH or superoxide sensor? J. Gen. Physiol. *140*, 567–570.

Qureshi, W.T., and Nasir, U.B. (2017). Principals and clinical applications of magnetic resonance cardiac spectroscopy in heart failure. Heart Fail. Rev. *22*, 491–499.

Radak, Z., Ishihara, K., Tekus, E., Varga, C., Posa, A., Balogh, L., Boldogh, I., and Koltai, E. (2017). Exercise, oxidants, and antioxidants change the shape of the bell-shaped hormesis curve. Redox Biol. *12*, 285–290.

Ramirez F., D., Motazedian, P., Jung, R. G., Di Santo, P., MacDonald Z., Simard, T., Clancy, A. A., Russo, J. J., Welch, V., Wells, G. A., et al. (2017). Sex Bias Is Increasingly Prevalent in Preclinical Cardiovascular Research: Implications for Translational Medicine and Health Equity for Women. Circulation *135*, 625–626.

Ramsay, R.R. (2019). Electron carriers and energy conservation in mitochondrial respiration. ChemTexts *5*, 9.

Rebek, J., Costello, T., and Wattley, R. (1985). Binding forces and catalysis. The use of bipyridyl-metal chelation to enhance reaction rates. J. Am. Chem. Soc. *107*, 7487–7493.

Reed, G.W., Rossi, J.E., and Cannon, C.P. (2017). Acute myocardial infarction. The Lancet *389*, 197–210.

Rees, J.F., Wergifosse, B. de, Noiset, O., Dubuisson, M., Janssens, B., and Thompson, E.M. (1998). The origins of marine bioluminescence: turning oxygen defence mechanisms into deep-sea communication tools. J. Exp. Biol. *201*, 1211–1221.

Reily, C., Mitchell, T., Chacko, B.K., Benavides, G.A., Murphy, M.P., and Darley-Usmar, V.M. (2013). Mitochondrially targeted compounds and their impact on cellular bioenergetics. Redox Biol. *1*, 86–93.

Requejo, R., Hurd, T.R., Costa, N.J., and Murphy, M.P. (2010). Cysteine residues exposed on protein surfaces are the dominant intramitochondrial thiol and may protect against oxidative damage. FEBS J. *277*, 1465–1480.

Rider, O.J., and Tyler, D.J. (2013). Clinical Implications of Cardiac Hyperpolarized Magnetic Resonance Imaging. J. Cardiovasc. Magn. Reson. *15*, 93.

Rigo, A., Stevanato, R., Finazzi-Agro, A., and Rotilio, G. (1977). An attempt to evaluate the rate of the Haber-Weiss reaction by using OH radical scavengers. FEBS Lett. *80*, 130–132.

Robb, E.L., Gawel, J.M., Aksentijević, D., Cochemé, H.M., Stewart, T.S., Shchepinova, M.M., Qiang, H., Prime, T.A., Bright, T.P., James, A.M., et al. (2015). Selective superoxide generation within mitochondria by the targeted redox cycler MitoParaquat. Free Radic. Biol. Med.

Robb, E.L., Hall, A.R., Prime, T.A., Eaton, S., Szibor, M., Viscomi, C., James, A.M., and Murphy, M.P. (2018). Control of mitochondrial superoxide production by reverse electron transport at complex I. J. Biol. Chem. *293*, 9869–9879.

Ronchi, J.A., Figueira, T.R., Ravagnani, F.G., Oliveira, H.C.F., Vercesi, A.E., and Castilho, R.F. (2013). A spontaneous mutation in the nicotinamide nucleotide transhydrogenase gene of C57BL/6J mice results in mitochondrial redox abnormalities. Free Radic. Biol. Med. *63*, 446–456.

Ross, A.J., Yang, Z., Berr, S.S., Gilson, W.D., Petersen, W.C., Oshinski, J.N., and French, B.A. (2002). Serial MRI evaluation of cardiac structure and function in mice after reperfused myocardial infarction. Magn. Reson. Med. *47*, 1158–1168.

Ross, M.F., Kelso, G.F., Blaikie, F.H., James, A.M., Cochemé, H.M., Filipovska, A., Ros, T.D., Hurd, T.R., Smith, R. a. J., and Murphy, M.P. (2005). Lipophilic triphenylphosphonium cations as tools in mitochondrial bioenergetics and free radical biology. Biochem. Mosc. *70*, 222–230.

Rottbauer, W., Greten, T., Müller-Bardorff, M., Remppis, A., Zehelein, J., Grünig, E., and Katus, H.A. (1996). Troponin T: a diagnostic marker for myocardial infarction and minor cardiac cell damage. Eur. Heart J. *17 Suppl F*, 3–8.

Rowe, I., and Boletta, A. (2013). Mitochondrial Transmembrane Potential (ψm) Assay Using TMRM. BIO-Protoc. *3*.

Russo, A., DeGraff, W., Friedman, N., and Mitchell, J.B. (1986). Selective Modulation of Glutathione Levels in Human Normal versus Tumor Cells and Subsequent Differential Response to Chemotherapy Drugs. Cancer Res. *46*, 2845–2848.

Sakellariou, G.K., Vasilaki, A., Palomero, J., Kayani, A., Zibrik, L., McArdle, A., and Jackson, M.J. (2013). Studies of Mitochondrial and Nonmitochondrial Sources Implicate Nicotinamide Adenine Dinucleotide Phosphate Oxidase(s) in the Increased Skeletal Muscle Superoxide Generation That Occurs During Contractile Activity. Antioxid. Redox Signal. *18*, 603–621.

Sanadi, D.R., and Fluharty, A.L. (1963). On the Mechanism of Oxidative Phosphorylation. VII. The Energy-Requiring Reduction of Pyridine Nucleotide by Succinate and the Energy-Yielding Oxidation of Reduced Pyridine Nucleotide by Fumarate*. Biochemistry *2*, 523–528.

Saotome, M., Katoh, H., Yaguchi, Y., Tanaka, T., Urushida, T., Satoh, H., and Hayashi, H. (2009). Transient opening of mitochondrial permeability transition pore by reactive oxygen species protects myocardium from ischemia-reperfusion injury. Am. J. Physiol. - Heart Circ. Physiol. *296*, H1125–H1132.

Sauer, H., Wartenberg, M., and Hescheler, J. (2001). Reactive Oxygen Species as Intracellular Messengers During Cell Growth and Differentiation. Cell. Physiol. Biochem. *11*, 173–186.

Sawyer, D.T., and Valentine, J.S. (1981). How super is superoxide? Acc. Chem. Res. *14*, 393–400.

Scarlett, J.L., Packer, M.A., Porteous, C.M., and Murphy, M.P. (1996). Alterations to glutathione and nicotinamide nucleotides during the mitochondrial permeability transition induced by peroxynitrite. Biochem. Pharmacol. *52*, 1047–1055.

Schranner, D., Kastenmüller, G., Schönfelder, M., Römisch-Margl, W., and Wackerhage, H. (2020). Metabolite Concentration Changes in Humans After a Bout of Exercise: a Systematic Review of Exercise Metabolomics Studies. Sports Med. - Open *6*, 11.

Sharma, S., Jackson, P.G., and Makan, J. (2004). Cardiac troponins. J. Clin. Pathol. *57*, 1025–1026.

Sharman, I.M., Down, M.G., and Sen, R.N. (1971). The effects of vitamin E and training on physiological function and athletic performance in adolescent swimmers. Br. J. Nutr. *26*, 265–276.

Shchepinova, M.M., Cairns, A.G., Prime, T.A., Logan, A., James, A.M., Hall, A.R., Vidoni, S., Arndt, S., Caldwell, S.T., Prag, H.A., et al. (2017). MitoNeoD: A Mitochondria-Targeted Superoxide Probe. Cell Chem. Biol. *24*, 1285-1298.e12.

Sibbing, D., Pfeufer, A., Perisic, T., Mannes, A.M., Fritz-Wolf, K., Unwin, S., Sinner, M.F., Gieger, C., Gloeckner, C.J., Wichmann, H.-E., et al. (2011). Mutations in the mitochondrial thioredoxin reductase gene TXNRD2 cause dilated cardiomyopathy. Eur. Heart J. *32*, 1121–1133.

Smith, R.A.J., and Murphy, M.P. (2010). Animal and human studies with the mitochondria-targeted antioxidant MitoQ. Ann. N. Y. Acad. Sci. *1201*, 96–103.

Smith, P.K., Krohn, R.I., Hermanson, G.T., Mallia, A.K., Gartner, F.H., Provenzano, M.D., Fujimoto, E.K., Goeke, N.M., Olson, B.J., and Klenk, D.C. (1985). Measurement of protein using bicinchoninic acid. Anal. Biochem. *150*, 76–85.

Smith, R.A.J., Porteous, C.M., Gane, A.M., and Murphy, M.P. (2003). Delivery of bioactive molecules to mitochondria in vivo. Proc. Natl. Acad. Sci. U. S. A. *100*, 5407–5412.

Smith, R.A.J., Kelso, G.F., James, A.M., and Murphy, M.P. (2004). Targeting coenzyme Q derivatives to mitochondria. Methods Enzymol. *382*, 45–67.

Smith, R.A.J., Hartley, R.C., and Murphy, M.P. (2011). Mitochondria-Targeted Small Molecule Therapeutics and Probes. Antioxid. Redox Signal. *15*, 3021–3038.

Strøm, C.C., Aplin, M., Ploug, T., Christoffersen, T.E.H., Langfort, J., Viese, M., Galbo, H., Haunsø, S., and Sheikh, S.P. (2005). Expression profiling reveals differences in metabolic gene expression between exercise-induced cardiac effects and maladaptive cardiac hypertrophy. FEBS J. *272*, 2684–2695.

Tait, S.W.G., and Green, D.R. (2012). Mitochondria and cell signalling. J. Cell Sci. *125*, 807–815.

Taylor, R.S., Brown, A., Ebrahim, S., Jolliffe, J., Noorani, H., Rees, K., Skidmore, B., Stone, J.A., Thompson, D.R., and Oldridge, N. (2004). Exercise-based rehabilitation for patients with coronary heart disease: systematic review and meta-analysis of randomized controlled trials. Am. J. Med. *116*, 682–692.

Thornton, J., Striplin, S., Liu, G.S., Swafford, A., Stanley, A.W., Van Winkle, D.M., and Downey, J.M. (1990). Inhibition of protein synthesis does not block myocardial protection afforded by preconditioning. Am. J. Physiol.-Heart Circ. Physiol. *259*, H1822–H1825.

Toledano, M.B., Planson, A.-G., and Delaunay-Moisan, A. (2010). Reining in H2O2 for Safe Signaling. Cell *140*, 454–456.

Tong, G., Aponte, A.M., Kohr, M.J., Steenbergen, C., Murphy, E., and Sun, J. (2014). Postconditioning leads to an increase in protein S-nitrosylation. Am. J. Physiol. - Heart Circ. Physiol. *306*, H825–H832.

Topf, U., Suppanz, I., Samluk, L., Wrobel, L., Böser, A., Sakowska, P., Knapp, B., Pietrzyk, M.K., Chacinska, A., and Warscheid, B. (2018). Quantitative proteomics identifies redox switches for global translation modulation by mitochondrially produced reactive oxygen species. Nat. Commun. *9*, 1–17.

Toyokuni, S., Okamoto, K., Yodoi, J., and Hiai, H. (1995). Persistent oxidative stress in cancer. FEBS Lett. *358*, 1–3.

Tritto, I., D'Andrea, D., Eramo, N., Scognamiglio, A., Simone, C.D., Violante, A., Esposito, A., Chiariello, M., and Ambrosio, G. (1997). Oxygen Radicals Can Induce Preconditioning in Rabbit Hearts. Circ. Res. *80*, 743–748.

Tucker, W.J., Beaudry, R.I., Liang, Y., Clark, A.M., Tomczak, C.R., Nelson, M.D., Ellingsen, O., and Haykowsky, M.J. (2019). Meta-analysis of Exercise Training on Left Ventricular Ejection Fraction in Heart Failure with Reduced Ejection Fraction: A 10-year Update. Prog. Cardiovasc. Dis. *62*, 163–171.

Tullio, F., Angotti, C., Perrelli, M.-G., Penna, C., and Pagliaro, P. (2013). Redox balance and cardioprotection. Basic Res. Cardiol. *108*, 392.

Turrens, J.F. (2003). Mitochondrial formation of reactive oxygen species. J. Physiol. *552*, 335–344.

Turrens, J.F., Alexandre, A., and Lehninger, A.L. (1985). Ubisemiquinone is the electron donor for superoxide formation by complex III of heart mitochondria. Arch. Biochem. Biophys. *237*, 408–414.

Urig, S., and Becker, K. (2006). On the potential of thioredoxin reductase inhibitors for cancer therapy. Semin. Cancer Biol. *16*, 452–465.

Valls-Lacalle, L., Barba, I., Miró-Casas, E., Alburquerque-Béjar, J.J., Ruiz-Meana, M., Fuertes-Agudo, M., Rodríguez-Sinovas, A., and García-Dorado, D. (2015). Succinate dehydrogenase inhibition with malonate during reperfusion reduces infarct size by preventing mitochondrial permeability transition. Cardiovasc. Res. cvv279.

Vercesi, A.E., Castilho, R.F., Kowaltowski, A.J., de Oliveira, H.C.F., de Souza-Pinto, N.C., Figueira, T.R., and Busanello, E.N.B. (2018). Mitochondrial calcium transport and the redox nature of the calcium-induced membrane permeability transition. Free Radic. Biol. Med. *129*, 1–24.

Vina, J., Sanchis-Gomar, F., Martinez-Bello, V., and Gomez-Cabrera, M. (2012). Exercise acts as a drug; the pharmacological benefits of exercise. Br. J. Pharmacol. *167*, 1–12.

de Waard, M.C., van Haperen, R., Soullié, T., Tempel, D., de Crom, R., and Duncker, D.J. (2010). Beneficial effects of exercise training after myocardial infarction require full eNOS expression. J. Mol. Cell. Cardiol. *48*, 1041–1049.

Wang, Z.-H., Liu, J.-L., Wu, L., Yu, Z., and Yang, H.-T. (2014). Concentration-dependent wrestling between detrimental and protective effects of H2O2 during myocardial ischemia/reperfusion. Cell Death Dis. *5*, e1297.

Warburton, D.E.R., and Bredin, S.S.D. (2017). Health benefits of physical activity: a systematic review of current systematic reviews. [Miscellaneous Article]. Curr. Opin. Cardiol. *32*, 541–556.

Weigert, C. (1880). Ueber die pathologischen Gerinnungsvorgänge. Arch. Für Pathol. Anat. Physiol. Für Klin. Med. *79*, 87–123.

West, R.R., Jones, D.A., and Henderson, A.H. (2012). Rehabilitation after myocardial infarction trial (RAMIT): multi-centre randomised controlled trial of comprehensive cardiac rehabilitation in patients following acute myocardial infarction. Heart Br. Card. Soc. *98*, 637–644.

Wilson, M.A., and Cascarano, J. (1970). The energy-yielding oxidation of NADH by fumarate in submitochondrial particles of rat tissues. Biochim. Biophys. Acta BBA - Bioenerg. *216*, 54–62.

Winter, S., Strik, H., Rieger, J., Beck, J., Meyermann, R., and Weller, M. (2000). Glutathione S-transferase and drug sensitivity in malignant glioma. J. Neurol. Sci. *179*, 115–121.

Winterbourn, C.C., and Metodiewa, D. (1999). Reactivity of biologically important thiol compounds with superoxide and hydrogen peroxide. Free Radic. Biol. Med. *27*, 322–328.

Wojtovich, A.P., Nadtochiy, S.M., Urciuoli, W.R., Smith, C.O., Grunnet, M., Nehrke, K., and Brookes, P.S. (2013). A non-cardiomyocyte autonomous mechanism of cardioprotection involving the SLO1 BK channel. PeerJ *1*, e48.

Wong, H.L., and Shimamoto, K. (2009). Sending ROS on a Bullet Train. Sci. Signal. *2*, pe60–pe60.

Yaguchi, Y., Satoh, H., Wakahara, N., Katoh, H., Uehara, A., Terada, H., Fujise, Y., and Hayashi, H. (2003). Protective Effects of Hydrogen Peroxide Against Ischemia/Reperfusion Injury in Perfused Rat Hearts. Circ. J. *67*, 253–258.

Yamamoto, M., Yang, G., Hong, C., Liu, J., Holle, E., Yu, X., Wagner, T., Vatner, S.F., and Sadoshima, J. (2003). Inhibition of endogenous thioredoxin in the heart increases oxidative stress and cardiac hypertrophy. J. Clin. Invest. *112*, 1395–1406.

Yancy, C.W., Jessup, M., Bozkurt, B., Butler, J., Casey, D.E., Drazner, M.H., Fonarow, G.C., Geraci, S.A., Horwich, T., Januzzi, J.L., et al. (2013). 2013 ACCF/AHA guideline for the management of heart failure: a report of the American College of Cardiology Foundation/American Heart Association Task Force on Practice Guidelines. J. Am. Coll. Cardiol. *62*, e147-239.

Yang, L., Yu, D., Mo, R., Zhang, J., Hua, H., Hu, L., Feng, Y., Wang, S., Zhang, W., Yin, N., et al. (2016). The Succinate Receptor GPR91 Is Involved in Pressure Overload-Induced Ventricular Hypertrophy. PLOS ONE *11*, e0147597.

Yang, Y., Ago, T., Zhai, P., Abdellatif, M., and Sadoshima, J. (2011). Thioredoxin 1 negatively regulates angiotensin II-induced cardiac hypertrophy through upregulation of miR-98/let-7. Circ. Res. *108*, 305–313.

Ye, Y., Li, J., and Yuan, Z. (2013). Effect of Antioxidant Vitamin Supplementation on Cardiovascular Outcomes: A Meta-Analysis of Randomized Controlled Trials. PLOS ONE *8*, e56803.

Ytrehus, K., Liu, Y., Tsuchida, A., Miura, T., Liu, G.S., Yang, X.M., Herbert, D., Cohen, M.V., and Downey, J.M. (1994). Rat and rabbit heart infarction: effects of anesthesia, perfusate, risk zone, and method of infarct sizing. Am. J. Physiol.-Heart Circ. Physiol. *267*, H2383–H2390.

Ytrehus, K., Walsh, R.S., Richards, S.C., and Downey, J.M. (1995). Hydrogen peroxide as a protective agent during reperfusion A study in the isolated perfused rabbit heart subjected to regional ischemia. Cardiovasc. Res. *30*, 1033–1037.

Yu, H., Kalogeris, T., and Korthuis, R.J. (2019). Reactive species-induced microvascular dysfunction in ischemia/reperfusion. Free Radic. Biol. Med. *135*, 182–197.

Yuan, K., Liu, Y., Chen, H.-N., Zhang, L., Lan, J., Gao, W., Dou, Q., Nice, E.C., and Huang, C. (2015). Thiol-based redox proteomics in cancer research. PROTEOMICS *15*, 287–299.

Yuan, Y., Xu, Y., Xu, J., Liang, B., Cai, X., et al. (2017). Succinate promotes skeletal muscle protein synthesis via Erk1/2 signaling pathway. Mol. Med. Rep. *16*, 7361–7366.

Yun, J., and Finkel, T. (2014). Mitohormesis. Cell Metab. *19*, 757–766.

Zacharias, N.M., Chan, H.R., Sailasuta, N., Ross, B.D., and Bhattacharya, P. (2012). Real-Time Molecular Imaging of Tricarboxylic Acid Cycle Metabolism in Vivo by Hyperpolarized 1-13C Diethyl Succinate. J. Am. Chem. Soc. *134*, 934–943.

Zamzami, N., Maisse, C., Métivier, D., and Kroemer, G. (2001). Measurement of membrane permeability and permeability transition of mitochondria. Methods Cell Biol. *65*, 147–158.

Zhang, H., Jay Forman, H., and Choi, J. (2005). γ-Glutamyl Transpeptidase in Glutathione Biosynthesis. In Methods in Enzymology, H. Sies, and L. Packer, eds. (Academic Press), pp. 468–483.

Zhang, J., Wang, Y.T., Miller, J.H., Day, M.M., Munger, J.C., and Brookes, P.S. (2018a). Accumulation of Succinate in Cardiac Ischemia Primarily Occurs via Canonical Krebs Cycle Activity. Cell Rep. *23*, 2617–2628.

Zhang, X., Gibhardt, C., Cappello, S., Zimmermann, K., Vultur, A., and Bogeski, I. (2018b). Measuring Mitochondrial ROS in Mammalian Cells with a Genetically Encoded Protein Sensor. BIO-Protoc. *8*.

Zhao, D., Sun, Y., Tan, Y., Zhang, Z., Hou, Z., Gao, C., Feng, P., Zhang, X., Yi, W., and Gao, F. (2018). Short-Duration Swimming Exercise after Myocardial Infarction Attenuates Cardiac Dysfunction and Regulates Mitochondrial Quality Control in Aged Mice. Oxid. Med. Cell. Longev. *2018*.

Zhou, M., Diwu, Z., Panchuk-Voloshina, N., and Haugland, R.P. (1997). A Stable Nonfluorescent Derivative of Resorufin for the Fluorometric Determination of Trace Hydrogen Peroxide: Applications in Detecting the Activity of Phagocyte NADPH Oxidase and Other Oxidases. Anal. Biochem. *253*, 162–168.

Zhou, Y.-Q., Foster, F.S., Nieman, B.J., Davidson, L., Chen, X.J., and Henkelman, R.M. (2004). Comprehensive transthoracic cardiac imaging in mice using ultrasound biomicroscopy with anatomical confirmation by magnetic resonance imaging. Physiol. Genomics *18*, 232–244.

Zielonka, J., and Kalyanaraman, B. (2010). Hydroethidine- and MitoSOX-derived red fluorescence is not a reliable indicator of intracellular superoxide formation: Another inconvenient truth. Free Radic. Biol. Med. *48*, 983–1001.

Zorov, D.B., Filburn, C.R., Klotz, L.-O., Zweier, J.L., and Sollott, S.J. (2000). Reactive Oxygen Species (Ros-Induced) Ros Release A New Phenomenon Accompanying Induction of the Mitochondrial Permeability Transition in Cardiac Myocytes. J. Exp. Med. *192*, 1001–1014.

Zuo, L., Youtz, D.J., and Wold, L.E. (2011). Particulate Matter Exposure Exacerbates High Glucose-Induced Cardiomyocyte Dysfunction through ROS Generation. PLoS ONE *6*.

Zweier, J.L., Flaherty, J.T., and Weisfeldt, M.L. (1987). Direct measurement of free radical generation following reperfusion of ischemic myocardium. Proc. Natl. Acad. Sci. U. S. A. *84*, 1404–1407.

## Appendix

### Synthesis of MitoPQ control compound 2

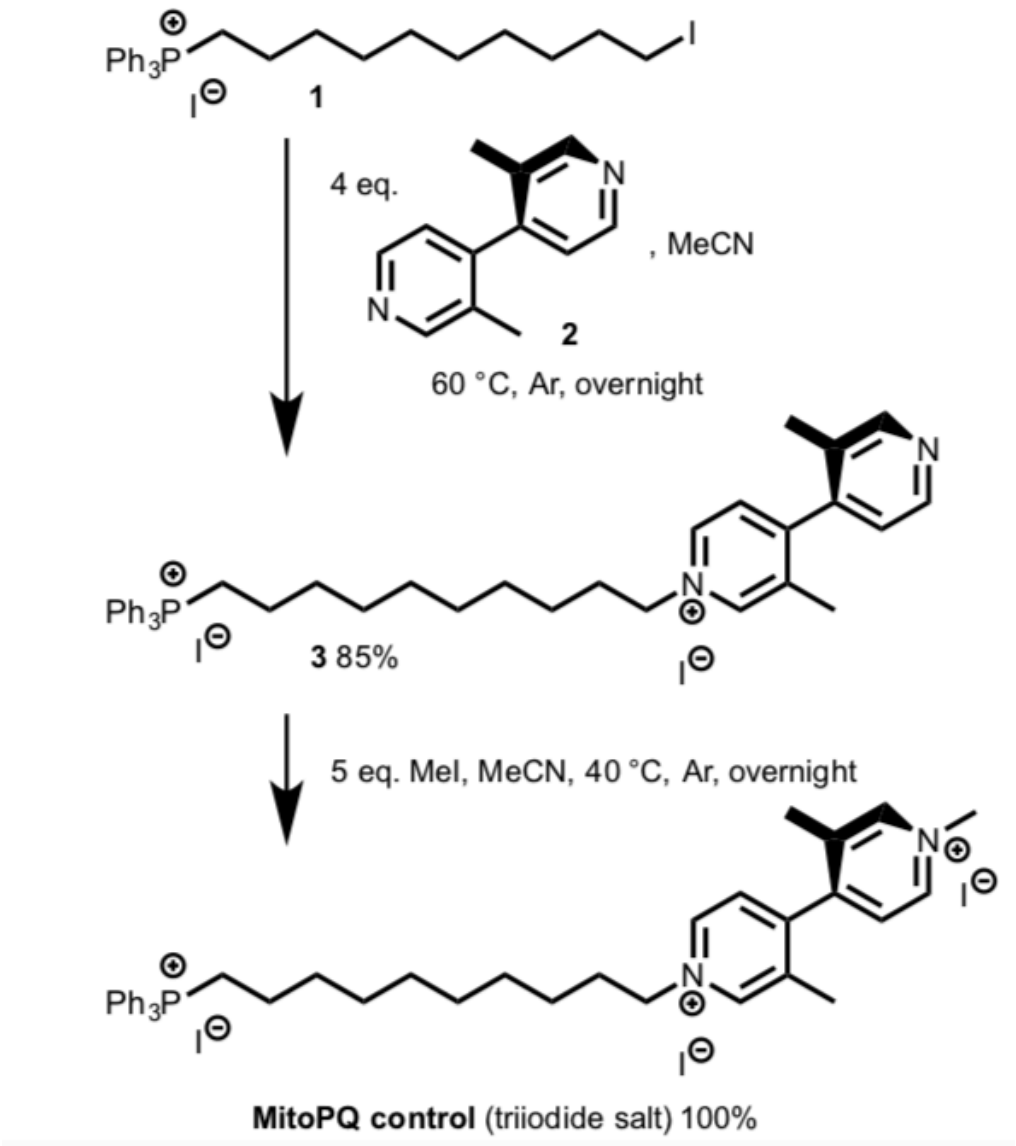


**Figure S1 Schematic showing the synthesis of MitoPQ control compound 2.**

MitoPQ was synthesized from iododecyl-TPP salt 1, which was prepared as described previously. This was reacted with an excess of dimethyl-4,4'-dipyridyl 2, prepared by the procedure of Rebek et al. (1985), to minimise dialkylation. The monoalkylated product 3 was isolated in excellent year and was then methylated to give complete conversion to MitoPQ control.

**Publications arising from this work**

Antonucci S*, **Mulvey JF***, Burger N, Di Sante M, Hall AR, Hinchy EC, Caldwell ST, Gruszczyk AV, Deshwal S, Hartley RC, Kaludercic N, Murphy MP, Di Lisa F, Krieg T **Selective mitochondrial superoxide generation *in vivo* is cardioprotective through hormesis.** Free Radic Biol Med. 2019 Feb 4;134:678-687
*these authors contributed equally to this work

Booty L, Gawal J, Cvetko F, Cadlwell S, Hall A, **Mulvey J**, James A, Hinchy E, Prime T, Arndt S, Beninca A, Bright T, Clatworthy M, Ferdinand J, Prag H, Logan A, Prudent J, Krieg T, Murphy M Hartley R **Organelle-specific Disruption of Mitochondrial Thiol Redox State in Cells and In Vivo**. Cell Chem Biol. 2019 Mar 21;26(3):449-461.e8

Kohlhauer M, Pell VR, Burger N, Spiroski AM, Gruszczyk A, **Mulvey JF**, Mottahedin A, da Costa ASH, Frezza C, Murphy mP, Tissier R, Krieg T. **Protection against cardiac ischemia-reperfusion injury by hypothermia and by inhibition of succinate accumulation and oxidation are additive.** Basic Res Cardiol. 2019 Mar 15;114(3):18

Pell VR, Spiroski AM, **Mulvey J**, Burger N, Costa ASH, Logan A, Gruszczyk AV, Rosa T, James AM, Frezza C, Murphy MP, Krieg T. **Ischemic preconditioning protects against cardiac ischemia reperfusion injury without affecting succinate accumulation or oxidation.** J Mol Cell Cardiol. 2018 Oct;123:88-91

Shchepinova MM, Cairns AG, Prime TA, Logan A, James AM, Hall AR, Vidoni S, Arndt S, Caldwell ST, Pragg HA, Pell VR, Krieg T, **Mulvey JF,** Yadav P, Cobley JN, Bright TP, Senn HM, Anderson RF, Murphy MP, Hartley RC. **MitoNeoD: A Mitochondria-Targeted Superoxide Probe.** Cell Chem Biol. 2017 Oct 19;24(10):1285-1298.e12

Egea J, Fabregat I… **Mulvey J**, … Schmidt HHHW, Di Lisa F, Daiber A. **European contribution to the study of ROS: A summary of the findings and prospects for the future from the COST action BM1203 (EU-ROS**). Redox Biol. 2017 Oct;13:94-162.

**Presentations and prizes resulting from this work**

International Society of Heart Research World Congress 2019: invited co-chair for session on “Mitochondrial homeostasis and Cardioprotection”, poster presentation

International Society of Heart Research-European Section meeting 2017: Oral communication, poster presentation

Cambridge cardio-metabolic early career researchers meeting 2017: awarded poster prize

Cambridge Cardiovascular SRI and British Heart Foundation Centre of Research Excellence Annual conference 2017: awarded poster prize

British Society of Cardiovascular Research Spring meeting 2017: poster presentation